Die approbierte Originalversion dieser Dissertation ist an der Hauptbibliothek der Technischen Universität Wien aufgestellt (http://www.ub.tuwien.ac.at).

The approved original version of this thesis is available at the main library of the Vienna University of Technology (http://www.ub.tuwien.ac.at/englweb/).

DISSERTATION

QCT based Finite Element Models of the Human Vertebra and Femur: Validation with Experiments and comparison with Bone Densitometry

ausgeführt zum Zwecke der Erlangung des akademischen Grades eines Doktors der technischen Wissenschaften unter der Leitung von

Assoc.Prof. Dipl.-Ing. Dr.techn. Dieter H. PAHR
E317
Institut für Leichtbau und Struktur-Biomechanik

Und

Prof. Dipl.-Ing. Dr.techn. Philippe K. ZYSSET
Institut für chirurgische Technologien und Biomechanik
Universität Bern

eingereicht an der Technischen Universität Wien
Fakultät für Maschinenwesen und Betriebswissenschaften

Von

Dipl.-Ing. Enrico DALL'ARA
Matrikelnummer: 0828490
Eisvogelgasse 6/24
A-1060 Wien,

im October 2012 Enrico Dall'Ara

To myself I am only a child playing on the beach,
while vast oceans of truth lie undiscovered before me.
Sir Isaac Newton

…ai miei genitori Graziella e Renzo,
…ai miei nonni Fernanda e Mario,
…e all'Amore della mia vita, Felicia.

Acknowledgements

I would like to take this space to sincerely and warmly thank some of the people who contributed directly or indirectly to the realisation of this thesis in the last years.

First I would like to state my gratitude to Prof Dieter Pahr and Prof Philippe Zysset for giving me the opportunity of working in such stimulating research group and for the outstanding and continuous supervision during the last years. It was really a pleasure being supervised by such great scientists, engineers and brilliant minds. I hope that during the numerous fruitful discussions and meetings over the years I could absorb and learn not only how to deal with scientific problems but also how to keep such passion and energy that they invest in their work.
I would like to thank also Prof Zohar Yosibash for taking the time for reading and evaluating my thesis.

I would like to thank also all the colleagues whose contributions have been essential in different ways for the accomplishment of the sub-studies that compose this thesis. Particular thanks to Prof Franz Kainberger and Janina Patsch for opening the doors of the radiology department at the AKH, Prof Michael Pretterklieber for collecting the samples, Reinhard Schmidt for the bloody job ;-) , Yan Chevalier and Peter Varga for sharing their knowledge. Yan, Peter it was a pleasure working with you at ILSB, I really enjoy still collaborating with you and I hope it will be the same in the future!
Moreover, during the last (almost) five years at the ILSB I had the opportunity to work with a group of people who brought something into this thesis through every single discussion. It was a pleasure working with them and sharing ideas, thoughts in front of a (relatively) good coffee in the MuFuZi, time in the MMLAB, AKH and/or workshop. In this regard I would like to thank in particular Benoit Luisier, Michael Kinzl (thanks for the translation of the abstract!!), Prof Heinz Pettermann, Robert Exler, Jakob Schwiedrzik and Thomas Gross. Special thanks also to Gerhard Schneider for the great help with the computing resources and to Maria Steininger for standing my bad German and for helping with all the paper work! I would like also to acknowledge the past and present heads of the ILSB (Prof Helmut Böhm, Prof Philippe Zysset and Prof Franz Rammerstorfer) for having created a great and friendly working environment.

I would like to thank my parents Renzo&Graziella and grandparents Mario&Fernanda…well I will switch to Italian for this…dicevo, vorrei ringraziare i miei genitori e i miei nonni per avermi motivato sin da quando ero bambino a cercare di raggiungere i traguardi che piu' mi stimolassero…se ho completato questo traguardo e' anche grazie ai vostri insegnamenti di vita!

Finally, I would like to thank Felicia, the love of my life, for her constant support in all the steps of this adventure and for having spent so many hours on the trains to be able to meet again during the weekends. I hope there will be a time, soon, when we will be looking at all this travelling with a smile, and I will have you close to my side in the everyday life.

Abstract

Osteoporosis is a skeletal disease which dramatically increases mortality and morbidity. In Europe the total direct cost for osteoporotic fractures are expected to be more than €76 billions in 2050. The current method to estimate the risk of fracture and therefore to decide which patients should be treated against bone loss is based on bone mineral density (BMD) analysis of the hip or of the spine, by means of dual energy X-rays absorptiometry (DXA) or quantitative computed tomography (QCT). However, such techniques have been found not to be reliable in predicting bone strength in *in vitro* studies. In the last decades the finite element (FE) method has been extensively used to try to enhance the prediction of bone strength *in vitro*. Nevertheless, such models should be meticulously validated through reliable experiments *in vitro* to evaluate to which extent they can accurately predict the reality. Therefore, the goal of this thesis was to apply QCT-based FE models of the human vertebra and femur, validate them versus accurate experiments performed *in vitro* on a large number of specimens and compare their predictive ability with the ones of densitometric measurements usually used in clinical applications.

The first study presented a methodology to compute bone volume fraction (BV/TV) from QCT BMD which could be applied for both vertebra and femur and used to define the material properties of the FE models. The second and third studies reported the results for the human vertebra, while the fourth and fifth studies reported the ones for the proximal femora. In particular, for both anatomical sites novel testing setups were designed to generate fractures which are usually observed in clinics on 37 vertebral bodies and on 72 femora as well as to compute their mechanical properties at the organ level. Moreover, these studies presented the developed automatic procedure to generate the specimen specific nonlinear homogenized voxel FE (hvFE) models from the QCT scans and the procedures to evaluate volumetric/areal BMD from QCT or DXA.

The results of the Thesis showed that 1) similar calibration laws for both anatomical sites can be used to relate QCT BMD to BV/TV, 2) the hvFE models are better predictors of the vertebral and femoral mechanical properties than standard densitometric measurements, 3) and provided meaningful information about fracture location, 4) an improvement in scanning resolution would not improve prediction of vertebral body strength, 5) the DXA is capable to predict well femoral mechanical properties if loaded in a simulated fall and only moderately if loaded by simulating a one legged stance.

In conclusion a large dataset of experimental results (mechanical properties and 3D images) were generated and used to successfully validate QCT-based nonlinear specimen specific hvFE models of the human femur and vertebral body. The experimental results can be used in future studies to validate a number of numerical models based on QCT datasets. Moreover, the developed hvFE models could be used without major modification for pre-clinical and clinical studies in the next future to improve the prediction of the bone strength and indirectly of the risk of fracture *in vivo*.

Kurzfassung

Osteoporose ist eine Erkrankung des Skeletts durch die Mortalität und Morbidität dramatisch erhöht werden. In Europa wird erwartet, dass die gesamten direkten Kosten für osteoporotische Frakturen im Jahr 2050 mehr als €76 Milliarden betragen. Die derzeitige Methode mittels der das erwartete Frakturrisiko abgeschätzt wird und somit entschieden wird welche Patienten gegen Knochenabbau behandelt werden basiert auf der Messung Knochendichte (BMD) in Hüfte und Wirbelsäule mittels Dual-Röntgen-Absorptiometrie (DXA) oder quantitativer Computertomographie (QCT). Es wurde jedoch in *in vitro* Studien festgestellt, dass diese Techniken nicht in der Lage sind die Festigkeit des Knochens zuverlässig vorherzusagen. Im vergangen Jahrzehnt wurde die Finite Elemente (FE) Methode extensiv verwendet um die *in vitro* Prädiktion der Knochenfestigkeit zu verbessern. Allerdings müssen solche Simulationsmodelle sorgfältig gegen zuverlässige *in vitro* Experimente validiert werden um festzustellen inwiefern sie in der Lage sind die Realität akkurat vorherzusagen. Daher war das Ziel dieser Arbeit QCT-basierte FE Modelle des menschlichen Femur und Wirbelkörpers gegen akkurat durchgeführte *in vitro* Experimente mit großer Probenzahl zu validieren und die Genauigkeit der Prädiktionen mit der klinisch verwendeten Densitometrie zu vergleichen.

Die erste Studie präsentiert eine Methode um den Anteil des Knochenvolumens (BV/TV) mittels QCT basierter BMD Messung zu berechnen, wodurch die Materialeigenschaften des FE Modells sowohl für den Femur als auch für den Wirbelkörper berechnet werden können. In der zweiten und dritten Studie werden die Ergebnisse für den menschlichen Wirbelkörper dargelegt, und in der vierten und fünften Studie jene für den proximalen Femur. Für beide anatomische Positionen wurden spezielle experimentelle Konfigurationen entwickelt um in den 37 Wirbelkörper und 72 Femora klinisch relevante Frakturen zu erzeugen und ihre mechanischen Eigenschaften auf der Organebene zu berechnen. Des Weitern präsentieren diese Studien die entwickelte automatische Prozedur um Proben-spezifische, nichtlineare, homogenisierte Voxel-FE (hvFE) Modelle aus den QCT-Bildern zu generieren, sowie Methoden um den BMD basierend auf QCT oder DXA zu berechnen.

Die Ergebnisse dieser Arbeit zeigten, dass 1) ähnliche Kalibriergesetze für Wirbelkörper und Femur verwendet werden können um QCT BMD mit BV/TV zu verknüpfen, dass 2) die hvFE Modelle für beide Knochen bessere Prädiktoren der mechanische Eigenschaften sind als die standardmäßige Densitometrie und 3) zusätzlich bedeutende Informationen über die Frakturposition liefern, dass 4) eine höhere CT-Auflösung nicht zu besseren Festigkeitsprädiktionen der Wirbelkörper führt, dass 5) DXA in der Lage ist die mechanischen Eigenschaften des Femur bei Belastungen während eines simulierten Falls gut vorherzusagen, jedoch nur moderat für die Belastungen während eines simulierten Stehens auf einem Bein.

Schlussendlich wurde eine umfassend Datenbank an experimentellen Ergebnissen (mechanische Eigenschaften und 3D Bilder) gewonnen und wurde erfolgreich verwendet um QCT-basierte, nichtlineare, Proben-spezifische hvFE Modelle des menschlichen Femur und Wirbelkörpers zu generieren. Die experimentellen Ergebnisse können in Zukunft verwendet werden um verschiedenartige, auf QCT-Daten basierende, numerische Modelle zu validieren. Zudem, können die entwickelten hvFE Modelle ohne erhebliche Modifikationen für präklinische und klinische Studien verwendet werden um die Prädiktion der Knochenfestigkeit, und somit indirekt des Frakturrisikos, *in vivo* zu verbessern.

Contents

Introduction ***1***

1.1 Motivations 1

1.2 Bone 2

1.2.1 Bone physiology 2

1.2.2 Bone Mechanics 4

Trabecular bone morphology 4

Elasticity 6

Post-yield behaviour 7

1.3 Osteoporotic bone fractures 10

1.3.1 General problem 10

1.3.2 Clinical Evaluation of the BMD 12

DXA 12

QCT 13

HR-pQCT 15

1.4 The human vertebra 16

1.4.1 Vertebral anatomy 16

1.4.2 Vertebral biomechanics 17

1.4.3 Vertebral fractures 19

1.5 The human proximal femur 20

1.5.1 Proximal femur anatomy 20

1.5.2 Femoral biomechanics 21

1.5.3 Femoral fractures 22

1.6 Specimen specific finite element models 23

1.6.1 QCT-based homogenized models 24

1.6.2 HR-pQCT MicroFE models 26

1.6.3 Model Validation 27

Validation studies for the human vertebra 28

Validation studies for the human femur 30

1.6.4 Requirements and simplifications for QCT-based FE models 32

1.7 Objectives of the thesis 33

1.8 Outline of the thesis 34

Bibliography 35

BMD to BV/TV calibration study ***47***

2.1 Introduction 49

2.2 Materials and methods 50

2.2.1 Samples 50

2.2.2 Scanning 51

2.2.3 Image processing 51

2.2.4 Data analysis 52

2.3 Results 52

2.4 Discussion 55

Bibliography 58

hvFE validation study for the human vertebral body ***60***

3.1 Introduction....62
3.2 Materials and methods....63
3.2.1 Sample selection....63
3.2.2 Slice preparation....63
3.2.3 CT Scanning and vBMD analysis....63
3.2.4 Mechanical tests....65
3.2.5 Calibration curve....67
3.2.6 Voxel models....67
3.3 Results....69
3.4 Discussion....69
Bibliography....73
hvFE of the human vertebral body versus DXA ***75***
4.1 Introduction....77
4.2 Materials and methods....78
4.2.1 Sample preparation....78
4.2.2 Scanning procedures and image processing....79
4.2.3 Mechanical tests....80
4.2.4 QCT-based hvFE models....80
4.2.5 HR-pQCT-based μFE models....80
4.2.6 Data analysis and statistics....81
4.3 Results....81
4.4 Discussion....85
Bibliography....88
hvFE validation study for the human proximal femur ***92***
5.1 Introduction....94
5.2 Materials and methods....95
5.2.1 Sample preparation....95
5.2.2 QCT Scanning....96
5.2.3 Mechanical tests....96
5.2.4 Computation of the BMD to BV/TV calibration....98
5.2.5 Homogenized voxel FE models....98
5.3 Results....101
5.4 Discussion....105
5.5 Conclusions....108
Bibliography....108
Appendix: Material model for the QCT-based FE....113
DXA versus experiments for the human proximal femur ***116***
6.1 Introduction....118
6.2 Materials and methods....119
6.2.1 Sample preparation....119
6.2.2 DXA analysis....119
6.2.3 Mechanical tests....121
6.2.4 Post test radiographs and classification of fractures....121
6.2.5 Statistics....121
6.3 Results....122
6.4 Discussion....124
Bibliography....129
Conclusions ***133***
7.1 Original contributions....133

7.2 General Discussion 134
7.2.1 Sample preparation 135
7.2.2 CT scanning and densitometry 135
7.2.3 Mechanical testing 136
7.2.4 Generation of hvFE models 136
Calibration of BV/TV 137
Constitutive model 137
7.2.5 Prediction ability of the hvFE models 137
7.2.6 Limitations of the study 138
7.3 Outlook 139
7.3.1 Clinical and Pre-clinical application of the hvFE models 140
7.3.2 Model improvements 140
7.3.3 Experimental datasets 141
Bibliography 141

Chapter 1

Introduction

1.1 Motivations

The main motivation of the present thesis is to apply and validate numerical methods, based on clinical 3D images, to improve the prediction of bone strength and, in long term, to contribute to the assessment of fracture risk.
The society invests every year a large amount of economical resources to treat osteoporotic fractures (for more details please refer to section *1.3*). Osteoporosis is a major clinical problem which is characterized by a severe reduction in bone density and bone quality. This pathology has a growingly impact on our society due to the ageing of the human population. By increasing dramatically the number of vertebral and femoral fractures, osteoporosis is related to an enhancement of mortality and morbidity and to a reduction of the patient's quality of life.
To date, the best clinical approach to evaluate the risk of fracture is based on the measurement of the bone mineral density (BMD) with dual X-ray absorptiometry (DXA, see section *1.3.2*). However, it has been demonstrated that this method is not reliable enough and a large portion of biomechanicians worldwide focus their research challenges in finding more accurate tools to improve the ability of predicting the bone strength and, indirectly, the risk of fracture.
Engineering techniques such as quantitative computed tomography (QCT)-based finite element (FE) models, thanks to the improvement of the diagnostic machines and computational capability, can help basic and clinical research in the race against the increasing number of patients. By adding to the standard BMD measurements information about the bone geometry, bone dimension, tissue material properties, loading conditions, etc. these methods are becoming increasingly popular to predict the bone strength. In the last decades part of the bone research community invested large resources in finding more and more complex models that include more details about the bone geometry and microarchitecture acquired by using high resolution QCT scans, more accurate numerical solutions (e.g. by increasing the grade of the FE models), more detailed and complex material models and boundary conditions (e.g. by including material nonlinearities and contacts), more complex loading scenarios (e.g. by including muscle forces) and multi-

scale approaches which take into account the hierarchical fashion of the bone. Although it remains fundamental to develop new and more accurate methods, the required large computational resources and/or the increase in radiation dose induced to the patient to obtain more information from the CT images (by increasing their resolution), reduce their short term clinical applicability. Therefore, it is necessary to focus in finding tools which are fast, robust and easy to be implemented in a clinical environment, like for example QCT-based homogenized voxel based FE models (hvFE).
However, I will stress throughout all chapter of this thesis that every model, at least to some extent, should be validated through meticulous experiments in the laboratory to check its ability in predicting accurately the reality. The validation experiments presented here focus on vertebral and femoral fractures and are used to compare the ability of hvFE with the one of standard clinical tools in predicting the bone stiffness and failure (ultimate) load to better understand the potential of such models. This, as I shall show in the end of this chapter, is the main objective of this thesis. This introductory chapter will provide the basic state of the art about the features which are then used in the body of the thesis to generate, calibrate, validate and interpret the output of QCT-based hvFE models of the human vertebra and femur. In particular, it will begin with a brief description of bone physiology and mechanics, of the impact of osteoporotic fractures in our society, followed by two sections where the biomechanics of the human vertebra and femur are reported and then the application of specimen specific FE models to bone at the organ level will be described. Finally, I shall conclude the chapter with the objectives and outline of the thesis.

1.2 Bone

1.2.1 Bone physiology

Bone is one of the main constituents of the muscular-skeletal system together with muscles, ligaments, tendons and cartilage. This connective tissue is mainly responsible for body support, organ protection, supplying bone marrow and mineral (i.e. calcium and phosphorus) and to guaranteeing the body movement by transmitting muscular forces. Bone mass is constituted by 65% mineral (largely impure hydroxyapatite $Ca_{10}(PO_4)_6(OH)_2$), and for the remaining 35% by organic matrix (90% collagen type I and 10% noncollagenous proteins) and water (Webster, 2001). Mineral crystals are embedded in the organic matrix by forming collagen fibrils. Packages of fibrils are bound together to form collagen fibers which generates lamellar bone. Depending on the bone local function, the lamellae are arranged in two types of microstructures: cortical and trabecular bone. Cortical bone (compact bone or cortex) is formed of cylindrical substructures called Haversian systems (or osteons), where circular rings of 3-7 μm in thickness lamellae surround a longitudinal vascular channel, or Volkmann canals, where the vascular channel is oriented transversely to the bone axis. Haversian and Volkmann systems (blood vessel plus the concentric lamellae around it) are 100-300 μm in diameter, can be some mm long and are embedded in interstitial tissue, which is the remnant of old osteons (Guo, 2001). Cortical bone constitutes the diaphysis of long bones (e.g. femur, tibia) and the external shell of short bones (e.g. tarsus, carpus), flat bones (e.g. pelvis) and irregular bones (e. g. vertebrae). Trabecular bone (spongeous bone or cancellous bone) consists of an array of interconnected beams, called trabeculae, which are constituted by parallel packages of lamellae. The trabecular mean thickness can vary between 100 and 640 μm (Guo, 2001).

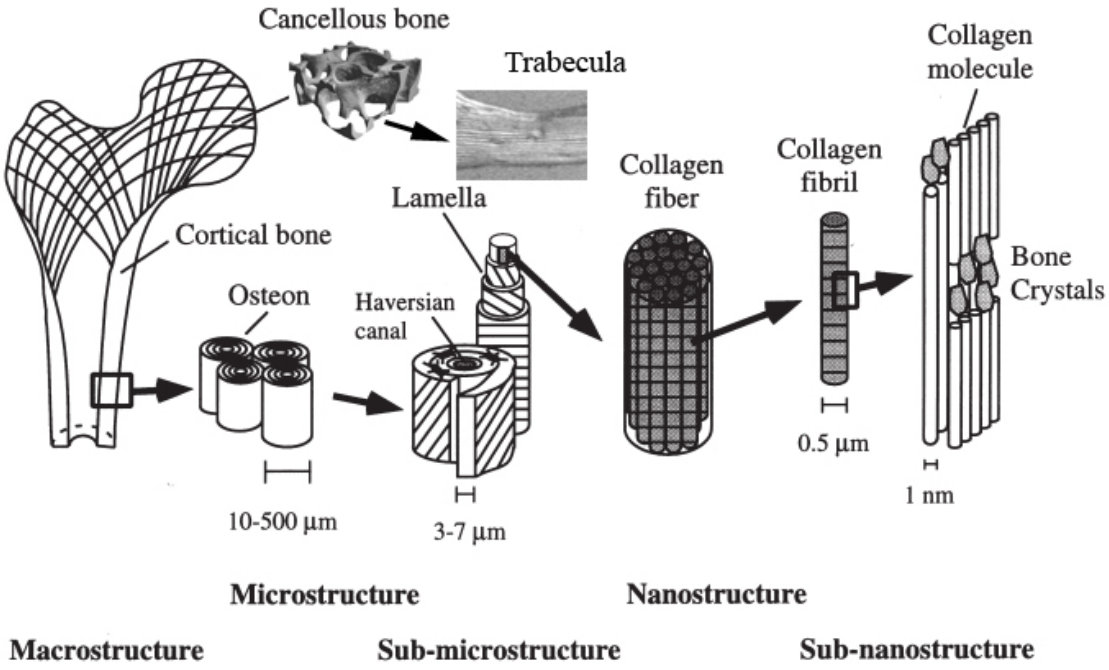

Figure 1. 1: Hierarchical structure of bone. Adapted from (Rho, et al., 1998).

This microstructure is located in the epiphysis of the long bones and in the central core of flat, short and irregular bones.

The organization of the bone's three main constituents in a complex hierarchical structure (Figure 1.1) provides a multifunctional material with stiffness and hardness (provided mainly by the mineral phase) high enough to resist external loads, and ductility (provided mainly by the organic phase and the arrangement of the collagen fibres) high enough to resist against fracture (Turner, 2006).

Furthermore, thanks to the activity of the cells embedded in it, bone is a self-healing material capable of repairing the microcracks induced by the daily activities and overloads. In facts, each bone is a leaving organ which is continuously remodelled by the work of three types of cells: osteocytes, osteoclasts and osteoblasts. Osteocytes are embedded in the bone matrix in small cavities called lacunae which are interconnected by a net of tubular channels, the canaliculi. These cells play an important role in the restructuring process of bone mass. In fact, they control the efflux of calcium ions, detect micro-damage and respond to the amount and distribution of strain by activating the other cells to remove (osteoclasts) or add (osteoblasts) bone where needed (Webster, 2001). Some authors also distinguish a fourth type of cells, called lining cell, which are quiescent osteoblasts laying on the extracellular matrix surface without any remodelling activity (Viceconti, 2012). If the osteoclastic and osteblastic activities are unbalanced the bone is too much reabsorbed or deposited, leading to pathologies like osteoporosis or osteopetrosis, respectively.

1.2.2 Bone Mechanics

Even though cortical and trabecular bone show a similar microscopic mechanical behaviour, due to their similar material composition, they behave differently at the macroscopic level, due to the differences in their architecture and bone volume fraction (BV/TV). In both microstructures the porosity (determined by the space between the trabeculae in trabecular bone and by the vascular systems in the cortical bone) plays a dominant role in the determination of the mechanical properties. The low resolution of the clinical QCT images does not allow for an accurate differentiation between trabecular and cortical bone and therefore the QCT based hvFE generated in this thesis assumed cortical bone such as dense trabecular bone. Thus, in the next paragraphs I will focus on the mechanics of trabecular bone, beginning from the descriptions of the method to characterize its density and micro-architecture.
Furthermore, even though experimental studies performed at the biopsy level on cortical bone have shown that bone is a viscoelastic material (Hansen, et al., 2008) (i.e. its mechanical properties are dependant from the loading rate, Figure 1.2), in this thesis the viscous-dependent behaviour of bone was not included in the hvFE models and experimental tests were performed in quasi static conditions. Therefore, in this chapter I will focus only on the elasticity and post-yield behaviour of bone, by leaving the description of viscoelasticity to other more specialized literature.

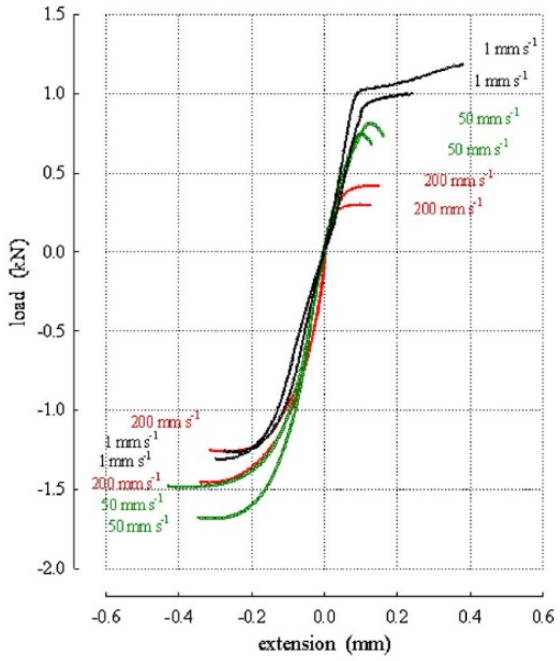

Figure 1. 2: Effect of strain rate on cortical bone samples extracted from the human femur and tested in compression and tension. Adapted from (Hansen, et al., 2008).

Trabecular bone morphology

Macroscopically, trabecular bone is a highly heterogeneous and in general anisotropic material due to its adaptation to physiological loading. Its mechanical properties are driven by the amount of bone in the considered volume, by the geometrical arrangement of its

substructures (trabeculae) and, to some extent, by the mineralization and composition at the microscopic level.
The amount of bone within a specified volume of trabecular bone can be evaluated with:

- Apparent density (ρ_{app}) (Morgan, et al., 2003), defined as the bone weight over the total volume;
- Apparent ash density (ρ_{ash}) (Kaneko, et al., 2004), defined as the weight of mineral phase over the total volume;
- Tissue mineral density (TMD) (Tassani, et al., 2010), defined as the weight of mineral phase over the bone volume;
- Bone volume fraction (BV/TV or hereby referred to as ρ in the equations) (Ding, et al., 1999), defined as bone volume over total volume. It provides a scalar architectural property that accounts for the volume occupied by the pores.

While the amount of bone was shown to be the most important determinant of trabecular bone mechanical properties (Kaneko, et al., 2004; Perilli, et al., 2007), also the trabecular architecture was found to contribute to them (Matsuura, et al., 2007; Ohman, et al., 2007).
In human bone, quantification of trabecular bone 3D morphology can be done with desktop imaging techniques such as micro computed tomography (μCT, usual voxel size down to 6 μm) for *in vitro* investigations or with high resolution peripheral computed tomography (HR-pQCT) for *in vivo* investigations on peripheral anatomical sites (typically distal radius and tibia, voxel size down to 42μm). With both machines, the trabecular structure can be reconstructed in 3D (Boyd and Muller, 2006; Ruegsegger, et al., 1996; Varga and Zysset, 2009) after proper segmentation of the acquired grey scale images and standardized morphological indices can be evaluated. Typical measurements consists in BV/TV, bone volume (BV), trabecular thickness (Tb.Th), trabecular number (Tb.N) and trabecular spacing (Tb.Sp) (Hildebrand, et al., 1999). Moreover, the anisotropy of trabecular bone can be quantified by measuring the main trabecular orientation in the considered region of interest. Although different methodologies for evaluating trabecular anisotropy (fabric) can be used (Varga, 2009), currently the most common method to measure it is the Mean Intercept length (MIL) which was first developed for histomorphometric analysis (Whitehouse, 1974) and only afterwards applied to 3D scans (Harrigan and Mann, 1984). Briefly, the method superimposes a ray field in direction **e**(ϑ, ϕ) and measures the mean interceptions of the ray with the bone defined as MIL(ϑ, ϕ), where ϑ and ϕ are the in plane and out of plane angles as described in Figure 1.3A.

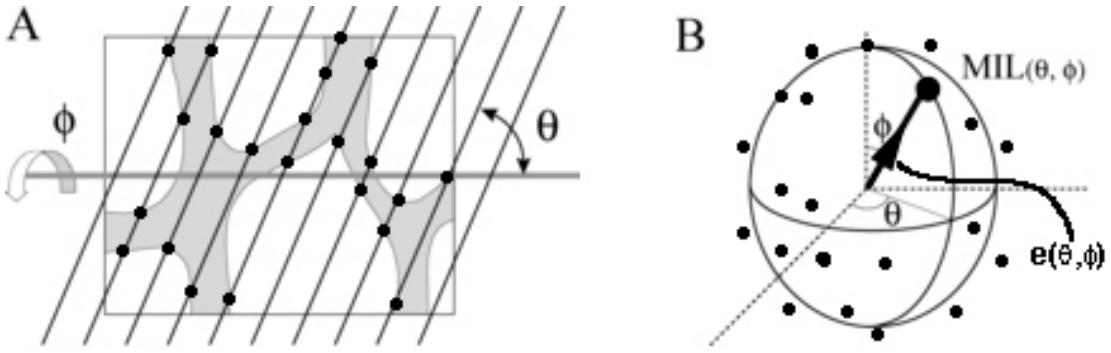

Figure 1. 3: Explanation of the mean intercept length (MIL) method. The average bone–marrow distances are measured in several directions in function of the values of the two in-plane (in A shown as ϑ) and out of plane (in A shown as ϕ) angles by counting the interfaces. The resulting MIL in function of the two angles ϑ and ϕ is approximated with an ellipsoid (B).

By changing discretely the values of ϑ and ϕ, the resulting cloud of point (Figure 1.3B) was found to fit with an ellipsoid, which can be described as the quadratic form of a second order tensor which is denoted as fabric tensor ***M*** (Harrigan and Mann, 1984):

$$\boldsymbol{M} = \sum_{i=1}^{3} m_i \boldsymbol{M}_i = \sum_{\boldsymbol{i=1}}^{\boldsymbol{3}} m_i (\boldsymbol{m}_i \otimes \boldsymbol{m}_i) \tag{1.1}$$

where $\mathbf{m}_i$ are the normalized eigenvectors providing the orientation of the principal directions, and m_i are strictly positive eigenvalues of ***M***. With this procedure the eigenvectors $\mathbf{m}_i$ of the fabric tensor ***M*** represents the main orientation of the trabeculae. The degree of anisotropy (DA) is defined as the ratio between the maximum and minimum eigenvalues.

Elasticity

The macroscopic elastic behavior of both cortical and trabecular bone is characterized by linear relationships between strains and stress, with similar tensile and compressive elastic constants (Rohl, et al., 1991). The Hooke's law can be used to relate the symmetric stress (**S**) and strain (**E**) second order tensors via the symmetric positive definite fourth order stiffness tensor ($\mathbb{S}$) or its inverse, the compliance tensor ($\mathbb{E}$):

$$\boldsymbol{S} = \mathbb{S}\,\boldsymbol{E} \tag{1.2}$$

$$\boldsymbol{E} = \mathbb{E}\,\boldsymbol{S} \tag{1.3}$$

For a general anisotropic material, the elasticity and compliance tensors are defined by 21 independent constants. As bone is normally considered as orthotropic material (i.e. materials with three planes of elastic symmetry), only nine constants remain independent. Furthermore, by using the Voigt-Mandel notation Equation 1.3 can be expressed as following:

$$\begin{bmatrix} \mathrm{E}_{11} \\ \mathrm{E}_{22} \\ \mathrm{E}_{33} \\ \sqrt{2}\mathrm{E}_{23} \\ \sqrt{2}\mathrm{E}_{31} \\ \sqrt{2}\mathrm{E}_{12} \end{bmatrix} = \begin{bmatrix} \frac{1}{\varepsilon_1} & \frac{-\upsilon_{21}}{\varepsilon_2} & \frac{-\upsilon_{31}}{\varepsilon_3} & 0 & 0 & 0 \\ \frac{-\upsilon_{12}}{\varepsilon_1} & \frac{1}{\varepsilon_2} & \frac{-\upsilon_{32}}{\varepsilon_3} & 0 & 0 & 0 \\ \frac{-\upsilon_{13}}{\varepsilon_1} & \frac{-\upsilon_{23}}{\varepsilon_2} & \frac{1}{\varepsilon_3} & 0 & 0 & 0 \\ 0 & 0 & 0 & \frac{1}{2\mu_{23}} & 0 & 0 \\ 0 & 0 & 0 & 0 & \frac{1}{2\mu_{31}} & 0 \\ 0 & 0 & 0 & 0 & 0 & \frac{1}{2\mu_{12}} \end{bmatrix} \begin{bmatrix} \mathrm{S}_{11} \\ \mathrm{S}_{22} \\ \mathrm{S}_{33} \\ \sqrt{2}\mathrm{S}_{23} \\ \sqrt{2}\mathrm{S}_{31} \\ \sqrt{2}\mathrm{S}_{12} \end{bmatrix} \tag{1.4}$$

where the engineering constants ε_i , υ_{ij} and μ_{ij} are the Young's moduli, the Poisson's ratios and the shear moduli, respectively and the indices i=1,2,3 correspond to the three principal axes of symmetry. Due to the necessary symmetry of the compliance tensor the following equation holds:

$$\frac{\upsilon_{ij}}{\varepsilon_i} = \frac{\upsilon_{ji}}{\varepsilon_j} \tag{1.5}$$

In order to evaluate the mechanical properties of trabecular bone, the concept of representative volume element (RVE) should be introduced. An RVE is a volume large enough to allow for sensible definition of apparent properties.
Several homogenization approaches have been proposed to describe the apparent or homogenized trabecular bone mechanical properties (Zysset, 2003). The one adopted in this thesis has been proposed by Zysset and Curnier (Zysset and Curnier, 1996) and describes the relation of the apparent elastic properties of trabecular bone with bone volume fraction and the fabric tensor. It was shown that this model works also for cortical bone which is considered as high density trabecular bone, under the assumption of same microstructural properties of the two bone structures. With this theory, bone is considered orthotropic and its plane of mechanical symmetry coincident with the planes of morphological symmetry (i.e. the planes of symmetry of the fabric tensor) (Goulet, et al., 1994; Odgaard, et al., 1997; Turner, et al., 1990).
Moreover, *in vitro* studies at the biopsy level showed that trabecular bone's elastic modulus is related to its density through a power law (Currey, 1969; Hernandez, et al., 2001; Schaffler and Burr, 1988; Zysset, et al., 1994), even though there is not yet agreement about the exponent. Under these assumptions, the compliance tensor is dependent from bone volume fraction (ρ) and fabric tensor (**M**) and takes the following form:

$$\mathbb{E}(\rho, \boldsymbol{M}) = \frac{1}{\rho^k}\begin{bmatrix} \frac{1}{\varepsilon_0 {m_1}^{2l}} & \frac{-\upsilon_0}{\varepsilon_0 {m_1}^l {m_2}^l} & \frac{-\upsilon_0}{\varepsilon_0 {m_1}^l {m_3}^l} & 0 & 0 & 0 \\ \frac{-\upsilon_0}{\varepsilon_0 {m_2}^l {m_1}^l} & \frac{1}{\varepsilon_0 {m_2}^{2l}} & \frac{-\upsilon_0}{\varepsilon_0 {m_2}^l {m_3}^l} & 0 & 0 & 0 \\ \frac{-\upsilon_0}{\varepsilon_0 {m_3}^l {m_1}^l} & \frac{-\upsilon_0}{\varepsilon_0 {m_3}^l {m_2}^l} & \frac{1}{\varepsilon_0 {m_3}^{2l}} & 0 & 0 & 0 \\ 0 & 0 & 0 & \frac{1}{2\mu_0 {m_2}^l {m_3}^l} & 0 & 0 \\ 0 & 0 & 0 & 0 & \frac{1}{2\mu_0 {m_3}^l {m_1}^l} & 0 \\ 0 & 0 & 0 & 0 & 0 & \frac{1}{2\mu_0 {m_1}^l {m_2}^l} \end{bmatrix} \tag{1.6}$$

Where the constants ε_0, υ_0, μ_0, k and l are material properties of a poreless material (ρ=1) and can be investigated with experimental multi-axial testing of human trabecular bone samples extracted from different anatomical locations (Rincon-Kohli and Zysset, 2009).

Post-yield behaviour

Microcracks and diffuse micro-damage were found to affect the mechanical properties of bone both at micro- (Dall'Ara, et al., 2012) and macro-scale (Ager, et al., 2006). After yielding, bone shows a nonlinear behavior in the stress-strain relationship (Figures 1.4 and 1.5) until a maximum stress (strength or failure stress, Figure 1.4). From experimental tests at the biopsy level, it was shown that bone strength is related to bone volume fraction with a power law with an exponent close to two (Keaveny, et al., 1994; Rice, et al., 1988; Wolfram, et al., 2011), is dependent on the trabecular

microarchitecture (Bayraktar, et al., 2004; Rice, et al., 1988), is asymmetric with respect to tension and compression regimes (Keaveny, et al., 1994; Keaveny, et al., 1999; Rice, et al., 1988; Rincon-Kohli and Zysset, 2009; Wolfram, et al., 2011) and is independent by the anatomical site (Turner, 1989).

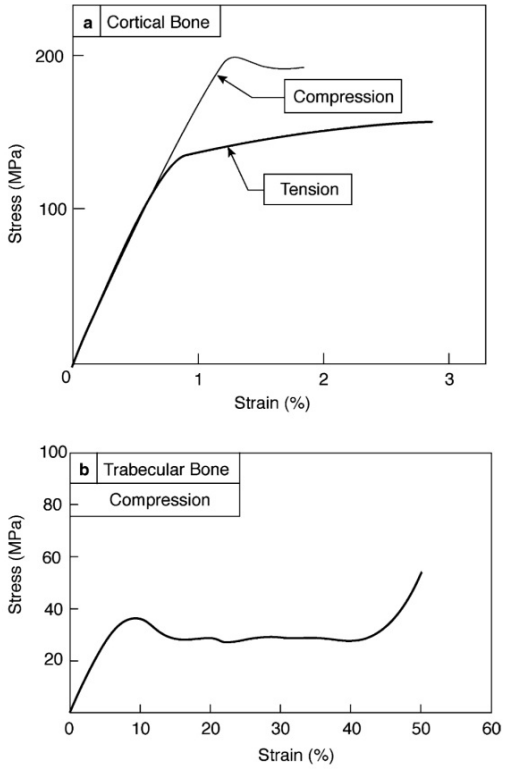

Figure 1. 4: Mechanical properties of cortical (a) and trabecular (b) bone (adapted from (Mercer, et al., 2006))

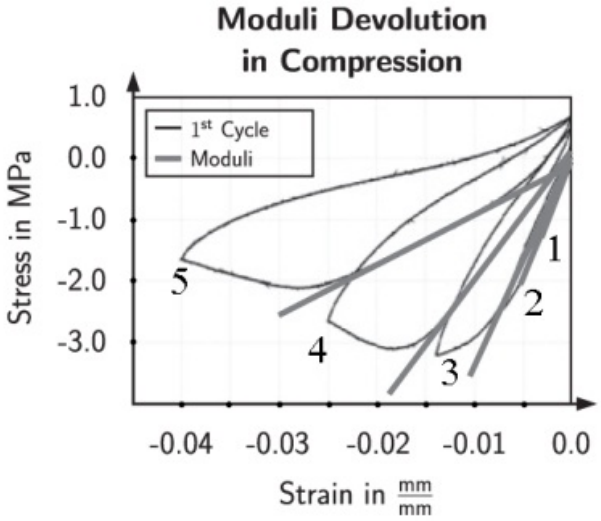

Figure 1. 5: Mechanical behavior of trabecular bone in cyclic compression (from (Wolfram, et al., 2011)) for five cycles.

In the literature the apparent yield and damage behaviour of trabecular bone is modelled by considering a Drucker-Prager yield surface together with a fixed yield strain (Bessho, et al., 2007) or by using a perfectly-plastic material whose elastic modulus is reduced in function of the yield strains when bone is loaded beyond a Von Mises yield surface (Wilcox, 2006). Alternatively, more complex yield surfaces such as Tsai-Wu (Schwiedrzik and Zysset, 2012), piecewise Hill (Garcia, et al., 2009) or modified super-ellipsoidal (Bayraktar, et al., 2004) can be used to take into account for the anisotropy of trabecular bone.
In the present thesis the post-yield behavior of bone was modeled by simplifying the elasto-plastic-damage constitutive model proposed by Garcia et al. (Garcia, et al., 2009). In particular, to reduce the computational time, plasticity was not modeled. This assumption was taken to reduce the computational time and was allowed by the fact that, in both FE simulations and experiments, bone was loaded only monotonically without any unloading. Moreover, as for elasticity, no distinction was made between the two bone types (i.e. cortical bone was considered as a dense trabecular bone).
With these assumptions the rheological model becomes a simple damageable spring and the relationship between the stress tensor **S** and the strain tensor **E** is:

$$\boldsymbol{S} = (1 - D)\,\mathbb{S}\,\boldsymbol{E} \tag{1.7}$$

where D is a scalar variable between 0 (no damage) and 1 (total damage) that represents the damage accumulation in the element and reduces the element stiffness isotropically.
Damage starts accumulating when the element is loaded beyond a generalized Hill damage criterion, that is defined in function of the BV/TV and fabric and that is asymmetric for tension and compression.

$$Y^D = \begin{cases} \sqrt{\boldsymbol{S}:\mathbb{F}^{+}\boldsymbol{S}} - r^D(D) \le 0 \ \text{ if } m(\boldsymbol{S}) \ge 0 \\ \sqrt{\boldsymbol{S}:\mathbb{F}^{-}\boldsymbol{S}} - r^D(D) \le 0 \ \text{ if } m(\boldsymbol{S}) < 0 \end{cases} \tag{1.8}$$

where m(**S**) is the plane separating the two stress domains for compression and tension, $r^D(D)$ represents the radius of the damage criterion and $\mathbf{F}^{\pm}$ are two fourth order tensors for tension and compression defined in function of the bone volume fraction (ρ) and fabric eigenvalues (m_1, m_2 and m_3):

$$\mathbb{F}^{\pm}(\rho, \boldsymbol{M}) = \frac{1}{{\sigma_0}^{\pm 2}\rho^{2p}} \begin{bmatrix} \frac{1}{{m_1}^{4q}} & \frac{-\chi_0{}^{\pm}}{{m_1}^{2q}{m_2}^{2q}} & \frac{-\chi_0{}^{\pm}}{{m_3}^{2q}{m_1}^{2q}} & 0 & 0 & 0 \\ \frac{-\chi_0{}^{\pm}}{{m_2}^{2q}{m_1}^{2q}} & \frac{1}{{m_2}^{4q}} & \frac{-\chi_0{}^{\pm}}{{m_3}^{2q}{m_2}^{2q}} & 0 & 0 & 0 \\ \frac{-\chi_0{}^{\pm}}{{m_1}^{2q}{m_3}^{2q}} & \frac{-\chi_0{}^{\pm}}{{m_2}^{2q}{m_3}^{2q}} & \frac{1}{{m_3}^{4q}} & 0 & 0 & 0 \\ 0 & 0 & 0 & \frac{{\sigma_0}^{\pm 2}}{2\tau_0{m_2}^{2q}{m_3}^{2q}} & 0 & 0 \\ 0 & 0 & 0 & 0 & \frac{{\sigma_0}^{\pm 2}}{2\tau_0{m_3}^{2q}{m_1}^{2q}} & 0 \\ 0 & 0 & 0 & 0 & 0 & \frac{{\sigma_0}^{\pm 2}}{2\tau_0{m_1}^{2q}{m_2}^{2q}} \end{bmatrix} \tag{1.9}$$

The coefficients σ_0^+, σ_0^- are the uniaxial strength (in tension and in compression), χ_0^+ and χ_0^- are the multi-axial coupling terms (in tension and in compression) and τ_0 is the ultimate shear stress, all for idealized poreless bone (ρ=1). These material constants, together with the exponents p and q, where investigated with experimental multi-axial testing of human trabecular bone samples extracted from different anatomical locations (Rincon-Kohli and Zysset, 2009). The damage criterion is assumed to evolve isotropically with the following exponential law (an increase in the level of damage leads to a reduced stiffness and hardening):

$$r^D(D) = R(1 + \chi_D(1 - e^{-\upsilon D})) \tag{1.10}$$

where χ_D and υ are damage hardening coefficients defined according to the results from uniaxial testing of trabecular bone samples (Garcia, et al., 2009). Furthermore, R is a coefficient that defines the radius of the damage criterion (this coefficient is redundant and could be included in the $\mathbf{F}^{\pm}$ tensors).

1.3 Osteoporotic bone fractures

1.3.1 General problem

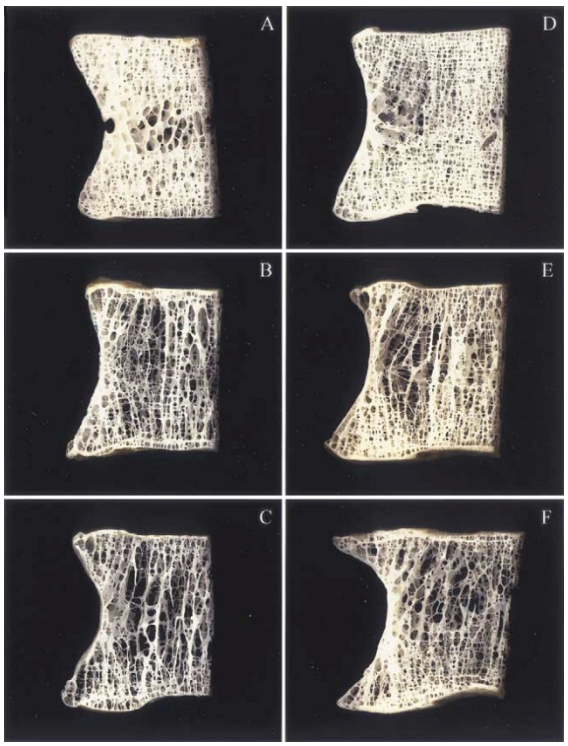

Figure 1. 6: sections of human vertebra showing the degradation of BMD and trabecular structure from healthy (A,D), osteopenic (B, E) and osteoporotic subjects (females on the left, males on the right) (Thomsen, et al., 2002).

Osteoporosis (OP) is a common pathology of human musculoskeletal system which impairs the bone remodelling balance in favour of reabsorption. The resulting reductions in BMD, cortical thickness and bone quality (e.g. degradation of trabecular bone microstructure, Figure 1.6) results in a lower apparent bone strength, increased bone fragility and higher risk of fracture (RoF). OP was found to increase human mortality and morbidity (Cummings and Melton, 2002; Jalava, et al., 2003; Johnell and Kanis, 2005; Kanis, et al., 2004; Mnif, et al., 2009). Both genders are affected, but post-menopause women have a higher probability to suffer from it (Melton, et al., 1997).
The World Health Organization (WHO) suggests to discriminate between normal and pathologic patients on the basis of measurements of areal BMD (aBMD) or bone mineral content (BMC) (WHO, 1994) with the following thresholds:

- Normal: value of BMD or BMC ≤ 1 standard deviation below the average value of young adult
- Low bone mass or osteopenia: a value for BMD or BMC between 1 and 2.5 standard deviations below the young adult average
- Osteoporosis: a value of BMD or BMC >2.5 standard deviations below the young adult average value
- Severe osteoporosis (established osteoporosis): a value of BMD or BMC >2.5 standard deviations below the young adult average value and presence of one or more fragility fractures

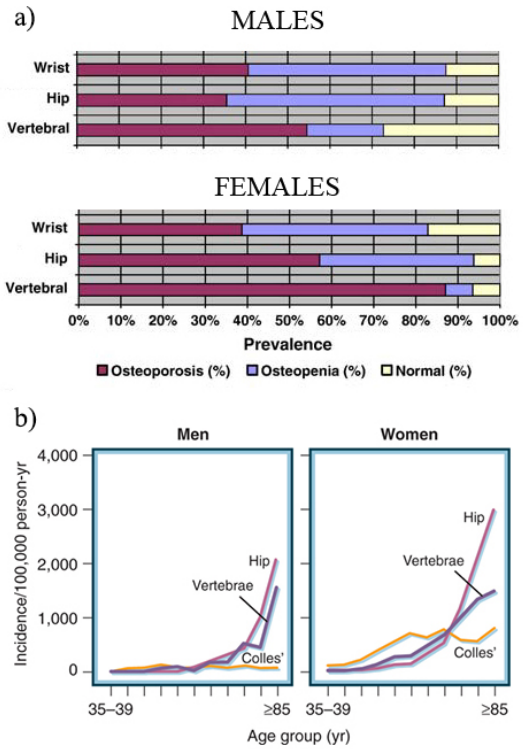

Figure 1. 7: a) reports the incidence of wrist, hip and vertebral fractures in osteoporotic, osteopenic and normal patients (n=804 females and n=254 males) defined according to WHO criteria (adapted from (Blonk, et al., 2007)). b) shows the incidence of vertebral, hip and wrist (Colles') fractures in function of age (Cooper and Melton, 1992).

The three more common fractures are the ones of the wrist, of the vertebrae and of the hip. The wrist (Colles') fractures are usually related to a trauma and their incidence increases moderately with age only for woman after menopause (Figure 1.7). Vertebral and hip fractures increase dramatically in subjects older than 70 years and have a huge impact on the society by increasing mortality and morbidity (Johnell and Kanis, 2005). Only in the United States 25% of the postmenopausal woman and 40% of those who are nearly 80 years old suffer of a vertebral fracture (Old and Calvert, 2004). Just as example on the economical impact of osteoporotic fractures due to the aging population, the cost for hip fractures for the society has been estimated in $ 132 billions in 2050 (Johnell, 1997).

1.3.2 Clinical Evaluation of the BMD

Although BMD does not provide information about bone quality (Bouxsein, 2003) (e.g. trabecular architecture, cortical thickness, microdamage, …), it is considered as surrogate of bone strength as it was found to explain, at least in a few cases, up to the 92% of its variance at the organ level (Bouxsein, et al., 1999; Ebbesen, et al., 1999; Varga, et al., 2009). In clinical practice BMD is measured by analysing images acquired by X-rays (or in a few cases γ-rays) based techniques after a proper calibration with calibration phantoms to obtain BMD equivalent based grey scale images. Higher the resolution and the quality of the image analysed, more precise is the evaluation of BMD and therefore the assessment of RoF. However, the increased image resolution is usually achieved by increasing the intensity of the X-rays beam and, therefore, by exposing the body to a higher radiation dose (Burghardt, et al., 2011). Therefore, in everyday clinical practice the radiologists are challenged in finding the balance between a reasonable amount of radiation dose and a measurement which allows a reliable and accurate evaluation of BMD. The next sections provide a short description of the techniques used in clinical practice to evaluate BMD.

DXA

Dual energy X-rays absorptiometry (DXA or DEXA) is still the gold standard technique in most hospital to evaluate BMD with a low radiation dose (approximately 10 μSv for lumbar spine scan, and 2 μSv for a hip scan) and low cost (Griffith and Genant, 2008; Njeh and Shepherd, 2004). The measurement of radiation at two energy levels allows for correction of soft tissues and fat, making this technique suitable for central site measurements (spine and hip) (Njeh and Shepherd, 2004). Although the hip is suggested as anatomical site to define osteoporotic subjects (WHO, 1994), the best assessment of the RoF in specific sites is to measure BMD at that location (Marshall, et al., 1996).
The lumbar spine, due to its sensitivity to causes of bone loss, is probably the most common skeletal site investigated with DXA. The lumbar spine is usually scanned in anterior-posterior direction (AP) due to the easier alignment of the patient in the machine. While the main interest is in evaluating the BMD of the vertebral body which carries most of the axial and bending load (Asano, et al., 1992), AP scans are affected by the superimposition of the posterior element (Figure 1.8 top, left). Therefore, lateral scans (LAT) of the lumbar spine have become more common to reduce the intrinsic artifacts introduced by an AP scan (Figure 1.8, top, right). Indeed, with this approach a region of interest (ROI) can be selected to exclude the posterior element. Nevertheless, during LAT DXA examinations, the BMD measures are affected by the presence of the ribs and the pelvis in measurements of the thoracic and lumbar vertebrae, respectively (Jergas, et al., 1995).

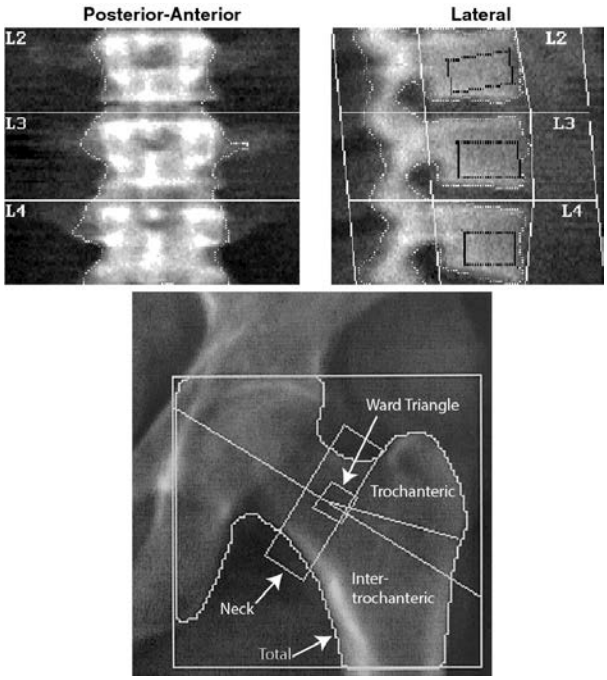

Figure 1. 8: Top: anterior-posterior (left) and lateral (right) DXA of the lumbar spine (Leonard, 2007). Bottom: example of DXA of the hip (adapted from (Lentle and Prior, 2003)).

The proximal femur is a common site of osteoporotic fractures too and, therefore, is frequently analysed by DXA. Due to its complex geometry, the BMD is usually investigated in different sub-regions. The most commonly defined ROI are: total hip, femoral neck, intertrochanteric and trochanteric regions (Figure 1.8 bottom). The BMD of each single region has been found to be related to femoral mechanical properties evaluated by means of *in vitro* testing ($0.39<R^2<0.92$ (Bouxsein, et al., 1999; Lochmuller, et al., 2003)). Ward's triangle represents the earliest site of post-menopausal lost and is usually included in the analysis by most of the DXA manufacturers. However, due to poor precision, its usage has been limited in clinical practice (Njeh and Shepherd, 2004).
The long-term precision error for DXA analysis was found to be 1.12% for total spine, 2.21% for femoral neck and 1.32% for total hip (Patel, et al., 1997).

QCT

Quantitative computed tomography (QCT) is a relatively recent method for measuring BMD in central sites of the human body. The typical output of such technique is a grey scale 3D image. The grey levels are originally provided in Hounsfield units (HU) scale which is related to the X-ray attenuation coefficients of the scanned material. The HU scale can be then converted into equivalent BMD values by using a calibration phantom (Cann, et al., 1985) (Figure 1.9a and 1.9b). During the analysis of the QCT image, a ROI is defined within each insertion of the calibration phantom and linear regression analysis is used to determine the relationship between the mean HU measured in the each ROI and the known concentration of bone equivalent material (Lang, 2004). QCT can produce 3D images (Figure 1.9c) which can be used to perform size-independent measurements of BMD. However, the radiation dose on the patient is much larger than for a DXA exam (for

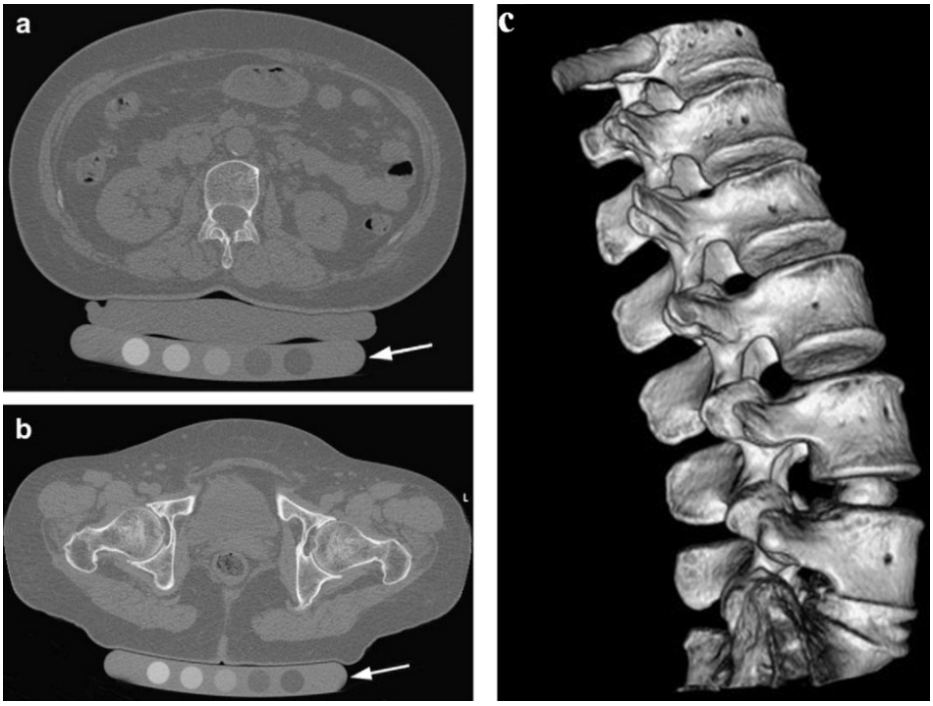

Figure 1. 9: Examples of transverse section of QCT scans of the spine (a) and hip (b). The calibration phantom is indicated with the arrows. An example of QCT 3D reconstruction of the lumbar spine is shown in (c). Sources: www.sciencephoto.com and (Griffith and Genant, 2008)

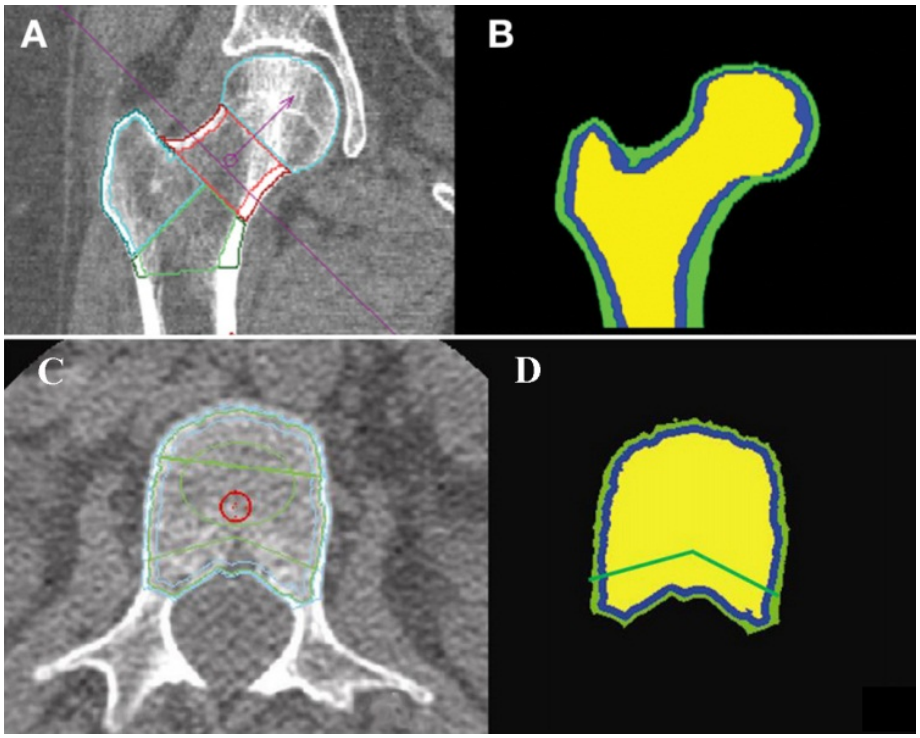

Figure 1. 10: Evaluation of different ROI for the BMD analysis in the proximal femur (A) and vertebra (C). The software allows to investigate also cortical, sub-cortical and trabecular regions independently (B, D). Source: (Engelke, et al., 2010)

the spine approximately 30-100 μSv for 8-10mm in thickness single slice, up to 2500 μSv for hip analysis with a slice thickness equal to 2.5mm (Griffith and Genant, 2008)).
Moreover, due to the relatively low resolution (0.8-1.0 mm in plane, 0.5-10.0mm slice thickness), the QCT images can not accurately represent the trabecular microstructure or the thin cortical shell which can be found for example in the vertebral body. The partial volume averaging is the major source of error in QCT scans (Lang, 2004). Moreover, the measurements can be affected by some properties of the patients such as the fat percentile in the analysed bone. In fact, single-energy QCT can measure the mass of bone in a volume with two components (for example bone and red marrow). However, the presence of fat (which has a value of ~200 HU compared to the ~30 HU for red marrow and the 300-3000 HU for bone) causes single-energy QCT to underestimate the BMD.
Although a dual-energy QCT scanner would reduce this error, until now the single-energy QCT has been considered sufficient for clinical practice and is preferable for lower radiation dose to the patient. Moreover, when performing longitudinal studies, the precision error of QCT is reported to be in the order of 1-2% for analysis of the spine (Lang, et al., 1999). This error is mainly due to the positioning of the ROI and scanner instability. For spine and hip analysis minor variations in ROI positioning can largely affect BMD. Therefore, to reduce this operator-sensitive problem, software is being developed to automatize the process of BMD evaluation in the 3D images reconstructed by QCT scanners. Recently, Engelke et al. has developed a software which can also evaluate cortical and trabecular compartments separately and can provide BMD analysis of different sub-regions of the vertebra and of the femur (Figure 1.10, (Engelke, et al., 2010)).
Moreover, specimen specific FE models can be generated from QCT images to evaluate the vertebral and femoral mechanical properties. This last issue point will be intensively discussed in section *1.6*.

HR-pQCT

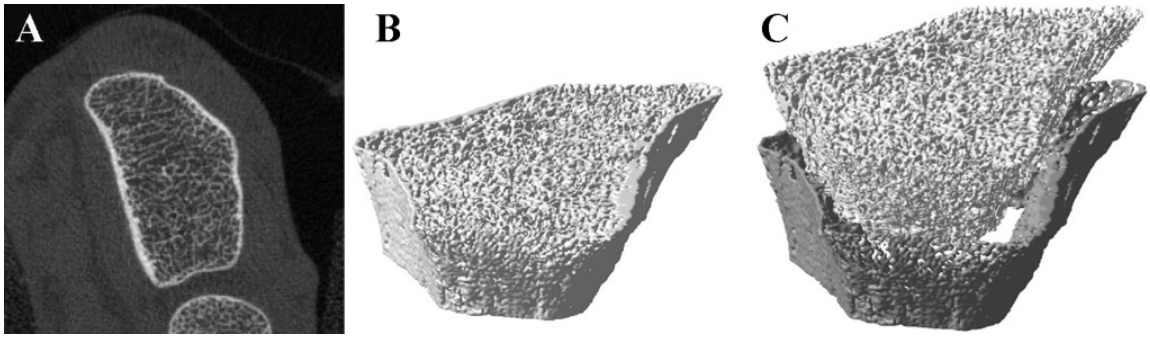

Figure 1. 11: A) shows an example of distal radius scan with HR-pQCT (adapted from (Burghardt, et al., 2010a)). B) and C) show 3D reconstructions of the distal radius and the segmentation between cortical and trabecular compartments (adapted from (Mueller, et al., 2009))

High-resolution peripheral QCT (HR-pQCT) has recently been used as a noninvasive method for *in vivo* 3D characterization of the peripheral skeleton (distal radius and tibia, Figure 1.11 (Burghardt, et al., 2010a)).
With its high image resolution (~100μm) and the low radiation dose for 9 mm in thickness slices of peripheral sites (~3 μSv for the distal radius (Griffith and Genant, 2008)), HR-

pQCT has become an attractive approach to evaluate both densitometric and morphometric bone parameters. Moreover, at such resolution it becomes possible to segment between cortical and trabecular compartments. HR-pQCT has been recently used in pre-clinical studies to evaluate the effect of gender and age (Sode, et al., 2010), drug treatments (Burghardt, et al., 2010b) or pathologies (Burghardt, et al., 2010a) on densitometric measurements (BMD, BMC, and BV/TV) and microstructural properties (trabecular microarchitecture, cortical thickness, and/or cortical porosity). Moreover, HR-pQCT provides 3D images which can be used to generate both homogenized FE and Micro-FE (µFE) models. Again, more details about these approaches are reported in section *1.6*.

1.4 The human vertebra

1.4.1 Vertebral anatomy

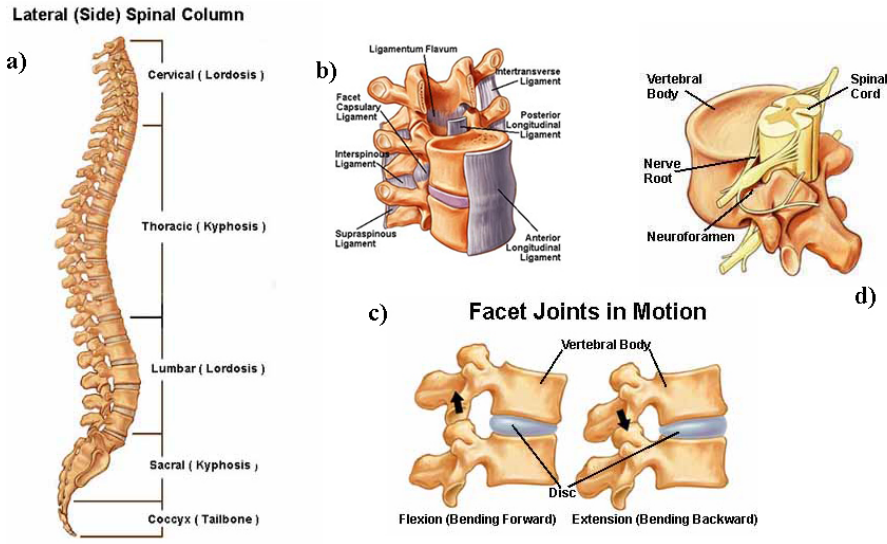

Figure 1. 12: Anatomy of the spine. a) and b) show schematic views of the spine from a lateral view with indication of the spinal portions and a representation of a spinal unit with the ligament structures, respectively. c) shows a particular of the movement allowed by the intervertebral disc in the sagittal plane. d) represents the typical shape of a lumbar vertebra. Source: www.spineuniverse.com

The spine is divided in five regions: cervical (7 vertebrae), thoracic (12 vertebrae), lumbar (5 vertebrae), sacrum and coccyx, Figure 1.12a. The sacrum and the coccyx are fusions of five and four rudimentary vertebrae, respectively. Each vertebra of the cervical, thoracic and lumbar spine is connected to the adjacent ones via a fibro-cartilaginous intervertebral disc which is placed between two laminae of hyaline cartilage. The intervertebral disc (Figure 1.12b) is composed by an external region of annular layers of fibrocartilage (annolus fibrosus) and an inner jelly nucleus (nucleus pulposus). Its main functions are to distribute homogeneously the load to the next vertebra and to allow relative motions in the spinal segments. Stabilization of the spine is guaranteed by the superior and inferior articular facet joints of each vertebra and by two systems of ligaments (inter- and intra-segmental systems) (Gray, 1989).

Each vertebra (Figure 1.12d) is an irregular shaped bone composed of a vertebral body which curries most of the axial load transmitted by the intervertebral discs, and of a posterior element which protects the spinal cord and articulates with other vertebrae and ribs (Gray, 1989). The vertebral body consists of a core of trabecular bone (70-80% of the total weight (Eastell, et al., 1990)) surrounded by a thin shell of cortical bone (approximately 0.38 mm in thickness (Eswaran, et al., 2006)) and two thin cortical endplates (approximately 0.35-0.44 mm in thickness (Hulme, et al., 2007; Silva, et al., 1994)) adjacent to the hyaline cartilage layers on the most cranial and most caudal sides of the vertebral body. Due to aging and load distribution unbalance, sometimes two or more vertebral bodies are "bridged" with a fibrocartilage-capped bony outgrowth called osteophyte. Osteophytes usually grow laterally to the original bone at the articular surface of a synovial joint and are therefore often associated with osteoarthritis (OA) and other degenerative spine diseases.

1.4.2 Vertebral biomechanics

The vertebral cross section area increases from the cranial to the caudal direction to overcome the higher portion of the body's weight which has to be supported by the lumbar spine. The vertebral body carries most of the load (75%) while the remaining 25% is carried by the posterior element (in particular the facets joints) (Asano, et al., 1992). While the posterior element is important for the spinal stability and to transfer the loads to the ribs, its effect on the mechanical properties of human vertebra will not be included in the present thesis and was not modelled in the FE. The endplates, during the daily activities, act as load distributors to the adjacent trabecular centrum and cortical shell structures. They have a large impact in vertebral structural properties in case of vertebral disc replacement and vertebroplasty, where the integrity of the vertebral structure and the load distribution between one vertebra and the other have a major importance. Moreover, the endplate failure was also suggested to be one of the early events during high-speed injury formation (Ochia, et al., 2003). However, during physiological activities they can be considered as rigid structures in first approximation.

Typically, the vertebra fails with a wedge shape fracture (Jelsma, et al., 1982) induced by an overload of the anterior side of the vertebral body with some eccentric loading (therefore a combination of compression and bending) fair higher than the usual physiological conditions. The vertebral body axial strength is mainly a function of the mechanical properties of the trabecular centrum and of the cortical shell. The load sharing between these two compartments of the vertebral body is not clear yet. From FE simulations, Eswaran et al. (Eswaran, et al., 2006) showed that the maximal load fraction taken by the shell in the mid cross section of the vertebral body ranged from 38 to 54%. These results are consistent with the ones found through experimental tests on vertebral bodies before and after removal of trabecular bone, where the cortical bone showed to take approximately 45% of the load (Kilincer, et al., 2007). The mechanical properties of the trabecular centrum are driven by its BV/TV, heterogeneously distributed in the vertebral body (Hulme, et al., 2007; Hussein and Morgan, 2012). Trabecular bone architecture changes with age (Figure 1.6). In particular, aging was shown to reduce the trabecular BV/TV, trabecular connectivity, to increase the ratio between rod-like and plate-like trabecular structures and to strengthen the orientation of the trabeculae along the cranio-caudal axis (Gong, et al., 2005; Hildebrand and Ruegsegger, 1997).

Typically, an experimental load-displacement curve for the vertebral body loaded in compression (Figure 1.13) shows an initial nonlinear toe region (dependent on the

experimental setup, vertebral body preparation and boundary conditions) followed by a linear elastic region, and a nonlinear yielding until a minimum ultimate load (*Fu*).
After *Fu*, the load-displacement curve shows a softening due to the accumulated damage and plastic deformation in the trabecular and cortical bone (Garcia, et al., 2009; Keaveny, et al., 2001). The *Fu* was found to range between 0.8kN and 13kN (Buckley, et al., 2007; Chevalier, et al., 2009; Crawford, et al., 2003). Similar results were found if the cortical endplates were removed (Ebbesen, et al., 1999). Moreover, the structural stiffness (*S*) of the vertebral body, defined by the slope of the linear portion of the load-displacement curve, was found to range between 2kN/mm and 12.7kN/mm (Buckley, et al., 2007; Chevalier, et al., 2009). These mechanical properties were found to be correlated with BMD (Ebbesen, et al., 1999) and BMC (Perilli, et al., 2012). If data about vertebral cross section area were added to densitometric measures the prediction of vertebral *Fu* was shown to improve (Buckley, et al., 2007; Crawford, et al., 2003).

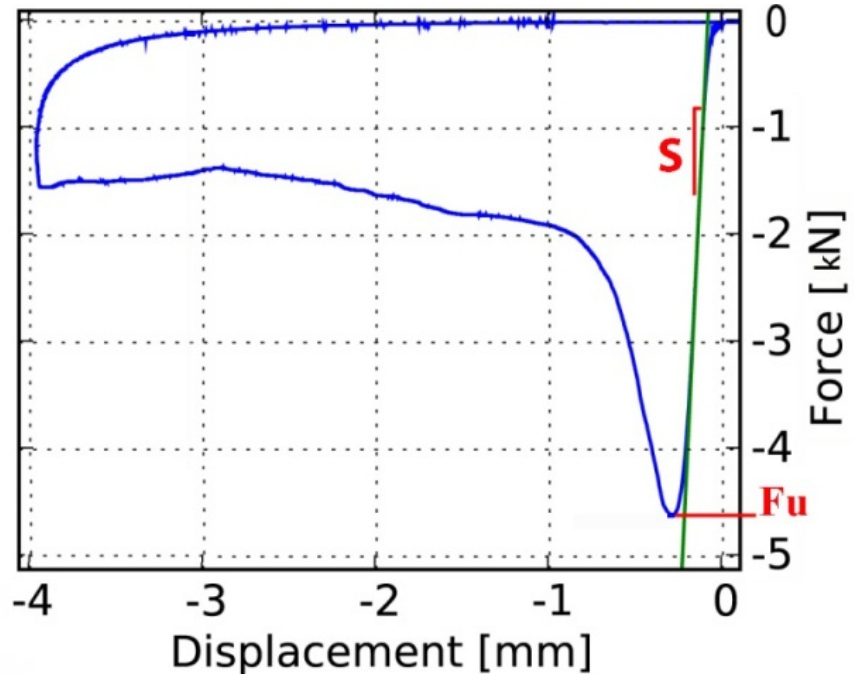

Figure 1. 13: Typical Load-Displacement curve from a compression test of a human lumbar vertebral body. *S* represents the structural stiffness and *Fu* the ultimate force.

1.4.3 Vertebral fractures

Vertebral compression fractures occur usually under a combination of axial compression and bending and are the most common complication due to a reduction in bone density, consequence of osteoporosis. Clinically, they are examined through radiography analysis and defined as a reduction of the vertebral height larger than 20% (see fracture classification in Figure 1.14). Moreover, the fractured vertebral body most commonly shows a wedge-shaped due to a larger deformation of the anterior portion of the bone.

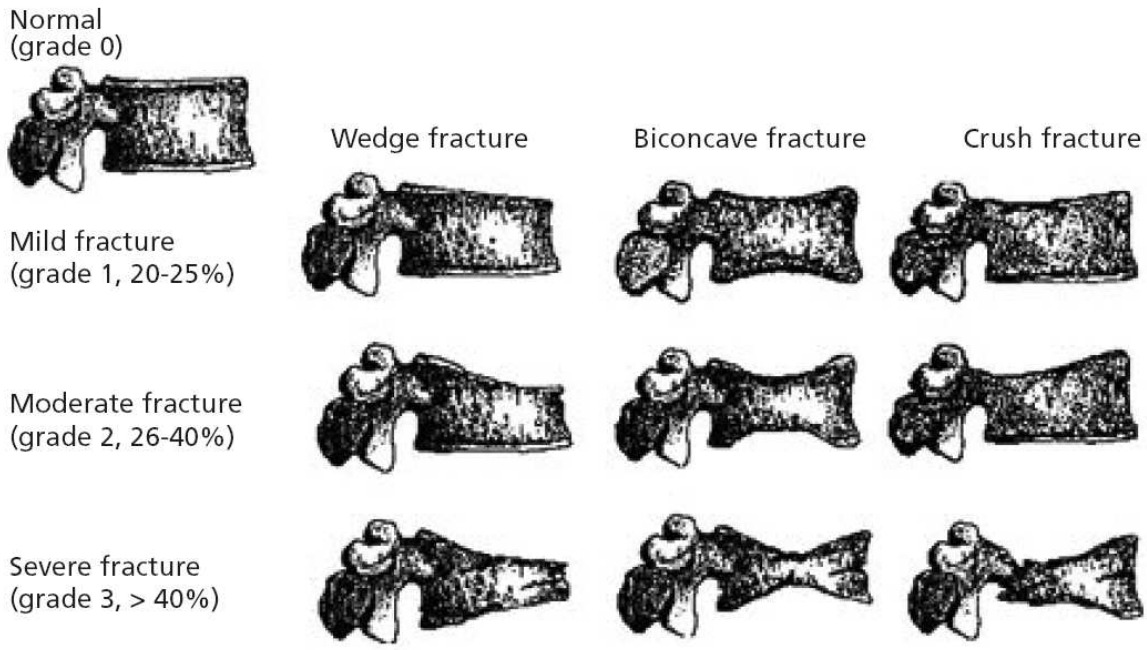

Figure 1. 14: Classification of vertebral fractures according to Genant et al. (Genant, et al., 1996).

Two thirds of the vertebral fractures are asymptomatic and in most cases aren't even detected (Kado, et al., 1999). However, the consequences of severe vertebral fractures include reduction of quality of life (severe pain due to compression of the spinal cord, loss of height, crowding of internal organs and physical deconditioning) (Dionyssiotis, 2010), increase the risk of other fractures (Klotzbuecher, et al., 2000) and increase mortality (Kanis, et al., 2004). The assessment of vertebral fracture risk in the clinical practice is based on the evaluation of vertebral BMD by means of DXA or QCT. However, *in vitro* studies have shown how areal or volumetric BMD are not accurate predictors of vertebral strength (R^2=0.16-0.83 (Buckley, et al., 2007; Faulkner, et al., 1991; Granhed, et al., 1989)). Therefore, an improvement of the estimation of vertebral strength is necessary for a better identification and follow-up of patients who require treatment.

1.5 The human proximal femur

1.5.1 Proximal femur anatomy

The human femur is the longest and strongest bone in the human body. Proximally it articulates with the pelvis in the hip joint (Figure 1.15). In standing position the femora are oblique, with higher inclination angle for women than for men. The proximal femur comprises of a head, neck, greater trochanter and lesser trochanter. The femoral head, which articulates with the acetabulum, is almost half-spherical and covered by a thick layer of cartilage (except for a small portion called fovea, where there is the insertion of the ligament of the head of the femur). The femoral neck is approximately 5 cm long and connects the head to the shaft at an angle of approximately 125°. The greater trochanter is a large quadrangular superior projection from the attachment between the neck and the shaft.

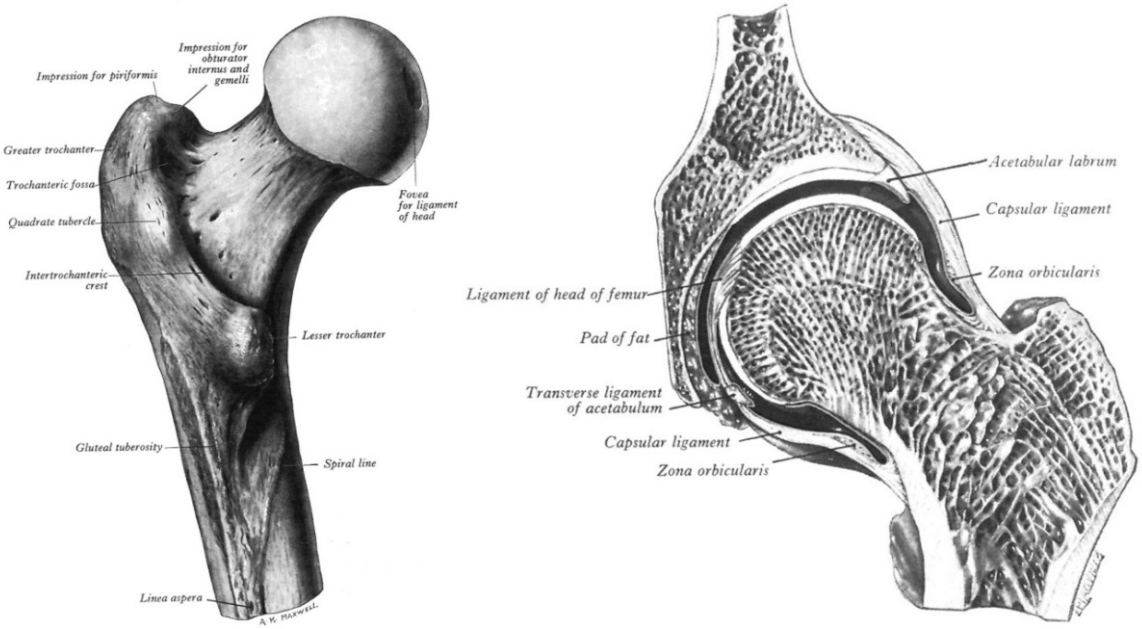

Figure 1. 15: the human proximal femur (left) and a section of the hip (right). Source: (Gray, 1989)

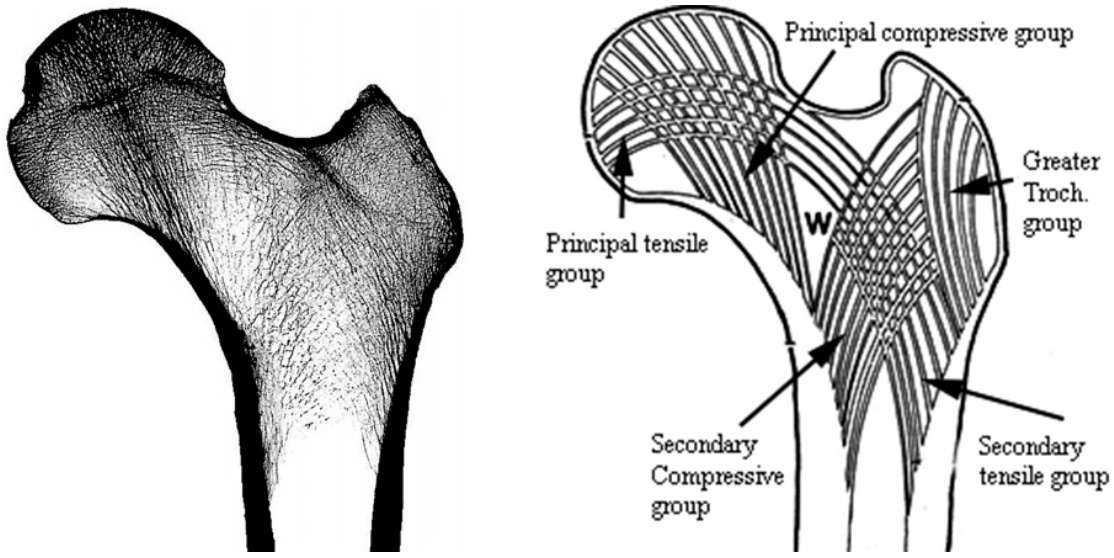

Figure 1. 16: trabecular structure in the middle-frontal section of the proximal femur (left, adapted from (Fratzl and Weinkamer, 2007)) and scheme of the trabecular groups of the proximal femur (adapted from (Bucholz, et al., 2009))

It provides attachment for the gluteus minimus, gluteus medius, piriformis, obturator internus and the gemelli. The lesser trochanter is a conical posteromedial projection on the connection between the shaft and the posterior-inferior portion of the femoral neck. It provides attachment for the psoas major, iliacus and adductor magnus (Gray, 1989). The

femoral shaft is approximately a cylinder of cortical bone with a large medullary cavity. Conversely, the proximal part of the femur is mainly made of trabecular bone, surrounded by a shell of cortical bone with different thickness according to the location. The trabecular orientation of the proximal femur is probably the best example of an anisotropic cellular architecture which adapts to external loads (Figure 1.16, (Fratzl and Weinkamer, 2007; Wolff, 1892)).

1.5.2 Femoral biomechanics

In the last two decades the mechanical properties of the human femur have been investigated in both physiological and accidental conditions. In the first case, the assessment of femoral mechanics in one-legged stance provided valuable information to study the behavior of the hip during daily activities, the designing of new implants and the stress redistribution on the femur after hip surgery, the load sharing between cortical and trabecular bone, as well as the effect of pathologies like bone metastasis on bone strength and the investigation of spontaneous fractures. Conversely, the study of accidental loading conditions is fundamental to investigate the majority of femoral fractures (for more details see section *1.5.3*).
As for the vertebrae body, a typical load-displacement curve from a compression test performed in the laboratory (Figure 1.17) shows an initial nonlinear toe region, followed by a linear portion and again a nonlinear behaviour after yielding with a subsequent minimum ultimate load followed by a softening. However, similar femora tested in two loading conditions behave differently. If the femur is tested in a position to simulate a physiological condition (Figure 1.17, blue curve) it fails in most cases in a fragile way after the ultimate load. Conversely, when the femur is tested by simulating the position during a fall (Figure 1.17, black curve), it shows a more ductile behaviour, underlined by a lower structural stiffness and ultimate force, and a higher displacement at ultimate force (Keyak, 2000).

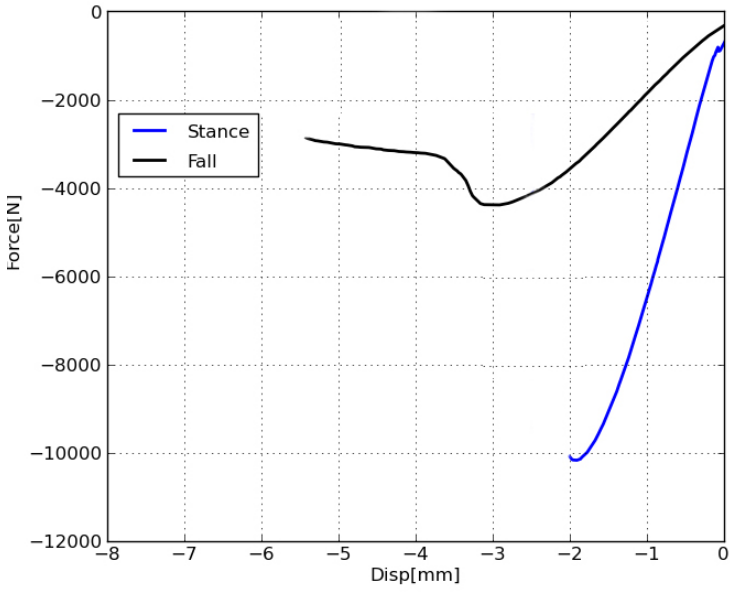

Figure 1. 17: Example of load displacement curves from compression test of one pair of femora extracted from the same subject. One was tested in a position that simulates a one-legged stance (blue) and the other in a position that simulates a fall on the side backward (black).

In vitro studies have shown how the range of mechanical properties varies substantially for femora tested in the physiological (*Fu*=1.3-16.0 kN and *S*=1.8-10.0 kN/mm (Cristofolini, et al., 2007; Eckstein, et al., 2002; Keyak, 2000; Keyak, 2001)) and in accidental loading conditions (*Fu*=1.0-7.0 kN and *S*=0.8-2.5 kN/mm (Dragomir-Daescu, et al., 2011; Eckstein, et al., 2002; Keyak, 2000)). Moreover, the results from experimental and computational studies have shown that the inclination angles (simulated adduction and internal rotation) in both loading conditions affect the femoral mechanical properties (Keyak, et al., 2001b) and the strain distribution (Cristofolini, et al., 2012; Zani, et al., 2010).

1.5.3 Femoral fractures

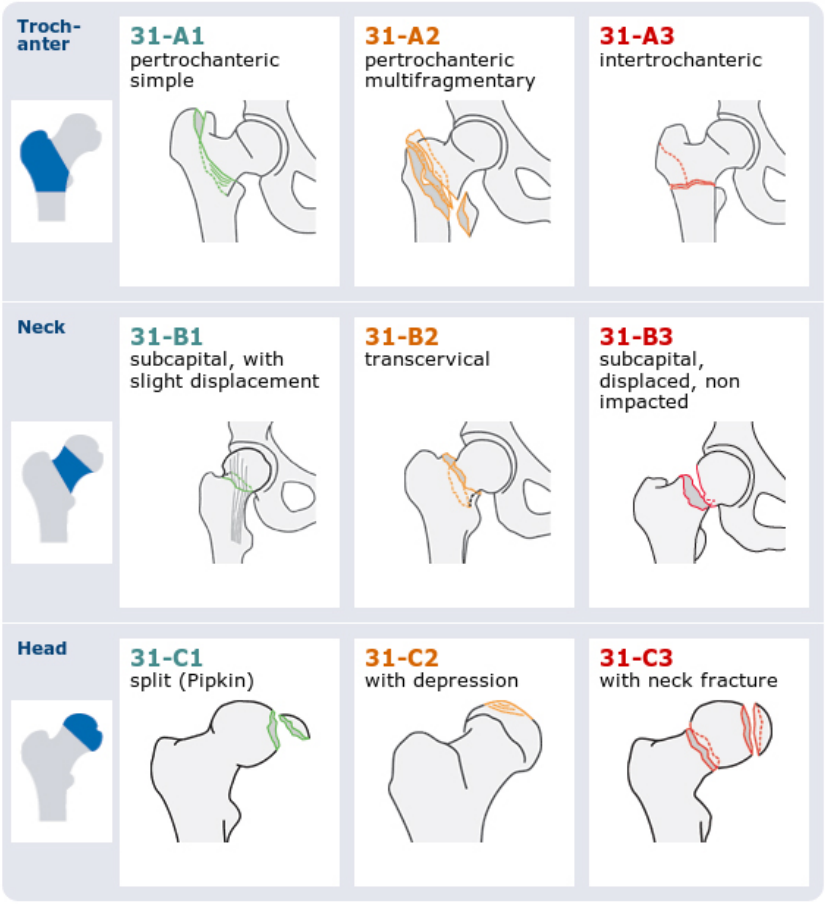

Figure 1. 18: AO classification of the most common proximal femoral fractures (adapted from www2.aofoundation.org)

Femoral fractures decrease dramatically the patient's quality of life and increase both mortality and morbidity (Cummings and Melton, 2002; Mnif, et al., 2009). Spontaneous fractures might happen in absence of any accident and are probably due to the intrinsic reduction of bone quantity in the femur, due to osteoporosis. However, even though their occurrence was not excluded by computational considerations (Viceconti, et al., 2012),

only 2% of the fractures can be considered such as spontaneous (Parkkari, et al., 1999) while in all other cases they are related to a trauma. The most common fracture sites generated after a low energy trauma (for example a fall on the side) are the subcapital region, the neck or the pertrochanteric region. In a study on a large number of cases of femoral fractures (1664) in an urban population (Malmö, Sweden), Alffram P. registered 44% of subcapital fractures, 19% of neck fractures and 37% of trochanteric fractures (Alffram, 1964). Nevertheless, to better define the approach to treat them, a more detailed classification of the fracture localization is becoming more conventional (as example the classification proposed by the AO foundation is reported in Figure 1.18).
The femoral risk of fracture is investigated in clinical practice with DXA or QCT by measuring BMD or BMC. However, these densitometric measures showed a wide range of accuracies in predicting the variation of femoral mechanical properties in *in vitro* studies where the femora were tested in different loading configurations (R^2=0.35-0.92 (Bouxsein, et al., 1999; Lochmuller, et al., 2003)). Therefore, a further rigorous investigation of the relationship between the femoral mechanical properties and its densitometric distribution is necessary to better clarify this issue. Moreover, it would be essential to develop methodologies like FE models which are more reliable than densitometry for the prediction of femoral strength. Indeed, it is reasonable to think that by enhancing the prediction of femoral strength, also the prediction of risk of fracture would improve and therefore such tools would become fundamental to better identify patients who require treatment.

1.6 Specimen specific finite element models

The FE method has been applied extensively in the last decades to study the mechanical competences of bone at different dimensional levels (Crawford, et al., 2003; Jones and Wilcox, 2008; Keyak, et al., 2001a; Lenaerts and van Lenthe, 2009; Mueller, et al., 2011; Pahr and Zysset, 2009; Schileo, et al., 2007; Trabelsi and Yosibash, 2011; Viceconti, 2012; Wolfram, et al., 2010). One of the challenges when generating FE models of the human biological tissues is the definition of the complex geometry of the specimens to be modelled. While some researchers used generic models (i.e. the geometry is fully defined on the basis of generic anatomical measurements) to investigate mechanical properties of bone (Higgins, et al., 2007; Whyne, et al., 2003), nowadays the most common approach is to generate specimen specific FE models, where the geometry of each specimen is taken from 3D CT scan of it. At the organ level this method has been used in many pre-clinical and basic research applications. Some examples are: the estimation of bone mechanical properties (Chevalier, et al., 2009; Faulkner, et al., 1991; Keyak, 2001; Lotz, et al., 1991a; Lotz, et al., 1991b; Mueller, et al., 2011), of the damage distribution (Chevalier, et al., 2008; Keyak, et al., 2001a; Varga, et al., 2009), of the strain distribution in some regions of the external bone surface (Schileo, et al., 2007; Wille, et al., 2012), of the effect of drug treatments on the bone mechanical properties (Burghardt, et al., 2010b; Chevalier, et al., 2010; Keaveny, et al., 2008; Rizzoli, et al., 2012), of the effect of pathologies like diabetes (Burghardt, et al., 2010a) or bone metastasis (Keyak, et al., 2007; Whyne, et al., 2003) on the bone mechanical properties, of the risk of fracture (Falcinelli, et al., 2012; Wang, et al., 2012) and of the stability of bone after fracture fixation with implants (Martelli, et al., 2012) or biomaterials (Kinzl, et al., 2012; Tschirhart, et al., 2006).
Principally, two approaches have been used to study the mechanical properties of the human femur and vertebra: the *continuum level finite element approach* (see section *1.6.1*) and the *micro-finite element (μFE) approach* (see section *1.6.2*).

1.6.1 QCT-based homogenized models

In clinical applications for the central skeleton (e.g. for human spine and hip), the only possibility to model the bones at the organ level is to use a continuum level approach (i.e. the bone microarchitecture and porosities are not resolved, but heterogeneous material properties are assigned in function of the BMD value which is averaged and assumed constant in each element). In fact, QCT can operate with a maximum resolution of 0.3-0.5 mm^3 (but usually much lower for large scans of the whole lumbar spine and the hip) and, therefore, can provide only qualitatively information about the trabecular structure and the cortical thickness. Although some researchers have recently attempted to extract information about the trabecular orientation from QCT images (Lenaerts and van Lenthe, 2009; Trabelsi and Yosibash, 2011; Wolfram, et al., 2009), no accurate and reliable method have been validated yet. Continuum level FE models can be generated from the QCT images by importing the scanned geometry, by converting the HU unit scale to BMD equivalent scale by means of calibration phantoms (as described in section *1.3.2*), by meshing the bone outer geometry, and by applying the heterogeneous material properties in function of the average BMD within the element and based on the bone mechanics theory presented in section *1.2.2*. The element size used in the FE method has to be large enough to hold the continuum hypothesis and small enough to be able to properly describe the outer bone geometry.

The most convenient and straightforward generation of the mesh for QCT-based FE models is to convert the voxels of the coarsened QCT images into hexahedron elements (these models are usually called homogenized voxel FE models or hvFE, Figure 1.19). This method allows for a fast mesh generation and material properties assignment and has been therefore used in a number of clinical applications (Graeff, et al., 2009; Keaveny, et al., 2008; Keaveny, et al., 2012). However, the usage of this simplified mesh increases the partial volume errors and decreases the accuracy in representing the external typically curved surface of the modelled bone. For this reason the voxel mesh was found to be less accurate than a smooth one (Viceconti, et al., 1998). Moreover, the thin cortical shell which is composing the external surface of the vertebral body and of the head of the femur can not be accurately modelled with hvFE and in most cases it is considered such as a dense trabecular bone. More sophisticated QCT-based FE models can account for a smooth surface based geometry which can be represented by tetrahedral elements (Chevalier, et al., 2009; Imai, et al., 2006; Schileo, et al., 2008) or attempt to distinguish between cortical and trabecular bone by assuming a constant shell thickness (Imai, et al., 2006).

Moreover, due to the poor resolution and the impossibility to extract accurate and reliable information about the orientation of the trabecular and cortical structures, in most QCT-based FE models the femoral bone is considered such as isotropic (Imai, et al., 2006; Taddei, et al., 2006). Recently, some researchers have tried to improve the material model by assuming a constant geometry-dependent anisotropy in the whole bone (Chevalier, et al., 2008; Crawford, et al., 2003) or by defining orthotropic material properties by assuming that the main orthotropic trajectories follow the principal strains (Trabelsi and Yosibash, 2011). However, up to date no proper validation studies have been shown if these assumptions can significantly improve the ability of the FE models for predicting vertebral and femoral mechanical properties.

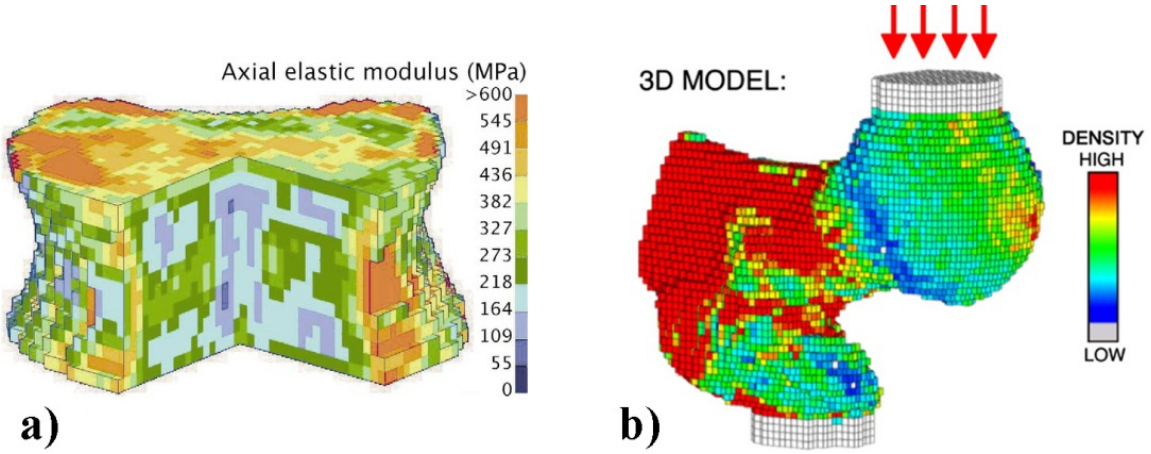

Figure 1. 19: Example of voxel based continuum level FE model of the human vertebra (a, adapted from (Crawford, et al., 2003)) and of the human proximal femur (b, adapted from (Keaveny, et al., 2012))

As the goal of the present study was to generate FE models which provide a good compromise between simplicity, efficiency and accuracy, the above mentioned refinements (smooth mesh, splitting between trabecular and cortical bone, orthotropic material properties) were not included in the modelling approach selected for this thesis. Albeit these simplifications, QCT-based hvFE models are ideal for nonlinear material analysis (Chevalier, et al., 2009; Keyak, 2001) thanks to the low number of degrees of freedom. Therefore, QCT-based hvFE models are a powerful tool to predict post-yield mechanical properties as fracture load and damage localization. To introduce the material nonlinearities different yield/failure criteria have been used in the literature for both vertebra and femur. When bone was assumed such as isotropic, both strain-based (Bessho, et al., 2007; Imai, et al., 2006) or stress-based (Wilcox, 2007) failure criteria, provided realistic results. When anisotropy is assumed from geometrical considerations, a more complex yield/failure criterion can be defined (Chevalier, et al., 2009). One of the subtasks of this thesis was to adapt the constitutive model for bone developed by Garcia et al. (Garcia, et al., 2009) to fulfil the requirements of the present study (more details in sections *1.6.4*, Chapter 3 and Chapter 5).

1.6.2 HR-pQCT MicroFE models

µFE models are generated by converting the "bone voxels" of a high resolution binary (bone-not bone) image directly into hexahedral elements (Figure 1.20). The main requirement for the original image is to have a resolution high enough to describe properly the trabecular bone microstructure and the thin cortical shells. In example, to well describe the bending behaviour of the trabeculae the original images should not go below a minimum resolution of 30µm (Guldberg, et al., 1998; Varga, 2009). In such dimensional scale, the material properties of bone are usually considered constant and isotropic within each element. A recent computational study based on synchrotron images has confirmed that at a resolution of 10.3µm, mineral heterogeneity plays only a minor role in the apparent properties of trabecular bone samples (Gross, et al., 2012).
While originally such models were generated from µCT images to study the mechanical behaviour of trabecular and cortical bone samples (Nazarian, et al., 2006; van Rietbergen,

et al., 1995), nowadays this approach has been extensively used also from HR-pQCT images. As HR-pQCT can be used to scan peripheral sites such as distal radius and tibia *in vivo*, this methodology has become more and more popular in longitudinal clinical studies to address the change of the bone apparent stiffness (Boutroy, et al., 2008; Rizzoli, et al., 2012; Vilayphiou, et al., 2010). However, for basic research applications µFE models have been also applied *in vitro* to other anatomical sites (proximal femur (Van Rietbergen, et al., 2003; Verhulp, et al., 2008) and vertebral body (Chevalier, et al., 2009; Eswaran, et al., 2006; Homminga, et al., 2004; Kinzl, et al., 2012)).

Nevertheless, the typical resolution of HR-pQCT images (approximately 100 µm) does not allow an accurate description of the geometry of the trabecular structure (the trabeculae are approximately 200 µm thick) and makes such µFE strongly dependent from the image processing procedure, namely the segmentation technique used to generate the binary images from the original grey scale ones (Laib and Ruegsegger, 1999), which induces errors into the model (e.g. underestimation or overestimation of the BV/TV in different regions of the sample). Moreover, the large number of elements and, therefore, of degrees of freedom limit nowadays this type of model to linear analysis which are already computational demanding. Nevertheless, even if restricted to linear analysis, high parallel computers are needed to run organ level µFE analysis due to the high number of degrees of freedom (typically several millions). Albeit these considerations, the HR-pQCT µFE models have been found to accurately compute the stiffness (R^2=0.96) and accurately estimate the strength (R^2=0.95) of the distal radius (Varga, et al., 2011). Furthermore, a recent study (Pistoia, et al., 2002) proposed to estimate, from HR-pQCT based linear µFE, the failure load of the radius by assuming that the failure would be initiated when a significant part of the bone tissue (2%) was strained beyond a critical limit (7000 microstrain). Moreover, with the development of Supercomputing centres it seems realistic that in the next decade nonlinear HR-pQCT based organ level µFE could be run to predict directly the bone strength. However, it has to be investigated how much this approach would be applicable in clinics. In fact, even though we might be able to solve the FE models, it is not clear what would be the payback, in terms of radiation dose to the patient, to be able to decrease the CT voxel size at least down to 82µm for central anatomical sites.

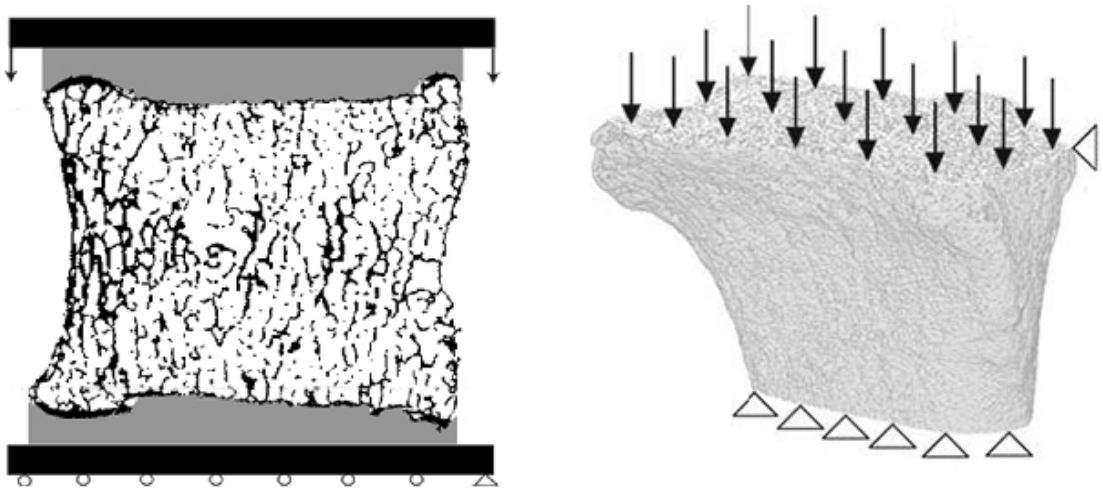

Figure 1. 20: Examples of HR-pQCT based µFE of the vertebral body (sagittal section on the left, adapted from (Eswaran, et al., 2006)) and of the distal radius (adapted from (Varga, et al., 2011)).

1.6.3 Model Validation

The term validation indicates the process that ensures that a numerical model accurately predicts the physical phenomenon it was designed to replicate (Anderson, et al., 2007; ASME, 2006; Viceconti, et al., 2005). Although numerical models designed to simulate the behaviour of complex natural systems can not be totally validated (Oreskes, et al., 1994), they should succeed against several attempts of falsification (Popper, 1959) (i.e. to construct experiments whose goal is to prove that the model is not correct in predicting the reality it was designed for) before considering them accurate enough to predict the reality. In biomechanical application, the usual method to validate numerical models is to compare their outcomes with the ones measured during well controlled *in vitro* experiments. It should be stressed that also the *in vitro* experiment is a conceptual model of the clinical reality (what happens to the patient *in vivo*) (Cristofolini, et al., 2010) and therefore even though a validated numerical model through *in vitro* experiments is likely to do not provide completely wrong results, caution should be taken before considering its outcomes true when applied *in vivo*.
There are a number of studies in which the results of QCT-based FE models designed to predict the mechanical properties of human femur and vertebra were validated through experiments *in vitro*. Usually only a few features of the prediction ability of the models are validated:

- The strains and/or displacement in points of the external surface of the bone (Schileo, et al., 2007);
- The apparent mechanical properties of the bone as stiffness and/or fracture load (Crawford, et al., 2003);
- The region where the damage (or strain) localizes (Keyak, et al., 2001a).

A more detailed overview of the validation studies for the human vertebra and femur found in the literature is reported in the next two sections.

Validation studies for the human vertebra

Several studies have attempted to validate the outcomes of QCT-based FE model of the human vertebra. Principally three approaches with different degrees of complexities have been used so far.
First: Full vertebra (Figure 1.21a). In this approach, one vertebra is completely disarticulated from the spine segment. The posterior element is kept but is not articulating with any other bone. The ligaments and intervertebral discs are completely removed. This approach has the advantage of guaranteeing continuity in the vertebral structure. The load is usually distributed through the endplates by embedding a thin portion of the vertebral body in PMMA. As there is only a body involved, the validation procedure focuses in predicting the structural properties of the vertebra (Jones and Wilcox, 2008). The material properties are assigned to each element in function of the BMD value, of the trabecular orientation (usually assumed for models based on QCT images due to the impossibility of extracting information about the fabric) and of the defined constitutive law which might also include nonlinearities (Jones and Wilcox, 2008). While it was found that the posterior element through the facet joints takes almost one fourth of the axial load, its complex geometry makes challenging both capturing and meshing procedures (Jones and Wilcox, 2008).
Second: Vertebral body (Figure 1.21b). In this configuration, the posterior portion of the full vertebra is removed by cutting adjacent to the vertebral body to reduce the above mentioned complexity in meshing the posterior element. As for full vertebrae, an uniaxial

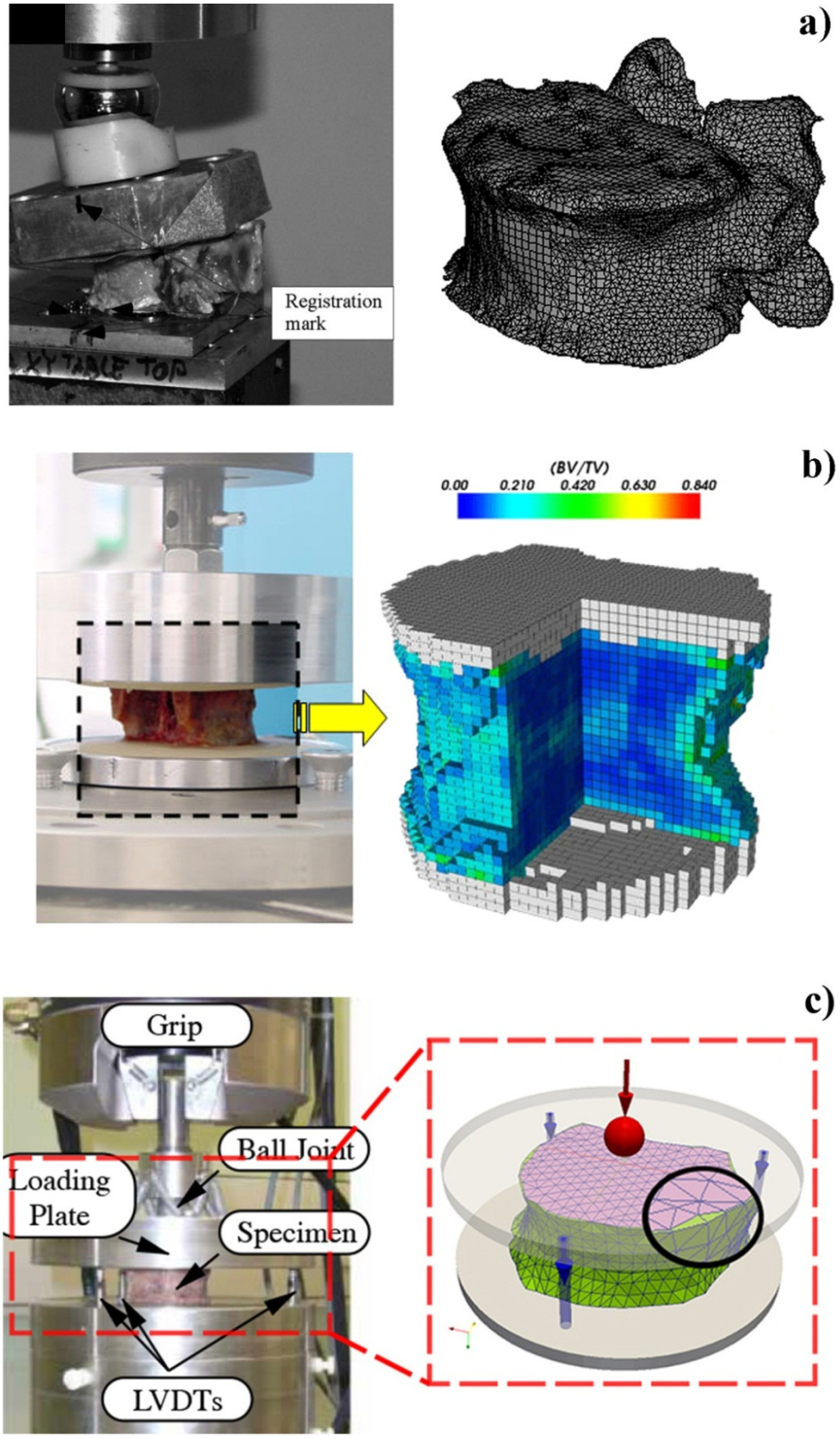

Figure 1. 21: Comparison of experiments and models in case of validation studies for the full vertebra (a, adapted from (Alkalay, et al., 1976; Wijayathunga, et al., 2008)) for the vertebral body (b, adapted from (Chevalier, et al., 2008)) and for the vertebral body section (c, adapted from (Pahr, et al., 2012)).

compressive load is usually distributed to the cortical endplates through layers made of PMMA or rubber which are modelled in the FE (Chevalier, et al., 2008; Imai, et al., 2006; Mirzaei, et al., 2009). In this approach, as for the previous one, the apparent mechanical properties of the vertebral body (apparent stiffness, ultimate force and work to failure) are compared with the simulations.
Third: Vertebral body section (Figure 1.21c). This is the simplest model with the most controllable loading conditions. From the vertebral body configuration the endplates are further removed by using a diamond blade (Ebbesen, et al., 1999) and a further step of polishing can be used to improve their flatness and roughness. With this approach the displacement can be directly applied and measured at the two parallel surfaces without the need of introducing any other material in between. Therefore, this methodology not only guarantees a simple and reproducible way of matching the boundary conditions between experiments and simulations, but also improves the experimental evaluation of the vertebral body stiffness and, therefore, its comparison with the one found in the models. Moreover, a ball joint above the loading plate can be used to easily induce a more realistic anterior wedge fractures. In a recent study Maquer et al. (Maquer, et al., 2012) showed that the removal of the endplates in hvFE models of the vertebral body has only a minor effect on the vertebral stiffness, ultimate force and damage distribution compared to the vertebral body approach. Finally, the removal of the posterior element and of the endplates makes this approach attractive for μFE models that benefit from the lower number of elements.

Validation studies for the human femur

A number of validation studies for FE model of the femur can be found in the literature. As mentioned in the section *1.6.3*, even the experiments can be considered a model of the real physical situation as it would not be possible to reproduce in a controlled experiment the *in vivo* loading conditions. Therefore, in the framework of validation studies for the human femur the following simplifications are usually accepted.
First, in the majority of the cases only the proximal portion is considered (Dragomir-Daescu, et al., 2011; Keyak, et al., 1998; Yosibash, et al., 2007) instead of testing the whole femur (Cristofolini, et al., 2007). Both configurations have shown to be able to reproduce typical femoral fractures (see section *1.5.3*). Therefore, the isolation of the proximal portion of the femur is preferred for the better control of the boundary conditions, easier image processing and smaller dimension of the FE models.
Second, normally no muscle forces are simulated and the load is applied to the femoral head. The distal portion of the proximal femur is fixed usually by means of embedding material. The load is distributed on a large portion of the femoral head to do not localize the damage in regions where is usually not observed (proximal portion of the femoral head). Moreover, from numerical investigations the exclusion of the abductor muscles in the model (Figure 1.22) has shown a minor effect on strain distribution (Cristofolini, et al., 2007; Cristofolini, et al., 1995) and femoral strength (Keyak, et al., 2005).
Third, in most studies only two loading scenarios are investigated. A physiological loading is usually examined by placing the femur in a simulated one-legged stance position. Moreover, as in 95% of the cases a femoral fracture is associated with a fall, the mechanical properties of the femur have been investigated in such configuration too. While it was shown that the mechanical properties of the femur are strongly dependent from the considered loading scenarios (i.e. stance versus fall, Figure 1.23 (Keyak, 2000)), the effect of the loading direction within each scenario is still debated.

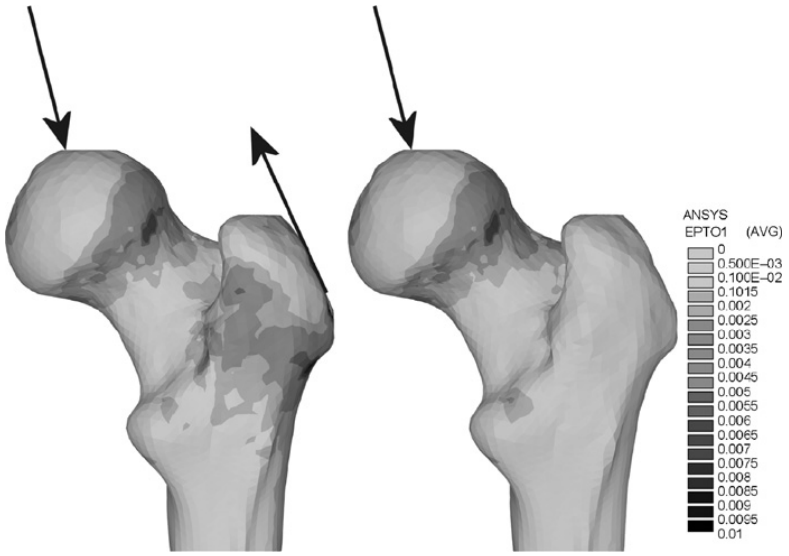

Figure 1. 22: strain distribution with and without inclusion of the abductor force in the FE model (Cristofolini, et al., 2007).

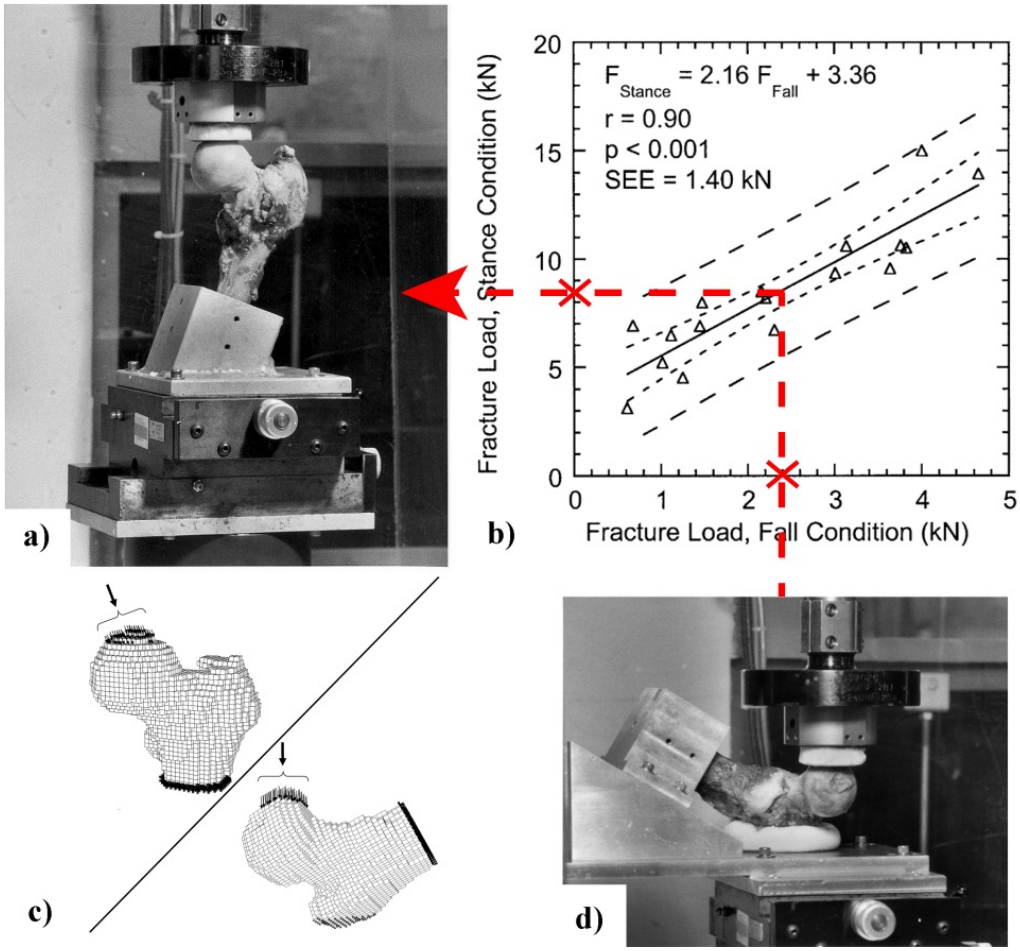

Figure 1. 23: b) represents the relationship between experimental femoral ultimate load for stance (a) and fall (d) configurations (adapted from (Keyak, 2000)). c) shows examples of QCT-based hvFE model from the same author (Keyak, 2001).

From computational studies it was found that both adduction and rotation angles affect the femoral mechanical properties in both stance and fall configurations (Bessho, et al., 2009; Keyak, et al., 2001b; Wakao, et al., 2009). Similar results have been shown through experimental studies which have demonstrated that the loading direction in a simulated fall affects the femoral strength (Pinilla, et al., 1996) and the strain distribution (Zani, et al., 2010). However, no exhaustive validation studies where both experimental and numerical approaches were considered have been done so far. The choice of the loading direction for validation studies which investigate the mechanical properties of the femur in a stance configuration is usually based on the results shown by Bergman et al. (Bergmann, et al., 2001), who measured with instrumented implants the range of loading direction during physiological gait. Based on these measurements, the loading direction is usually tested with an inclination of 0º to 27º in the frontal plane and of -3º to +18º in the sagittal plane from the femur axis (Cristofolini, et al., 2012). On the other side, there are no *in vivo* data about the loading direction in case of a simulated fall, yet. Most researchers choose a loading direction corresponding to an abduction angle between 0º and 30º and an internal rotation between 0º and 30º (Cong, et al., 2011; Cristofolini, et al., 2012; Grassi, et al., 2012; Koivumaki, et al., 2012). Fourth, although it is well known that the mechanical properties of bone are dependent from the loading rate (viscoelastic) and from the loading direction (anisotropic, in particular orthotropic), in most cases the FE models do not account for them. Therefore, the mechanical tests are performed or in quasi-static conditions (Keyak, et al., 1998) for better controlling the experiments, or by simulating velocities which might induce a fracture *in vivo* (Schileo, et al., 2007). Furthermore, even though recently an estimation of trabecular orientation from low resolution QCT images has been attempted (Lenaerts and van Lenthe, 2009) by extending to 3D CT images the method of line fraction deviation (Geraets, 1998), the femoral bone material properties are usually considered such as isotropic. The impact of this assumption on the FE models' ability to predict femoral mechanical properties is still debated (Peng, et al., 2006; Verhulp, et al., 2006; Yang, et al., 2010). While the last mentioned studies used only a numerical approach, recently a study based on both computational and experimental results showed that the difference between the accuracy of FE models based on isotropic or orthotropic (defined by geometrical and micromechanical considerations) assumptions are minor if the femur was loaded in one-legged stance configuration (Trabelsi and Yosibash, 2011). No data have been shown so far for the fall configuration.

1.6.4 Requirements and simplifications for QCT-based FE models

According to the literature review provided in the previous sections, in the present thesis the models were designed and validated by considering possible short term pre-clinical and clinical applications. Therefore, they had to fulfil the following requirements:

- Specimen-specific FE models had to be generated from QCT images with standard clinical resolution;
- The validation procedure had to be applied to human vertebra and femur;
- The whole procedure to validate the models had to be performed for a relatively large amount of samples (~40 for each loading configuration);
- The loading scenarios considered in the validation study had to reproduce vertebral and femoral fractures typically observed during clinical practice;
- The image processing and model generation had to be done in a semi-automatic way, by guaranteeing a reasonable pre-processing time;

- At least structural stiffness and ultimate force had to be computed from the models and then compared to the same properties measured in the experiments. If possible a qualitative comparison between predicted and observed failure localization had to be included in the analysis;
- The ability of the FE models in predicting bone mechanical properties had to be compared with the one of standard clinical tools.

To fulfil the above mentioned requirements, the following assumptions were taken:

- The effect of ligament, tendons, cartilage and muscles were considered negligible for the investigation of bone mechanical properties and therefore not included in the models nor in the experiments;
- The existence of load configurations representative for clinical vertebral and femoral fractures was assumed;
- In case of vertebra, the effect of the posterior element and of the cortical endplate on the vertebral body's mechanical properties was considered negligible. In case of the human femur the distal portion of the bone was considered not to affect its proximal mechanical properties;
- Bone viscous dependency was not included in the model and, therefore, the experiments were performed in quasi-static conditions;
- Due to the impossibility of extracting reliable information about the trabecular microarchitecture from the QCT images, bone was considered such as isotropic in case of the human femur and transverse isotropic in case of the human vertebral body (according to geometrical considerations);
- In order to simplify the meshing procedure and to reduce the pre-processing time, trabecular and cortical bone were modelled in the same way and a simple voxel based mesh was used;
- Material nonlinearities were included by using an already published constitutive law developed for bone (Garcia, et al., 2009), which was adapted for the numerical simulations of the present thesis as described in the next chapters. The modelling procedures were defined in a flexible way to allow an accurate estimation of the model's sensitivity to the used constitutive law in future works.

1.7 Objectives of the thesis

The aim of this thesis was to validate nonlinear specimen specific QCT-based voxel homogenized FE models for the human vertebra and femur and to compare their ability in predicting bone mechanical properties at the organ level measured with *in vitro* experiments versus the one of standard clinical tools. While several validation studies for FE models of bone at the organ level can be found in the literature (see section *1.6.3*), the goal of this thesis was to perform a comprehensive validation study to push forward our understanding about this topic. To overcome most of the limitations of the previously published studies in the present thesis the following points were considered:

- In the studies presented in this thesis a relatively large number of samples from two anatomical sites were considered;

- The samples included in the projects presented in this thesis were stored fresh frozen to do not affect bone mechanical properties with chemical preservation procedures (like alcohol or formalin solutions);
- Each sample underwent a densitometric exam to evaluated its BMD with standard clinical tools (QCT and DXA analysis);
- The samples were tested until failure with reliable experiments to be able to evaluate not only bone stiffness but also bone strength. Novel experimental setups were designed to accurately control the boundary conditions for a more accurate match between numerical and experimental approaches. Moreover, the experiments were used to induce fractures typically observed in clinics and to perform machine compliance free measurements of stiffness;
- The FE models included material nonlinearities to be able to directly predict the failure load and the failure localization without estimating them from linear models;

The sub-goals of the thesis included:

- The development of a method to estimate BV/TV from QCT images. This step is necessary to be able to apply the material properties in the hvFE models. In particular, the bone mechanical properties were modelled with an already published BV/TV and fabric based nonlinear constitutive model (Garcia, et al., 2009) which was slightly modified. While isotropy (for femur) or transverse isotropy (for vertebra) was assumed from geometrical considerations, the BV/TV needed to be accurately estimated from the BMD measured in the QCT images;
- The design of three different mechanical setups to be able to induce clinical relevant vertebral and femoral fractures in physiological and accidental loading configurations *in vitro*. These setups should guarantee accurate control of the boundary conditions and accurate measurement of the bone mechanical properties for a reproducible comparison with the numerical outcomes;
- The definition of a well automated procedure to generate, with a low level of operator interaction, hvFE models from the QCT 3D images. In fact, the procedure has to guarantee in a reasonable time an accurate extraction of the specimen geometry, the meshing of it, the assignment of material properties and the interface with a commercial software used for the computation and the evaluation of the required mechanical properties for a large set of vertebrae (~40 samples) and femora (~80 samples);
- The comparison between the ability of the applied hvFE models and of standard densitometric clinical tools such as DXA and QCT in predicting vertebral and femoral stiffness and failure load.

1.8 Outline of the thesis

Chapter 1 provided a description of the state of the art in the topic of this thesis. The next five Chapters are based on a collection of five manuscripts published (Chapters 2, 3 and 4), accepted (Chapter 5), and submitted (Chapter 6) to peer reviewed journals and report the sub-studies performed to achieve the goals mentioned in the previous section.

Chapter 2 presents a new methodology to estimate µCT BV/TV from QCT BMD. This calibration law is necessary for the estimation and assignment of the material properties in

the FE models. The main motivation for this chapter was the lack in the literature of a reliable methodology to estimate such calibration law for high BMD range, especially in bones with thin cortical shell. The methodology to compute the calibration equation is presented for the human vertebra. The results for the human femur obtained with the same methodology presented in this chapter are reported in Chapter 5;

Chapter 3 presents a novel setup to induce wedge shape failure to the human vertebral body. Moreover, this chapter shows the procedure for generating nonlinear QCT-based hvFE models of the human vertebra to evaluate its stiffness, the failure load and the damage localization. Furthermore, the methodology to evaluate the volumetric BMD with one of the standard clinical tools is reported. The chapter shows how the hvFE models predict the femoral mechanical properties better than BMD;

Chapter 4 presents a more clinical application of the above mentioned hvFE models. It investigates whether densitometric or FE-based measurements would predict better structural or material properties. Moreover, this chapter presents the effect of a possible improvement of the scanning resolution of the CT images up to 82µm on the predictive ability of the densitometric and FE methods. While an improvement in scanning resolution was found not to improve the prediction ability of densitometric parameters, HR-pQCT models were found to better predict vertebral stiffness than QCT-based FE models.

Chapter 5 shows a validation study for QCT-based hvFE models of the human femur. In particular it presents a novel setup to perform reliable mechanical testing on the proximal femur by inducing femoral fractures in both physiological and accidental loading configurations. Moreover, this chapter shows the procedure for calibrating QCT BMD and µCT BV/TV for the human femur, based on the methodology described in Chapter 2. This chapter describes the procedure used to generate the nonlinear hvFE models, by including in the appendix the modifications of the constitutive model necessary to take into account for thick cortical bone. The results of this chapter show that hvFE models can predict femoral mechanical properties better than QCT based densitometric measures and can provide meaningful information about the femoral load-displacement curves and the fracture location.

Chapter 6 presents more in details the experimental methodology used to validate the hvFE models for the femur. In particular, the results from the two loading configurations (physiological and accidental) were compared for the different pairs of femora. Moreover, the chapter shows how the gold standard clinical tool to investigate the risk of fracture (DXA) can predict with more accuracy the femoral mechanical properties in a simulated fall while its accuracy decreases for simulated spontaneous fractures.

Finally, **Chapter 7** shall provide a general conclusion of the whole thesis, by underlining its strengths, limitations and future perspectives.

Bibliography

Ager J.W., Balooch G., Ritchie R.O., 2006. Fracture, aging, and disease in bone. J Mat Res 21, 1878-1892

Alffram P.A., 1964. An epidemiolologic study of cervical and trochanteric fractures of the femur in an urban population. Analysis of 1,664 cases with special reference to etiologic factors. Acta Orthopaedica Scandinavica Supplementum 65, 1-109.

Alkalay R.N., von Stechow D., Torres K., Hassan S., Sommerich R., Zurakowski D., 1976. The effect of cement augmentation on the geometry and structural response of recovered osteopenic vertebrae: an anterior-wedge fracture model. Spine 33, 1627-1636.

Anderson A.E., Ellis B.J., Weiss J.A., 2007. Verification, validation and sensitivity studies in computational biomechanics. Computer Methods in Biomechanics and Biomedical Engineering 10, 171-184

Asano S., Kaneda K., Umehara S., Tadano S., 1992. The mechanical properties of the human L4-5 functional spinal unit during cyclic loading. The structural effects of the posterior elements. Spine (Phi Pa 1976) 17, 1343-1352.

ASME Standards Committee on Verification and Validation in Computational Solid Mechanics, 2006. Guide for Verification and Validation in Computational Solid Mechanics

Bayraktar H.H., Gupta A., Kwon R.Y., Papadopoulos P., Keaveny T.M., 2004. The modified super-ellipsoid yield criterion for human trabecular bone. J Biomed Eng 126, 677-684.

Bergmann G., Deuretzbacher G., Heller M., Graichen F., Rohlmann A., Strauss J., Duda G.N., 2001. Hip contact forces and gait patterns from routine activities. Journal of Biomechanics 34, 859-871.

Bessho M., Ohnishi I., Matsumoto T., Ohashi S., Matsuyama J., Tobita K., Kaneko M., Nakamura K., 2009. Prediction of proximal femur strength using a CT-based nonlinear finite element method: differences in predicted fracture load and site with changing load and boundary conditions. Bone 45, 226-231. Epub 2009 May 2003.

Bessho M., Ohnishi I., Matsuyama J., Matsumoto T., Imai K., Nakamura K., 2007. Prediction of strength and strain of the proximal femur by a CT-based finite element method. Journal of Biomechanics 40, 1745-1753

Blonk M.C., Erdtsieck R.J., Wernekinck M.G., Schoon E.J., 2007. The fracture and osteoporosis clinic: 1-year results and 3-month compliance. Bone 40, 1643-1649. Epub 2007 Mar 1641.

Boutroy S., Van Rietbergen B., Sornay-Rendu E., Munoz F., Bouxsein M.L., Delmas P.D., 2008. Finite element analysis based on in vivo HR-pQCT images of the distal radius is associated with wrist fracture in postmenopausal women. Journal of Bone and Minereral Research 23, 392-399.

Bouxsein M.L., 2003. Bone quality: where do we go from here? Osteoporososis International 14 Suppl 5, S118-127

Bouxsein M.L., Coan B.S., Lee S.C., 1999. Prediction of the strength of the elderly proximal femur by bone mineral density and quantitative ultrasound measurements of the heel and tibia. Bone 25, 49-54.

Boyd S.K., Muller R., 2006. Smooth surface meshing for automated finite element model generation from 3D image data. Journal of Biomechanics 39, 1287-1295

Bucholz R.W., Heckman J.D., Court-Brown C.M., Tornetta P., 2009. Rockwood and Green's Fractures in Adults. Lippincott Williams & Wilkins,

Buckley J.M., Loo K., Motherway J., 2007. Comparison of quantitative computed tomography-based measures in predicting vertebral compressive strength. Bone 40, 767-774

Burghardt A.J., Issever A.S., Schwartz A.V., Davis K.A., Masharani U., Majumdar S., Link T.M., 2010a. High-resolution peripheral quantitative computed tomographic imaging of cortical and trabecular bone microarchitecture in patients with type 2 diabetes mellitus. J Clin Endocrinol Metab 95, 5045-5055. Epub 2010 Aug 5018.

Burghardt A.J., Kazakia G.J., Sode M., de Papp A.E., Link T.M., Majumdar S., 2010b. A longitudinal HR-pQCT study of alendronate treatment in postmenopausal women with low bone density: Relations among density, cortical and trabecular microarchitecture, biomechanics, and bone turnover. Journal of Bone and Mineral Research 25, 2558-2571. doi: 2510.1002/jbmr.2157. Epub 2010 Jun 2518.

Burghardt A.J., Link T.M., Majumdar S., 2011. High-resolution computed tomography for clinical imaging of bone microarchitecture. Clinical Orthopaedics Relatated Research 469, 2179-2193

Cann C.E., Genant H.K., Kolb F.O., Ettinger B., 1985. Quantitative computed tomography for prediction of vertebral fracture risk. Bone 6, 1-7

Chevalier Y., Charlebois M., Pahra D., Varga P., Heini P., Schneider E., Zysset P., 2008. A patient-specific finite element methodology to predict damage accumulation in vertebral bodies under axial compression, sagittal flexion and combined loads. Computer Methods in Biomechanics and Biomedical Engineering 11, 477-487

Chevalier Y., Pahr D., Zysset P.K., 2009. The role of cortical shell and trabecular fabric in finite element analysis of the human vertebral body. J Biomed Eng 131, 111003

Chevalier Y., Quek E., Borah B., Gross G., Stewart J., Lang T., Zysset P., 2010. Biomechanical effects of teriparatide in women with osteoporosis treated previously with alendronate and risedronate: results from quantitative computed tomography-based finite element analysis of the vertebral body. Bone 46, 41-48. Epub 2009 Oct 2001.

Cong A., Buijs J.O., Dragomir-Daescu D., 2011. In situ parameter identification of optimal density-elastic modulus relationships in subject-specific finite element models of the proximal femur. Medical Engineering and Physics 33, 164-173. Epub 2010 Oct 2027.

Cooper C., Melton L.J., 3rd, 1992. Epidemiology of osteoporosis. Trends in Endocrinology and Metababolism: TEM 3, 224-229.

Crawford R.P., Cann C.E., Keaveny T.M., 2003. Finite element models predict in vitro vertebral body compressive strength better than quantitative computed tomography. Bone 33, 744-750

Cristofolini L., Juszczyk M., Martelli S., Taddei F., Viceconti M., 2007. In vitro replication of spontaneous fractures of the proximal human femur. Journal of Biomechanics 40, 2837-2845

Cristofolini L., Juszczyk M., Zani L., Viceconti M., 2012. For which loading scenarios is the proximal femur optimized? 18th Congress of the ESB, Lisbon, Portugal, 01-04 July. Poster Presentation

Cristofolini L., Schileo E., Juszczyk M., Taddei F., Martelli S., Viceconti M., 2010. Mechanical testing of bones: the positive synergy of finite-element models and in vitro experiments. Philosophical Transactions Series A Mathematical Physical and Engineering Sciences 368, 2725-2763

Cristofolini L., Viceconti M., Toni A., Giunti A., 1995. Influence of thigh muscles on the axial strains in a proximal femur during early stance in gait. Journal of Biomechanics 28, 617-624.

Cummings S.R., Melton L.J., 2002. Epidemiology and outcomes of osteoporotic fractures. Lancet 359, 1761-1767.

Currey J.D., 1969. The relationship between the stiffness and the mineral content of bone. Journal of Biomechanics 2, 477-480

Dall'Ara E., Schmidt R., Zysset P., 2012. Microindentation can discriminate between damaged and intact human bone tissue. Bone 50, 925-929. Epub 2012 Jan 2014.

Ding M., Odgaard A., Hvid I., 1999. Accuracy of cancellous bone volume fraction measured by micro-CT scanning. Journal of Biomechanics 32, 323-326

Dionyssiotis Y., 2010. Management of osteoporotic vertebral fractures. International Journal of General Medicine 3, 167-171.

Dragomir-Daescu D., Op Den Buijs J., McEligot S., Dai Y., Entwistle R.C., Salas C., Melton L.J., 3rd, Bennet K.E., Khosla S., Amin S., 2011. Robust QCT/FEA models of proximal femur stiffness and fracture load during a sideways fall on the hip. Annals of Biomedical Engineering 39, 742-755

Eastell R., Mosekilde L., Hodgson S.F., Riggs B.L., 1990. Proportion of human vertebral body bone that is cancellous. Journal of Bone and Mineral Research 5, 1237-1241.

Ebbesen E.N., Thomsen J.S., Beck-Nielsen H., Nepper-Rasmussen H.J., Mosekilde L., 1999. Lumbar vertebral body compressive strength evaluated by dual-energy X-ray absorptiometry, quantitative computed tomography, and ashing. Bone 25, 713-724

Eckstein F., Lochmuller E.M., Lill C.A., Kuhn V., Schneider E., Delling G., Muller R., 2002. Bone strength at clinically relevant sites displays substantial heterogeneity and is best predicted from site-specific bone densitometry. Journal of Bone and Mineral Research 17, 162-171.

Engelke K., Fuerst T., Dasic G., Davies R.Y., Genant H.K., 2010. Regional distribution of spine and hip QCT BMD responses after one year of once-monthly ibandronate in postmenopausal osteoporosis. Bone 46, 1626-1632. Epub 2010 Mar 1610.

Eswaran S.K., Gupta A., Adams M.F., Keaveny T.M., 2006. Cortical and trabecular load sharing in the human vertebral body. Journal of Bone and Mineral Research 21, 307-314

Falcinelli C., Schileo E., Morawska M., Viceconti M., Taddei F., 2012. FE-based strength estimation for the prediction of femoral neck fractures. 18th Congress of the ESB, Lisbon, Portugal, 01-04 July. Oral Presentation

Faulkner K.G., Cann C.E., Hasegawa B.H., 1991. Effect of bone distribution on vertebral strength: assessment with patient-specific nonlinear finite element analysis. Radiology 179, 669-674

Fratzl P., Weinkamer R., 2007. Nature's hierarchical materials. Prog Mat Sci 52, 1263-1334

Garcia D., Zysset P.K., Charlebois M., Curnier A., 2009. A three-dimensional elastic plastic damage constitutive law for bone tissue. Biomechanics and Modeling in Mechanobiology 8, 149-165

Genant H.K., Jergas M., Palermo L., Nevitt M., Valentin R.S., Black D., Cummings S.R., 1996. Comparison of semiquantitative visual and quantitative morphometric assessment of prevalent and incident vertebral fractures in osteoporosis The Study of Osteoporotic Fractures Research Group. Journal of Bone and Mineral Research 11, 984-996.

Geraets W.G., 1998. Comparison of two methods for measuring orientation. Bone 23, 383-388

Gong H., Zhang M., Yeung H.Y., Qin L., 2005. Regional variations in microstructural properties of vertebral trabeculae with aging. Journal of Bone and Mineral Metabolism 23, 174-180.

Goulet R.W., Goldstein S.A., Ciarelli M.J., Kuhn J.L., Brown M.B., Feldkamp L.A., 1994. The relationship between the structural and orthogonal compressive properties of trabecular bone. Journal of Biomechanics 27, 375-389.

Graeff C., Chevalier Y., Charlebois M., Varga P., Pahr D., Nickelsen T.N., Morlock M.M., Gluer C.C., Zysset P.K., 2009. Improvements in vertebral body strength under teriparatide treatment assessed in vivo by finite element analysis: results from the EUROFORS study. Journal of Bone and Mineral Research 24, 1672-1680.

Granhed H., Jonson R., Hansson T., 1989. Mineral content and strength of lumbar vertebrae. A cadaver study. Acta Orthopaedica Scandinavica 60, 105-109

Grassi L., Schileo E., Taddei F., Zani L., Juszczyk M., Cristofolini L., Viceconti M., 2012. Accuracy of finite element predictions in sideways load configurations for the proximal human femur. Journal of Biomechanics 45, 394-399. Epub 2011 Nov 2012.

Gray H., 1989. Gray's anatomy. Williams P.L., Warwick R., Dyson M., Bannister L.H., Churchill Livingstone, Edinburgh

Griffith J.F., Genant H.K., 2008. Bone mass and architecture determination: state of the art. Best Practice & Research Clinical Endocrinology & Metabolism 22, 737-764

Gross T., Pahr D.H., Peyrin F., Zysset P.K., 2012. Mineral heterogeneity has a minor influence on the apparent elastic properties of human cancellous bone: a SRmuCT-based finite element study. Computer Methods in Biomechanics and Biomedical Engineering 23, 23

Guldberg R.E., Hollister S.J., Charras G.T., 1998. The accuracy of digital image-based finite element models. J Biomed Eng 120, 289-295

Guo X.E., 2001. Mechanical Properties of Cortical bone and Cancellous Bone Tissue. In Cowin S.C. (ed) Bone Mechanics Handbook. Informa Healthcare USA, Inc., New York, pp 10.11-10.23

Hansen U., Zioupos P., Simpson R., Currey J.D., Hynd D., 2008. The effect of strain rate on the mechanical properties of human cortical bone. J Biomed Eng 130, 011011.

Harrigan T.P., Mann R.W., 1984. Characterization of microstructural anisotropy in orthotropic materials using a second rank tensor. J Mater Sci 19, 761-767

Hernandez C.J., Beaupre G.S., Keller T.S., Carter D.R., 2001. The influence of bone volume fraction and ash fraction on bone strength and modulus. Bone 29, 74-78.

Higgins K.B., Sindall D.R., Cuitino A.M., Langrana N.A., 2007. Biomechanical alterations in intact osteoporotic spine due to synthetic augmentation: finite element investigation. J Biomed Eng 129, 575-585.

Hildebrand T., Laib A., Muller R., Dequeker J., Ruegsegger P., 1999. Direct three-dimensional morphometric analysis of human cancellous bone: microstructural data from spine, femur, iliac crest, and calcaneus. Journal of Bone and Mineral Reasearch 14, 1167-1174.

Hildebrand T., Ruegsegger P., 1997. Quantification of Bone Microarchitecture with the Structure Model Index. Computer methods in biomechanics and biomedical engineering 1, 15-23

Homminga J., Van-Rietbergen B., Lochmuller E.M., Weinans H., Eckstein F., Huiskes R., 2004. The osteoporotic vertebral structure is well adapted to the loads of daily life, but not to infrequent "error" loads. Bone 34, 510-516

Hulme P.A., Boyd S.K., Ferguson S.J., 2007. Regional variation in vertebral bone morphology and its contribution to vertebral fracture strength. Bone 41, 946-957. Epub 2007 Aug 2017.

Hussein A.I., Morgan E.F., 2012. The effect of intravertebral heterogeneity in microstructure on vertebral strength and failure patterns. Osteoporosis International 16, 16

Imai K., Ohnishi I., Bessho M., Nakamura K., 2006. Nonlinear finite element model predicts vertebral bone strength and fracture site. Spine 31, 1789-1794

Jalava T., Sarna S., Pylkkanen L., Mawer B., Kanis J.A., Selby P., Davies M., Adams J., Francis R.M., Robinson J., McCloskey E., 2003. Association between vertebral fracture and increased mortality in osteoporotic patients. Journal of Bone and Mineral Research 18, 1254-1260

Jelsma R.K., Kirsch P.T., Rice J.F., Jelsma L.F., 1982. The radiographic description of thoracolumbar fractures. Surgical Neurology 18, 230-236

Jergas M., Breitenseher M., Gluer C.C., Black D., Lang P., Grampp S., Engelke K., Genant H.K., 1995. Which vertebrae should be assessed using lateral dual-energy X-ray absorptiometry of the lumbar spine. Osteoporosis International 5, 196-204.

Johnell O., 1997. The socioeconomic burden of fractures: today and in the 21st century. American Journal of Medicine 103, 20S-25S; discussion 25S-26S.

Johnell O., Kanis J., 2005. Epidemiology of osteoporotic fractures. Osteoporosis International 16 Suppl 2, S3-7

Jones A.C., Wilcox R.K., 2008. Finite element analysis of the spine: towards a framework of verification, validation and sensitivity analysis. Medical Engineering and Physics 30, 1287-1304. Epub 2008 Nov 1284.

Kado D.M., Browner W.S., Palermo L., Nevitt M.C., Genant H.K., Cummings S.R., 1999. Vertebral fractures and mortality in older women: a prospective study. Study of Osteoporotic Fractures Research Group. Archives of Internal Medicine 159, 1215-1220.

Kaneko T.S., Bell J.S., Pejcic M.R., Tehranzadeh J., Keyak J.H., 2004. Mechanical properties, density and quantitative CT scan data of trabecular bone with and without metastases. Journal of Biomechanics 37, 523-530.

Kanis J.A., Oden A., Johnell O., De Laet C., Jonsson B., 2004. Excess mortality after hospitalisation for vertebral fracture. Osteoporosis International 15, 108-112

Keaveny T.M., Guo X.E., Wachtel E.F., McMahon T.A., Hayes W.C., 1994. Trabecular bone exhibits fully linear elastic behavior and yields at low strains. Journal of Biomechanics 27, 1127-1136.

Keaveny T.M., Hoffmann P.F., Singh M., Palermo L., Bilezikian J.P., Greenspan S.L., Black D.M., 2008. Femoral bone strength and its relation to cortical and trabecular changes after treatment with PTH, alendronate, and their combination as assessed by finite element analysis of quantitative CT scans. Journal of Bone and Mineral Research 23, 1974-1982.

Keaveny T.M., McClung M.R., Wan X., Kopperdahl D.L., Mitlak B.H., Krohn K., 2012. Femoral strength in osteoporotic women treated with teriparatide or alendronate. Bone 50, 165-170. Epub 2011 Oct 2017.

Keaveny T.M., Morgan E.F., Niebur G.L., Yeh O.C., 2001. Biomechanics of trabecular bone. Annu Rev Biomed Eng 3, 307-333.

Keaveny T.M., Wachtel E.F., Kopperdahl D.L., 1999. Mechanical behavior of human trabecular bone after overloading. Journal of Orthopaedic Research 17, 346-353.

Keyak J.H., 2000. Relationships between femoral fracture loads for two load configurations. Journal of Biomechanics 33, 499-502.

Keyak J.H., 2001. Improved prediction of proximal femoral fracture load using nonlinear finite element models. Medical Engineering and Physics 23, 165-173

Keyak J.H., Kaneko T.S., Rossi S.A., Pejcic M.R., Tehranzadeh J., Skinner H.B., 2005. Predicting the strength of femoral shafts with and without metastatic lesions. Clinical Orthopaedics and Related Research 439, 161-170

Keyak J.H., Kaneko T.S., Skinner H.B., Hoang B.H., 2007. The effect of simulated metastatic lytic lesions on proximal femoral strength. Clinical Orthopaedics and Related Research 459, 139-145

Keyak J.H., Rossi S.A., Jones K.A., Les C.M., Skinner H.B., 2001a. Prediction of fracture location in the proximal femur using finite element models. Medical Engineering and Physics 23, 657-664.

Keyak J.H., Rossi S.A., Jones K.A., Skinner H.B., 1998. Prediction of femoral fracture load using automated finite element modeling. Journal of Biomechanics 31, 125-133.

Keyak J.H., Skinner H.B., Fleming J.A., 2001b. Effect of force direction on femoral fracture load for two types of loading conditions. Journal of Orthopaedic Research 19, 539-544.

Kilincer C., Inceoglu S., Sohn M.J., Ferrara L.A., Bakirci N., Benzel E.C., 2007. Load sharing within a human thoracic vertebral body: an in vitro biomechanical study. Turkish Neurosurgery 17, 167-177.

Kinzl M., Benneker L.M., Boger A., Zysset P.K., Pahr D.H., 2012. The effect of standard and low-modulus cement augmentation on the stiffness, strength, and endplate pressure distribution in vertebroplasty. European Spine Journal 21, 920-929. Epub 2011 Dec 2015.

Klotzbuecher C.M., Ross P.D., Landsman P.B., Abbott T.A., 3rd, Berger M., 2000. Patients with prior fractures have an increased risk of future fractures: a summary of the literature and statistical synthesis. Journal of Bone and Mineral Research 15, 721-739.

Koivumaki J.E., Thevenot J., Pulkkinen P., Kuhn V., Link T.M., Eckstein F., Jamsa T., 2012. Ct-based finite element models can be used to estimate experimentally measured failure loads in the proximal femur. Bone 50, 824-829. Epub 2012 Jan 2028.

Laib A., Ruegsegger P., 1999. Calibration of trabecular bone structure measurements of in vivo three-dimensional peripheral quantitative computed tomography with 28-microm-resolution microcomputed tomography. Bone 24, 35-39.

Lang T.F., 2004. Quantitative computed tomography. In Langton C.M., Njeh C.F. (eds) The physical measurement of bone. Institute of Physics Publishing, London, pp 308-318

Lang T.F., Li J., Harris S.T., Genant H.K., 1999. Assessment of vertebral bone mineral density using volumetric quantitative CT. J Comput Assist Tomogr 23, 130-137.

Lenaerts L., van Lenthe G.H., 2009. Multi-level patient-specific modelling of the proximal femur. A promising tool to quantify the effect of osteoporosis treatment. Philosophical Transactions Series A, Mathematical, Physical, and Engineering Sciences 367, 2079-2093.

Lentle B.C., Prior J.C., 2003. Osteoporosis: What a clinician expects to learn from a patient's bone density examination. Radiology 228, 620-628

Leonard M.B., 2007. A structural approach to the assessment of fracture risk in children and adolescents with chronic kidney disease. Pediatric Nephrology 22, 1815-1824. Epub 2007 Jul 1811.

Lochmuller E.M., Muller R., Kuhn V., Lill C.A., Eckstein F., 2003. Can novel clinical densitometric techniques replace or improve DXA in predicting bone strength in osteoporosis at the hip and other skeletal sites? Journal of Bone and Mineral Research 18, 906-912.

Lotz J.C., Cheal E.J., Hayes W.C., 1991a. Fracture prediction for the proximal femur using finite element models: Part I--Linear analysis. J Biomed Eng 113, 353-360.

Lotz J.C., Cheal E.J., Hayes W.C., 1991b. Fracture prediction for the proximal femur using finite element models: Part II--Nonlinear analysis. J Biomed Eng 113, 361-365.

Maquer G., Dall'Ara E., Zysset P.K., 2012. Removal of the cortical endplates has little effect on ultimate load and damage distribution in QCT-based voxel models of human lumbar vertebrae under axial compression. Journal of Biomechanics 45, 1733-1738. Epub 2012 Apr 1713.

Marshall D., Johnell O., Wedel H., 1996. Meta-analysis of how well measures of bone mineral density predict occurrence of osteoporotic fractures. BMJ (Clinical Research ad) 312, 1254-1259

Martelli S., Taddei F., Schileo E., Cristofolini L., Rushton N., Viceconti M., 2012. Biomechanical robustness of a new proximal epiphyseal hip replacement to patient variability and surgical uncertainties: a FE study. Medical Engineering and Physics 34, 161-171. Epub 2011 Aug 2012.

Matsuura M., Eckstein F., Lochmuller E.M., Zysset P.K., 2007. The role of fabric in the quasi-static compressive mechanical properties of human trabecular bone from various anatomical locations. Biomechanics and modeling in mechanobiology 19, 19

Melton L.J., 3rd, Thamer M., Ray N.F., Chan J.K., Chesnut C.H., 3rd, Einhorn T.A., Johnston C.C., Raisz L.G., Silverman S.L., Siris E.S., 1997. Fractures attributable to osteoporosis: report from the National Osteoporosis Foundation. Journal of Bone and Mineral Research 12, 16-23

Mercer C., He M.Y., Wang R., Evans A.G., 2006. Mechanisms governing the inelastic deformation of cortical bone and application to trabecular bone. Acta Biomaterialia 2, 59-68. Epub 2005 Oct 2005.

Mirzaei M., Zeinali A., Razmjoo A., Nazemi M., 2009. On prediction of the strength levels and failure patterns of human vertebrae using quantitative computed tomography (QCT)-based finite element method. Journal of Biomechanics 42, 1584-1591

Mnif H., Koubaa M., Zrig M., Trabelsi R., Abid A., 2009. Elderly patient's mortality and morbidity following trochanteric fracture. A prospective study of 100 cases. Orthopaedics&traumatology, surgery&research 95, 505-510. Epub 2009 Sep 2026.

Morgan E.F., Bayraktar H.H., Keaveny T.M., 2003. Trabecular bone modulus–density relationships depend on anatomic site. Journal of Biomechanics 36, 897-904.

Mueller T.L., Christen D., Sandercott S., Boyd S.K., van Rietbergen B., Eckstein F., Lochmuller E.M., Muller R., van Lenthe G.H., 2011. Computational finite element bone mechanics accurately predicts mechanical competence in the human radius of an elderly population. Bone 48, 1232-1238. Epub 2011 Mar 1232.

Mueller T.L., Stauber M., Kohler T., Eckstein F., Muller R., van Lenthe G.H., 2009. Non-invasive bone competence analysis by high-resolution pQCT: an in vitro

reproducibility study on structural and mechanical properties at the human radius. Bone 44, 364-371

Nazarian A., Stauber M., Zurakowski D., Snyder B.D., Muller R., 2006. The interaction of microstructure and volume fraction in predicting failure in cancellous bone. Bone 39, 1196-1202. Epub 2006 Aug 1121.

Njeh C.F., Shepherd J.A., 2004. Absorptionmetric measurement. In Langton C.M., Njeh C.F. (eds) The physical measurement of bone. Institute of Physics Publishing, London, pp 267-307

Ochia R.S., Tencer A.F., Ching R.P., 2003. Effect of loading rate on endplate and vertebral body strength in human lumbar vertebrae. Journal of Biomechanics 36, 1875-1881.

Odgaard A., Kabel J., van Rietbergen B., Dalstra M., Huiskes R., 1997. Fabric and elastic principal directions of cancellous bone are closely related. Journal of Biomechanics 30, 487-495.

Ohman C., Baleani M., Perilli E., Dall'Ara E., Tassani S., Baruffaldi F., Viceconti M., 2007. Mechanical testing of cancellous bone from the femoral head: experimental errors due to off-axis measurements. Journal of Biomechanics 40, 2426-2433

Old J.L., Calvert M., 2004. Vertebral compression fractures in the elderly. American Family Physician 69, 111-116.

Oreskes N., Shrader-Frechette K., Belitz K., 1994. Verification, validation, and confirmation of numerical models in the Earth sciences. Science 263, 641-646.

Pahr D.H., Dall'ara E., Varga P., Zysset P.K., 2012. HR-pQCT-based homogenised finite element models provide quantitative predictions of experimental vertebral body stiffness and strength with the same accuracy as muFE models. Computer Methods in Biomechanics and Biomedical Engineering 15, 711-720. Epub 2011 May 2024.

Pahr D.H., Zysset P.K., 2009. From high-resolution CT data to finite element models: development of an integrated modular framework. Computer Methods in Biomechanics and Biomedical Engineering 12, 45-57

Parkkari J., Kannus P., Palvanen M., Natri A., Vainio J., Aho H., Vuori I., Jarvinen M., 1999. Majority of hip fractures occur as a result of a fall and impact on the greater trochanter of the femur: a prospective controlled hip fracture study with 206 consecutive patients. Calcified Tissue International 65, 183-187.

Patel R., Blake G.M., Herd R.J., Fogelman I., 1997. The effect of weight change on DXA scans in a 2-year trial of etidronate therapy. Calcified Tissue International 61, 393-399.

Peng L., Bai J., Zeng X., Zhou Y., 2006. Comparison of isotropic and orthotropic material property assignments on femoral finite element models under two loading conditions. Medical Engineering and Physics 28, 227-233. Epub 2005 Aug 2001.

Perilli E., Baleani M., Ohman C., Baruffaldi F., Viceconti M., 2007. Structural parameters and mechanical strength of cancellous bone in the femoral head in osteoarthritis do not depend on age. Bone 41, 760-768. Epub 2007 Aug 2001.

Perilli E., Briggs A.M., Kantor S., Codrington J., Wark J.D., Parkinson I.H., Fazzalari N.L., 2012. Failure strength of human vertebrae: prediction using bone mineral density measured by DXA and bone volume by micro-CT. Bone 50, 1416-1425. Epub 2012 Mar 1410.

Pinilla T.P., Boardman K.C., Bouxsein M.L., Myers E.R., Hayes W.C., 1996. Impact direction from a fall influences the failure load of the proximal femur as much as age-related bone loss. Calcified Tissue International 58, 231-235.

Pistoia W., van Rietbergen B., Lochmuller E.M., Lill C.A., Eckstein F., Ruegsegger P., 2002. Estimation of distal radius failure load with micro-finite element analysis

models based on three-dimensional peripheral quantitative computed tomography images. Bone 30, 842-848

Popper K., 1959. The Logic of Scientific Discovery. Hutchinson & Co, New York

Rho J.Y., Kuhn-Spearing L., Zioupos P., 1998. Mechanical properties and the hierarchical structure of bone. Medical Engineering and Physics 20, 92-102.

Rice J.C., Cowin S.C., Bowman J.A., 1988. On the dependence of the elasticity and strength of cancellous bone on apparent density. Journal of Biomechanics 21, 155-168.

Rincon-Kohli L., Zysset P.K., 2009. Multi-axial mechanical properties of human trabecular bone. Biomechanics and Modeling in Mechanobiology 8, 195-208

Rizzoli R., Chapurlat R.D., Laroche J.M., Krieg M.A., Thomas T., Frieling I., Boutroy S., Laib A., Bock O., Felsenberg D., 2012. Effects of strontium ranelate and alendronate on bone microstructure in women with osteoporosis. Results of a 2-year study. Osteoporosis International 23, 305-315. Epub 2011 Sep 2010.

Rohl L., Larsen E., Linde F., Odgaard A., Jorgensen J., 1991. Tensile and compressive properties of cancellous bone. Journal of Biomechanics 24, 1143-1149.

Ruegsegger P., Koller B., Muller R., 1996. A microtomographic system for the nondestructive evaluation of bone architecture. Calcified Tissue International 58, 24-29.

Schaffler M.B., Burr D.B., 1988. Stiffness of compact bone: effects of porosity and density. Journal of Biomechanics 21, 13-16

Schileo E., Dall'ara E., Taddei F., Malandrino A., Schotkamp T., Baleani M., Viceconti M., 2008. An accurate estimation of bone density improves the accuracy of subject-specific finite element models. Journal of Biomechanics 41, 2483-2491

Schileo E., Taddei F., Malandrino A., Cristofolini L., Viceconti M., 2007. Subject-specific finite element models can accurately predict strain levels in long bones. Journal of Biomechanics 40, 2982-2989

Schwiedrzik J.J., Zysset P.K., 2012. An anisotropic elastic-viscoplastic damage model for bone tissue. Biomechanics and Modelling in Mechanobiology

Silva M.J., Wang C., Keaveny T.M., Hayes W.C., 1994. Direct and computed tomography thickness measurements of the human, lumbar vertebral shell and endplate. Bone 15, 409-414

Sode M., Burghardt A.J., Kazakia G.J., Link T.M., Majumdar S., 2010. Regional variations of gender-specific and age-related differences in trabecular bone structure of the distal radius and tibia. Bone 46, 1652-1660. Epub 2010 Feb 1625.

Taddei F., Cristofolini L., Martelli S., Gill H.S., Viceconti M., 2006. Subject-specific finite element models of long bones: An in vitro evaluation of the overall accuracy. Journal of Biomechanics 39, 2457-2467. Epub 2005 Oct 2456.

Tassani S., Ohman C., Baruffaldi F., Baleani M., Viceconti M., 2010. Volume to density relation in adult human bone tissue. Journal of biomechanics

Thomsen J.S., Ebbesen E.N., Mosekilde L., 2002. Zone-dependent changes in human vertebral trabecular bone: clinical implications. Bone 30, 664-669.

Trabelsi N., Yosibash Z., 2011. Patient-specific finite-element analyses of the proximal femur with orthotropic material properties validated by experiments. J Biomed Eng 133, 061001.

Tschirhart C.E., Finkelstein J.A., Whyne C.M., 2006. Optimization of tumor volume reduction and cement augmentation in percutaneous vertebroplasty for prophylactic treatment of spinal metastases. J Spinal Disord Tech 19, 584-590.

Turner C.H., 1989. Yield behavior of bovine cancellous bone. J Biomed Eng 111, 256-260.

Turner C.H., 2006. Bone strength: current concepts. Annals of the New York Academy of Science 1068, 429-446

Turner C.H., Cowin S.C., Rho J.Y., Ashman R.B., Rice J.C., 1990. The fabric dependence of the orthotropic elastic constants of cancellous bone. Journal of Biomechanics 23, 549-561.

Van Rietbergen B., Huiskes R., Eckstein F., Ruegsegger P., 2003. Trabecular bone tissue strains in the healthy and osteoporotic human femur. Journal of Bone and Mineral Reasearch 18, 1781-1788.

van Rietbergen B., Weinans H., Huiskes R., Odgaard A., 1995. A new method to determine trabecular bone elastic properties and loading using micromechanical finite-element models. Journal of Biomechanics 28, 69-81.

Varga P., 2009. Prediction of Distal Radius Fracture Load Using HR–pQCT–based Finite Element Analysis. Ph. D. thesis, Vienna University of Technology, Vienna.

Varga P., Baumbach S., Pahr D., Zysset P.K., 2009. Validation of an anatomy specific finite element model of Colles' fracture. Journal of Biomechanics 42, 1726-1731

Varga P., Dall'Ara E., Pahr D.H., Pretterklieber M., Zysset P.K., 2011. Validation of an HR-pQCT-based homogenized finite element approach using mechanical testing of ultra-distal radius sections. Biomechanics and Modelling in Mechanobiology 10, 431-444

Varga P., Zysset P.K., 2009. Assessment of volume fraction and fabric in the distal radius using HR-pQCT. Bone 45, 909-917

Verhulp E., van Rietbergen B., Huiskes R., 2006. Comparison of micro-level and continuum-level voxel models of the proximal femur. Journal of Biomechanics 39, 2951-2957. Epub 2005 Dec 2915.

Verhulp E., van Rietbergen B., Huiskes R., 2008. Load distribution in the healthy and osteoporotic human proximal femur during a fall to the side. Bone 42, 30-35

Viceconti M., 2012. Multiscale modeling of the skeletal system. Cambridge University Press, Cambridge

Viceconti M., Bellingeri L., Cristofolini L., Toni A., 1998. A comparative study on different methods of automatic mesh generation of human femurs. Medical Engineering and Physics 20, 1-10.

Viceconti M., Olsen S., Nolte L.P., Burton K., 2005. Extracting clinically relevant data from finite element simulations. Clinical Biomechanics (Bristol, Avon) 20, 451-454.

Viceconti M., Taddei F., Cristofolini L., Martelli S., Falcinelli C., Schileo E., 2012. Are spontaneous fractures possible? An example of clinical application for personalised, multiscale neuro-musculo-skeletal modelling. Journal of Biomechanics 45, 421-426. Epub 2011 Dec 2026.

Vilayphiou N., Boutroy S., Sornay-Rendu E., Van Rietbergen B., Munoz F., Delmas P.D., Chapurlat R., 2010. Finite element analysis performed on radius and tibia HR-pQCT images and fragility fractures at all sites in postmenopausal women. Bone 46, 1030-1037

Wakao N., Harada A., Matsui Y., Takemura M., Shimokata H., Mizuno M., Ito M., Matsuyama Y., Ishiguro N., 2009. The effect of impact direction on the fracture load of osteoporotic proximal femurs. Medical Engineering and Physics 31, 1134-1139. Epub 2009 Aug 1138.

Wang X., Sanyal A., Cawthon P.M., Palermo L., Jekir M., Christensen J., Ensrud K.E., Cummings S.R., Orwoll E., Black D.M., Keaveny T.M., 2012. Prediction of new

clinical vertebral fractures in elderly men using finite element analysis of CT scans. Journal of Bone and Mineral Research 27, 808-816. doi: 810.1002/jbmr.1539.

Webster S.J., 2001. Integrated Bone Tissue Physiology: Anatomy and Physiology. In Cowin S.C. (ed) Bone Mechanics Handbook, Second edn. Informa Healthcare USA, Inc., New York, pp 1.1-1.68

Whitehouse W.J., 1974. The quantitative morphology of anisotropic trabecular bone. J Microsc 101, 153-168.

WHO, 1994. Assessment of fracture risk and its application to screening for postmenopausal osteoporosis. Technical Report Series. WHO, Geneve

Whyne C.M., Hu S.S., Lotz J.C., 2003. Burst fracture in the metastatically involved spine: development, validation, and parametric analysis of a three-dimensional poroelastic finite-element model. Spine 28, 652-660

Wijayathunga V.N., Jones A.C., Oakland R.J., Furtado N.R., Hall R.M., Wilcox R.K., 2008. Development of specimen-specific finite element models of human vertebrae for the analysis of vertebroplasty. Proceedingd of the Institution of Mechanical Engineering Part H, journal of engineering in medicine 222, 221-228.

Wilcox R.K., 2006. The biomechanical effect of vertebroplasty on the adjacent vertebral body: a finite element study. Proceedings of the Institution of Mechanical Engineering: Part H 220, 565-572

Wilcox R.K., 2007. The influence of material property and morphological parameters on specimen-specific finite element models of porcine vertebral bodies. Journal of Biomechanics 40, 669-673

Wille H., Rank E., Yosibash Z., 2012. Prediction of the mechanical response of the femur with uncertain elastic properties. Journal of Biomechanics 45, 1140-1148. Epub 2012 Mar 1113.

Wolff J., 1892. Das Gesetz der Transformation der Knochen. Hirschwald, A., Berlin

Wolfram U., Schmitz B., Heuer F., Reinehr M., Wilke H.J., 2009. Vertebral trabecular main direction can be determined from clinical CT datasets using the gradient structure tensor and not the inertia tensor--a case study. Journal of Biomechanics 42, 1390-1396. Epub 2009 May 1317.

Wolfram U., Wilke H.J., Zysset P.K., 2010. Valid micro finite element models of vertebral trabecular bone can be obtained using tissue properties measured with nanoindentation under wet conditions. Journal of Biomechanics 43, 1731-1737. Epub 2010 Mar 1735.

Wolfram U., Wilke H.J., Zysset P.K., 2011. Damage accumulation in vertebral trabecular bone depends on loading mode and direction. Journal of Biomechanics 44, 1164-1169. Epub 2011 Feb 1164.

Yang H., Ma X., Guo T., 2010. Some factors that affect the comparison between isotropic and orthotropic inhomogeneous finite element material models of femur. Medical Engineering and Physics 32, 553-560.

Yosibash Z., Trabelsi N., Milgrom C., 2007. Reliable simulations of the human proximal femur by high-order finite element analysis validated by experimental observations. Journal of Biomechanics 40, 3688-3699. Epub 2007 Aug 3613.

Zani L., Juszczyk M., Grassi L., Cristofolini L., Viceconti M., 2010. Developing a set-up for sideway fall testing of the proximal neck of the human femur. 17th Congress of the ESB, Edinburgh, UK, 05-08 July. Poster Presentation

Zysset P.K., 2003. A review of morphology-elasticity relationships in human trabecular bone: theories and experiments. Journal of Biomechanics 36, 1469-1485.

Zysset P.K., Curnier A., 1996. A 3D damage model for trabecular bone based on fabric tensors. Journal of Biomechanics 29, 1549-1558

Zysset P.K., Sonny M., Hayes W.C., 1994. Morphology-mechanical property relations in trabecular bone of the osteoarthritic proximal tibia. J Arthroplasty 9, 203-216.

Chapter 2

BMD to BV/TV calibration study

From the manuscript:

A Calibration methodology of QCT BMD for Human Vertebral Body with Registered Micro-CT images

E. Dall'Ara, P. Varga , D. Pahr , P. Zysset

Institute of Lightweight Design and Structural Biomechanics, Vienna University of Technology, Vienna, Austria

Published in: Medical Physics Vol. 38, 2602-08, 2011

Abstract

Purpose: The accuracy of QCT-based homogenized Finite Element (FE) models is strongly related to the accuracy of the prediction of bone volume fraction (BV/TV) from bone mineral density (BMD). The goal of this study was to establish a calibration methodology to relate the BMD computed with QCT with the BV/TV computed with Micro-CT (μCT) over a wide range of bone mineral densities and to investigate the effect of region size in which BMD and BV/TV are computed.

Method: Six human vertebral bodies were dissected from the spine of six donors and scanned submerged in water with QCT (voxel size: 0.391x0.391x0.450 mm^3) and μCT (isotropic voxel size: 0.018^3 mm^3). The μCT images were segmented with a single level threshold. Afterwards QCT-greyscale, μCT-greyscale and μCT-segmented images were registered. Two isotropic grids of 1.230 mm (small) and 4.920 mm (large) were superimposed on every image and QCT_{BMD} was compared both with μCT_{BMD} and $\mu CT_{BV/TV}$ for each grid cell.

Results: The ranges of QCT_{BMD} for large and small regions were 9-559 mg/cc and (-90)-1006 mg/cc, respectively. QCT_{BMD} was found to overestimate μCT_{BMD}. No significant differences were found between the QCT_{BMD}-$\mu CT_{BV/TV}$ regression parameters of the two grid sizes. However, the R^2 was higher and the SEE was lower for large regions when compared to small regions. For the pooled data, an extrapolated QCT_{BMD} value equal to 1062 mg/cc was found to correspond to 100% $\mu CT_{BV/TV}$.

Conclusion: A calibration method was defined to evaluate BV/TV from QCT_{BMD} values for cortical and trabecular bone *in vitro*. The QCT_{BMD}-$\mu CT_{BV/TV}$ calibration was found to be dependent on the scanned vertebral section, but not on the size of the regions. However, the higher SEE computed for small regions suggests that the deleterious effect of QCT image noise on FE modelling increases with decreasing voxel size.

Keywords: Human vertebrae, Bone density, Bone Volume Fraction, Computed Tomography, CT Calibration

2.1 Introduction

The FE method has been largely used in the last decades to predict bones stiffness and strength from clinical diagnostic images (Crawford, et al., 2003; Dall'Ara, et al., 2010; Keyak and Falkinstein, 2003; Varga, et al., 2009; Vilayphiou, et al., 2010). While high-resolution images of the wrist and of the ankle can be acquired *in vivo* with a high resolution peripheral QCT (HR-pQCT, down to an isotropic voxel size of 0.082^3 mm^3) only low resolution (isotropic voxel size in the order of 0.5^3-1^3 mm^3) images from QCT are currently available for clinical applications in the spine and the hip. Although micro-FE models can be generated from HR-pQCT images through identification of trabecular structure (Macneil and Boyd, 2008; Mueller, et al., 2009), for femur and vertebrae the low resolution of QCT allows only for homogenized FE (Chevalier, et al., 2008; Crawford, et al., 2003; Dall'Ara, et al., 2010; Keyak and Falkinstein, 2003; Schileo, et al., 2007). It has recently been shown that BV/TV-based homogenized FE models predict vertebral stiffness and strength accurately (Crawford, et al., 2003; Dall'Ara, et al., 2010; Pahr and Zysset, 2009a). Moreover, when subject specific cortical thickness were included in the model, the predictions improved (Chevalier, et al., 2009). Therefore, both trabecular BV/TV and cortical thickness should be computed to correctly assign homogenized material properties, which are defined by using experimentally validated constitutive laws (Ciarelli, et al., 2000; Goulet, et al., 1994; Rincon-Kohli and Zysset, 2009). BV/TV can be computed from segmented images generated from micro-CT grey-scale images by reducing high frequency noise with a Gaussian filter and applying a threshold value to distinguish bone from marrow (Kazakia, et al., 2008). Polychromatic desktop X-ray µCT has been shown to measure BV/TV accurately compared to Archimedes' method (Ding, et al., 1999), but to underestimate tissue mineralization compared to synchrotron radiation µCT (SR-µCT) and to ash density (ρ_{ash}) measurements by approximately 15% and 20%, respectively (Kazakia, et al., 2008). However in humans, due to the high radiation dose and small volume of analysis, µCT can only be used to scan *ex vivo* biopsies. On the other hand, the low resolution of QCT images does not allow to measure BV/TV, but only BMD, that is computed in every voxel using a calibration phantom, which contains inserts of HA-equivalent-resin mixtures with well known density (Adams, 2009). Moreover, the dimension of the finite elements generated from QCT images for vertebral bodies are usually about 1-1.5mm (Buckley, et al., 2007; Chevalier, et al., 2009; Dall'Ara, et al., 2010; Kazakia, et al., 2008) in order to achieve a good compromise between accuracy of the prediction and computation time (Jones and Wilcox, 2007). As the dimension of the finite elements is roughly three times larger then the cortical shell's thickness, cortical and trabecular bone can not be accurately distinguished. In particular, there are elements close to the shell, which are partially composed by trabecular and cortical bone. For the above-mentioned reasons, QCT-based FE models require a calibration law between BV/TV and QCT_{BMD} valid for a wide range of density to assign material properties to each element. The QCT_{BMD}-$\mu CT_{BV/TV}$ relationship might be defined by combining already published correlations between QCT_{BMD}-ρ_{ash} (Schileo, et al., 2008) and ρ_{ash}-$\mu CT_{BV/TV}$ (Tassani, et al., 2010) recently defined for trabecular and cortical bone extracted from the human femur. However, this methodology has a main limitation when applied to the vertebral body. In fact, while ρ_{ash} is a reliable measurement when applied to cortical bone samples extracted from the human long bones, the evaluation of ρ_{ash} for cortical bone tissue extracted from human vertebral body is affected by large experimental errors, due to the thin cortical shell and endplates (typically about 0.38mm (Eswaran, et al., 2006) and 0.35mm (Silva, et al., 1994) thick, respectively). To circumvent this limitation, in the present study we propose a

method to calibrate the QCT images with BV/TV measured in registered and segmented images obtained with μCT.
The main aim of this study was to develop a method applicable to human vertebral bodies *in vitro* to calibrate the bone mineral density computed with QCT with the bone volume fraction computed with μCT over a wide range of densities. The specific aims were to determine:

- The QCT_{BMD}-μCT_{BMD} relationship to compare the BMD calibration values of the two scanners;
- The μCT_{BMD}-$\mu CT_{BV/TV}$ relationship to evaluate tissue mineral density;
- The QCT_{BMD}-$\mu CT_{BV/TV}$ relationship to be used for calibration of homogenized FE based on BV/TV *in vitro*;
- The effect of the size of the region in which BMD and BV/TV are computed on the above relationships.

2.2 Materials and methods

2.2.1 Samples

Six vertebrae (T11-L4) were extracted from six human cadavers (males, age 44-82) and then prepared as described in a previous study (Dall'Ara, et al., 2010). The vertebrae were received from the Clinical Department of Pathology, Medical University of Vienna, Austria. The Medical University of Vienna ethics commission approved the procedures applied during the present study. Soft tissues, posterior element and cortical endplates were removed to obtain vertebral body sections. The specimens were stored at -20 °C when not processed.

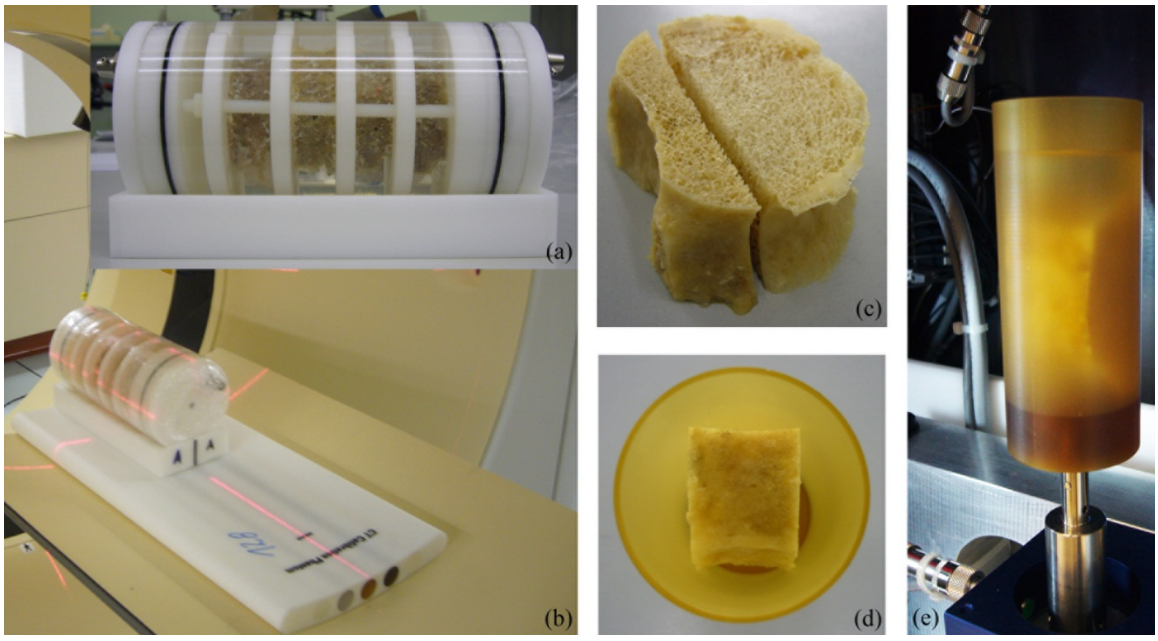

Figure 2. 1: Scanning procedure. Samples were placed in a home made sample holder (a) and then scanned with a QCT (b). After reducing the size (c-d) each slice was scanned with a μCT (e).

2.2.2 Scanning

Each vertebra was submerged in 0.9% NaCl saline solution, exposed to vacuum for ten minutes to remove air bubbles and placed in a custom made Plexiglas chamber (Figure 2.1a). The sections were then scanned (Figure 2.1b) together with a K_2HPO_4 calibration phantom (*Model 3 CT Calibration Phantom, Mindways Software, U.S.A.*) in a clinical QCT (*Brilliance64, Philips, Germany*) with the same settings used for clinical analysis of the lumbar spine: Voltage 140 kV, Intensity 200 mA, Matrix 512x512, in-plane pixel size 0.391x0.391 mm^2, slice thickness 0.450 mm. The standard beam hardening correction developed by the manufacturer was used. Afterwards, the most posterior parts of three vertebral bodies (one example in Figure 2.1c), or two parts on the lateral sides for the remaining three samples, were removed by means of a band saw (*300 CP, Exakt Gmbh, Germany*) to fit the dimension of the largest sample holder (Figure 2.1d) of a μCT *(μCT40, Scanco Medical AG, Switzerland*). The removed parts were selected to keep as much cortical shell as possible. After other ten minutes of vacuum exposure to remove residual air bubbles, the samples were scanned submerged in 0.9% NaCl (Fig. 1e) with the μCT (Voltage 70 kV, Intensity: 114 mA, Matrix 2048x2048, isotropic voxel size 0.018^3 mm^3). To minimize the influence of specimen geometry on reconstructed linear attenuation values, a beam hardening correction, based on a step wedge phantom composed of a HA-resin mixture (200 mg HA/cm^3), was applied. The equivalent BMD in mg/cm^3 was computed in each voxel of both QCT and μCT images by converting the grey-scale with the respective calibration phantoms. For μCT the standard procedure suggested by the manufacturer was used. The BMD range was restricted to -100 and 1059 mg/cm^3 for each voxel (Chevalier, et al., 2008; Dall'Ara, et al., 2010), to exclude extreme values due to image noise, residual bubbles or to hypermineralized tissue located in the inner part of osteophytes. The upper limit was found to concern less than 0.01% of the number of the evaluated voxels and was therefore considered as appropriate.

2.2.3 Image processing

Each QCT image was rotated and translated to roughly match the corresponding μCT image and then re-sampled to a final voxel size of 0.410^3 mm^3. The QCT and μCT images were then registered (3D rigid registration; *ITK, Kitware, U.S.A.*) and cropped to fit the size of the smaller μCT images. Afterwards, the QCT and μCT images of each vertebra were divided in three regions to reduce the file dimension and therefore the computer's memory required during processing. A filling-out algorithm was used to identify the external surface of the cortical shell (Pahr and Zysset, 2009b) in the QCT images and the resulting mask was used to crop both QCT and μCT images (Figure 2.2a-b). A Gaussian filter (σ=1.2, radius equal to two voxels) was applied to the μCT images (Pahr and Zysset, 2009a) to remove high frequency noise. A single level threshold was then computed using the iterative selection method of Ridler and Calvard (Ridler and Calvard, 1978) for each of the 18 obtained regions. The average of the 18 computed iterative thresholds values was applied to each region to obtain segmented images (Figure 2.2c). For each region two isotropic grids of different size (4.920 and 1.230 mm, respectively) were superimposed to the three registered images (QCT-greyscale, μCT-greyscale and μCT-segmented). The 1.230 mm size was chosen as it is representative of the voxel size typically used in QCT based FE analyses and allowed to obtain high density regions by including the cortical shell. The larger grid was used to investigate the effect of the image's noise on the evaluated quantities. For each cube defined by both grids, QCT_{BMD} and μCT_{BMD} were

computed from QCT-greyscale and μCT-greyscale images, respectively. $\mu CT_{BV/TV}$ was computed from μCT-segmented images by dividing the volume of bone by the total volume of the selected cube of the grid. In all three cases the volume outside the mask was not included in the calculation of the total volume.

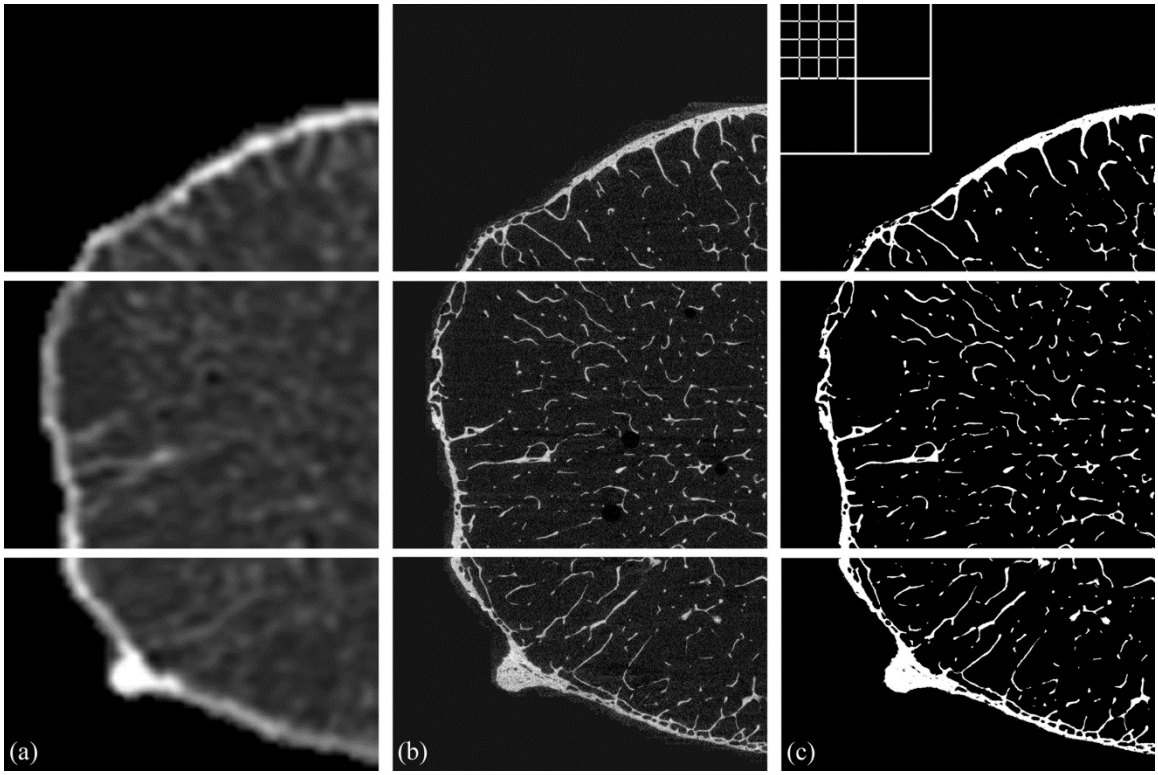

Figure 2. 2: Cross sections of masked QCTgreyscale (a), μCTgreyscale and (b) and μCTsegmented (c) images for one vertebral section divided in three regions. The white large and small squares represent the large and small grid size, respectively.

2.2.4 Data analysis

All statistical analyses were performed with R (R Foundation for Statistical Computing, (Crawley, 2005)). Linear regressions were used to model the relationships between QCT_{BMD}-μCT_{BMD}, μCT_{BMD}-$\mu CT_{BV/TV}$ and QCT_{BMD}-$\mu CT_{BV/TV}$. The regression lines computed for the data separated for different grid sizes were analyzed with analysis of covariance (ANCOVA). The coefficient of determination (R^2) and standard error of the estimate (SEE) were computed from the above-mentioned linear regressions both for the pooled data including large and small regions together and for the data separated for different grid size.

2.3 Results

The QCT_{BMD} range for large and small regions was 9-559 mg/cm³ (N=328) and -90-1006 mg/cm³ (N=29109), respectively. Linear regressions between μCT_{BMD} and QCT_{BMD} for different grid sizes were not statistically different (Figure 2.3, p=0.399). Moreover the linear regression for the pooled data (μCT_{BMD} = 0.671 QCT_{BMD} + 30.156) was statistically

distinct from identity (95% confidence interval intercept 29.545-30.767, confidence interval slope 0.668-0.674).

A significant but small difference was found between the μCT_{BMD}-$\mu CT_{BV/TV}$ regressions separated for the two different grid sizes (Figure 2.4, p=0.038). In particular, slopes and intercepts differed by approximately 2%. Accordingly, the extrapolated μCT_{BMD} values corresponding to 100% $\mu CT_{BV/TV}$ differed by approximately 2% (747 and 763 mg/cm³ for small and large regions, respectively).

No significant difference was found for different grid sizes between the regressions QCT_{BMD}-$\mu CT_{BV/TV}$ (Figure 2.5, p=0.142). However, in case of large regions R^2 was higher and SEE was lower than the ones for small regions (R^2=0.95 and R^2=0.83, respectively; SEE=1.69 and SEE=4.17, respectively). For the pooled data, the extrapolated QCT_{BMD} value corresponding to 100% $\mu CT_{BV/TV}$ was 1062 mg/cm³ (1061 and to 1106 mg/cm³ for small and large regions, respectively) and the intercept of the regression was found to be not significantly different from zero (95% confidence interval between -0.115 and 0.061). Moreover, significantly different regression lines (in all cases p<0.02) were obtained when the data were grouped in vertebral sections (the ranges of slope, intercept and QCT_{BMD} values corresponding to 100% $\mu CT_{BV/TV}$ were 0.086-0.107 %*cm³/mg, (-2.79) -1.68 % and 961-1142 mg/cm³, respectively).

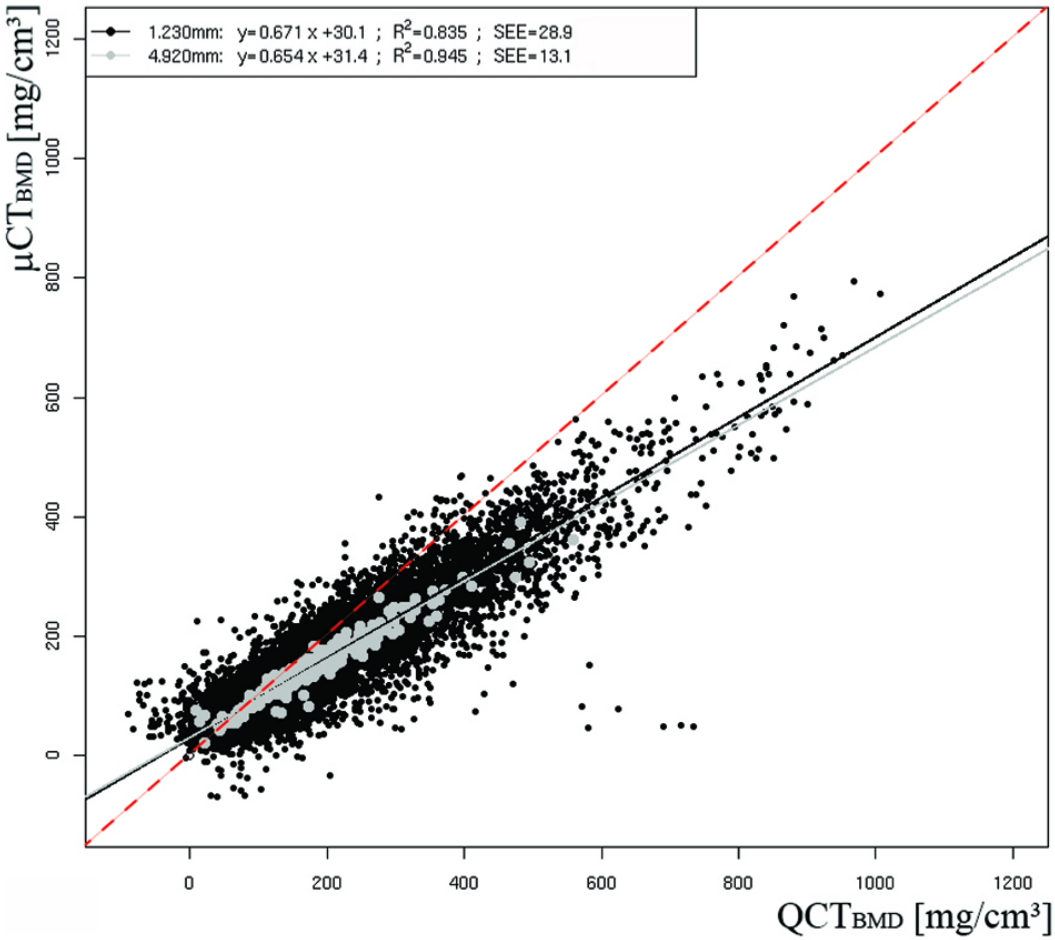

Figure 2. 3: Correlations between QCT_{BMD} and μCT_{BMD} separated for small (black dots) and large (grey dots) grid size. The legend reports grid size, regression equation, coefficient of determination, standard error of the estimate and QCT_{BMD} extrapolated value for 100% BV/TV, respectively. The dashed red line represents the 1:1 relationship.

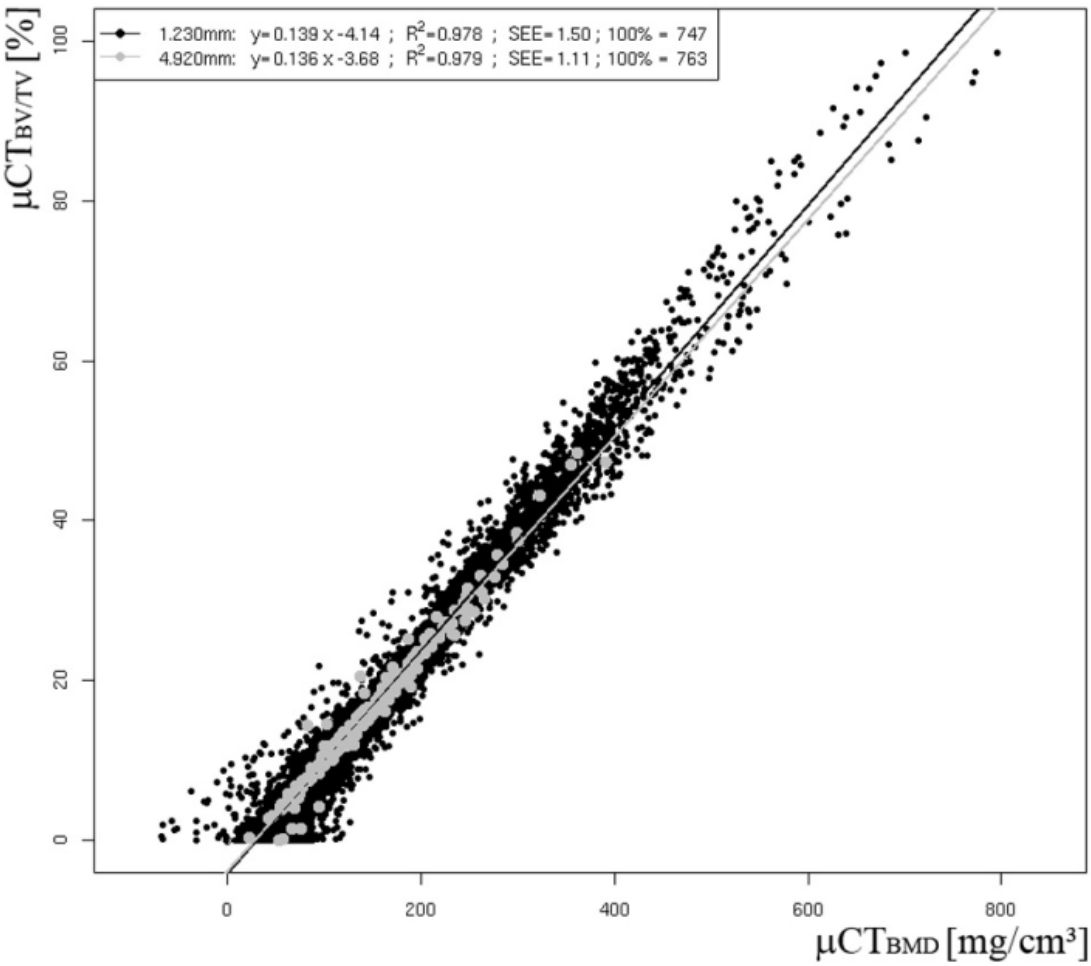

Figure 2. 4: Correlations between μCT_{BMD} and $\mu CT_{BV/TV}$ separated for small (black dots) and large (grey dots) grid size. The legend reports grid size, regression equation, coefficient of determination, standard error of the estimate and μCT_{BMD} extrapolated value for 100% BV/TV, respectively.

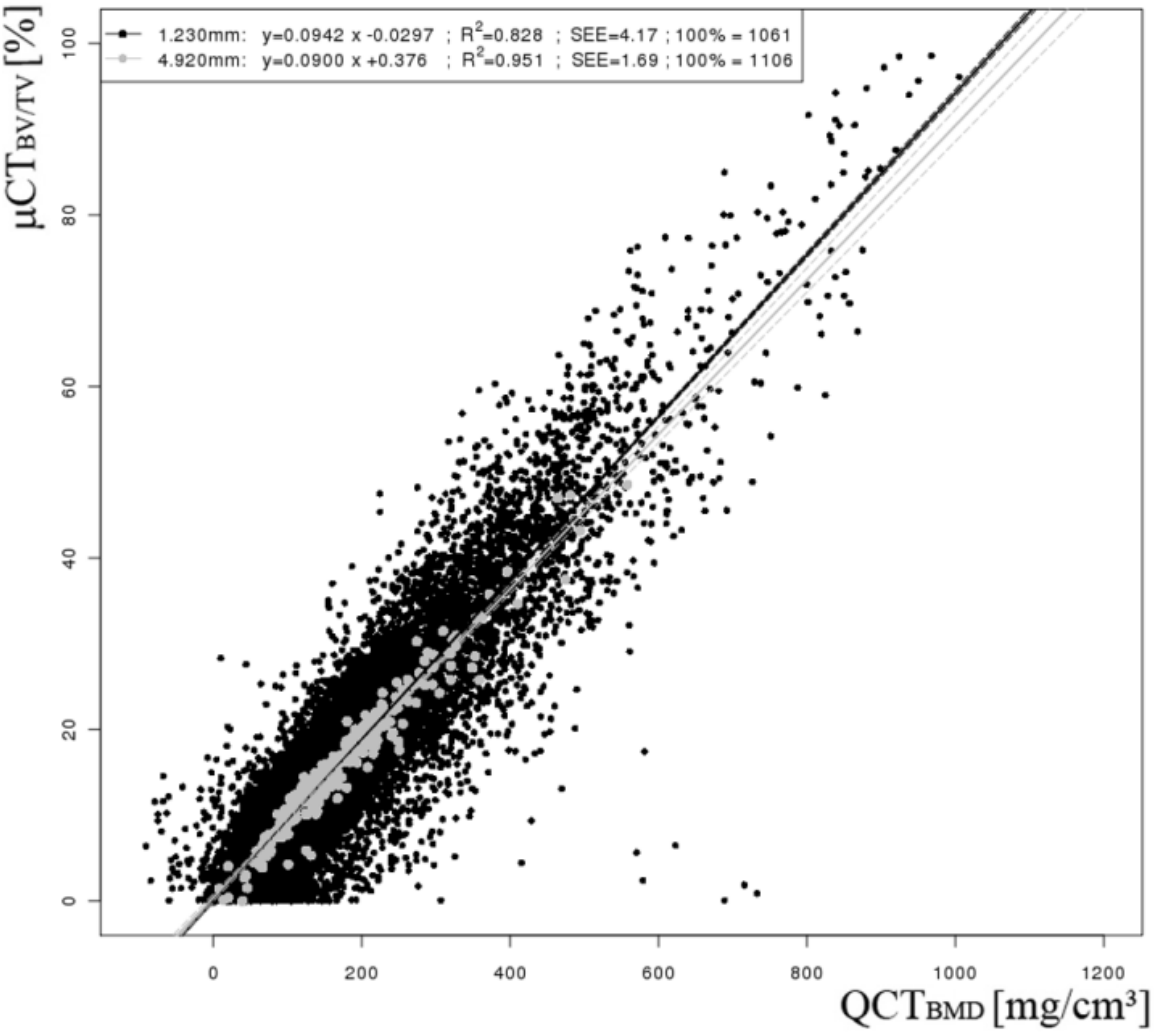

Figure 2. 5: Correlations between QCT_{BMD} and $\mu CT_{BV/TV}$ separated for small (black dots) and large (grey dots) grid size. The legend reports grid size, regression equation, coefficient of determination and standard error of the estimate, respectively. Dashed lines represent the 95% confidence intervals (black for the small and grey for the large grid sizes). The high density regions ($\mu CT_{BV/TV}$ greater than 65%) are the 0.3% of the total number of points.

2.4 Discussion

The aim of this study was to develop a method to compute BV/TV from BMD measured in QCT images of human vertebral body *in vitro* for the whole density range by using registered QCT and µCT images.

A significant difference between the 1:1 line and the linear regression QCT_{BMD}-μCT_{BMD} was found. Even if the intercept of the linear regression is significantly different but not far from zero (3.8% of the maximum value), the slope was substantially lower than one. Moreover, the extrapolated value of μCT_{BMD} for 100% $\mu CT_{BV/TV}$ is much lower than experimental values reported recently in the literature (747-763 mg/cm³ vs. 900-1200 mg/cm³ from ρ_{ash} measurements of the femur (Schileo, et al., 2008; Tassani, et al., 2010) and 1060-1160 mg/cm³ from SR-µCT analysis of different anatomical sites (Kazakia, et al., 2008; Raum, et al., 2006)). The underestimation of tissue density computed with µCT in

the present study is in line with the results reported by Kazakia et al. (2008) who didn't find any difference between $\mu CT_{BV/TV}$ and SR-$\mu CT_{BV/TV,}$ although they found an underestimation of tissue mineral density computed with µCT compared to the one computed with SR-µCT. Conversely, the extrapolated value of QCT_{BMD} for 100% $\mu CT_{BV/TV}$ (1062 mg/cm³) found in the present study for the pooled data is in line with the above reported experimental results. The difference between the BMD values measured with the two scanners might be due to the different calibration procedure used to compute BMD from greyscale images. The few points far from the regression lines of the QCT_{BMD}-μCT_{BMD} and $\mu CT_{BV/TV}$-QCT_{BMD} relationships were probably due to the presence of a few bubbles, which were not removed by the vacuum procedure. Indeed, if in a certain region of the vertebral body a bubble was removed before the QCT scan but not before the µCT one, after image registration a high QCT_{BMD} could correspond to $\mu CT_{BV/TV}$ or μCT_{BMD} values close to 0.

The slope of the μCT_{BMD}-$\mu CT_{BV/TV}$ relation for the small regions was found to be significantly but only slightly higher than the one for large regions. The 2% difference in the slope and therefore in the μCT_{BMD} at 100% $\mu CT_{BV/TV}$ found in the present study seem to indicate a slight dependence of the tissue mineral density estimated with µCT on the dimension of the regions. This effect is due to the different ranges of BV/TV for the small and the large regions. Indeed, if the range of BV/TV computed for small regions was restricted to the same computed for the large ones, the difference between the two regression lines were not significantly different anymore (p=0.605).

Furthermore, if the linear law between $\mu CT_{BV/TV}$-QCT_{BMD} computed combining the linear regressions found by Tassani et al. (Tassani, et al., 2010) (ρ_{ash}-$\mu CT_{BV/TV}$) and Schileo et al. (Schileo, et al., 2008) (ρ_{ash}-QCT_{BMD}) was used, the QCT_{BMD} value for extrapolated 100% $\mu CT_{BV/TV}$ was higher than the one found in the present study for the pooled data (1268 vs 1062 mg/cm³). This might be due to the different measurement techniques, sample size and anatomical site investigated in the two mentioned studies.

For smaller grid size, as expected, the range of values for $\mu CT_{BV/TV}$ and QCT_{BMD} substantially increased, however the variability in the measurements increased as well (lower R^2, higher SEE). Moreover, the absence of significant difference between $\mu CT_{BV/TV}$-QCT_{BMD} regression lines for data separated for grid sizes suggests that the used linear model is valid also for high-density regions. For the pooled data, the regression line remained similar to the one for small regions (10% difference between the intercepts and 4% difference between the slopes). The few high density points (only 0.3% of the points with $\mu CT_{BV/TV}$ greater than 65%) fit well with the regression lines computed for the pooled data even though the SEE was higher (11.7) compared to the one of low density regions for the same regression line. This finding has an important impact on the generation of subject specific FE models from QCT images of the human vertebrae: it suggests that a unique linear (with intercept equal to zero) calibration equation for the whole range of BMD is appropriate. Moreover the extrapolated value of BMD for pure bone tissue (100% BV/TV) was found to be 1062 mg/cm³ that can be used as an upper bound to limit the BMD range during the generation of FE models. Furthermore, the higher SEE computed for small regions suggests that the deleterious effect of QCT image noise on FE modelling increases with decreasing voxel dimension. Therefore, a possible solution to increase the prediction ability of FE models might be to increase the size of the volume in which the BMD is averaged for each voxel. It remains to be demonstrated if the inaccuracies of BV/TV, introduced by the higher standard error in the QCT_{BMD}-$\mu CT_{BV/TV}$ relationship for small grid size, would increase the heterogeneity in the mechanical properties of adjacent voxels and therefore the errors in the prediction of stiffness and strength due to stress localization.

This consideration is in line with the results found by Johns and Wilcox (Jones and Wilcox, 2007), who performed an accuracy study to investigate the effect of voxel size on the ability of FE model to predict experimental stiffness and strength, by testing porcine vertebrae *in vitro*. They found the predictive ability to increase (R^2 from 0.83 to 0.98 for stiffness and from 0.74 to 0.88 for strength) if voxel size increased from 1x1x1 mm^3 to 2x2x2 mm^3, followed by a drop of R^2 for stiffness if voxel size was larger. However, if the calibration found in the present study was used to generate QCT-based FE models for vertebral bodies scanned *in vitro*, a good quantitative agreement with experimental results was found for mechanical properties (for elastic modulus: R^2=0.70, slope=0.92, intercept=-50 MPa; for strength: R^2=0.80, slope=0.90, intercept=41 MPa, data adapted from (Dall'Ara, et al., 2010)). Therefore, the random error introduced with the wide scatter in the QCT_{BMD}-$\mu CT_{BV/TV}$ calibration law for the small regions, seems to be somehow balanced during the computation of the global mechanical properties of the samples with the FE models. Furthermore, the regression lines of the data separated for subject were found to be significantly different. While for the low-density range the lines are similar, for higher densities the differences become larger. In particular, when separated for subject, a wide range of extrapolated QCT_{BMD} for 100% $\mu CT_{BV/TV}$ is found (961-1142 mg/cm^3). This differences could be due to different marrow composition, density, mass, dimension and shape of the six samples, which have been shown to affect reconstruction artefacts and therefore BMD and BV/TV measurements (Fajardo, et al., 2009). However, as the goal of this study was to define a general method to investigate the QCT_{BMD}-$\mu CT_{BV/TV}$ calibration law, valid for different subjects, pooling the data appeared to be the best choice.

This study has also a number of limitations. First, direct experimental measurements of the real mineral density in the investigated sub-regions were not performed. Second, the standard beam hardening correction based on a wedge phantom with 200 mg HA/cm^3 insertions was used, even though it was found (Kazakia, et al., 2008) that the correction based on wedge phantom with higher density insertions (1200 mg HA/cm^3) increases the accuracy of the µCT measurements by decreasing the cupping artefacts (Barrett and Keat, 2004) of the reconstructed images. Third, as cortical endplates, posterior elements and soft tissues around the vertebrae were removed, we studied an ideal scanning configuration. In fact, the vertebrae were not scanned *in situ* and neither a body phantom was used but the samples were placed in a Plexiglas chamber filled with saline solution to simulate the soft tissues. The quantity of water around the samples might not be enough to simulate the large amount of soft tissues around the body during an *in vivo* scan. Therefore, the noise in our images was lower than for *in vivo/in situ* images and the calibration may as well be affected. Fourth, the six vertebrae which were included in the present study likely do not represent a full range of human bone variation. Considering the above mentioned differences among the regression lines grouped for vertebral sections, increasing the sample number and performing the scans *in vivo* would lead to a more general calibration law.

In conclusion, a new method to calibrate the QCT_{BMD} with the $\mu CT_{BV/TV}$ over a wide range of densities in human vertebral bodies *in vitro* was successfully applied. In particular: 1) The BMD values measured with µCT and QCT were significantly different. 2) µCT was found to underestimate BMD computed without any beam hardening correction compared to QCT and previously published experimental data. 3) QCT_{BMD}-$\mu CT_{BV/TV}$ calibration was computed successfully and was found to be dependent on the scanned vertebral section. 4) The size of the region in which the variables were averaged affected marginally the μCT_{BMD}-$\mu CT_{BV/TV}$ but not the QCT_{BMD}-$\mu CT_{BV/TV}$ and QCT_{BMD}-μCT_{BMD} regressions. In all cases, the SEE computed from large regions was higher than the one for small regions.

The calibration found in this study was used to generate BV/TV-based FE models from QCT scans performed *in vitro* (Dall'Ara, et al., 2010). In particular, the equations found are valid only for the two scanners used in the present work. However, the same method applied to human vertebrae scanned *in situ* could be used to generate BV/TV-based FE models *in vivo*.

Acknowledgements
The authors acknowledge a grant for an interuniversity computer tomography network from the UniInfrastruktur Program III of the Austrian Ministry for Science and Research (bm: bwk). The authors gratefully acknowledge DR Reinhard Schmidt for having collected the bone tissue used in the present study and Prof Franz Kainberger for giving us the opportunity to use the QCT.

Bibliography

Adams J.E., 2009. Quantitative computed tomography. European Journal of Radiology 12, 12

Barrett J.F., Keat N., 2004. Artifacts in CT: recognition and avoidance. Radiographics 24, 1679-1691

Buckley J.M., Loo K., Motherway J., 2007. Comparison of quantitative computed tomography-based measures in predicting vertebral compressive strength. Bone 40, 767-774

Chevalier Y., Charlebois M., Pahra D., Varga P., Heini P., Schneider E., Zysset P., 2008. A patient-specific finite element methodology to predict damage accumulation in vertebral bodies under axial compression, sagittal flexion and combined loads. Computer Methods in Biomechanics and Biomedical Engineering 11, 477-487

Chevalier Y., Pahr D., Zysset P.K., 2009. The role of cortical shell and trabecular fabric in finite element analysis of the human vertebral body. J Biomed Eng 131, 111003

Ciarelli T.E., Fyhrie D.P., Schaffler M.B., Goldstein S.A., 2000. Variations in three-dimensional cancellous bone architecture of the proximal femur in female hip fractures and in controls. Journal of Bone and Mineral Reasearch 15, 32-40.

Crawford R.P., Cann C.E., Keaveny T.M., 2003. Finite element models predict in vitro vertebral body compressive strength better than quantitative computed tomography. Bone 33, 744-750

Crawley M.J. (2005) Statistics - an introduction using R. John Wiley & Sons, Chichester

Dall'Ara E., Schmidt R., Pahr D., Varga P., Chevalier Y., Patsch J., Kainberger F., Zysset P., 2010. A nonlinear finite element model validation study based on a novel experimental technique for inducing anterior wedge-shape fractures in human vertebral bodies in vitro. Journal of Biomechanics 43, 2374-2380

Ding M., Odgaard A., Hvid I., 1999. Accuracy of cancellous bone volume fraction measured by micro-CT scanning. Journal of Biomechanics 32, 323-326

Eswaran S.K., Gupta A., Adams M.F., Keaveny T.M., 2006. Cortical and trabecular load sharing in the human vertebral body. Journal of Bone and Mineral Research 21, 307-314

Fajardo R.J., Cory E., Patel N.D., et al., 2009. Specimen size and porosity can introduce error into microCT-based tissue mineral density measurements. Bone 44, 176-184

Goulet R.W., Goldstein S.A., Ciarelli M.J., Kuhn J.L., Brown M.B., Feldkamp L.A., 1994. The relationship between the structural and orthogonal compressive properties of trabecular bone. Journal of Biomechanics 27, 375-389.

Jones A.C., Wilcox R.K., 2007. Assessment of factors influencing finite element vertebral model predictions. J Biomed Eng 129, 898-903

Kazakia G.J., Burghardt A.J., Cheung S., Majumdar S., 2008. Assessment of bone tissue mineralization by conventional x-ray microcomputed tomography: comparison with synchrotron radiation microcomputed tomography and ash measurements. Medical Physics 35, 3170-3179

Keyak J.H., Falkinstein Y., 2003. Comparison of in situ and in vitro CT scan-based finite element model predictions of proximal femoral fracture load. Medical Engineering and Physics 25, 781-787

Macneil J.A., Boyd S.K., 2008. Bone strength at the distal radius can be estimated from high-resolution peripheral quantitative computed tomography and the finite element method. Bone 42, 1203-1213

Mueller T.L., Stauber M., Kohler T., Eckstein F., Muller R., van Lenthe G.H., 2009. Non-invasive bone competence analysis by high-resolution pQCT: an in vitro reproducibility study on structural and mechanical properties at the human radius. Bone 44, 364-371

Pahr D.H., Zysset P.K., 2009a. A comparison of enhanced continuum FE with micro FE models of human vertebral bodies. Journal of Biomechanics 42, 455-462

Pahr D.H., Zysset P.K., 2009b. From high-resolution CT data to finite element models: development of an integrated modular framework. Computer Methods in Biomechanics and Biomedical Engineering 12, 45-57

Raum K., Leguerney I., Chandelier F., Talmant M., Saied A., Peyrin F., Laugier P., 2006. Site-matched assessment of structural and tissue properties of cortical bone using scanning acoustic microscopy and synchrotron radiation muCT. Physics in Medicine and Biology 51, 733-746

Ridler T.W., Calvard S., 1978. Picture Thresholding Using an Iterative Selection Method. IEEE Transactions on Systems, Man and Cybernetics 8, 630-632

Rincon-Kohli L., Zysset P.K., 2009. Multi-axial mechanical properties of human trabecular bone. Biomechanics and Modeling in Mechanobiology 8, 195-208

Schileo E., Dall'ara E., Taddei F., Malandrino A., Schotkamp T., Baleani M., Viceconti M., 2008. An accurate estimation of bone density improves the accuracy of subject-specific finite element models. Journal of Biomechanics 41, 2483-2491

Schileo E., Taddei F., Malandrino A., Cristofolini L., Viceconti M., 2007. Subject-specific finite element models can accurately predict strain levels in long bones. Journal of Biomechanics 40, 2982-2989

Silva M.J., Wang C., Keaveny T.M., Hayes W.C., 1994. Direct and computed tomography thickness measurements of the human, lumbar vertebral shell and endplate. Bone 15, 409-414

Tassani S., Ohman C., Baruffaldi F., Baleani M., Viceconti M., 2010. Volume to density relation in adult human bone tissue. Journal of biomechanics

Varga P., Baumbach S., Pahr D., Zysset P.K., 2009. Validation of an anatomy specific finite element model of Colles' fracture. Journal of Biomechanics 42, 1726-1731

Vilayphiou N., Boutroy S., Sornay-Rendu E., Van Rietbergen B., Munoz F., Delmas P.D., Chapurlat R., 2010. Finite element analysis performed on radius and tibia HR-pQCT images and fragility fractures at all sites in postmenopausal women. Bone 46, 1030-1037

Chapter 3

hvFE validation study for the human vertebral body

From the manuscript:

A nonlinear finite element model validation study based on a novel experimental technique for inducing anterior wedge-shape fractures in human vertebral bodies *in vitro*

E. Dall'Ara [a], R. Schmidt [b], D. Pahr [a], P. Varga [a], Y. Chevalier [a], J. Patsch [c], F. Kainberger[c], P. Zysset [a]

a Institute of Lightweight Design and Structural Biomechanics, Vienna University of Technology, Austria
b Department of Traumatology, Medical University of Vienna, Austria
c Department of Radiology, Medical University of Vienna, Austria

Published in: Journal of Biomechanics Vol. 43(12), 2374-80, 2010

Abstract
Vertebral compression fracture is a common medical problem in osteoporotic individuals. The quantitative computed tomography (QCT)-based Finite Element (FE) method may be used to predict vertebral strength *in vivo*, but needs to be validated with experimental tests. The aim of this study was to validate a nonlinear anatomy specific QCT-based FE model by using a novel testing setup. Thirty-seven human thoracolumbar vertebral bone slices were prepared by removing cortical endplates and posterior elements. The slices were scanned with QCT and the volumetric bone mineral density (vBMD) was computed with the standard clinical approach. A novel experimental setup was designed to induce a realistic failure in the vertebral slices *in vitro*. Rotation of the loading plate was allowed by means of a ball joint. To minimize device compliance, the specimen deformation was measured directly on the loading plate with three sensors. A nonlinear FE model was generated from the calibrated QCT images and computed vertebral stiffness and strength were compared to those measured during the experiments. In agreement with clinical observations, most of the vertebrae underwent an anterior wedge-shape fracture. As expected, the FE method predicted both stiffness and strength better than vBMD (R^2 improved from 0.27 to 0.49 and from 0.34 to 0.79, respectively). Despite the lack of fitting parameters, the linear regression of the FE prediction for strength was close to the 1:1 relation (slope and intercept close to one (0.86) and to zero (0.72 kN), respectively). In conclusion, a nonlinear FE model was successfully validated through a novel experimental technique for generating wedge-shape fractures in human thoracolumbar vertebrae.

Keywords: Finite Element modelling, Bone mineral density, Bone strength, Osteoporosis, Mechanical testing

3.1 Introduction

Osteoporosis is a common skeletal disease causing bone mass reduction and bone microstructural changes. In osteoporotic individuals, vertebral compression fracture is a major clinical problem with high morbidity and mortality (Jalava, et al., 2003; Kanis, et al., 2004). Accurate prediction of bone properties and the associated risk of fracture is necessary to identify whether an appropriate drug treatment is required to prevent a vertebral failure. Both dual energy X-ray absorptiometry (DXA) and quantitative computer tomography (QCT) are extensively used in clinics to non-invasively evaluate the vertebral fracture risk (Grampp, et al., 1997) by computing the vertebral areal bone mineral density (aBMD) and vBMD, respectively. The correlation between vertebral strength and aBMD or vBMD measured *in vitro* shows a wide range of predictive capability: R^2=0.46-0.83 for DXA (Faulkner, et al., 1991; Granhed, et al., 1989) and R^2=0.16-0.67 for QCT (Buckley, et al., 2007; Faulkner, et al., 1991). The vertebral strength is better correlated if the minimum cross sectional area (minCSA), measured from QCT images, is combined with vBMD (Buckley, et al., 2007; Cheng, et al., 1997; Crawford, et al., 2003; Singer, et al., 1995). Even though correlations may be strong, bone mineral density (BMD) alone or its product with minCSA can predict neither stiffness nor vertebral strength quantitatively.

FE models based on QCT images include information about the vertebral body geometry and bone density inhomogeneity. Therefore they may be used to predict vertebral stiffness and strength *in vivo*, but they need to be accurately validated with experimental tests *in vitro*. Recent studies showed good correlations between the predicted and the experimental vertebral strength ((Buckley, et al., 2007) N=77; (Chevalier, et al., 2009) N=12; (Crawford, et al., 2003) N=13; (Imai, et al., 2006) N=12; (Liebschner, et al., 2003) N=13; (Mirzaei, et al., 2009) N=13). However the modest correlation between experimental and predicted vertebral stiffness (R^2=0.54 in (Chevalier, et al., 2009); R^2=0.27 in (Buckley, et al., 2007)) supports that further refinements are needed both in the models and in the experimental setup.

Particular emphasis should be put on the definition of the boundary conditions during the experimental tests and consequently in their correct reproduction in the FE model. In most of the studies (Buckley, et al., 2007; Chevalier, et al., 2009; Crawford, et al., 2003; Liebschner, et al., 2003) the vertebral body cortical endplates were embedded in Poly-methyl-methacrylate during the compression test. In another case, rubber discs were positioned between the loading plate and the vertebra (Mirzaei, et al., 2009) introducing an undetermined deformation component during the test. In the first case an unrealistic situation was modelled. These constraints introduce complications in modelling the behaviour of the material inserted between the vertebra and the loading plate. Moreover, the embedding material constrains the vertebral body in a non-physiological way and may affect its failure mechanics. Furthermore, the anterior wedge-shape fracture of the vertebral body, that typically occurs *in vivo* (Jelsma, et al., 1982), can not be reproduced by loading the vertebra between two parallel planes. Therefore, in some studies the rotation of the loading plate was allowed by means of a ball joint (Furtado, et al., 2007; Imai, et al., 2006; Liebschner, et al., 2003). In all the mentioned cases, especially when a ball joint was used, the system machine-setup compliance analysis were not included into the calculation and may have affected the experimental vertebral stiffness measurement.

The aim of this study was to validate a nonlinear FE model for predicting vertebral stiffness and strength in a large number of human vertebral bodies *in vitro*, by means of a novel testing setup developed to induce anterior wedge-shape fractures.

3.2 Materials and methods

3.2.1 Sample selection

Ten human thoracolumbar spines (T12-L5) were received from the Clinical Department of Pathology, Medical University of Vienna, Austria. The donors (seven males, three females with age 44-82) did not suffer of any bone or cartilage disease. The Medical University of Vienna ethics commission approved the procedures applied during the present study. Three to five vertebrae were dissected from each spine (in total 43 specimens) and their soft tissues were removed. The bone tissue was kept frozen at -20°C until the beginning of the sample preparation and in between the procedure steps.

3.2.2 Slice preparation

Two parallel cuts perpendicularly to the cranio-caudal axis were performed to remove both endplates (*300 CP, Exakt Gmbh, Germany*). The posterior elements were then separated from the vertebral body. To obtain plane and parallel surfaces, a 0.5 mm layer was removed from both sides of the vertebral body by polishing with a silicon carbide paper (*P500, PM5, Logitech Ltd, Scotland*). Cutting and polishing operations were performed under constant water irrigation. Twelve measurements of the slice thickness were performed along its perimeter with a digital calliper. The polishing procedure was repeated, removing 0.25mm per iteration, until the difference between maximum and minimum became less than the 1% of the average thickness.

3.2.3 CT Scanning and vBMD analysis

Each vertebra was submerged in 0.9% NaCl saline solution and exposed to vacuum for 10 minutes to remove air bubbles. A custom made Plexiglas chamber was used to position the immerged specimens and to align the cranio-caudal axes of the slice with the scanners. First, each slice was scanned together with a K_2HPO_4 calibration phantom (*Model 3 CT Calibration Phantom, Mindways Software, U.S.A.*) using a clinical QCT (*Brilliance64, Philips, Germany*) at two different resolutions. A lower resolution (LR-QCT, Figure 3.1a-c) was used to evaluate the vBMD and a higher resolution (HR-QCT, Figure 3.1d) was used to generate the FE models (Figure 3.1e) and calculate the minCSA. Afterwards, each vertebra was scanned with a High Resolution peripheral-QCT (HR-pQCT: *XtremeCT, Scanco Medical AG, Switzerland*) to obtain a more accurate representation of the vertebral bone geometry, and therefore to better control the specimen positioning in the testing machine (described in the next section). An overview of the scanning procedures can be found in Table 3.1.

	LR-QCT	**HR-QCT**	**HR-pQCT**	**μCT**
Voltage [kV]	120	140	60	70
Intensity [mA]	100	200	1	114
Matrix [number of pixels]	512x512	512x512	1536x1536	2048x2048
Isotropic in plane pixel size [mm]	0.391	0.391	0.082	0.018
Slice spacing [mm]	2.500	0.450	0.082	0.018

Table 3. 1: Parameters defined for each individual scanning procedure

The QCT and HR-pQCT images were then rotated and cropped to correct the small misalignments between the plane surfaces of the specimen and the scanning slices. Then, the images were registered, by using a rigid registration algorithm (*ITK, Kitware, U.S.A.*), to match the coordinate systems of the mechanical setup and of the FE models.
vBMD was computed from the LR-QCT images of each specimen with a commercial software (*QCT Pro, Mindways Software, U.S.A.*) using the standard clinical approach applied for lumbar spine analysis. An experienced QCT analyst defined a region of interest (ROI) in the trabecular bone of the vertebral body. The ROI was defined selecting manually the position of an elliptical area in the mid-vertebral transverse section (Figure 3.1a), while maximizing its in-plane dimension by excluding the trabecular tissue close to the cortical shell and to the posterior wall. The area was then extended symmetrically into superior and inferior QCT slices to reach a nominal thickness of 9mm (Figure 3.1b,c). vBMD was calculated as the mineral content in the ROI divided by its volume. The calibration phantom was used to convert Hounsfield Units to equivalent vBMD in g/cm³ (Crawford, et al., 2003; Kopperdahl, et al., 2002)) for both QCT images.

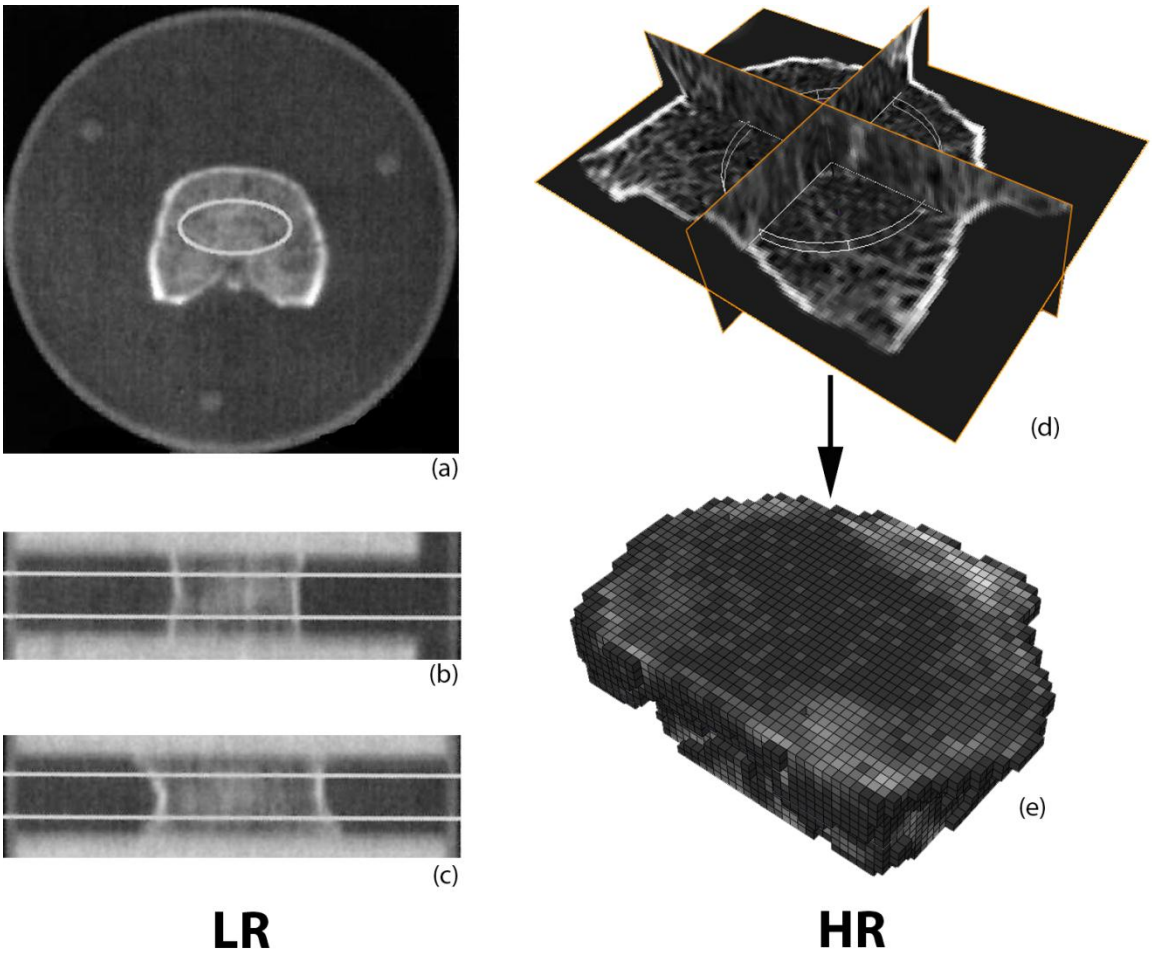

Figure 3. 1 Left: an example of a LR-QCT scan (a-c) used to compute the vBMD with the bright line representing the bounds of the ROI. Right: orthogonal sections from an example of HR-QCT image (d) and the corresponding FE model (e).

3.2.4 Mechanical tests

Thirty-seven specimens were randomly selected for mechanical testing (Table 3.2).

Gender	Age	Nr	T12	L1	L2	L3	L4	L5
M	44	3		x	x		x	
M	48	4		x	x	x	x	
M	50	3			x	x	x	
M	59	3		x	x	x		
F	64	3				x	x	x
F	65	5	x	x	x	x	x	
M	70	4		x	x	x	x	
F	71	5		x	x	x	x	x
M	78	3		x		x	x	
M	82	4	x	x	x	x		
7M/3F	64±12	37	2	8	8	9	8	2

Table 3. 2: Information about the subjects from which were extracted the vertebrae used for the compression test.

Samples with calcifications like osteophytes or with small lytic defects were intentionally not excluded. Each specimen was kept in 0.9% saline solution for at least one hour before testing and then carefully positioned in the machine as follows. From the segmented HR-pQCT images, the center of mass (CoM) of each specimen was computed. The projections of the sagittal and the frontal planes containing the CoM were then plotted on a sheet of paper, together with the most caudal slice of the HR-pQCT image. To induce an anterior wedge-shape fracture, the CoM projection was translated in the anterior direction (Figure 3.2a,b) of a fixed percentile of the width (W) of the most caudal slice of the vertebral body (0% in 2 cases, 5% in 21 cases and 10% in the left 14 cases). The loading axis was defined by the new reference point, and the projections of the reference planes were used for the correct alignment with the reference markers of the setup (Figure 3.2c,d). The specimen was then positioned in the machine by using the contour of the image of the slice (Figure 3.2d). A servohydraulic testing machine (*Mini-Bionix, MTS system, U.S.A.*) was used to compress the slices beyond 12% (Figure 3.3a). Rotation of the loading plate was allowed by means of a ball joint (Figure 3.3b). To avoid translations of the specimen the loading surfaces were sandblasted to increase friction (Figure 3.2c). To circumvent testing device compliance, the axial displacement of three points of the loading plate were measured with three sensors (LVDTs: *WA20, HBM, Germany*) (Figure 3.3c,d). The axial force was measured by means of a 100kN load cell (*U3 force transducer, HBM, Germany*) (Figure 3.3a). Ten preconditioning cycles were applied between 0 and 0.080 mm with a rate of 5 mm/min (Chevalier, et al., 2008) and then a monotonic compression was applied with the same rate. Vertebral strength (FM_Exp) was defined as the maximum compressive load (Figure 3.4b). From the measurement of the three LVDTs, that were placed at the same distance from the centre at 120°, the kinematics of the loading plate and therefore the axial displacement of its centre were computed. Stiffness (S_Exp) was calculated as the slope of the linear part of the "load - axial displacement" curve (Figure 3.4b). Furthermore, for evaluating the machine-setup compliance, an additional stiffness (S_MTS) was calculated from the linear part of the "load - actuator displacement" curve (Figure 3.5).

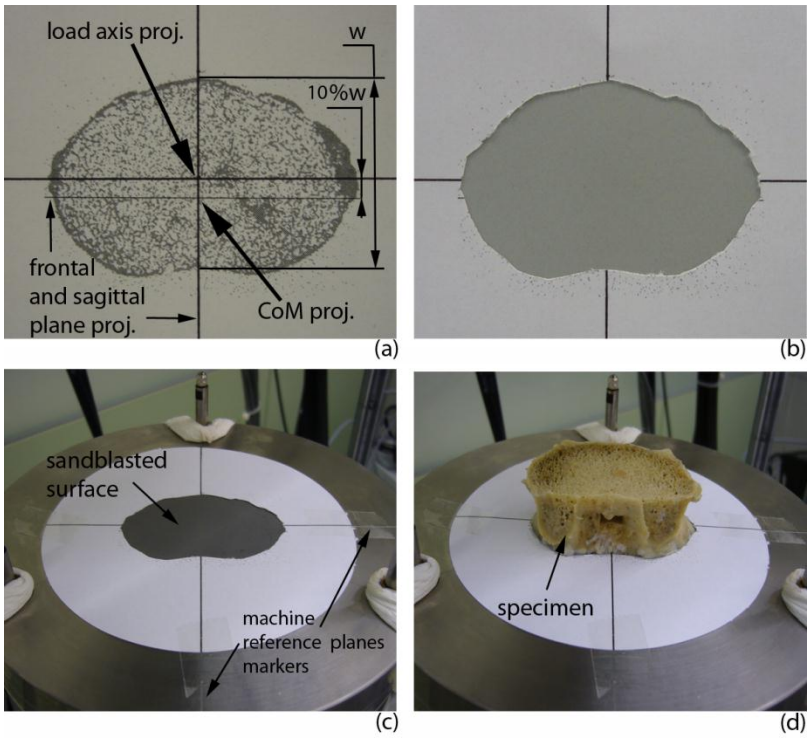

Figure 3. 2: Representation of the procedure to position the samples in the testing machine: the segmented HR-pQCT images of the most caudal slice was plotted on a sheet of paper (a) and it was cut along the slice contour (b). The sheet of paper was aligned with the setup reference markers (c) and used to position the specimen (d).

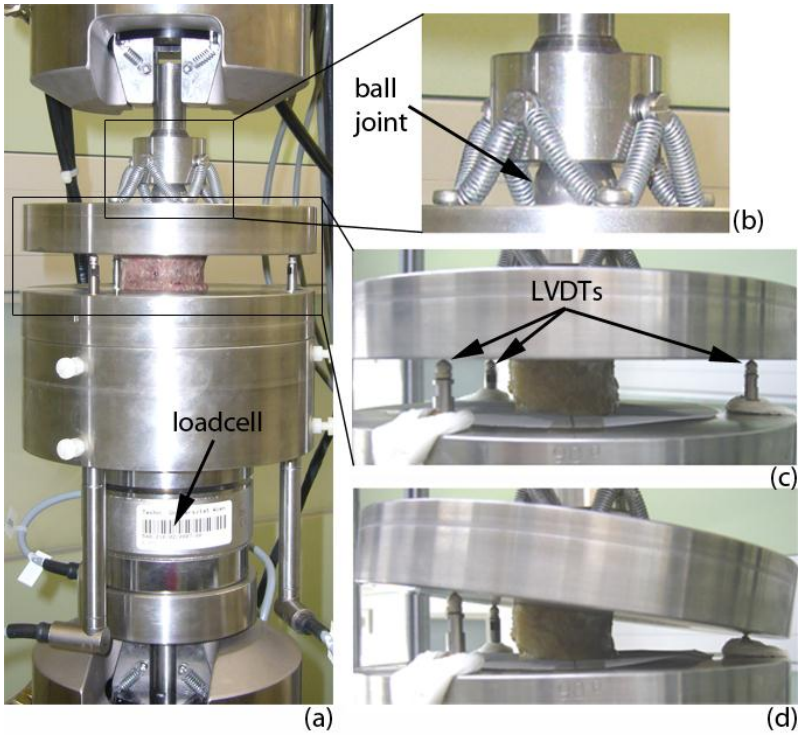

Figure 3. 3: Compression testing setup (a). The rotations were allowed by means of a ball joint (b) and the position of the loading plate was measured with three displacement sensors (c). An example of anterior wedge-shape fracture (d).

3.2.5 Calibration curve

A linear calibration equation defined by assuming 0% bone volume fraction (BV/TV) at 0 mg/cm³ and 100% BV/TV at 1059 mg/cm³ was used to assign a BV/TV value to each voxel of the HR-QCT images, that were coarsened to 1.3mm, from the vBMD. BV/TV was set to 0% and to 100% for vBMD lower than 0 mg/cm³ and higher than 1059 mg/cm³, respectively (Chevalier, et al., 2008). The accuracy of this equation was checked by applying to the six untested specimens the calibration procedure described in a previous study on radius slices (Varga and Zysset, 2009) adapted for QCT images. The specimens, after the above described scanning procedure, were cut to fit the dimensions of the largest sample holder of a μCT *(μCT40, Scanco Medical AG, Switzerland*, scanning parameters in Table 1). Following image registration between HR-QCT and μCT images (*ITK, Kitware, U.S.A.*), 355 cubes (5.33 mm side length) were cropped from both image sets. QCT vBMD and μCT BV/TV were calculated in each cube and compared. The coefficient of determination of the calibration equation (R^2=0.936) was almost equal with that computed from the best fit linear regression (R^2=0.940), therefore the above mentioned linear equation was considered appropriated and used in generating the FE models.

3.2.6 Voxel models

Vertebral stiffness and strength were computed with an FE model, based on a previously published procedure (Chevalier, et al., 2009), created using the HR-QCT images (Figure 3.1e). Two different sets of boundary conditions were applied. In both cases, the nodes of the most caudal section of the vertebral slice were completely constrained. In the first one (FE-NoRot), the loading plate was coupled with the most cranial slice and translated in axial direction with a linear ramp like in Chevalier et al. (2009). Conversely, in the second case (FE-Rot), the loading plate was modelled as a rigid element, whose kinematics was determined with the three axial displacements measured by the LVDTs during the experiments. A contact behaviour with high friction coefficient was defined between the loading plate and the surface defined by the nodes of the most cranial vertebral slice. The initial toe region was not modelled. Therefore in the FE-Rot the loading plate was kept horizontal until the force reached the value measured at the beginning of the linear range during the experiments (Figure 3.4b). Afterwards the rotations of the plate were applied. In both cases, analyses including geometrical and material nonlinearity were performed (*Abaqus 6.8, Simulia, Dassault Systemes, Velizy-Villacoublay, France*) until the centre of the loading plate was displaced by 0.8 mm in the axial direction. The elastic-damage constitutive model for bone developed by Garcia et al. (2009) was used to model material non linearity when it is loaded beyond a piecewise Hill criterion (Zysset and Rincon-Kohli, 2006). In this model, damage (Chevalier, et al., 2009; Zysset and Curnier, 1996) is included as a scalar variable (between 0 and 1), that describes the reduction of the elastic properties of the material. Elastic and strength properties were taken without any adjustment from Rincon-Kohli and Zysset (2009), who performed multi-axial mechanical testing on human trabecular bone. Transverse anisotropy in cranio-caudal direction was assumed. The load was computed as the sum of the axial reaction forces in the nodes of the most caudal surface. The displacement was computed as the axial displacement of the centre of the loading plate. The slice stiffness was calculated as the maximum slope of the load-displacement curve and the strength as the first peak of the load for the models with (S_FE-Rot and FM_FE-Rot, respectively) and without (S_FE-NoRot and FM_FE-NoRot, respectively) rotation of the loading plate.

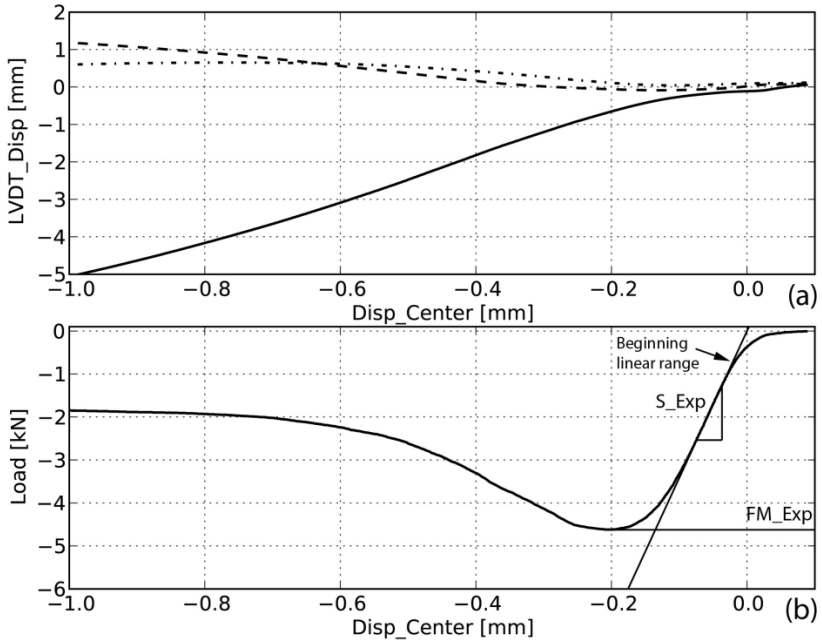

Figure 3. 4: Experimental results of a typical case: measurements of the three displacement sensors (a) and load-displacement curve. S_Exp and FM_Exp represent the vertebral stiffness and strength, respectively. The beginning of the elastic range was used to define the initial conditions of the FE model.

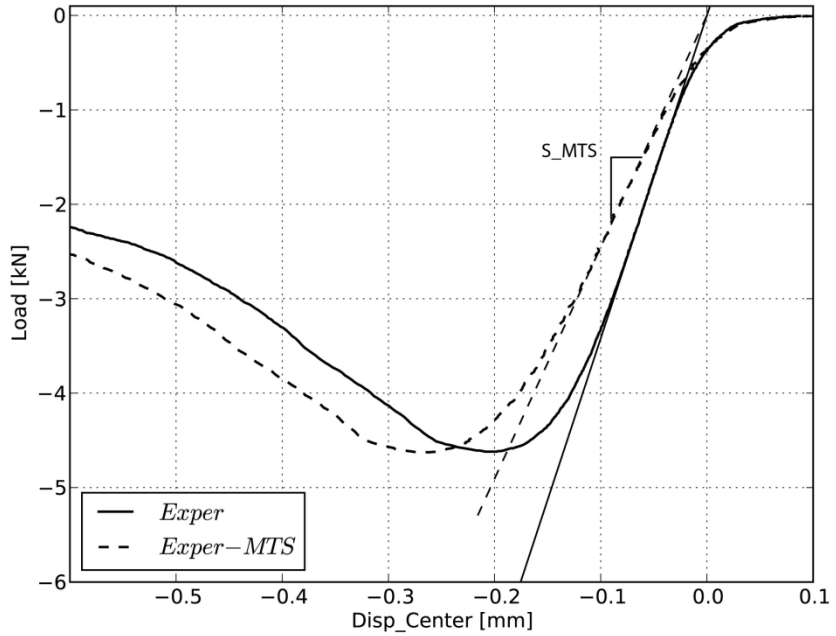

Figure 3. 5: Comparison between the load-displacement curves computing the displacement as the axial displacement of the center of the loading plate (continue line) and with the actuator position (dashed line).

3.3 Results

A modest correlation between age and vBMD (R^2=0.61) was found. The mean vBMD was 170±64 mg/cm³ (range 59-290 mg/cm³). Ten specimens showed a vBMD lower than 110 mg/cm³, which corresponds to the clinical QCT threshold value defining increased fracture risk (Cann, et al., 1985).
In most cases (N=35) an anterior wedge-shape fracture was induced (Figure 3.3d). However in two cases, when the loading axis projection was coincident with the CoM, the vertebrae failed with a posterior wedge shape fracture. The average vertebral strength and stiffness were 5.30±1.67 kN (range 2.31-9.19 kN) and 35.0±9.7 kN/mm (range 17.1-55.0 kN/mm), respectively. As expected, a strong correlation was found between experimental stiffness and strength ($p<0.001$, R^2=0.85). Moreover, large difference between S_MTS and S_Exp (mean 29±6%, range 19-40%) was found. The FE-Rot properly predicted the experimental load-displacement curves until the maximum force (Figure 3.6) and qualitatively well the damage pattern (Figure 3.7). Linear regressions were computed to correlate vBMD and vBMD*minCSA with both S_Exp and FM_Exp, because no improvements were shown in the prediction ability if more complex models were used. The FE models were found to better predict strength (N=37, $p<0.001$, R^2=0.79 for FM_FE-Rot Figure 3.8f, and $p<0.001$, R^2=0.78 for FM_FE-NoRot) than vBMD alone ($p<0.001$, R^2=0.34 Figure 3.8d) or vBMD*minCSA ($p<0.001$, R^2=0.70 Figure 3.8e). However, the stiffness was best predicted by the product vBMD*minCSA ($p<0.001$, R^2=0.59 Figure 3.8b) compared to vBMD alone ($p=0.001$, R^2=0.27 Figure 3.8a) and to the FE models ($p<0.001$, R^2=0.49 for S_FE-Rot Figure 3.8c, and R^2=0.52 for S_FE-NoRot). If samples with big osteophytes (three) or calcifications (one) were excluded the FE predictions improved both for strength (N=33, R^2=0.84 for FM_FE-Rot and R^2=0.83 for FM_FE-NoRot) and stiffness (R^2=0.63 for S_FE-Rot and R^2=0.67 for S_FE-NoRot).

3.4 Discussion

The aim of the present study was to validate a subject-specific QCT-based FE model by using an improved experimental technique that induces anterior wedge-shape vertebral fractures.
The measured vertebral strength was similar to the experimental results showed in other studies on thoracolumbar spine (Buckley, et al., 2007; Chevalier, et al., 2009; Crawford, et al., 2003; Ebbesen, et al., 1999; Liebschner, et al., 2003). Furthermore the higher values of vertebral stiffness compared with those reported in literature (Buckley, et al., 2007; Chevalier, et al., 2009; Liebschner, et al., 2003) might be due to the reduced vertebral thickness, as consequence of the cortical endplates removal, and to the improved testing protocol. In fact, it was shown that if the setup-machine compliance were not taken into account, the vertebral stiffness was highly underestimated (up to 40%). This result emphasizes the necessity of an appropriate mechanical testing setup when validating a new computational model.

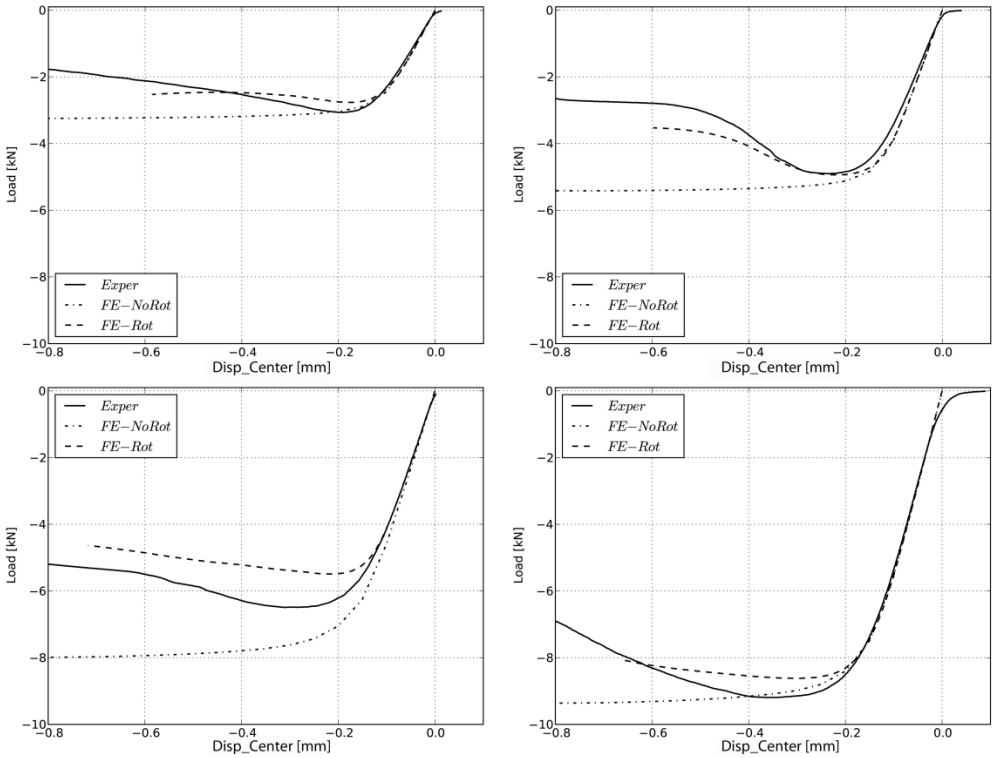

Figure 3. 6: Four examples of comparison between experimental and predicted curves. Dashed and dash-dot lines represent models including or not the rotation of the loading plate, respectively. The samples were selected to cover the entire range of vertebral strength.

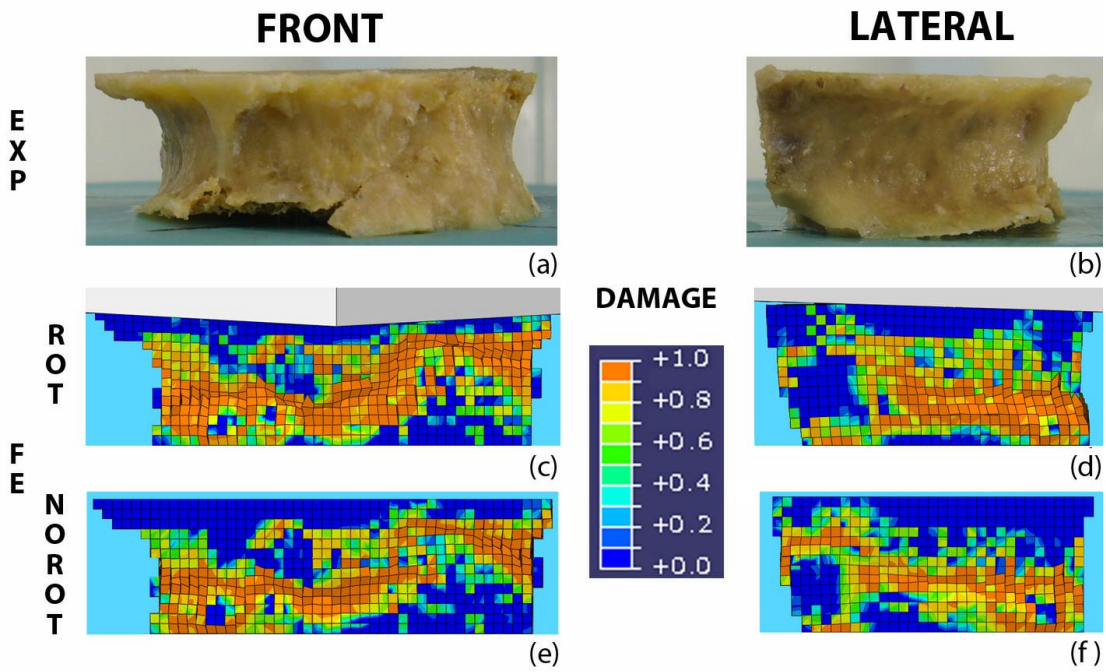

Figure 3. 7: Qualitative comparison between the experimental damage after large deformations (a, b) and the one predicted by the models including (c, d) or not (e, f) the rotation of the loading plate.

The improvement of the strength prediction from vBMD to vBMD*minCSA and further to FE models is in line with the study of Crawford et al. (2003). Furthermore the results of the present study support the finding that the coefficient of determination of the linear regressions for vertebral bone stiffness and strength predicted with FE method is around 0.5 (Chevalier, et al., 2009) and around 0.8 (Buckley, et al., 2007; Chevalier, et al., 2009)), respectively. The low predictive capability of the FE method for stiffness may be caused by the intrinsic low resolution of the QCT images and by the fact that cortical and trabecular bone were not distinguished in the models. The application of the rotations improved the prediction of strength (R^2 from 0.78 to 0.79, Slope from 0.67 to 0.86 and Intercept from 0.91 kN to 0.72 kN) and damage localization. In fact, the damage in the FE-Rot was mainly localized in the anterior part of the vertebral body. The same pattern could be qualitatively seen during the experiments. However, not surprisingly, the application of the rotation of the loading plate did not improve the stiffness prediction. Indeed until the maximum force, the angles of rotation projected in the two anatomical planes were smaller than 1° for each specimen. Considering the good correlation between FM_FE-NoRot and FM_Exp (R^2 = 0.78, difference of 24% in the mean values), and that the material constants for the models were taken directly from experiments without any adjustment (Rincon-Kohli and Zysset, 2009), the model may be adapted for a clinical application with few refinements. Furthermore if samples with big osteophytes and calcifications were excluded both predictions of stiffness and strength improved up to 63% and 84%, respectively. The stronger prediction of strength is in line with the finding of Crawford et al. (2003), who tested only vertebral bodies without osteophytes. Clarification of the mechanical properties of these structures will be one of our targets in future studies to better understand their impact in the mechanics of vertebral body failure.

The present study has two main limitations. First, the QCT scans were performed *in vitro* without using a body phantom. The soft and hard tissues around the spine and the fat content in the vertebral body, that may have been removed during the sample preparation, play an important role during the QCT scans *in vivo* and, therefore, their removal may affect the model prediction. Second, only 35% of the samples were extracted from female subjects and only 27% of the samples had to be considered at high fracture risk. Moreover, only a few thoracic vertebrae were included in the study. Considering that the population mostly affected by vertebral fracture consists of post-menopausal women with low vBMD and that the fractures usually occur between T6 and L3 (Cooper, et al., 1992; Melton, et al., 1989), it would be interesting to analyse the model prediction including more samples with those characteristics.

In conclusion, a nonlinear FE model was successfully validated by using an improved experimental technique for generating anterior wedge-shape fractures in a large number of human vertebral bodies. The obtained results will be exploited to identify the best FE modelling strategies to predict vertebral failure load *in vivo*.

Acknowledgements

The authors acknowledge a grant for an interuniversity computer tomography network from the UniInfrastruktur Program III of the Austrian Ministry for Science and Research (bm: bwk). The authors gratefully acknowledge Ms Plischke and Ms Merz for having performed the vBMD measurements and Mr Exler for having manufactured the experiment set-up tools.

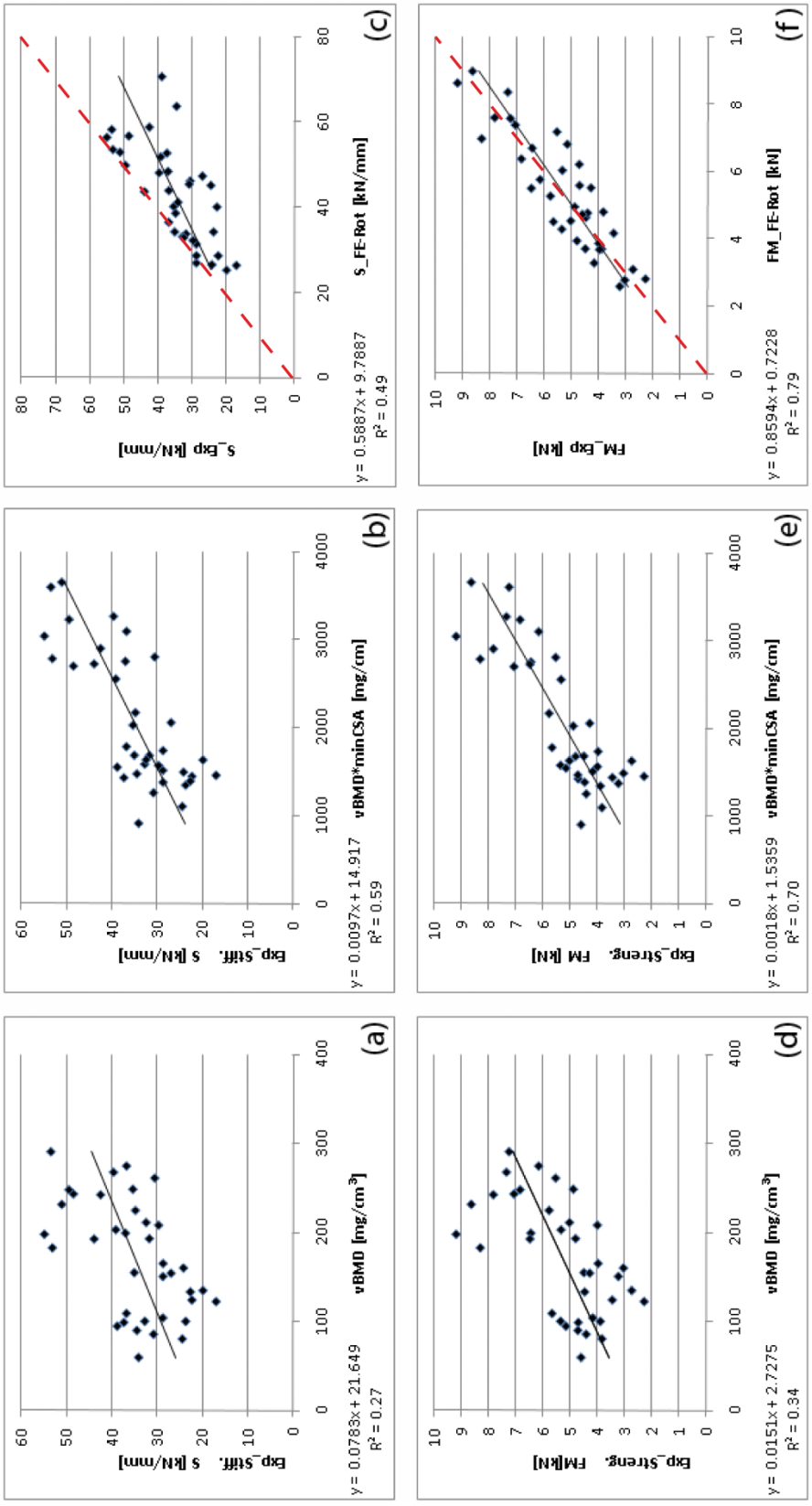

Figure 3. 8: Stiffness and Strength predictions with vBMD (a, d), vBMD*minCSA (b, e) and FE model including the rotations of the loading plate (c, f). The dashed line represents the quadrant bisector.

Bibliography

Buckley J.M., Loo K., Motherway J., 2007. Comparison of quantitative computed tomography-based measures in predicting vertebral compressive strength. Bone 40, 767-774

Cann C.E., Genant H.K., Kolb F.O., Ettinger B., 1985. Quantitative computed tomography for prediction of vertebral fracture risk. Bone 6, 1-7

Cheng X.G., Nicholson P.H., Boonen S., Lowet G., Brys P., Aerssens J., Van der Perre G., Dequeker J., 1997. Prediction of vertebral strength in vitro by spinal bone densitometry and calcaneal ultrasound. Journal of bone and Mineral Research 12, 1721-1728

Chevalier Y., Charlebois M., Pahra D., Varga P., Heini P., Schneider E., Zysset P., 2008. A patient-specific finite element methodology to predict damage accumulation in vertebral bodies under axial compression, sagittal flexion and combined loads. Computer Methods in Biomechanics and Biomedical Engineering 11, 477-487

Chevalier Y., Pahr D., Zysset P.K., 2009. The role of cortical shell and trabecular Fabric in Finite Element analysis of the human vertebral body. Journal of Biomechanical Engineering 131, epub

Cooper C., Atkinson E.J., O'Fallon W.M., Melton L.J., 3rd, 1992. Incidence of clinically diagnosed vertebral fractures: a population-based study in Rochester, Minnesota, 1985-1989. Journal of Bone and Mineral Research 7, 221-227

Crawford R.P., Cann C.E., Keaveny T.M., 2003. Finite element models predict in vitro vertebral body compressive strength better than quantitative computed tomography. Bone 33, 744-750

Ebbesen E.N., Thomsen J.S., Beck-Nielsen H., Nepper-Rasmussen H.J., Mosekilde L., 1999. Lumbar vertebral body compressive strength evaluated by dual-energy X-ray absorptiometry, quantitative computed tomography, and ashing. Bone 25, 713-724

Faulkner K.G., Cann C.E., Hasegawa B.H., 1991. Effect of bone distribution on vertebral strength: assessment with patient-specific nonlinear finite element analysis. Radiology 179, 669-674

Furtado N., Oakland R.J., Wilcox R.K., Hall R.M., 2007. A biomechanical investigation of vertebroplasty in osteoporotic compression fractures and in prophylactic vertebral reinforcement. Spine 32, E480-487

Grampp S., Genant H.K., Mathur A., Lang P., Jergas M., Takada M., Gluer C.C., Lu Y., Chavez M., 1997. Comparisons of noninvasive bone mineral measurements in assessing age-related loss, fracture discrimination, and diagnostic classification. Journal of Bone and Mineral Research 12, 697-711

Granhed H., Jonson R., Hansson T., 1989. Mineral content and strength of lumbar vertebrae. A cadaver study. Acta Orthopaedica Scandinavica 60, 105-109

Imai K., Ohnishi I., Bessho M., Nakamura K., 2006. Nonlinear finite element model predicts vertebral bone strength and fracture site. Spine 31, 1789-1794

Jalava T., Sarna S., Pylkkanen L., Mawer B., Kanis J.A., Selby P., Davies M., Adams J., Francis R.M., Robinson J., McCloskey E., 2003. Association between vertebral fracture and increased mortality in osteoporotic patients. Journal of Bone and Mineral Research 18, 1254-1260

Jelsma R.K., Kirsch P.T., Rice J.F., Jelsma L.F., 1982. The radiographic description of thoracolumbar fractures. Surgical Neurology 18, 230-236

Kanis J.A., Oden A., Johnell O., De Laet C., Jonsson B., 2004. Excess mortality after hospitalisation for vertebral fracture. Osteoporosis International 15, 108-112

Kopperdahl D.L., Morgan E.F., Keaveny T.M., 2002. Quantitative computed tomography estimates of the mechanical properties of human vertebral trabecular bone. Journal of Orthopaedic Research 20, 801-805

Liebschner M.A., Kopperdahl D.L., Rosenberg W.S., Keaveny T.M., 2003. Finite element modeling of the human thoracolumbar spine. Spine 28, 559-565

Melton L.J., 3rd, Kan S.H., Frye M.A., Wahner H.W., O'Fallon W.M., Riggs B.L., 1989. Epidemiology of vertebral fractures in women. American Journal of Epidemiology 129, 1000-1011

Mirzaei M., Zeinali A., Razmjoo A., Nazemi M., 2009. On prediction of the strength levels and failure patterns of human vertebrae using quantitative computed tomography (QCT)-based finite element method. Journal of Biomechanics 42, 1584-1591

Rincon-Kohli L., Zysset P.K., 2009. Multi-axial mechanical properties of human trabecular bone. Biomechanics and Modeling in Mechanobiology 8, 195-208

Singer K., Edmondston S., Day R., Breidahl P., Price R., 1995. Prediction of thoracic and lumbar vertebral body compressive strength: correlations with bone mineral density and vertebral region. Bone 17, 167-174

Varga P., Zysset P.K., 2009. Assessment of volume fraction and fabric in the distal radius using HR-pQCT. Bone 45, 909-917

Zysset P.K., Curnier A., 1996. A 3D damage model for trabecular bone based on fabric tensors. Journal of Biomechanics 29, 1549-1558

Zysset P.K., Rincon-Kohli L., 2006. An alternative fabric-based yield and failure criterion for treabecular bone. In Holzapfel G., Ogden R. (eds) Mechanics of biological tissue. Springer, Berlin, pp 457-470

Chapter 4

hvFE of the human vertebral body versus DXA

From the manuscript:

QCT-based Finite Element Models Predict Human Vertebral Strength *in vitro* Significantly Better than Simulated DEXA

E. Dall'Ara [a], D. Pahr [a], P. Varga [a], F. Kainberger [b], P. Zysset [a]

a Institute of Lightweight Design and Structural Biomechanics, Vienna University of Technology, Austria
b Department of Radiology, Medical University of Vienna, Austria

Published in: Osteoporosis International Vol. 23(2), 563-72, 2012

Abstract
Purpose Vertebral fracture is a common medical problem in osteoporotic individuals. Bone mineral density (BMD) is the gold standard measure to evaluate fracture risk *in vivo*. Quantitative computed tomography (QCT)-based finite element (FE) modeling is an engineering method to predict vertebral strength. The aim of this study was to compare the ability of FE and clinical diagnostic tools to predict vertebral strength *in vitro* using an improved testing protocol.
Methods Thirty-seven vertebral sections were scanned with QCT and high resolution peripheral QCT (HR-pQCT). Bone mineral content (BMC), total BMD (tBMD), areal BMD from lateral (aBMD-lat) and anterior-posterior (aBMD-ap) projections were evaluated for both resolutions. Wedge shape fractures were then induced in each specimen with a novel testing setup. Nonlinear homogenized FE models (hFE) and linear micro-FE (μFE) were generated from QCT and HR-pQCT images, respectively. For experiments and models both structural properties (stiffness, ultimate load) and material properties (apparent modulus and strength) were computed and compared.
Results Both hFE and μFE models predicted material properties better than structural ones and predicted strength significantly better than aBMD computed from QCT and HR-pQCT (hFE: R^2=0.79, μFE: R^2=0.88, aBMD-ap: R^2=0.48-0.47, aBMD-lat: R^2=0.41-0.43). Moreover, the hFE provided reasonable quantitative estimations of the experimental mechanical properties without fitting the model parameters.
Conclusions The QCT-based hFE method provides a quantitative and significantly improved prediction of vertebral strength *in vitro* when compared to simulated DXA. This superior predictive power needs to be verified for loading conditions that simulate even more the *in vivo* case for human vertebrae.

Keywords: Finite element modelling, Bone mineral density, DXA, Bone strength, Osteoporosis, Mechanical testing

4.1 Introduction

Osteoporosis is a systemic skeletal disease characterized by low bone mass and deterioration of the bone microstructure that lead to a high bone fragility. Among osteoporotic fractures, vertebral compression ones, with 490,000 cases each year in Europe (Johnell and Kanis, 2006), are a major clinical problem with high morbidity and mortality (Jalava, et al., 2003; Johnell and Kanis, 2005; Kanis, et al., 2004). In early nineties the World Health Organization recommended to diagnose osteoporoses for subjects with hip BMD more than 2.5 SD below the young adult average value (Kanis and Gluer, 2000; WHO, 1994). However, a previous study showed that the accuracy of the prediction of fracture risk increases with site-specific measurements (Marshall, et al., 1996). Therefore, direct BMD measurement of the spine is more accurate to predict vertebral fractures (Kanis, et al., 2006). Areal (aBMD) and volumetric (vBMD) BMD can be measured non-invasively by means of dual energy X-ray absorptiometry (DXA) and QCT, respectively. While DXA is considered nowadays the gold standard for the low radiation (5 μSv for DXA of the lumbar spine versus 2000 μSv for typical QCT of two vertebrae) (Griffith and Genant, 2008), low cost, high reliability and ease of use (Bergot, et al., 2001), QCT is being extensively used in clinics to evaluate the 3D bone geometry (Griffith, et al., 2010) and has been found to be more sensitive than DXA in explaining vertebral fractures (Bergot, et al., 2001). However, around 50% of the osteoporotic fractures occur in patients with BMD above the defined thresholds (Roux, et al., 2009; Siris, et al., 2004). Indeed, the risk of fracture can be defined as the ratio between the load under particular loading condition and the ultimate load supported by the bone, the bone strength (Hayes, 1991; Silva, 2007). The applied load is a function of patient variables (e.g. body height and mass), type of activity and can only be estimated for specific patients and loading scenarios. Conversely, bone strength has been investigated in several *in vitro* and *in silico* studies (review (Davison, et al., 2006)). Experimental studies have recently shown that bone strength is affected both by BMD, that remain the primary factor, and by bone quality (Ammann and Rizzoli, 2003; Bouxsein, 2003; McDonnell, et al., 2007; Viguet-Carrin, et al., 2006), that includes several parameters like cortical thickness and porosity (Augat and Schorlemmer, 2006; Dong and Guo, 2004; Turner, 2002), trabecular bone morphology (Ciarelli, et al., 2000; Homminga, et al., 2004; Matsuura, et al., 2007; Ulrich, et al., 1999), microdamage (Bouxsein, 2003; Keaveny, et al., 1994; Wenzel, et al., 1996) and properties of the matrix (Boivin, et al., 2000). The QCT-based FE method takes into account vertebral geometry, BMD and tissue material properties in order to better estimate vertebral strength. From the BMD values of the calibrated QCT images, the material properties are mapped in each element of the vertebral body by means of phenomenological laws (Rincon-Kohli and Zysset, 2009) (reviews (Helgason, et al., 2008; Zysset, 2003)) and constitutive assumptions (Garcia, et al., 2009; Zysset and Rincon-Kohli, 2006). The subject-specific QCT-based nonlinear FE models can predict the post yield behavior of bone and have been shown to predict vertebral stiffness and ultimate load *in vitro* better than BMD (Buckley, et al., 2007; Chevalier, et al., 2009b; Dall'Ara, et al., 2010; Imai, et al., 2006; Silva, et al., 1998; Zeinali, et al., 2010). Validated FE analysis (Cristofolini, et al., 2010) have been shown to predict quantitatively both stiffness and ultimate load and can be used to compute material mechanical properties normalized for bone geometry (Turner, 2002). Structural properties such as stiffness and ultimate load are often reported to discuss fracture risk. However, the evaluation of material properties might be even more interesting as they account for bone size and therefore for the magnitude of the loads that contributed to the growth and adaptation of that individual structure. Vertebral strength is defined by ultimate load

divided by cross-sectional area, while apparent modulus is determined by stiffness divided by the ratio of CSA over vertebral height. Using dimensional analysis under the reasonable assumption of geometrical self-similarity, bone ultimate load is theoretically proportional to $M^{2/3}$, displacement and bone length to $M^{1/3}$ and bone cross-sectional area to $M^{2/3}$ (Brianza, et al., 2007). Therefore, material variables such as apparent modulus and strength accounting for bone size are also independent of body mass.
Recently, the QCT image resolution of *in vivo* scans of human spine has been improved up to a voxel size of 150 μm (XperCT, Philips (Mulder, et al., 2010)) and in the next decades an even higher resolution with acceptable radiation dose can not be excluded. HR-pQCT-based FE models (nominal resolution equal to 82 μm) have been already validated with experimental tests of human vertebral bodies (Pahr, et al., 2010). While homogenization techniques are recently applied to high resolution images in order to take account of trabecular microstructure and cortical thickness (Chevalier, et al., 2009b; Pahr, et al., 2010; Varga, et al., 2009), the μFE models, in which the voxels of the CT image are directly converted in hexahedral elements, remain the gold standard (Macneil and Boyd, 2008; Mueller, et al., 2009; Varga, et al., 2010). Despite the well represented geometry and microstructure of the vertebra, a large number of degrees of freedom are included in the analysis (in the order of 100 mil for a vertebral body section (Pahr, et al., 2010)). Therefore, μFE analysis at the organ level are practically limited to linear elasticity and can be solved only by means of high performance computers with a large number of CPUs working in parallel.
In summary, the goals of this study were:

- To verify if material properties of vertebral sections are better predicted than structural properties by densitometric variables and FE analyses, respectively.
- To compare the predictive power of nonlinear QCT-based FE analyses with the one of BMC, vBMD and aBMD.
- To evaluate the potential of an improved QCT nominal resolution of 82 μm on the prediction of vertebral strength with densitometric variables and FE analysis.

4.2 Materials and methods

4.2.1 Sample preparation

Ten human thoracolumbar spines (T12-L5) were received from the Clinical Department of Pathology, Medical University of Vienna, Austria. The donors (seven males, three females with age 44-82) did not suffer of any bone or cartilage disease. The Medical University of Vienna ethics commission approved the procedures applied during the present study. In total 37 vertebrae were extracted and prepared as described in details in Chapter 3 (Dall'Ara, et al., 2010). In particular, soft tissues, cortical endplates and posterior elements were removed to obtain vertebral sections with two plane and parallel surfaces.

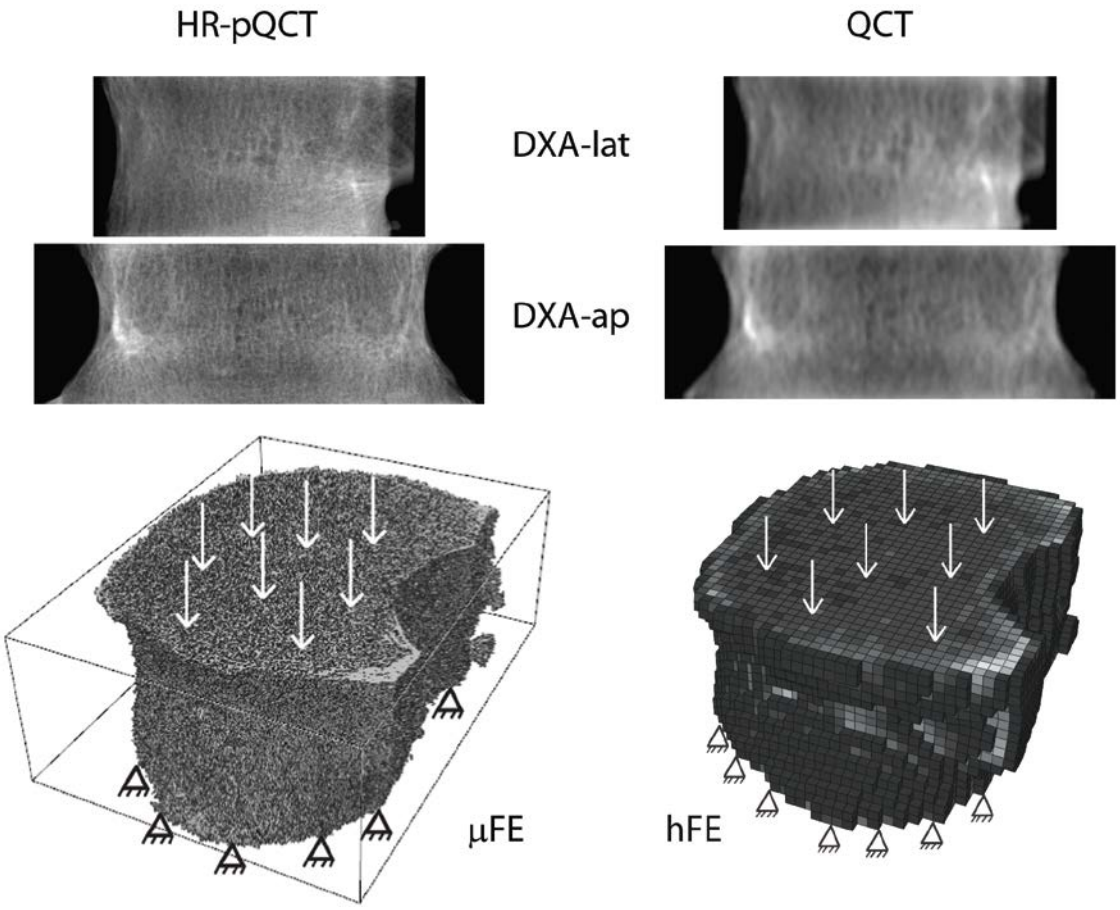

Figure 4. 1: Top: simulation of DXA in anterior-posterior and lateral directions for both HR-pQCT and QCT images. Bottom: example of μFE and hFE model generated from HR-pQCT and QCT, respectively.

4.2.2 Scanning procedures and image processing

After vacuum exposure to remove air bubbles, each section was scanned in saline solution using a clinical QCT (*Brilliance64, Philips, Germany*) and a high resolution peripheral-QCT (HR-pQCT: *XtremeCT, Scanco Medical AG, Switzerland*). The QCT (0.390x0.390x0.450 mm³ voxel size) and HR-pQCT (0.082x0.082x0.082 mm³ voxel size) images were then registered, by using a rigid registration algorithm (*ITK, Kitware, U.S.A.*), to match the coordinate systems of the experimental setup and both QCT-based homogenized FE and HR-pQCT-based μFE models (see paragraphs below). Original greyscale values were converted in BMD values by a linear calibration by means of calibration phantoms (*Model 3 CT Calibration Phantom, Mindways Software, U.S.A* for QCT and the standard one provided by the manufactures for HR-pQCT). The external bone contour (mask) was found for each image with a filling out algorithm (Pahr and Zysset, 2009) and the following quantities were calculated for both resolutions: bone mineral content (BMC) in the masked volume (i.e. including both trabecular and cortical bone), section's height (h), volume of the masked image (V), mean cross section area (CSA=V/h), projected area in the anterior-posterior and lateral directions (A-ap and A-lat, respectively), total vBMD (tBMD=BMC/V) including both cortical and trabecular bone and simulated aBMD (Burghardt, et al., 2009) (Figure 4.1, top) projected along the anterior-posterior and the lateral directions (aBMD-ap=BMC/A-ap and aBMD-lat=BMC/A-lat, respectively).

4.2.3 Mechanical tests

Each section was then prepared for experimental test. The samples were kept in 0.9% saline solution for at least one hour before testing and then carefully positioned in a servo-hydraulic testing machine (*Mini-Bionix, MTS system, U.S.A.*). The sections were compressed beyond 12% deformation. To induce wedge shape fractures, rotation of the loading plate was allowed by means of a ball joint, whose center was translated anteriorly with respect to the center of gravity of the vertebral section by 5-10% of its width. The position of the loading plate was determined by means of three sensors (*WA20, HBM, Germany*) and the axial displacement of the center was computed. The axial force was measured by means of a 100kN load cell (*U3 force transducer, HBM, Germany*). Ten preconditioning cycles between 0 and 0.080 mm followed by a monotonic compression were applied with a rate of 5 mm/min (Chevalier, et al., 2008). For more details about the positioning of the sections and the mechanical testing setup, please refer to Chapter 3 (Dall'Ara, et al., 2010).

4.2.4 QCT-based hvFE models

Bone volume fraction (BV/TV)-based homogenized FE (hFE) models were created using the QCT images coarsened to a voxel size of 1.3x1.3x1.3 mm³ (Figure 4.1, bottom right) to have a reasonable computation time (Chevalier, et al., 2009a; Dall'Ara, et al., 2010). The BMD value of each voxel was restricted between -100 and 1061 mg/cm³ and then converted in BV/TV by means of the calibration equation described in details in Chapter 2 (Dall'Ara, et al., 2010):

$$ {}^{BV}/_{TV} = \begin{cases} \sim 0, & BMD < -100 \\ 0.0942 * \mathrm{BMD} - 0.0297, & -100 \leq BMD \leq 1061 \\ 100, & BMD > 1061 \end{cases} \quad (4.1) $$

The nodes of the most caudal surface were constrained and the ones of the most cranial surface were displaced in axial direction until 0.8mm (*Abaqus 6.8, Simulia, Dassault Systemes, Velizy-Villacoublay, France*), while keeping the two planes parallel. Material and geometric non linearity were included in the analyses (Chevalier, et al., 2009a; Dall'Ara, et al., 2010). The elastic-damage constitutive model developed by Garcia et al. (Garcia, et al., 2009) was used to model the post-yield behavior of bone (Zysset and Rincon-Kohli, 2006). In particular material non linearity was included when bone was loaded beyond a yield criterion. In this model, damage (Chevalier, et al., 2009a; Zysset and Curnier, 1996) is included as a scalar variable (between 0 and 1), that describes the reduction of the elastic properties of the material. Elastic and strength properties were taken without any adjustment from Rincon-Kohli and Zysset (Rincon-Kohli and Zysset, 2009), who performed multi-axial mechanical testing on human trabecular bone. Transverse anisotropy in cranio-caudal direction was assumed (Chevalier, et al., 2009b).

4.2.5 HR-pQCT-based µFE models

The procedure used to generate the µFE was similar to the one applied by Pahr et al. (Pahr, et al., 2010). In summary, the HR-pQCT images were segmented, after the application of a Laplace-Hamming filter, with a fixed 40% threshold (Laib, et al., 1998) and the voxels were then directly converted to hexahedral elements (Figure 4.1, bottom left). A back-calculated tissue modulus of 8.78 GPa was found to best predict experimental results and

the same value was used in all computations. Correspondingly to the hFE, the nodes of the most caudal surface were constrained and the ones of the most cranial one were displaced axially of 0.1 mm. Linear μFE models were solved with ParFE (Arbenz, et al., 2008) on a CRAY XT3 using 256 CPUs in parallel.

4.2.6 Data analysis and statistics

Structural properties were computed from the load-displacement curves both for experiments and models. In particular stiffness (Exp_S, hFE_S and μFE_S) was defined as the slope of the linear portion of the curve and the ultimate load (Exp_Fu, hFE_Fu) as the maximum force of the nonlinear portion. Material properties were computed by normalizing the structural ones with the sample dimensions. In particular, apparent modulus (Exp_Y, hFE_Y, μFE_Y) was defined by dividing the stiffness by the ratio CSA/h and the strength (Exp_σu and hFE_σu) as the ultimate load divided by CSA.
The Williams's formula and the procedure proposed by Steiger et al. (Steiger, 1980) were used to compare the correlation coefficients of the different predictors (densitometric or FE variables vs experimental results and material or structural variables for all the predictors, significance p=0.05).

4.3 Results

The average, standard deviation, minimum and maximum values of the height, densitometric variables and mechanical properties computed from experiments and FE models are reported in Table 4.1. The coefficient of determination between the QCT or HR-pQCT derived variables and the structural or material mechanical properties of the vertebral sections are listed in Table 4.2. In the following paragraphs the p-values represent the significance of the difference between the correlation coefficients. The correlation coefficients were higher, sometimes significantly, for structural parameters than for the material ones in case of BMC ($p<0.001$ for ultimate load and stiffness), aBMD-lat ($p=0.018$ for ultimate load and $p=0.042$ for stiffness) and aBMD-ap ($p=0.179$ for ultimate load and $p=0.187$ for stiffness). Conversely, coefficient of determination were higher, sometimes significantly, for material properties than for structural ones in case of tBMD ($p=0.007$ for ultimate load and $p=0.011$ for stiffness), hFE ($p=0.417$ for ultimate load and $p=0.058$ for stiffness) and μFE ($p=0.003$ for ultimate load and $p=0.152$ for stiffness). Similar results were found both for QCT and HR-pQCT based measurements (Table 4.2).
hFE predicted strength Exp_σu significantly better than all the densitometric variables ($p=0.040$ for tBMD and $p<0.001$ for aBMD-ap, aBMD-lat and BMC) (Figure 4.2). Similar results were found for apparent modulus Exp_Y, except for tBMD for which the difference in prediction was not significant ($p=0.956$). Moreover hFE predicted ultimate load Exp_Fu significantly better than aBMD-ap ($p=0.002$), aBMD-lat ($p=0.011$) and tBMD ($p<0.001$). Even though the coefficient of determination for hFE vs Exp_Fu was higher than the one for BMC vs Exp_Fu, the difference was not significant ($p=0.163$).
The same densitometric variables measured by QCT and HR-pQCT were not equal but correlated very well.($R^2=0.99$ for BMC and $R^2=0.98$ for tBMD, aBMD-lat and aBMD-ap, Figure 4.3). As in case of hFE, μFE predicted both material variables (Exp_σu and Exp_Y)

		Avg ± SD	Min	Max
	Height [mm]	19.41 ± 2.11	15.58	23.49
QCT	**BMC [g]**	4.06 ± 1.38	1.99	7.66
	aBMD-ap [g/cm^2]	0.454 ± 0.106	0.295	0.643
	aBMD-lat [g/cm^2]	0.574 ± 0.146	0.353	0.936
	tBMD [mg/cm^3]	161.5 ± 38.7	96.0	236.6
HR-pQCT	**BMC [g]**	3.47 ± 1.25	1.73	6.98
	aBMD-ap [g/cm^2]	0.383 ± 0.097	0.239	0.548
	aBMD-lat [g/cm^2]	0.488 ± 0.132	0.280	0.765
	tBMD [mg/cm^3]	139.0 ± 34.9	74.7	197.4
Exp	**Exp-S [kN/mm]**	34.98 ± 9.73	17.09	54.36
	Exp-Fu [kN]	5.30 ± 1.67	2.31	9.19
	Exp-Y [MPa]	508.7 ± 165.2	269.1	781.6
	Exp-σu [MPa]	4.1 ± 1.3	1.8	6.0
hFE	**hFE-S [kN/mm]**	44.2 ± 11.9	26.8	69.7
	hFE-Fu [kN]	6.6 ± 2.2	3.0	10.6
	hFE-Y [MPa]	628.9 ± 159.2	380.8	875.7
	hFE-σu [MPa]	5.0 ± 1.6	2.6	7.6
μFE	**μFE-S [kN/mm]**	35.7 ± 11.7	11.5	56.8
	μFE-Y [MPa]	534.6 ± 195.5	191.5	827.0

Table 4. 1: Average, standard deviation, minimum and maximum values of the height, densitometric parameters and mechanical properties from experiments and FE models. The height was measured on the vertebral body sections after polishing

significantly better than aBMD-ap ($p<0.001$ in both cases), aBMD-lat ($p<0.001$ and $p=0.003$, respectively) and BMC ($p<0.001$ in both cases) (Figure 4.2). Both predictions of material properties using μFE were higher than the one found using tBMD but the

difference was significant only for strength (p=0.011 for Exp_σu and p=0.296 for Exp_Y). Considering structural properties, all coefficients of determination were higher for μFE but the difference was significant in one case only (μFE and tBMD vs Exp_S: p=0.035). μFE predicted stiffness Exp_S better than hFE (p=0.018), while all other predictions were not significantly different (p=0.398 for Exp_Fu, p=0.056 for Exp_σu and p=0.245 for Exp_Y).

		Structural/Extrinsic		***Material/Intrinsic***	
		Exp_Fu	**Exp_S**	**Exp_σu**	**Exp_Y**
QCT	BMC	0.70	0.62	0.31 **a, b**	0.25 **a, b**
	aBMD-ap	0.63 **b**	0.59	0.48 **b**	0.43 **b**
	aBMD-lat	0.67 **b**	0.66	0.41 **a, b**	0.42 **a, b**
	tBMD	0.46 **b**	0.42	0.74 **a, b**	0.71 **a**
	hFE	*0.78*	*0.52* **c**	*0.79*	*0.71*
HR-pQCT	BMC	0.72	0.66	0.27 **a, b**	0.33 **a, b**
	aBMD-ap	0.66	0.63	0.47 **b**	0.43 **b**
	aBMD-lat	0.70	0.69	0.43 **a, b**	0.45 **a, b**
	tBMD	0.51	0.48 **b**	0.74 **a, b**	0.71 **a**
	μFE	*0.72*	*0.72*	*0.88* **a**	*0.78*

Table 4. 2: Coefficients of determination (R^2) for linear regressions between predictive tools based on QCT or HR-pQCT for material and structural properties. While for nonlinear hFE all experimental measurements were predicted with the corresponding ones, for the linear μFE Exp_Fu and Exp_σu were predicted with μFE_S and μFE_Y, respectively. [a] represents significant differences between the predictions of material and structural properties. [b] represents significant differences between densitometric tools and FE generated from images with the same resolution. [c] represents significant differences between QCT based hFE and HR-pQCT based μFE predictions.

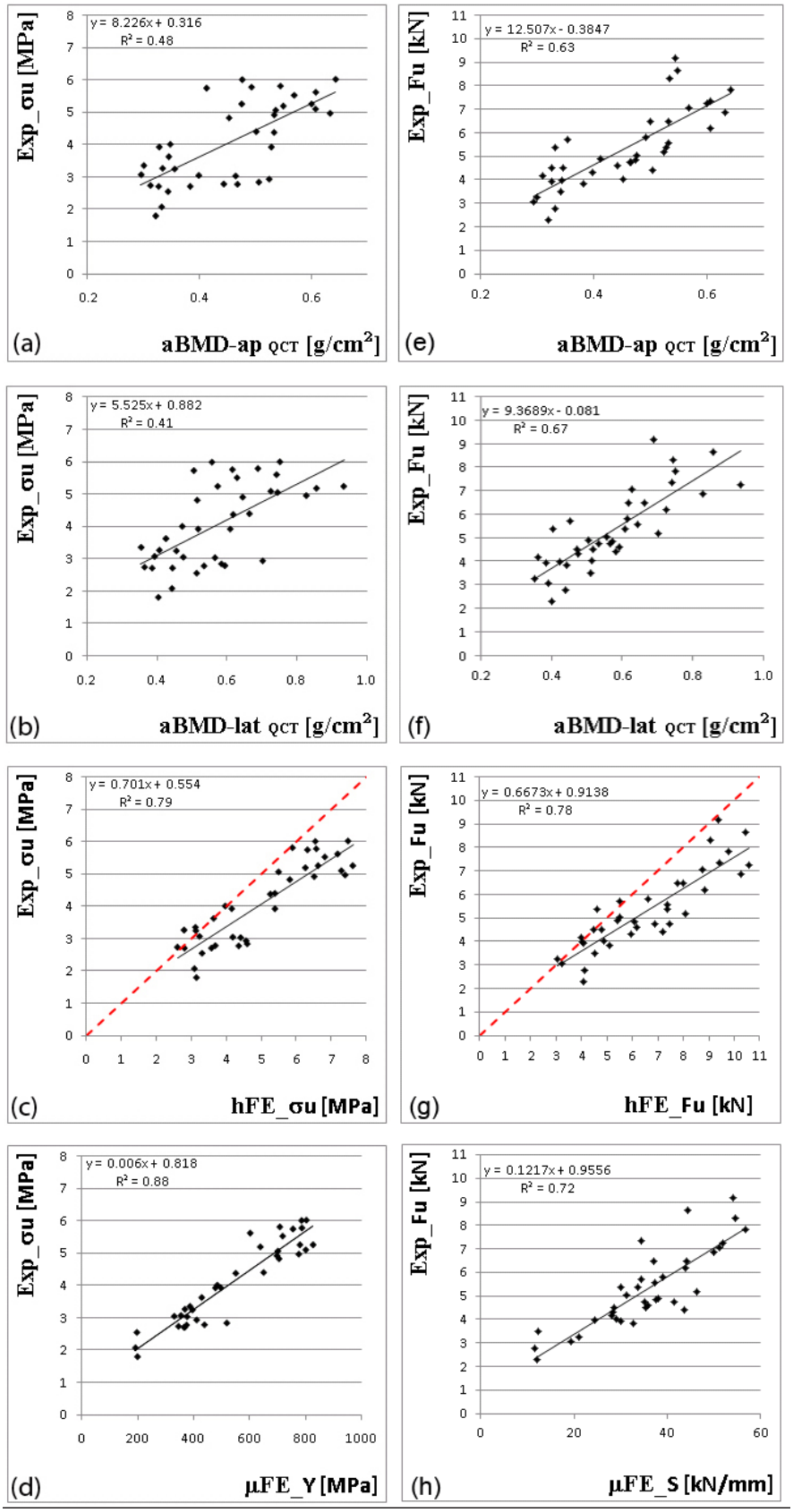

Figure 4. 2: Predictions of strength with aBMD-ap, aBMD-lat, hFE strength and μFE apparent modulus (a-d).Predictions of ultimate load with aBMD-ap, aBMD-lat, hFE ultimate load and μFE stiffness. The dashed lines represent the 1:1 relationships.

4.4 Discussion

The aim of the present study was to analyze the data from a large number of experimentally tested human thoracolumbar vertebrae and to compare the ability of the most common diagnostic tools and of FE models generated from clinical and high resolution CT images to predict both material and structural properties.

As expected, the results showed that BMC predicted the structural properties better than material ones and tBMD did the contrary. These findings underline the different nature of these two measured quantities. tBMD, defined as BMC normalized for the total volume, is obviously related to vertebral strength only if normalized for dimension. The same trend was found in previously reported results (Buckley, et al., 2007; Crawford, et al., 2003; Dall'Ara, et al., 2010). Conversely, it was not clear *a priori* if aBMD and FE models were better predictors of material or structural properties. In the present study both aBMD-ap and aBMD-lat were shown to predict better structural properties than material ones, even if the differences were not statistically significant for aBMD-ap, most probably due to the relatively low number of samples and to the strong statistical test used. This result might be explained considering that aBMD is related to body mass M. In fact it is defined as the ratio between BMC (that is proportional to M) and a projected area (that is proportional to $M^{2/3}$) and is therefore proportional to $M^{1/3}$. Conversely, even if the differences in the predictive ability was significant only in one case (strength for μFE), FE models were found to better predict material properties. In particular for hFE, the correlation improves from 0.52 to 0.71 if stiffness was normalized for dimensions. The improvement was mainly associated to the fact that samples with large osteophytes were found to be outliers only if stiffness was predicted (Dall'Ara, et al., 2010), but not for the apparent modulus. Therefore, the presence of osteophytes could significantly affect the FE model output, by changing the geometry of the vertebral body. However, this effect could be compensated by applying normalization for dimension.

The difference between the boundary conditions of the experiments, that were performed to simulate the typical wedge shape failure that occur *in vivo*, and the simplified ones defined in both hFE and μFE was justified by the two following considerations. First, the goal of the present study was to verify if the CT-based FE models could predict quantitatively the ultimate load and strength, using as inputs images and boundary conditions that could be easily extracted from *in vivo* scans. Therefore, only vertebral body sections were tested to avoid the segmentation between vertebral discs and cortical endplates or between posterior elements and the rest of the spine. Second, a previous study (Dall'Ara, et al., 2010) showed that both stiffness and ultimate load were very well correlated between models including or not the rotation of the loading plate. In fact during the experiments the rotation angles of the loading plate until the maximum force were less than one degree.

Both hFE_σu and μFE_Y predicted strength Exp_σu significantly better than almost all densitometric parameters. Moreover, it must be underlined that the FE models were generated from the same 3D images used to measure aBMD, BMC and tBMD. Therefore, the improvement in predictions could be obtained not only without additional diagnostic images, but also with reasonable computational time and costs in case of hFE. The ability of the nonlinear hFE in the present study to predict Exp_Fu and Exp_S was similar or better than the ones recently reported in the literature (Buckley, et al., 2007; Chevalier, et al., 2009b) and the prediction of Exp_Y is, in authors' knowledge, the best prediction of stiffness-related measurement reported in the literature for QCT-based FE of such a large number of samples. However, stiffness Exp_S was predicted with the same power by FE

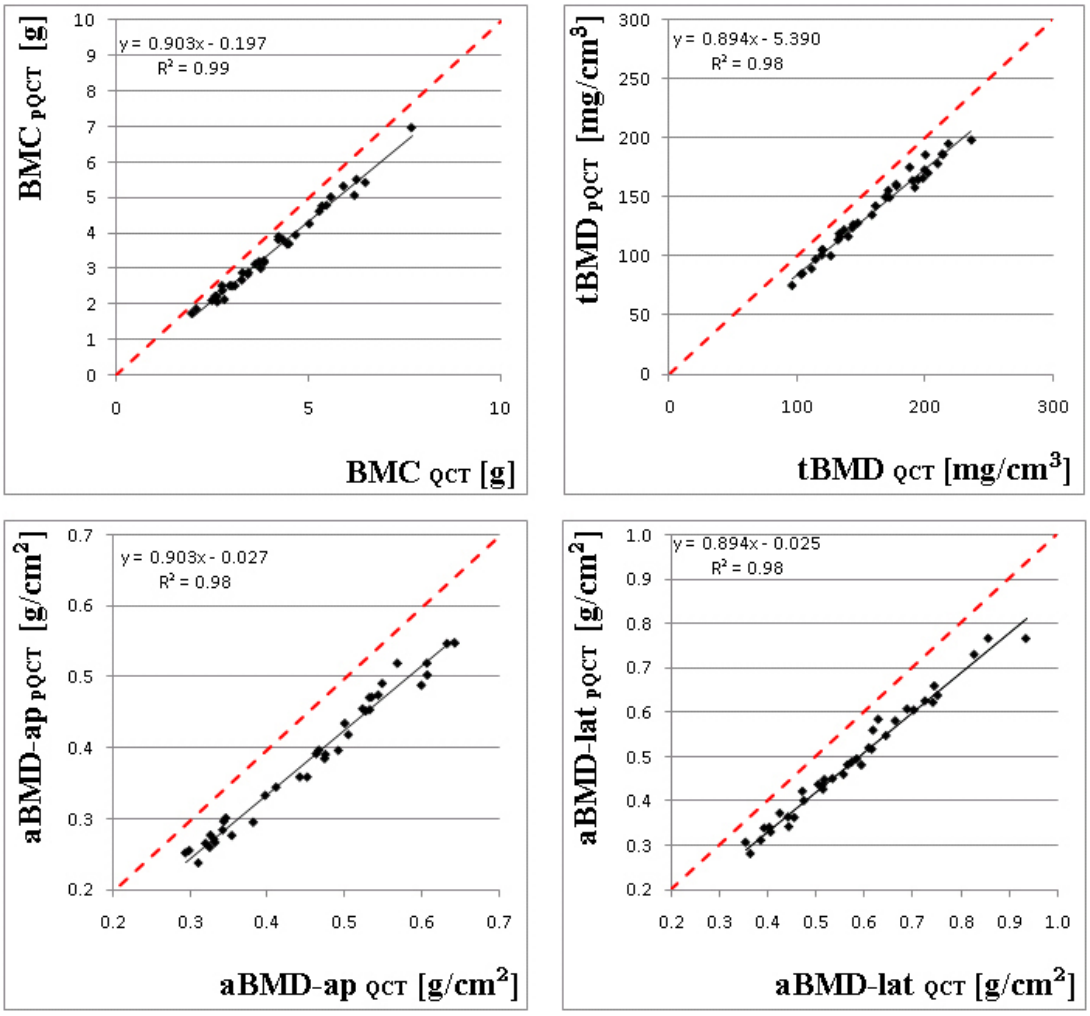

Figure 4. 3: Linear regressions for BMC, tBMD, aBMD-ap and aBMD-lat computed from QCT and HR-pQCT images. The dashed lines represent the 1:1 relationship.

models and densitometric parameters for both resolutions. BMC, tBMD and aBMD computed both with QCT and HR-pQCT predicted much better both Exp_S and Exp_Fu than the ones reported in a recent study using DXA and μCT (Roux, et al., 2009). This fact might be explained considering that the removal of posterior elements and the absence of the pelvis, that usually create artifacts in standard clinical analysis *in vivo* for anterior-posterior and lateral projections respectively, lead to an optimal artifact-free simulated DXA in the present study.

The tBMD surprisingly showed a similar ability to predict Exp_Y compared to the one of hFE (not significant difference). However, hFE, by using material properties directly from previously published experimental data (Rincon-Kohli and Zysset, 2009) without any fitting, showed a reasonable quantitative prediction of both Exp_σu and Exp_Y, which make this tool more attractive for the definition of vertebral strength and might improve the prediction of the risk of fracture. Both coefficient of determinations increased (even though not significantly) if HR-pQCT based μFE were used, even though in that case the slope of the regression line was optimized by back-calculating the tissue modulus. The stronger predictions obtained for μFE is related to the higher resolution of the images, which lead to a better representation of the bone microstructure and cortical thickness, that can not be

determined from QCT images. However, due to the high amount of time and resources needed to run the μFE, only linear analysis are feasible for large samples. Therefore, the strength could not be computed for μFE and a strong (R^2=0.88) but not quantitative prediction with μFE_Y was found. Moreover, as mentioned above, a clinical CT, that is able to scan the human spine with a resolution of 150 μm *in vivo*, was recently introduced in the market. However, an *in vivo* image voxel size for the human spine of 82 μm with a reasonable radiation dose is not expected in the close future. The strong correlations between the quantities computed from QCT and HR-pQCT images, and thus the similar predictions for the mechanical properties, showed that the increase of resolution might bring only a slight benefit for these predictions. On the contrary, the nonlinear hFE might still be improved by introducing more sophisticated material properties, an artificial smoothing of the cortical shell elements and evaluation of cortical thickness with higher resolution (Chevalier, et al., 2009b).

A first limitation of the study was that the vertebrae were scanned after extraction from the human body: the images used to generate all the data (both mass-, density-based properties and FE models) were therefore less affected by the noise that might appear in *in vivo* scans. In fact the amount of soft tissues around the spine and the different fat composition could increase noise and artifacts in the QCT images. However, the better ability of FE in predicting material properties compared to the one of aBMD might be even higher if standard DXA would be used instead of the artifact-free procedure applied in the present study. As a further limitation, bone sections were tested after removal of cortical endplates. While this model allows a simple image extraction from *in vivo* QCT scans, this choice might not mimic exactly the *in vivo* condition in which the vertebra is loaded through the vertebral disc and the cortical endplates. In particular, it cannot be inferred that the relatively small differences between some of the coefficients of determination would remain significant if the cortical endplates would be included. However, even if the model was validated in this simplified condition, it might be applied in the future to evaluate to what extent the removal of cortical endplates and of the posterior elements affects vertebral strength.

In conclusion:

- FE models were found to predict material properties of human vertebral sections as well as if not better as the structural ones. Suggested by its independence of body mass and indirectly of physiological loads, it remains to be shown if strength (σu) is a more relevant parameter for vertebral fracture risk than ultimate load.
- QCT-based hFE predicted *in vitro* strength significantly better than aBMD in both anterior-posterior and lateral directions. This superior predictive power of QCT-based variables needs to be confirmed for boundary conditions that resemble even more the *in vivo* loading conditions of human vertebrae.
- When the image resolution is improved to 82 μm, no benefits were found for prediction of any vertebral mechanical property using densitometric variables (BMC, tBMD, aBMD) and a significant improvement was seen only for prediction of stiffness using linear μFE.

Acknowledgements

The authors acknowledge a grant for an interuniversity computer tomography network from the UniInfrastruktur Program III of the Austrian Ministry for Science and Research (bm: bwk). The authors gratefully acknowledge Dr Reinhard Schmidt for having collected the samples.

Bibliography

Ammann P., Rizzoli R., 2003. Bone strength and its determinants. Osteoporosis International 14 Suppl 3, S13-18

Arbenz P., van Lenthe G.H., Mennel U., Mueller R., Sala M., 2008. A scalable multi-level preconditioner for matrix-free -finite element analysis of human bone structures. Int J Num Methods Eng 73, 927–947

Augat P., Schorlemmer S., 2006. The role of cortical bone and its microstructure in bone strength. Age and Ageing 35 Suppl 2, ii27-ii31

Bergot C., Laval-Jeantet A.M., Hutchinson K., Dautraix I., Caulin F., Genant H.K., 2001. A comparison of spinal quantitative computed tomography with dual energy X-ray absorptiometry in European women with vertebral and nonvertebral fractures. Calcified Tissue International 68, 74-82

Boivin G.Y., Chavassieux P.M., Santora A.C., Yates J., Meunier P.J., 2000. Alendronate increases bone strength by increasing the mean degree of mineralization of bone tissue in osteoporotic women. Bone 27, 687-694

Bouxsein M.L., 2003. Bone quality: where do we go from here? Osteoporososis International 14 Suppl 5, S118-127

Brianza S.Z., D'Amelio P., Pugno N., Delise M., Bignardi C., Isaia G., 2007. Allometric scaling and biomechanical behavior of the bone tissue: an experimental intraspecific investigation. Bone 40, 1635-1642

Buckley J.M., Loo K., Motherway J., 2007. Comparison of quantitative computed tomography-based measures in predicting vertebral compressive strength. Bone 40, 767-774

Burghardt A.J., Kazakia G.J., Link T.M., Majumdar S., 2009. Automated simulation of areal bone mineral density assessment in the distal radius from high-resolution peripheral quantitative computed tomography. Osteoporosis International 20, 2017-2024

Chevalier Y., Charlebois M., Pahra D., Varga P., Heini P., Schneider E., Zysset P., 2008. A patient-specific finite element methodology to predict damage accumulation in vertebral bodies under axial compression, sagittal flexion and combined loads. Computer Methods in Biomechanics and Biomedical Engineering 11, 477-487

Chevalier Y., Pahr D., Zysset P.K., 2009a. The role of cortical shell and trabecular Fabric in Finite Element analysis of the human vertebral body. Journal of Biomechanical Engineering 131, epub

Chevalier Y., Pahr D., Zysset P.K., 2009b. The role of cortical shell and trabecular fabric in finite element analysis of the human vertebral body. J Biomed Eng 131, 111003

Ciarelli T.E., Fyhrie D.P., Schaffler M.B., Goldstein S.A., 2000. Variations in three-dimensional cancellous bone architecture of the proximal femur in female hip fractures and in controls. Journal of Bone and Mineral Reasearch 15, 32-40.

Crawford R.P., Cann C.E., Keaveny T.M., 2003. Finite element models predict in vitro vertebral body compressive strength better than quantitative computed tomography. Bone 33, 744-750

Cristofolini L., Schileo E., Juszczyk M., Taddei F., Martelli S., Viceconti M., 2010. Mechanical testing of bones: the positive synergy of finite-element models and in vitro experiments. Philosophical Transactions Series A Mathematical Physical and Engineering Sciences 368, 2725-2763

Dall'Ara E., Varga P., Pahr D., Zysset P. (2010) Local BMD calibration of human vertebrae QCT using registered micro-CT images. European Symposium on Calcified Tissues 2010, Glasgow, UK, 26-30 June 2010.

Dall'Ara E., Schmidt R., Pahr D., Varga P., Chevalier Y., Patsch J., Kainberger F., Zysset P., 2010. A nonlinear finite element model validation study based on a novel experimental technique for inducing anterior wedge-shape fractures in human vertebral bodies in vitro. Journal of Biomechanics 43, 2374-2380

Davison K.S., Siminoski K., Adachi J.D., et al., 2006. Bone strength: the whole is greater than the sum of its parts. Seminars in Arthritis and Rheumatism 36, 22-31

Dong X.N., Guo X.E., 2004. The dependence of transversely isotropic elasticity of human femoral cortical bone on porosity. J Biomech 37, 1281-1287

Garcia D., Zysset P.K., Charlebois M., Curnier A., 2009. A three-dimensional elastic plastic damage constitutive law for bone tissue. Biomechanics and Modeling in Mechanobiology 8, 149-165

Griffith J.F., Engelke K., Genant H.K., 2010. Looking beyond bone mineral density : Imaging assessment of bone quality. Annales f the New York Academy of Science 1192, 45-56

Griffith J.F., Genant H.K., 2008. Bone mass and architecture determination: state of the art. Best Practice & Research Clinical Endocrinology & Metabolism 22, 737-764

Hayes W.C. (1991) Biomechanics of cortical and trabecular bone: Implications for assessment of fracture risk. In Hayes W.C. (ed) Basic orthopaedics biomechanics. Raven press, pp 93-142

Helgason B., Perilli E., Schileo E., Taddei F., Brynjolfsson S., Viceconti M., 2008. Mathematical relationships between bone density and mechanical properties: a literature review. Clinical Biomechanics (Bristol, Avon) 23, 135-146

Homminga J., Van-Rietbergen B., Lochmuller E.M., Weinans H., Eckstein F., Huiskes R., 2004. The osteoporotic vertebral structure is well adapted to the loads of daily life, but not to infrequent "error" loads. Bone 34, 510-516

Imai K., Ohnishi I., Bessho M., Nakamura K., 2006. Nonlinear finite element model predicts vertebral bone strength and fracture site. Spine 31, 1789-1794

Jalava T., Sarna S., Pylkkanen L., et al., 2003. Association between vertebral fracture and increased mortality in osteoporotic patients. Journal of Bone and Mineral Research 18, 1254-1260

Johnell O., Kanis J., 2005. Epidemiology of osteoporotic fractures. Osteoporosis International 16 Suppl 2, S3-7

Johnell O., Kanis J.A., 2006. An estimate of the worldwide prevalence and disability associated with osteoporotic fractures. Osteoporososis International 17, 1726-1733

Kanis J.A., Gluer C.C., 2000. An update on the diagnosis and assessment of osteoporosis with densitometry. Committee of Scientific Advisors, International Osteoporosis Foundation. Osteoporosis International 11, 192-202

Kanis J.A., Johnell O., Oden A., et al., 2006. The use of multiple sites for the diagnosis of osteoporosis. Osteoporosis International 17, 527-534

Kanis J.A., Oden A., Johnell O., De Laet C., Jonsson B., 2004. Excess mortality after hospitalisation for vertebral fracture. Osteoporosis International 15, 108-112

Keaveny T.M., Guo X.E., Wachtel E.F., McMahon T.A., Hayes W.C., 1994. Trabecular bone exhibits fully linear elastic behavior and yields at low strains. Journal of Biomechanics 27, 1127-1136.

Laib A., Hauselmann H.J., Ruegsegger P., 1998. In vivo high resolution 3D-QCT of the human forearm. Technol Health Care 6, 329-337

Macneil J.A., Boyd S.K., 2008. Bone strength at the distal radius can be estimated from high-resolution peripheral quantitative computed tomography and the finite element method. Bone 42, 1203-1213

Marshall D., Johnell O., Wedel H., 1996. Meta-analysis of how well measures of bone mineral density predict occurrence of osteoporotic fractures. BMJ (Clinical Research ad) 312, 1254-1259

Matsuura M., Eckstein F., Lochmuller E.M., Zysset P.K., 2007. The role of fabric in the quasi-static compressive mechanical properties of human trabecular bone from various anatomical locations. Biomechanics and modeling in mechanobiology 19, 19

McDonnell P., McHugh P.E., O'Mahoney D., 2007. Vertebral osteoporosis and trabecular bone quality. Annales of Biomedical Engineering 35, 170-189

Mueller T.L., Stauber M., Kohler T., Eckstein F., Muller R., van Lenthe G.H., 2009. Non-invasive bone competence analysis by high-resolution pQCT: an in vitro reproducibility study on structural and mechanical properties at the human radius. Bone 44, 364-371

Mulder L., Van Rietbergen B., Noordhoek N., Ito K. (2010) Determination of in-vivo vertebral and femural trabecular morphology and stiffness using a flat-panel CT fluoroscopy approach. 17th congress of the European society of biomechanics, University of Edinburgh, UK, 4-8 July 2010.

Pahr D., Dall'Ara E., Varga P., Zysset P. (2010) Homogenized continuum-level finite element models predict experimental vertebral stiffness and strength with the same accuracy as μFE models. 17th congress of the European society of biomechanics, University of Edinburgh, UK, 4-8 July 2010.

Pahr D.H., Zysset P.K., 2009. From high-resolution CT data to finite element models: development of an integrated modular framework. Computer Methods in Biomechanics and Biomedical Engineering 12, 45-57

Rincon-Kohli L., Zysset P.K., 2009. Multi-axial mechanical properties of human trabecular bone. Biomechanics and Modeling in Mechanobiology 8, 195-208

Roux J., Wegrzyn J., Arlot M., Guyen O., Delmas P., Chapurlat R., Bouxsein M., 2009. Contribution of trabecular and cortical components to biomechanical behavior of human vertebrae: an ex-vivo study. Journal of Bone and Mineral Research 25, 356-356.

Silva M.J., 2007. Biomechanics of osteoporotic fractures. Injury 38 Suppl 3, S69-76

Silva M.J., Keaveny T.M., Hayes W.C., 1998. Computed tomography-based finite element analysis predicts failure loads and fracture patterns for vertebral sections. Journal of Orthopaedic Research 16, 300-308

Siris E.S., Chen Y.T., Abbott T.A., Barrett-Connor E., Miller P.D., Wehren L.E., Berger M.L., 2004. Bone mineral density thresholds for pharmacological intervention to prevent fractures. Archives of Internal Medicine 164, 1108-1112

Steiger J.H., 1980. Tests for comparing elements of a correlation matrix. Psychological bullettin 87, 245-251

Turner C.H., 2002. Biomechanics of bone: determinants of skeletal fragility and bone quality. Osteoporosis International 13, 97-104.

Ulrich D., van Rietbergen B., Laib A., Ruegsegger P., 1999. The ability of three-dimensional structural indices to reflect mechanical aspects of trabecular bone. Bone 25, 55-60

Varga P., Baumbach S., Pahr D., Zysset P.K., 2009. Validation of an anatomy specific finite element model of Colles' fracture. Journal of Biomechanics 42, 1726-1731

Varga P., Pahr D., Dall'Ara E., Baumbach S., Pretterklieber M., Zysset P. (2010) Calibrated HR-pQCT-based microFE models of ultra-distal radius sections provide outstanding prediction of experimental Colles' fracture load. 17th congress of the European society of biomechanics, University of Edinburgh, UK, 4-8 July 2010.

Viguet-Carrin S., Garnero P., Delmas P.D., 2006. The role of collagen in bone strength. Osteoporosis International 17, 319-336

Wenzel T.E., Schaffler M.B., Fyhrie D.P., 1996. In vivo trabecular microcracks in human vertebral bone. Bone 19, 89-95

WHO (1994) Assessment of fracture risk and its application to screening for postmenopausal osteoporosis. Technical Report Series. WHO, Geneve

Zeinali A., Hashemi B., Akhlaghpoor S., 2010. Noninvasive prediction of vertebral body compressive strength using nonlinear finite element method and an image based technique. Physica Medica 26, 88-97

Zysset P.K., 2003. A review of morphology-elasticity relationships in human trabecular bone: theories and experiments. Journal of Biomechanics 36, 1469-1485.

Zysset P.K., Curnier A., 1996. A 3D damage model for trabecular bone based on fabric tensors. Journal of Biomechanics 29, 1549-1558

Zysset P.K., Rincon-Kohli L. (2006) An alternative fabric-based yield and failure criterion for treabecular bone. In Holzapfel G., Ogden R. (eds) Mechanics of biological tissue. Springer, Berlin, pp 457-470

Chapter 5

hvFE validation study for the human proximal femur

From the manuscript:

A nonlinear QCT-based finite element model validation study for the human femur tested in two configurations *in vitro*

E. Dall'Ara [a]*, B. Luisier [a], R. Schmidt [b], F. Kainberger [c], P. Zysset [d], D. Pahr [a]

a Institute of Lightweight Design and Structural Biomechanics, Vienna University of Technology, Austria
b Department of Trauma Surgery, Medical University of Vienna, Austria
c Department of Radiology, Medical University of Vienna, Austria
d Institute for Surgical Technology and Biomechanics, University of Bern, Switzerland

Accepted in: Bone, 2012

Abstract
Purpose Femoral fracture is a common medical problem in osteoporotic individuals. Bone mineral density (BMD) is the gold standard measure to evaluate fracture risk *in vivo*. Quantitative computed tomography (QCT)-based homogenized voxel finite element (hvFE) models have been proved to be more accurate predictors of femoral strength than BMD by adding geometrical and material properties. The aim of this study was to evaluate the ability of hvFE models in predicting femoral stiffness, strength and failure location for a large number of pairs of human femora tested in two different loading scenarios.
Methods Thirty-six pairs of femora were scanned with QCT and total proximal BMD and BMC were evaluated. For each pair, one femur was positioned in one-legged stance configuration (STANCE) and the other in a sideways configuration (SIDE). Nonlinear hvFE models were generated from QCT images by reproducing the same loading configurations imposed in the experiments. For experiments and models, the structural properties (stiffness and ultimate load), the failure location and the motion of the femoral head were computed and compared.
Results In both configurations, hvFE models predicted both stiffness (R^2=0.82 for STANCE and R^2=0.74 for SIDE) and femoral ultimate load (R^2=0.80 for STANCE and R^2=0.85 for SIDE) better than BMD and BMC. Moreover, the models predicted qualitatively well the failure location (66% of cases) and the motion of the femoral head.
Conclusions The subject specific QCT-based nonlinear hvFE model can not only predict femoral apparent mechanical properties better than densitometric measures, but can additionally provide useful qualitative information about failure location.

Keywords: Finite Element, BMD, Femoral Strength, Femoral Stiffness, Osteoporosis, Validation

5.1 Introduction

Osteoporosis is a common skeletal disease, which increases lifetime fracture risk (Johnell and Kanis, 2006). In osteoporotic individuals, femoral fracture is a major clinical problem with high morbidity and mortality (Cummings and Melton, 2002; Mnif, et al., 2009). As the factor of risk can be defined as the ratio between applied load and bone strength (Hayes, 1991), accurate prediction of femoral strength might help the identification and follow-up of patients who require treatment.

The evaluation and understanding of the mechanical properties of the human femur should be investigated for accidental and physiological loadings. In the first case, a fall scenario is important because femoral fractures are often associated with an impact load due to a sideways fall (Greenspan, et al., 1998; Kannus, et al., 2006; Parkkari, et al., 1999; Schwartz, et al., 1998). In the second case, the assessment of femoral mechanics in one-legged stance is necessary to study the incidence of spontaneous fractures (Cristofolini, et al., 2007; Viceconti, et al., 2012), the behavior of the hip during daily activities (Juszczyk, et al., 2011), the stress redistribution after hip surgery (Martelli, et al., 2012), the load sharing between cortical and trabecular bone (Holzer, et al., 2009), and the effect of pathologies like bone metastasis on bone strength (Keyak, et al., 2007).

Bone Mineral Density (BMD) measured at the hip is a surrogate of bone strength and is currently used to define osteoporosis (WHO, 1994). While dual energy x-rays absorptiometry (DXA) is the gold standard in measuring areal BMD for its low cost and radiation dose, quantitative computed tomography (QCT), with its 3D nature and the ability of distinguishing between bone microstructures (i.e. cortical vs trabecular bone), is being used intensively in the last decade as a research tool. For its higher precision in measuring BMD compared to DXA (Adams, 2009; Genant and Jiang, 2006), QCT has been recently used in clinical trials to estimate the effect of drug treatments on the femoral ultimate load (Borggrefe, et al., 2010; Engelke, et al., 2010; Lewiecki, et al., 2009) and to discriminate between patients who did or did not undergo a hip fracture (Black, et al., 2008; Bousson, et al., 2011). However, *in vitro* studies performed on bone tissue at the biopsy and organ levels showed that BMD alone can't explain the whole variance in the mechanical properties (Ammann and Rizzoli, 2003) and in particular its predictive ability for femoral strength has shown a wide range of variability (R^2=0.35-0.92) (Bouxsein, et al., 1999; Lochmuller, et al., 2003). Therefore, aspects other than BMD (e.g. geometry, cortical thickness, cortical and trabecular bone distribution, trabecular orientation, loading direction) may be relevant in the definition of femoral mechanical properties and should be taken into account when trying to diagnose its risk of fracture.

If applied to the proximal femur (Keyak, 2001; Lenaerts and van Lenthe, 2009; Viceconti, et al., 2004), QCT-based finite element (FE) models can improve the prediction of mechanical properties by combining information about BMD distribution, femoral geometry, femoral size, bone material properties and loading configuration. Homogenized continuum level voxel based FE models (hvFE, where coarsened voxels are directly converted to hexahedron elements) have been recently used in clinical studies to evaluate the effect of drug treatments compared to baseline femoral ultimate load (Keaveny, et al., 2008; Keaveny, et al., 2012), to investigate the effect of gender and age on femoral strength and fracture risk (Keaveny, et al., 2010; Keyak, et al., 2011), to investigate the hip fracture risk in older men (Orwoll, et al., 2009) or to investigate the effect of long-term spaceflight on bone strength (Keyak, et al., 2009). However, all computational models need first to be validated (i.e. have to be accurately compared with experimental outcomes *in vitro*) to understand how reliable they are in predicting specific mechanical properties under certain

conditions (Cristofolini, et al., 2010). *In vitro* studies have already shown QCT-based FE models to predict accurately the local strains/displacement in sub-regions of the external surface of the femur ($0.78<R^2<0.99$, (Grassi, et al., 2012; Schileo, et al., 2008; Trabelsi and Yosibash, 2011; Yosibash, et al., 2007)), to qualitatively predict the failure location (Keyak, et al., 2001a) and to predict the femoral ultimate load better than BMD (Cody, et al., 1999; Dragomir-Daescu, et al., 2011; Keyak, et al., 1998). In most validation studies, the models were validated for one particular load configuration (i.e. simulating one-legged stance or a fall on the side) and investigated solely one among structural properties (stiffness and/or ultimate force), local properties (displacements or strains in a few points of the femur) or fracture location (qualitatively). Due to the complexity of the experimental and modelling procedures, to the authors' knowledge, only a few studies have investigated both loading conditions with the same model (17 pairs in (Keyak, et al., 1998) and one pair in (Lotz, et al., 1991a; Lotz, et al., 1991b)) and no one has investigated all above mentioned structural and local predictions of the same model. Moreover, a relatively low number of samples was usually investigated ($1<N<25$ in the above mentioned studies) considering the highly time consuming validation procedure. Furthermore, in some cases the FE models were tuned i.e. parameters like yield strain (Dragomir-Daescu, et al., 2011) and Young's modulus-ash density relationship (Cong, et al., 2011) were defined from a training set to obtain more realistic results. While this procedure increases the performance of the model, at the same time it restricts its applicability to other configuration it was not trained for, thus it loses flexibility.
Even though the FE method is recognized as a powerful tool for both basic and clinical research to predict bone mechanical properties, there is still a lack of studies in the literature which investigate the ability of FE in predicting femoral structural and local mechanical properties for a large number of samples, for different loading scenario, and based on calibrated input parameters. The goal of the present study was to comprehensively validate a nonlinear QCT-based hvFE model of the human proximal femur loaded in an one-legged stance and in a sideways configuration (position which might occur during a fall onto the postero-lateral aspect) by comparing the stiffness and ultimate load, the failure location and the local motion of the femoral head to experimental tests performed on a large number of pairs of femora *in vitro*.

5.2 Materials and methods

5.2.1 Sample preparation

Seventy-five human femora were collected and prepared according to the prescriptions of the ethics commission of the Medical University of Vienna, which approved all procedures applied during the present study. Three femora (one from a 75 years old female and two from a 62 years old female) were used for a calibration study (see section *5.2.4*) while the remaining 36 pairs (17 males, 19 females with age 76±12 years, range 46-96) were prepared for scanning and paired mechanical testing in two different loading configurations as described in details in a previous publication (Dall'Ara, et al., 2012). Briefly, soft tissues were carefully removed from femoral shaft, greater trochanter and lesser trochanter. Each femur was cut at 80mm distally from the middle point of the lesser trochanter and the most distal 60 mm were embedded in Polyurethane (PU). Four dental cement markers were included in the PU to keep track of the position of the proximal femur in the scanned volume.

5.2.2 QCT Scanning

Samples were submerged in 0.9% NaCl saline solution and exposed to vacuum for ten minutes to remove air bubbles. Each pair of femora was then placed in a custom made plastic chamber and scanned with a clinical QCT (*Brilliance64, Philips, Germany*; intensity: 100 mA; voltage: 120 kV; filter type: B (+0.5 enhancement); voxel size: 0.33x0.33x1.0 mm^3). Samples were scanned together with a calibration phantom (*BDC Phantom, QMR Gmbh, Germany*) for converting the HU scale to equivalent BMD scale (in mgHA/cc). The BMD range was reduced to -100 and 1400 mgHA/cc to restrict the effect of remaining air bubbles and other artifacts. To match the position of the femora during the mechanical tests, each image was rotated and cropped according to the position of the dental cement markers included in the PU. The volumetric BMD (vBMD) and bone mineral content (vBMC) were computed in the portion of the proximal femur, which was not included in the embedding material.

5.2.3 Mechanical tests

After randomization between left and right, one sample of the pair was placed in the machine to simulate the position of the femur during a one-legged stance configuration (STANCE, angle between loading direction and proximal shaft axis equal to 20°) and the other was placed in the machine to simulate the position of the femur during a fall on the side backward (SIDE, angle between loading direction and proximal shaft axis equal to 60°). In both cases the load was applied on the femoral head (on the most cranial side in STANCE and on the medial side in SIDE) in the plane containing the neck axis and the proximal femur axis (Fessy, et al., 1997). This SIDE configuration was chosen because it was found to be most critical for the femoral strength (Keyak, et al., 2001b). The shaft was fixed in both configurations. To reduce transverse forces/moment a custom made bearing was designed to allow the rotation and the two translations perpendicular to the loading axis for the femoral head in STANCE and for both femoral head and greater trochanter in SIDE. Ten millimeters of the cranial portion of the femoral head in the STANCE configuration and 10 mm of the medial portion of the femoral head in the SIDE configuration were embedded in PU to distribute the applied load. In the SIDE configuration, 10 mm of the lateral portion of the greater trochanter were embedded in PU to distribute the reaction force during the mechanical test. An adjustment screw was used to guarantee a perfect contact between the greater trochanter and the embedding material during the test (Figure 5.1, right).
Six active infrared markers (diameter 7 mm) were gripped with custom-made clamps, which in turn were glued to each femur at six locations (see Figure 5.1). In particular, one marker was positioned on the lesser trochanter, two markers on the greater trochanter and three markers on the femoral head (STANCE: on the most posterior portion in the middle of the femoral head, on the most medial side and on the caudal-medial side; SIDE: on the most posterior portion in the middle of the femoral head, on the most cranial side and on the cranial-lateral side). More markers were applied to the setup and to the machine frame to define a local reference system, to measure the relative rotation of the femoral head in the frontal plane and to evaluate the compliance of the machine/setup. The position of the markers was acquired at 100Hz with a motion capture system placed in front of the tested femur (*Optotrak Certus, Northern Digital Inc., Canada*) and able to measure marker displacements with a precision of 10 μm.

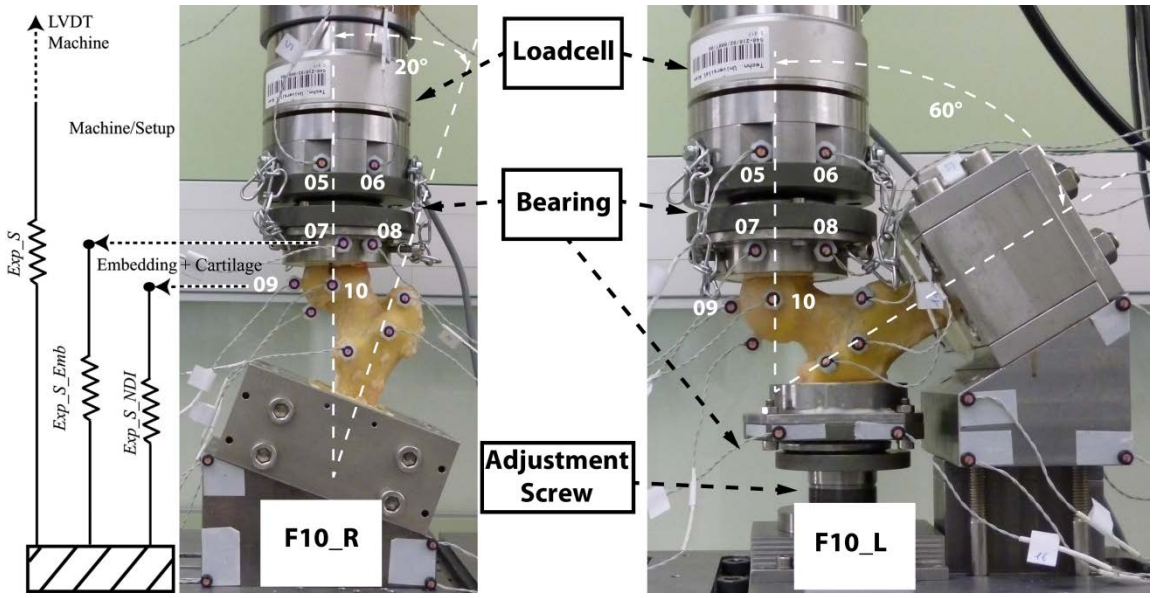

Figure 5. 1: *Experimental setup for the STANCE (left) and SIDE (right) configurations.* The positions of the load cell, of the bearings and of the screw used to adjust the position of the embedding on the greater trochanter in the SIDE configuration are indicated with the arrows. The numbers of the infrared markers used to evaluate the effect of the machine compliance and the motion of the femoral head are indicated in white. The scheme on the left hand side shows at which level the stiffness of the structure was computed.

Each specimen was kept in 0.9% NaCl saline solution for at least one hour before testing and then carefully positioned in the machine. A servo-hydraulic testing machine (*Mini-Bionix, MTS system, U.S.A.*) was used to compress the femoral head at a rate of 5 mm/min until failure. The axial force was measured by means of a 100 kN load cell (*U3 force transducer, HBM, Germany*) (Figure 5.1) mounted above the bearing of the femoral head.
Femoral ultimate force (Exp_Fu) was defined as the maximum compressive load. The markers positioned in the setup just below the femur showed a movement during the test in the order of the accuracy of the sensor (10 μm) and therefore the frame below the femur was considered as rigid. The stiffness was measured at different levels of the setup by using the integrated sensor of the machine and the output of the infrared markers (Figure 5.1 left). In particular the stiffness was calculated as the maximum slope of the linear part of the "load-displacement" curve where the axial displacement was computed as the displacement of the actuator of the testing machine (Exp_S), as the axial displacement of the marker Nr 10 (positioned on the most posterior side of the middle of the femoral head, Exp_S_NDI), or as the average axial displacement of the markers Nr 07 and Nr 08 (positioned on the rigid mold containing the embedding material above the femoral head, Exp_S_Emb). The rotation of the femoral head in the frontal plane (Exp_Rf) was computed as relative rotation between the vector defined by the markers Nr 09 and Nr 10 and the one defined by the markers Nr 07 and Nr 08. For each sample, the axial and lateral displacements of the markers Nr 09 (Exp_Disp_09ax and Exp_Disp_09lat, respectively) and Nr 10 (Exp_Disp_10ax and Exp_Disp_10lat, respectively) and the average axial displacement of the markers Nr 07 and Nr 08 (Exp_Disp_Emb) were computed when the load was equal to Exp_Fu.
After testing, plain radiographs were performed to classify the fracture location of each proximal femur according to four anatomical regions, as in clinical routine: head,

subcapital, neck and trochanter. Wherever the fracture location was in between two regions, the region involving the larger part of the fracture was considered as fracture site.

5.2.4 Computation of the BMD to BV/TV calibration

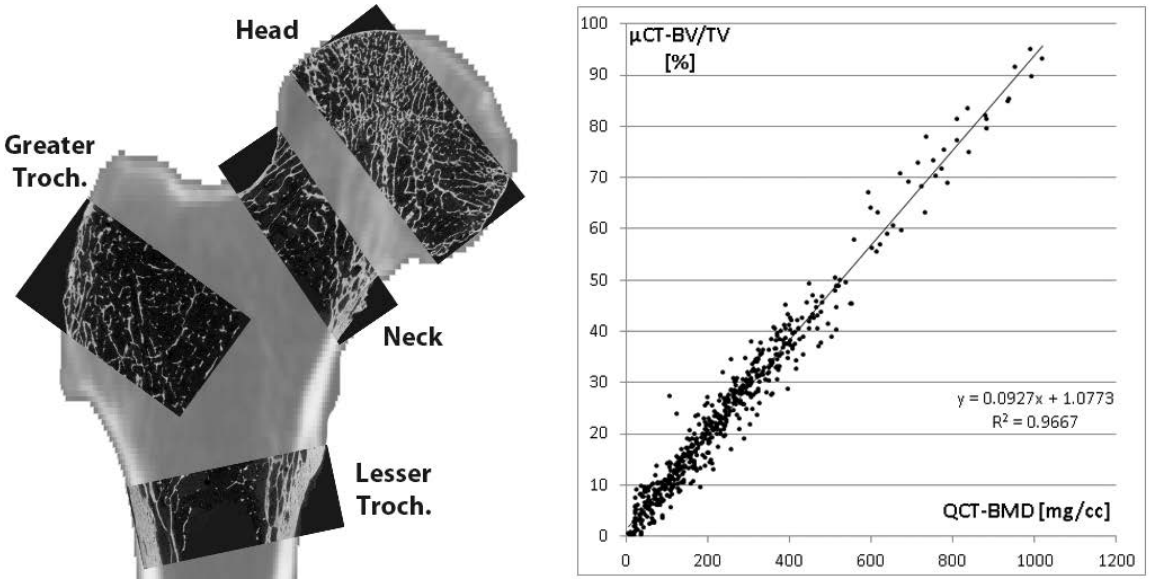

Figure 5. 2: *Overview of the calibration study.* After scanning with QCT, four regions were cut from each proximal femur (Head, Neck, Greater Trochanter and Lesser Trochanter), scanned with µCT and registered with the original QCT (left). A grid was superimposed on each registered image and the QCT_{BMD} was compared to the $\mu CT_{BV/TV}$ by means of linear regression (right).

A procedure similar to the one proposed by Dall'Ara et al. (Dall'Ara, et al., 2011) for the vertebral body was applied to find a calibration equation to compute $\mu CT_{BV/TV}$ from QCT_{BMD} for the proximal femur. In particular, the three remaining (not tested) femora were prepared and QCT-scanned with the same procedure described above. After QCT-scanning, four sub-regions were cut with a diamond band saw (*300 CP, Exakt Gmbh, Germany*) from each femur (head, greater trochanter, neck and lesser trochanter) to fit the dimensions of the largest sample holder of a µCT system (*µCT40, Scanco Medical AG, Switzerland*) and scanned in 0.9% NaCl saline solution (Voltage 70 kV, Intensity: 114 mA, Matrix 2048x2048, isotropic voxel size 0.018^3 mm^3). Afterwards, the cropped BMD-scale QCT and µCT images were superimposed with a rigid registration script (*ITK, Kitware, U.S.A.*, Figure 5.2 left). A Gaussian filter (σ=1.2, radius equal to two voxels) was applied to the µCT images to remove high frequency noise and an optimal single level threshold was computed using the iterative selection method of Ridler and Calvard (Ridler and Calvard, 1978) to segment the images. Finally, a grid with 4.32 mm in side length cubes was superimposed to both BMD-scale QCT and segmented µCT images and the QCT_{BMD} was compared to the $\mu CT_{BV/TV}$ in each cube (Dall'Ara, et al., 2011).

5.2.5 Homogenized voxel FE models

The obtained $\mu CT_{BV/TV}$-QCT_{BMD} calibration relationship was used to compute in each voxel the correspondent $\mu CT_{BV/TV}$ value from the original QCT_{BMD}.

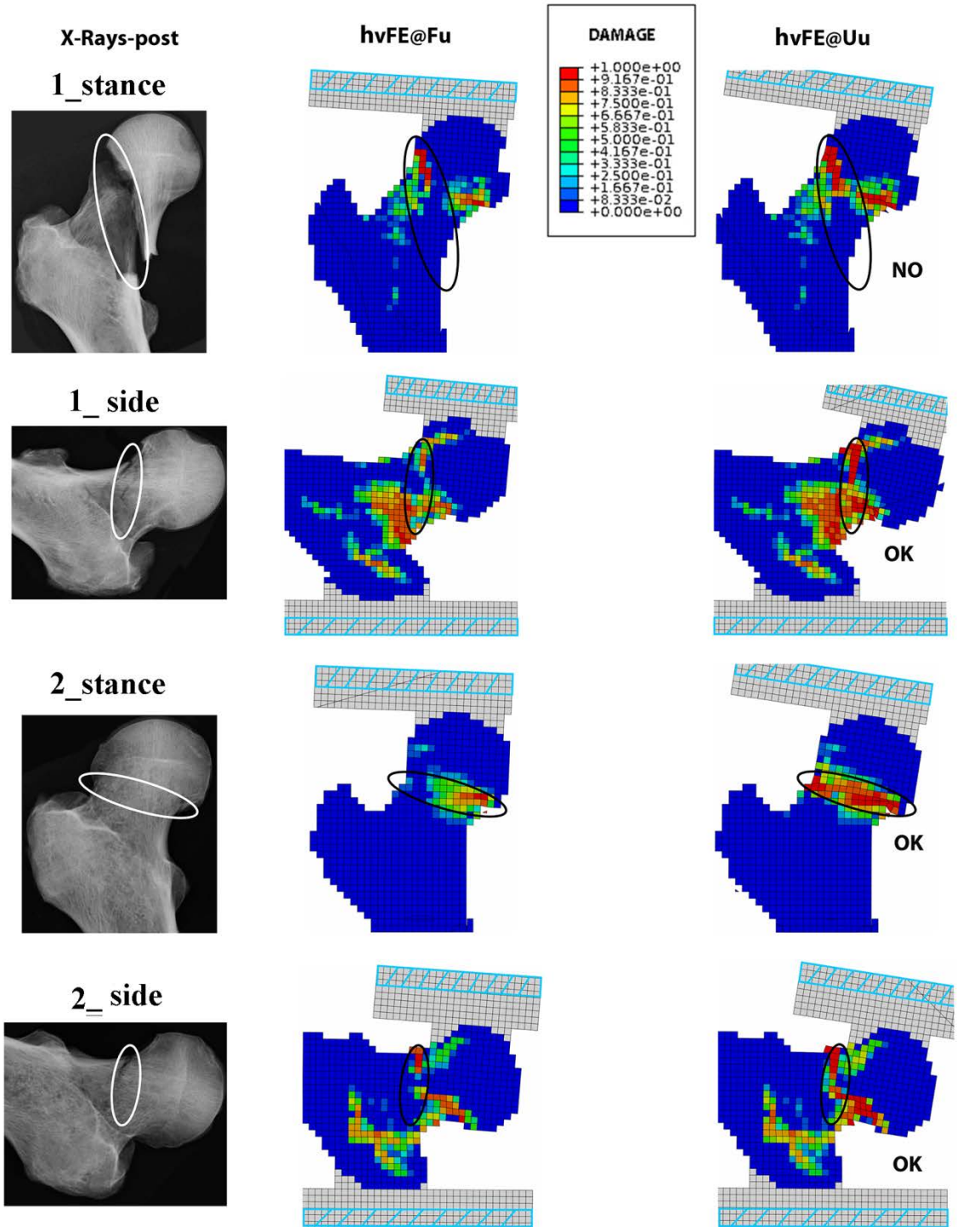

Figure 5. 3: *Prediction of failure location.* Evaluation of the ability of the model to predict the failure location in two pairs of femora. Left column shows the post-testing X-rays. hvFE cuts in the middle of the frontal plane are plotted both for the increment at the ultimate force (hvFE@Fu, middle column) and for the increment at the maximum displacement (hvFE@Uu, right column). The colors represent the value of the damage scalar variable from 0 (blue) to 1 (red). White circles highlight the failure location from the experiments and are reported in black on the models. Experiments showed three neck (1_stance, 1_side, 2_side) and one sub-capital (2_stance) fractures while the damage analysis on the 3D images of the models showed two neck (1_side and 2_side) and two sub-capital (1_stance and 2_stance) fractures. Consistent or not consistent qualitative predictions of the femoral location with the models are emphasized with "OK" or "NO", respectively. In the models steel elements are indicated with the light blue box.

The femoral QCT images were cut proximally to the embedding material and then coarsened to 3^3 mm³ voxels. The external bone contour was found for each image with a filling out algorithm (Pahr and Zysset, 2009b) as already described in a previous study for the human vertebra (Dall'Ara, et al., 2012). Voxels were directly converted to linear hexahedron elements. A PU layer (Figure 5.3, grey elements) and a steel plate (Figure 5.3, elements in the light blue boxes) were modeled to reproduce the experimental conditions. In both configurations, the nodes on the top of the steel layer above the femoral head were coupled to a reference node, located at the most top position (most cranial and most medial in case of STANCE and SIDE, respectively) of the femoral head (computed from the average positions of all finite element nodes of that portion of the femoral head). All translations and rotations of the reference node were left free except the axial translation, which was imposed to load the femoral head. In particular, the in-plane translations were left free to simulate the bearing and the rotations were left free to simulate the possible relative rotation between the embedding material and the femoral head, allowed during the experiments by the cartilage layer. In the SIDE configuration, the most lateral nodes of the steel elements (below the greater trochanter) were left free to translate and to rotate in the plane perpendicular to the loading axis (to simulate the boundary conditions imposed by the second bearing positioned under the greater trochanter). Furthermore, in both configurations the nodes of the most distal part of the shaft were fixed in all translations.
The material properties of the elements were defined as following. PU and steel elements were modeled as isotropic with Poisson ratio equal to 0.3 and Young's modulus equal to 1.36 (from tensile experimental tests performed in our laboratory on the utilized PU) and 210 GPa , respectively. Due to the limited resolution of the CT scans, no fabric measurement could be done and bone was therefore considered isotropic and was modeled with an elastic-damage constitutive law adapted from Garcia et al. (Garcia, et al., 2009) (for a more detailed formulation please see the Appendix). Briefly, material nonlinearity was applied when bone was loaded beyond a yield limit defined by a piecewise Hill criterion (Zysset and Rincon-Kohli, 2006) where the inelastic behavior was driven by a damage scalar variable (between 0 and 1) which represents the reduction of the material elastic modulus (Zysset and Curnier, 1996). Elastic and strength properties were adjusted from Rincon-Kohli and Zysset (2009) (Rincon-Kohli and Zysset, 2009), who performed multi-axial mechanical testing on human trabecular bone. Due to the fact that those material parameters were extrapolated from measurements performed on trabecular bone samples, a correction was necessary for the femur where cortical bone plays an important role. Therefore, a nonlinear scalar function (tissue function TF, Appendix) for both compression and tension was defined to provide, once extrapolated for poreless bone (BV/TV=ρ=1), an elastic modulus equal to 24 GPa (Emax), a compression ultimate stress equal to 266 MPa and a tension ultimate stress equal to 200 MPa. These values were based on published results for cortical bone (Bayraktar, et al., 2004; Ohman, et al., 2011). The material constants needed to define the elastic (defined in Appendix as ε_0, υ_0, μ_0) and yield (defined in Appendix as σ_0^+, σ_0^+, χ_0^+, χ_0^-, τ_0) behavior of bone were recalculated accordingly and were used to define the constitutive model.
Analyses including material nonlinearity were performed (*Abaqus 6.11, Simulia, Dassault Systemes, Velizy-Villacoublay, France*) until the reference point, placed on the top of the femoral head nodes and whose displacements where coupled to the top nodes of the steel part above the femoral head, was displaced in axial direction by 7mm. Although in most cases the simulation stopped before the reference point reached the target 7mm axial displacement, the load-displacement curve reached a clear maximum in all cases.

The axial load and axial displacement were computed as the reaction force and the displacement in axial direction of the reference point. Stiffness (hvFE_S) and ultimate force (hvFE_Fu) were calculated as the maximum slope and the maximum load of the load-displacement curve, respectively. Furthermore, two groups of four nodes closest to the position of the markers Nr 09 and Nr 10 were selected in the undeformed model for each sample. For comparison with experimental results, the average axial and lateral displacements for both groups of nodes (hvFE_Disp_09ax, hvFE_Disp_09lat for the one close to the position of marker Nr 09 and hvFE_Disp_10ax, hvFE_Disp_10lat for the one close to the position of the marker Nr 10), the displacement of the reference node in the axial direction (hvFE_Disp) and the rotation of the loading plate in the frontal plane (hvFE_Rf) were computed at the ultimate force hvFE_Fu.
For each model, the region where the damage localized mostly (head, subcapital, neck or trochanteric) was compared to the fracture location shown by the post-testing x-rays.

5.3 Results

The experimental setup was able to reproduce typical femoral fractures in most cases (subcapital: 24%, neck: 54%, trochanteric: 13%, atypical in the femoral head: 3%, not clear: 6%). The average experimental femoral ultimate force was 8.71±2.93 kN (range: 3.54-14.42 kN) and 3.12±1.14 kN (range: 1.46-5.26 kN) for STANCE and SIDE configurations, respectively.

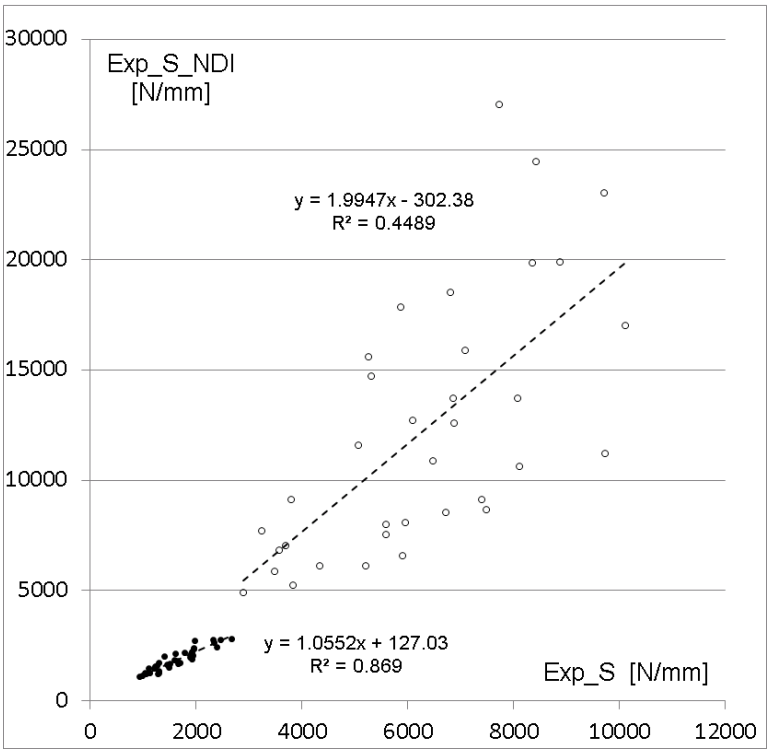

Figure 5. 4: *Experimental results for stiffness.* Relationship between the experimental stiffness calculated by using the displacement measured with the testing machine (Exp_S) or with the axial displacement of the marker Nr 10 positioned on the most posterior side in the middle of the femoral head (Exp_S_NDI). Open and filled circles represent the femora tested in the STANCE and SIDE configurations, respectively.

The stiffness computed with the machine displacement sensor (Exp_S) was 6.28±1.94 kN/mm (range: 2.90-10.12 kN/mm) for STANCE and 1.64±0.46 kN/mm (range: 0.95-2.68 kN/mm) for SIDE. As expected, a correlation was found between experimental stiffness and ultimate load ($p<0.001$, $R^2=0.73$ for both STANCE and SIDE). The good quantitative correlations between Exp_S and Exp_S_Emb ($R^2=0.997$, Intercept=-0.22kN/mm, Slope=1.09, respectively) showed a constant underestimation of the stiffness due to the compliance of the machine/setup of approximately 10%. Moreover, Exp_S was correlated with the stiffness computed from the displacement measured with the marker positioned on the femoral head (Exp_S_NDI) for both STANCE and SIDE configurations ($p<0.001$, Figure 5.4). However, high correlations were found only for the SIDE configuration (Range=1.08-2.81 kN/mm, $R^2=0.87$, SEE=0.18 kN/mm), while for the STANCE configuration the correlation was poor (Range=4.54-27.06kN/mm, $R^2=0.45$, SEE=4.29 kN/mm).

To define the element's material properties, two sub-studies were performed to investigate the relationship between BMD and BV/TV as well as to define a new set of material constants valid for both trabecular and cortical bone. The application of the pre-scan vacuum procedure resulted in almost bubble-free QCT and µCT images. The following linear regression between QCT_{BMD} and $\mu CT_{BV/TV}$ was found from the first sub-study (Figure 5.2 right):

$$\begin{cases} \boldsymbol{\mu CT_{BV/TV}}[\%] = 0.093 * \boldsymbol{QCT_{BMD}} \left[\frac{mgHA}{cc}\right] + 1.077 \text{ , for } -100 < \boldsymbol{QCT_{BMD}} \leq 1064 \\ \boldsymbol{\mu CT_{BV/TV}}[\%] = 100 \text{ , for } 1064 < \boldsymbol{QCT_{BMD}} \leq 1400 \end{cases} \quad (5.1)$$

The calibration equation was found to be linear for the full range of BMD ($R^2=0.97$ and SEE=3.2). The intercept of the linear regression was close to 0 (CI: 0.51-0.77%). A QCT_{BMD} equal to 1064 mgHA/cc was found to correspond to 100% $\mu CT_{BV/TV}$.

Furthermore, the set of material properties computed with the correction to account for cortical bone described in the previous section is reported in Table 5.1.

	Elasticity				**Yield/Strength**		
	ε_0 [GPa]	**υ_0 [-]**	**μ_0 [GPa]**	**k [-]**	**σ_0 [MPa]**	**χ_0 [-]**	**τ_0 [MPa]**
Tension	6.614	0.246	2.654	1.333	54.8	-0.246	44.6
Compression					72.9	0.333	

Table 5. 1: Material Constants. Set of material constants computed with the new tissue function TF to obtain meaningful values for pore-less bone material properties

Linear and power regressions were computed to investigate the correlation between QCT measurements (vBMD and vBMC) and femoral mechanical properties (Exp_S_Emb and Exp_Fu). An overview is given in Figure 5.5. The average number of nodes and elements in the hvFE models were approximately 13'000 and 10'000, respectively. The models were solved on a two CPU Desktop PC with 2.67 GHz each within approximately 30 minutes (average CPU time necessary 50 minutes, average necessary memory 480 Mb). For both configurations, the hvFE models were found to predict ultimate load (N=36, R^2=0.80, SEE=1.28kN for STANCE and R^2=0.85, SEE=0.44kN for SIDE) and stiffness (N=36, R^2=0.82, SEE=0.91kN/mm for STANCE and R^2=0.74, SEE=0.23kN/mm for SIDE) better than vBMD (R^2<0.61 and R^2<0.36 for STANCE; R^2<0.71 and R^2<0.61 for SIDE) and vBMC (R^2<0.74 and R^2<0.48 for STANCE; R^2<0.70 and R^2<0.60 for SIDE). The Pearson's coefficients of the linear regressions between mechanical properties and densitometric or hvFE outputs were found to be significantly different in almost all cases ($p<0.016$ in all comparisons except for vBMC vs hvFE_Fu for predictions of Exp_Fu in STANCE where p=0.108 and for vBMC vs hvFE_S for predictions of Exp_S_Emb in SIDE where p=0.060 (Steiger, 1980)).

Figure 5.6 shows the comparison between experimental and hvFE load-displacement curves for four different pairs of femora. The experimental curves for the femora tested in STANCE configuration were found to be steeper compared to the ones tested in SIDE configuration. In fact, the ultimate force was systematically higher for stance and the displacement at the ultimate force was systematically higher for SIDE (1.65±0.39mm for STANCE and 2.39±0.65mm for SIDE, paired t-test $p<0.001$). The same trend was found for the hvFE models (4.84±2.04kN and 1.14±0.19mm for STANCE and 2.65±1.16kN and 3.05±0.74mm for SIDE, paired t-test $p<0.001$ in both cases). The failure load in the STANCE configuration was correlated to the failure load in the SIDE configuration for both experiments (Slope=0.33, Intercept=0.24 kN, R^2=0.72, SEE=0.60 kN) and models (Slope=0.48, Intercept=0.33 kN, R^2=0.71, SEE=0.61 kN).

Moreover, the qualitative comparison between post-test X-rays and damage distribution in the hvFE models showed good agreement in 66% of cases (61% for the STANCE configuration and 71% for the SIDE configuration, examples in Figure 5.3). For the 65 fractures included in the analysis (after exclusion of the atypical and unclear fractures), the model predictions were in agreement with the experimental fracture location in 76% of the 17 sub-capital fractures (92% of the 13 for STANCE and 25% of the 4 for SIDE), in 74% of the 39 neck fractures (50% of the 16 for STANCE and 91% of the 23 for SIDE) and in 22% of the 9 trochanteric fractures (0% of the 3 for STANCE and 33% of the 6 for SIDE).

As the displacements of the markers applied to the greater trochanter and the lesser trochanter were small for both experiments and simulations, the kinematic analysis was performed only for the marker Nr 10 and Nr 09 placed on the femoral head. The hvFE were able to predict only qualitatively the axial and lateral displacements of the marker Nr 09 and Nr 10 and the rotation of the femoral head in the frontal plane computed at the maximum load (Figure 5.7). The linear regressions between the predicted and real values of these local measurements were only poorly or moderately correlated for STANCE ($p<0.001$; $0.28<R^2<0.68$) and poorly correlated in a few cases for SIDE (for Disp_10lat and Disp_09lat $p<0.001$ and R^2=0.40 and R^2=0.58, respectively) while in all other cases the correlation was not significant ($p>0.624$).

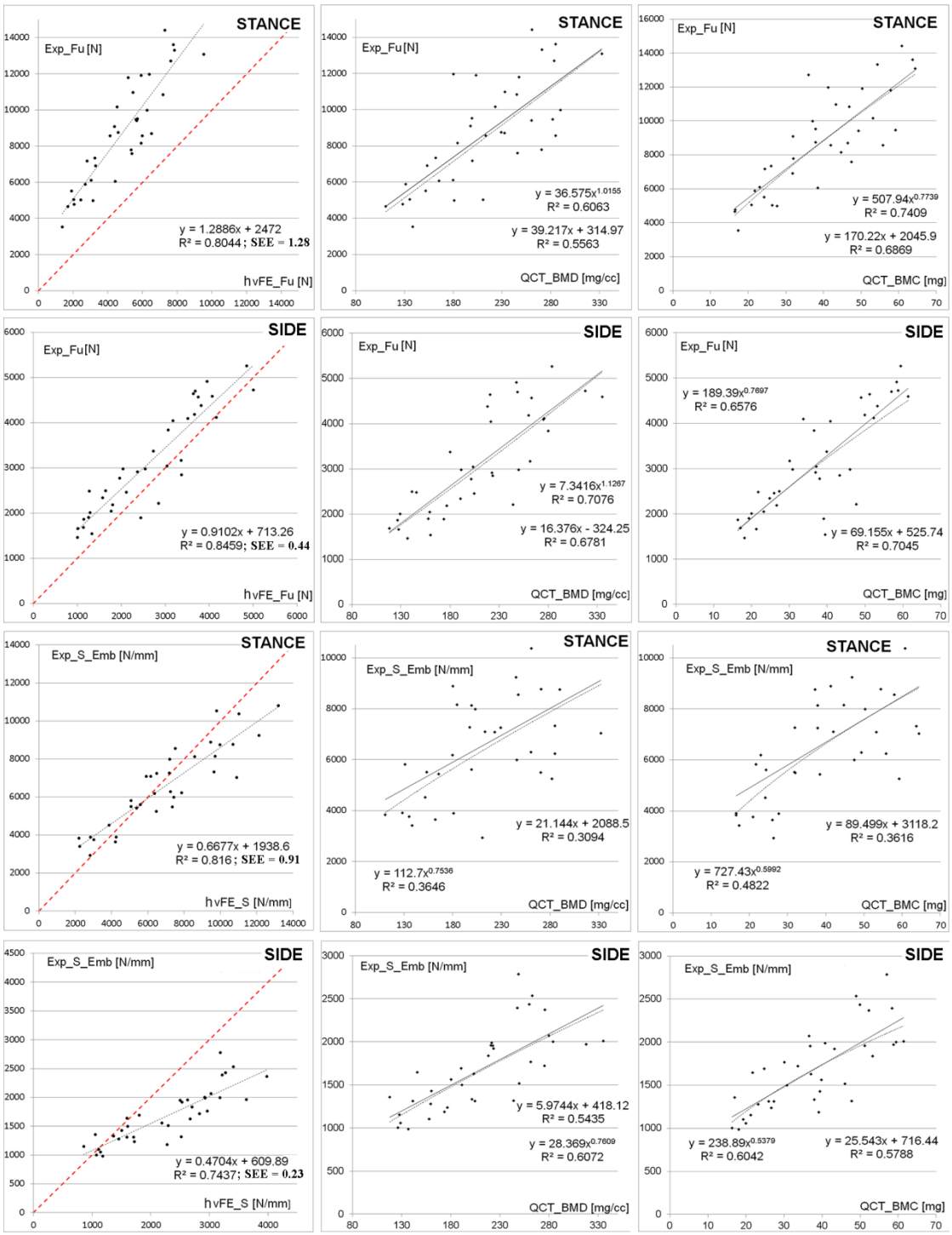

Figure 5. 5: *Results for prediction of the femoral mechanical properties.* Predictions of ultimate force (Exp_Fu) and stiffness (Exp_S_Emb) with hvFE (left), vBMD (center) and vBMC (right). All densitometric quantities were measured in the total proximal femur. The results are separated for STANCE and SIDE configurations. Dashed lines represent the 1:1 relationship.

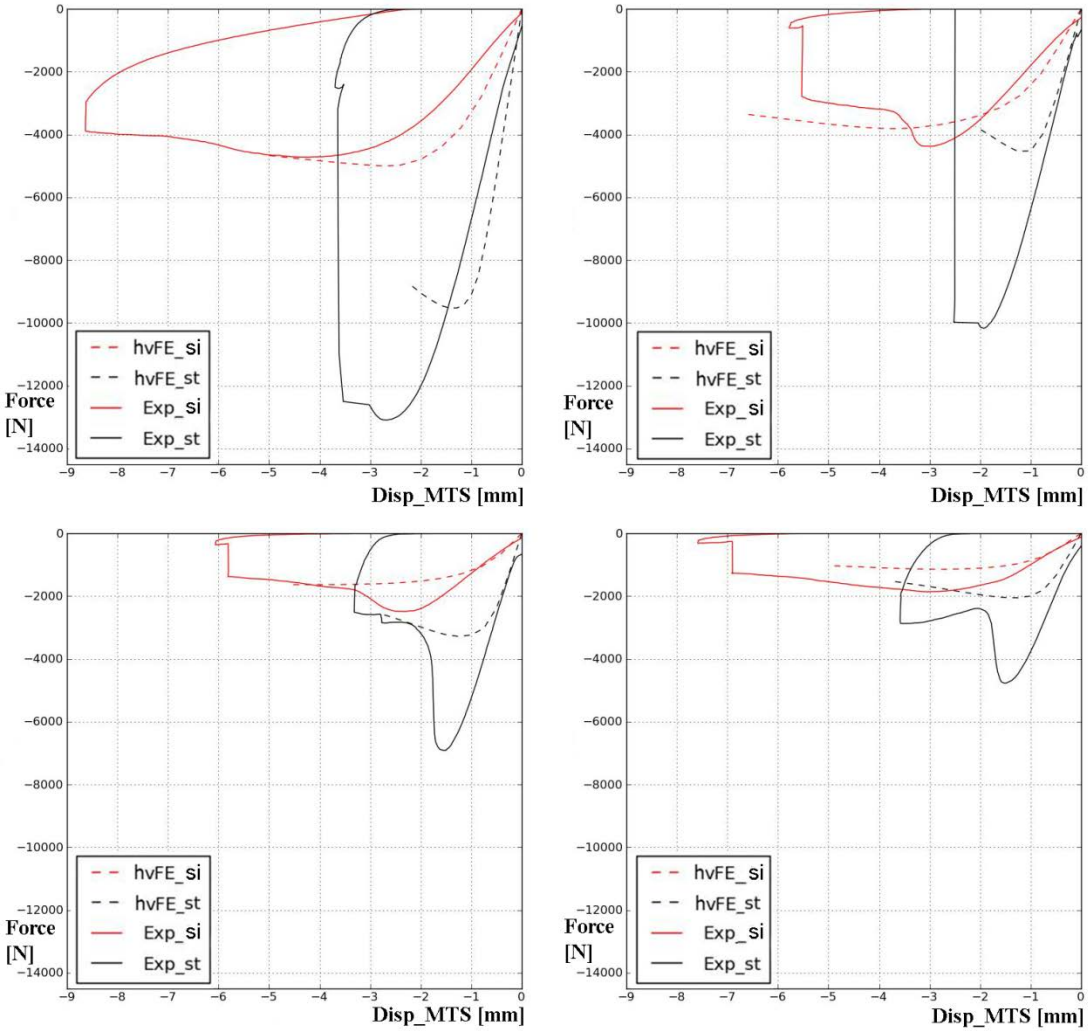

Figure 5. 6: Comparison between experimental and hvFE curves. Four examples of experimental (continuous lines) and hvFE (dashed lines) curves for pairs of femora. The pairs were selected to cover the full range of Exp_Fu. Red and black lines represent SIDE (Exp_si and hvFE_si) and STANCE (Exp_st and hvFE_st) configurations, respectively.

5.4 Discussion

The aim of the present study was to validate a nonlinear QCT-based hvFE model of the human proximal femur with respect to two different loading configurations on a large paired sample size.

The range of Exp_Fu and Exp_S for the two loading configurations were in line with the values reported in the literature for similar *in vitro* test on human femora (Cristofolini, et al., 2007; Keyak, 2000; Koivumaki, et al., 2012). If not included in the computation, the machine/setup compliance leads to a 10% underestimation of the femoral stiffness, constant in both configurations. The poor correlation between Exp_S and Exp_S_NDI (computed from the marker position in the center of the femoral head) for the STANCE configuration (R^2=0.45) compared to the one for the SIDE (R^2=0.87) is probably due to the inhomogeneous distribution of cartilage thickness in the femoral head. In fact, the cartilage thickness and its intra-subject variation are higher in the cranial side of the femoral head,

which was loaded in STANCE configuration, compared to the medial-caudal region of the femoral head, which was loaded in the SIDE configuration (Adam, et al., 1998). Higher variance in cartilage thickness leads to higher variance in the difference between the displacement measured below and above the femoral head, which increases the noise in the relationship between the computed stiffness values.

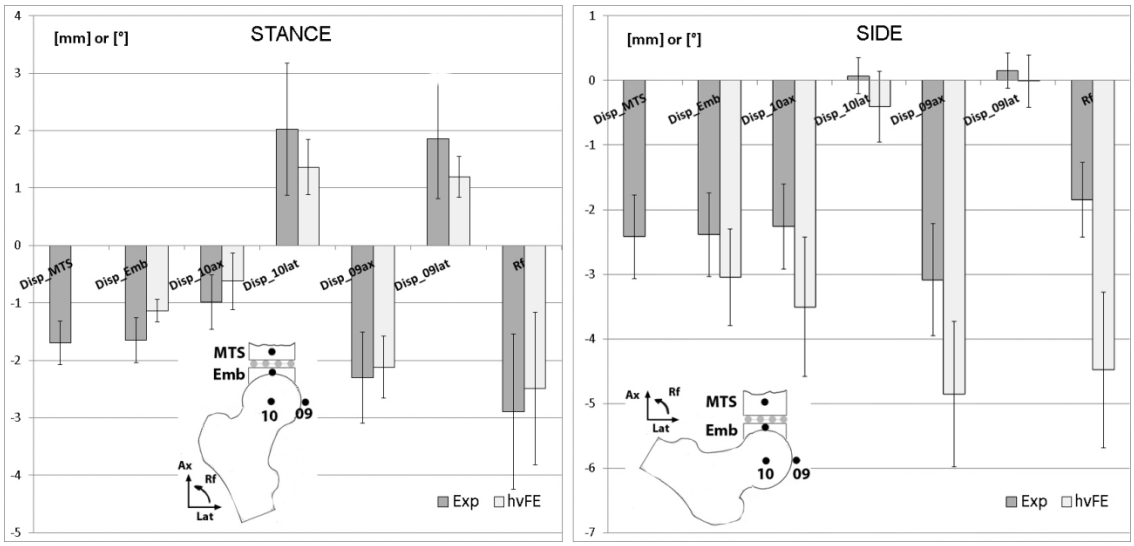

Figure 5. 7: Prediction of local measurements. Comparison between local measurements computed for experiments and hvFE. Results are separated for STANCE (left) and SIDE (right) configurations. Bar plots represent averages and standard deviations (error bars) of the axial displacement measured above the embedding material (Disp_Emb), of the axial and lateral displacements of the markers Nr 10 (Disp_10ax and Disp_10lat) and Nr 09 (Disp_09ax and Disp_09lat) and of the rotation in the frontal plane of the femoral head (Rf) computed for the experiments (dark) and models (bright). The most left column of both graphs represents the experimental displacement measured with the sensor of the testing machine (Disp_MTS).

The calibration equation found to compute $\mu CT_{BV/TV}$ from QCT_{BMD} with the methodology suggested by Dall'Ara et al. (Dall'Ara, et al., 2011) was found to be similar to the one previously found for the human vertebrae ($\mu CT_{BV/TV}=0.090*QCT_{BMD}+0.515$). This result suggests that the cortical thickness and BMD distribution (different for femora and vertebrae) do not affect the relationship between BMD and BV/TV and therefore the same calibration equation could be used for different anatomical sites.

Exp_Fu and Exp_S_Emb were better predicted by the hvFE outputs compared to vBMD or vBMC for both STANCE and SIDE. These results are in line with previous validation of nonlinear FE for either STANCE (Cody, et al., 1999; Keyak, et al., 1998) or SIDE (Dragomir-Daescu, et al., 2011; Keyak, et al., 1998). Due to the higher sample size and carefully designed testing concepts, we could also show that the differences in the prediction ability became in most cases significant. Moreover, if compared to already published densitometric data measured with DXA on the same set of samples (Dall'Ara, et al., 2012), for both configurations the hvFE models were better predictors of Exp_Fu compared to the areal BMD (aBMD) and BMC (R^2 increases of 4-30%, in most cases significantly, for measures performed on total proximal femur, femoral neck, trochanteric and intertrochanteric regions). Similar trends were found for prediction of Exp_S_Emb. Not only the hvFE models were able to predict more of the variation of the femoral

mechanical properties compared to BMD (both volumetric and areal), but the predictions close to the 1:1 relationship for SIDE (Slope=0.91, Intercept=0.71 kN) and for STANCE (Slope=1.29, Intercept=2.47 kN) suggest that the extrapolation procedure done to predict fair properties for poreless bone was reasonable. The modest underestimation found in case of STANCE might be due to the limited morphological information obtained from QCT data, which might have a dominant impact in this loading configuration. A further source of errors is the element size used in the hvFE (3mm in side length hexahedrons), which was chosen to reduce the computational and preprocessing time but is not able to model the smooth contour of the proximal femur and the real cortical thickness. A future study with improved smooth models (Pahr and Zysset, 2009a) will evaluate this uncertainty on the model outcome. Moreover, we would like to stress that no tuning was done on any material parameters (both elastic and yield properties) which were only extrapolated from the values reported in the literature for trabecular bone to obtain reasonable material properties for cortical bone. Even though a proper tuning of the material properties would probably lead to improved predictions closer to the 1:1 relationship, this was not the purpose of the present study.

The setup was able to generate fractures that are usually recorded during clinical practice (sub-capital, neck and trochanteric fractures) (Alffram, 1964; Cordey, et al., 2000). The failure localization predicted by the hvFE models was in agreement with the failure analysis performed with the X-rays in 66% of cases. The best predicted failure locations were the sub-capital region for samples tested in STANCE and the femoral neck for sample tested in SIDE. Compared to the only previous *in vitro* study in which hvFE failure location prediction was compared to experiments for the proximal femur (Keyak, et al., 2001a), similar prediction ability was found for SIDE (71% vs 67%) and for STANCE (61% vs 72%). Inaccuracies in failure location prediction are probably enhanced by the large hexahedron elements used in this study, which do not represent accurately the external smooth surface of the femur and introduce therefore geometrical artifacts (Viceconti, et al., 1998).

In most cases, the displacements and rotation of the femoral head at the ultimate load (measured in the experiments and predicted by the hvFE) were only in qualitative agreement. Some correlations between predicted and experimental local measurements became significant (but still only poorly or moderately correlated) for the samples tested in STANCE configuration. The inability of predicting quantitatively well the local displacements/rotation of the femoral head is probably due to the inaccuracy in the selection of the nodes closest to the marker position due to the relatively large dimensions of the markers and of the presence of the cartilage layer of unknown thickness, the missing simulation of the cartilage layer and the assumption of perfect relative rotation between cartilage and embedding material. Moreover, as the motion of the femoral head was compared at two different load levels (at the maximum force reached in the experiments and in the models), the intrinsic inaccuracy of the hvFE model added some uncertainties in the evaluation of the local displacements and rotation in the frontal plane. Further improvements of these modeling aspects could enhance the predictions of local measurements.

This study has three main limitations. First, the QCT scans of the femora were performed *in vitro*. Therefore, the image quality could be improved by the removal of soft (ligament, muscles …) and hard tissues (disarticulation from the pelvis) which were shown to affect (5-13%) the FE prediction of failure load in an *in vitro* study based on two subjects (Keyak and Falkinstein, 2003). Second, simplified model assumptions (e.g. isotropic bone behavior, similar damage behavior for trabecular and cortical bone, isotropic damage, no

softening in compression) and the usage of a coarse voxel type model limit the accuracy of the prediction, especially of the failure location and of the femoral head motion. In particular, the assumption of bone isotropy might play an important role in the estimation of mechanical properties and fracture location. In fact, it is well accepted that bone shows orthotropic material properties with plane of mechanical symmetry being coincident with the planes of morphological symmetry (Odgaard, et al., 1997). However, to the authors' knowledge no reliable techniques to measure the trabecular orientation from QCT data have been presented so far, and only one study has investigated the effect of including bone anisotropy (defined by geometrical and micromechanical considerations) into QCT-based FE models of the human femur (Trabelsi and Yosibash, 2011). While this last mentioned study came to the conclusion that ability of FE in predicting experimental femoral mechanical properties was not significantly enhanced by considering the bone such as orthotropic instead of as isotropic, there is still the need to further investigate this topic. Third, the SIDE configuration did not accurately represent an accidental fall, where the loading rate is much higher than the quasi-static one used in the experiments performed in the present study. Moreover, as the loading rate was found to affect the mechanical properties of the human femur in a STANCE configuration (Juszczyk, et al., 2011), it is likely that a similar effect would occur also for a SIDE configuration. However, as the model did not include any viscous dependence of bone mechanical properties, the loading rate was set to quasi-static to better control the experiments.

5.5 Conclusions

In conclusion, this study confirmed that the subject specific QCT-based nonlinear hvFE model can predict femoral structural properties better than BMD and BMC. Moreover, it can provide meaningful qualitative information about the failure location. It remains to be investigated if a more accurate prediction of femoral ultimate load *in vitro* is consistent with a better estimation of femoral fracture risk *in vivo*. However, the possible usage of clinical QCT data together with the low level of complexity, especially of the used mesh, and the moderate computational resources needed to perform the analyses, make this model suitable for clinical applications without major modifications.

Acknowledgements
The authors gratefully acknowledge Prof Pettermann and Dr Kinzl for the fruitful discussions about the setup design and the definition of the boundary conditions in the FE models, Mr Exler for having manufactured the experiment set-up, Mr Schwiedrzik for the adaptation of the UMAT, Mr Fritz for the help in the setup designing, Prof Pretterklieber, Mr Salmutter and Mr Seifert for the help with sample collection and preparation, Mr Bourgalet for the help with the calibration study, Ms Plischke and Ms Merz for the help during the QCT analysis, Prof Mayr and Mr Unger for the logistic help during the scanning.

Bibliography

Adam C., Eckstein F., Milz S., Putz R., 1998. The distribution of cartilage thickness within the joints of the lower limb of elderly individuals. J Anat 193, 203-214.

Adams J.E., 2009. Quantitative computed tomography. European Journal of Radiology 12, 12

Alffram P.A., 1964. An epidemiololologic study of cervical and trochanteric fractures of the femur in an urban population. Analysis of 1,664 cases with special reference to etiologic factors. Acta Orthopaedica Scandinavica Supplementum 65, 1-109.

Ammann P., Rizzoli R., 2003. Bone strength and its determinants. Osteoporosis International 14 Suppl 3, S13-18

Bayraktar H.H., Morgan E.F., Niebur G.L., Morris G.E., Wong E.K., Keaveny T.M., 2004. Comparison of the elastic and yield properties of human femoral trabecular and cortical bone tissue. Journal of Biomechanics 37, 27-35.

Black D.M., Bouxsein M.L., Marshall L.M., Cummings S.R., Lang T.F., Cauley J.A., Ensrud K.E., Nielson C.M., Orwoll E.S., 2008. Proximal femoral structure and the prediction of hip fracture in men: a large prospective study using QCT. Journal of bone and Mineral Research 23, 1326-1333.

Borggrefe J., Graeff C., Nickelsen T.N., Marin F., Gluer C.C., 2010. Quantitative computed tomographic assessment of the effects of 24 months of teriparatide treatment on 3D femoral neck bone distribution, geometry, and bone strength: results from the EUROFORS study. Journal of Bone and Mineral Research 25, 472-481.

Bousson V.D., Adams J., Engelke K., et al., 2011. In vivo discrimination of hip fracture with quantitative computed tomography: results from the prospective European Femur Fracture Study (EFFECT). Journal of Bone and Mineral Research 26, 881-893. doi: 810.1002/jbmr.1270.

Bouxsein M.L., Coan B.S., Lee S.C., 1999. Prediction of the strength of the elderly proximal femur by bone mineral density and quantitative ultrasound measurements of the heel and tibia. Bone 25, 49-54.

Chevalier Y., Pahr D., Zysset P.K., 2009. The role of cortical shell and trabecular fabric in finite element analysis of the human vertebral body. J Biomed Eng 131, 111003

Chevalier Y., Quek E., Borah B., Gross G., Stewart J., Lang T., Zysset P., 2010. Biomechanical effects of teriparatide in women with osteoporosis treated previously with alendronate and risedronate: results from quantitative computed tomography-based finite element analysis of the vertebral body. Bone 46, 41-48. Epub 2009 Oct 2001.

Cody D.D., Gross G.J., Hou F.J., Spencer H.J., Goldstein S.A., Fyhrie D.P., 1999. Femoral strength is better predicted by finite element models than QCT and DXA. Journal of Biomechanics 32, 1013-1020.

Cong A., Buijs J.O., Dragomir-Daescu D., 2011. In situ parameter identification of optimal density-elastic modulus relationships in subject-specific finite element models of the proximal femur. Medical Engineering and Physics 33, 164-173. Epub 2010 Oct 2027.

Cordey J., Schneider M., Buhler M., 2000. The epidemiology of fractures of the proximal femur. Injury 31, C56-61.

Cristofolini L., Juszczyk M., Martelli S., Taddei F., Viceconti M., 2007. In vitro replication of spontaneous fractures of the proximal human femur. Journal of Biomechanics 40, 2837-2845

Cristofolini L., Schileo E., Juszczyk M., Taddei F., Martelli S., Viceconti M., 2010. Mechanical testing of bones: the positive synergy of finite-element models and in vitro experiments. Philosophical Transactions Series A Mathematical Physical and Engineering Sciences 368, 2725-2763

Cummings S.R., Melton L.J., 2002. Epidemiology and outcomes of osteoporotic fractures. Lancet 359, 1761-1767.

Dall'Ara E., Luisier B., Schmidt R., Pretterklieber M., Kainberger F., Zysset P., Pahr D., 2012. DXA predictions of human femoral mechanical properties depend on the load configuration. Osteoporosis International submitted,

Dall'Ara E., Varga P., Pahr D., Zysset P., 2011. A calibration methodology of QCT BMD for human vertebral body with registered micro-CT images. Medical Physics 38, 2602-2608

Dall'Ara E., Pahr D., Varga P., Kainberger F., Zysset P., 2012. QCT-based Finite Element Models Predict Human Vertebral Strength in vitro Significantly Better than Simulated DEXA. Osteoporosis International 23, 563-572

Dragomir-Daescu D., Op Den Buijs J., McEligot S., Dai Y., Entwistle R.C., Salas C., Melton L.J., 3rd, Bennet K.E., Khosla S., Amin S., 2011. Robust QCT/FEA models of proximal femur stiffness and fracture load during a sideways fall on the hip. Annals of Biomedical Engineering 39, 742-755

Engelke K., Fuerst T., Dasic G., Davies R.Y., Genant H.K., 2010. Regional distribution of spine and hip QCT BMD responses after one year of once-monthly ibandronate in postmenopausal osteoporosis. Bone 46, 1626-1632. Epub 2010 Mar 1610.

Fessy M.H., Seutin B., Bejui J., 1997. Anatomical basis for the choice of the femoral implant in the total hip arthroplasty. Surgical and Radiologic Anatomy 19, 283-286.

Garcia D., Zysset P.K., Charlebois M., Curnier A., 2009. A three-dimensional elastic plastic damage constitutive law for bone tissue. Biomechanics and Modeling in Mechanobiology 8, 149-165

Genant H.K., Jiang Y., 2006. Advanced imaging assessment of bone quality. Annals of the New York Academy of Sciences 1068, 410-428.

Graeff C., Chevalier Y., Charlebois M., Varga P., Pahr D., Nickelsen T.N., Morlock M.M., Gluer C.C., Zysset P.K., 2009. Improvements in vertebral body strength under teriparatide treatment assessed in vivo by finite element analysis: results from the EUROFORS study. Journal of Bone and Mineral Research 24, 1672-1680.

Grassi L., Schileo E., Taddei F., Zani L., Juszczyk M., Cristofolini L., Viceconti M., 2012. Accuracy of finite element predictions in sideways load configurations for the proximal human femur. Journal of Biomechanics 45, 394-399. Epub 2011 Nov 2012.

Greenspan S.L., Myers E.R., Kiel D.P., Parker R.A., Hayes W.C., Resnick N.M., 1998. Fall direction, bone mineral density, and function: risk factors for hip fracture in frail nursing home elderly. American journal of medicine 104, 539-545.

Hayes W.C. (1991) Biomechanics of cortical and trabecular bone: Implications for assessment of fracture risk. In Hayes W.C. (ed) Basic orthopaedics biomechanics. Raven press, pp 93-142

Holzer G., von Skrbensky G., Holzer L.A., Pichl W., 2009. Hip fractures and the contribution of cortical versus trabecular bone to femoral neck strength. Journal of Bone and Mineral Research 24, 468-474.

Johnell O., Kanis J.A., 2006. An estimate of the worldwide prevalence and disability associated with osteoporotic fractures. Osteoporososis International 17, 1726-1733

Juszczyk M.M., Cristofolini L., Viceconti M., 2011. The human proximal femur behaves linearly elastic up to failure under physiological loading conditions. Journal of Biomechanics 44, 2259-2266. Epub 2011 Jun 2230.

Kannus P., Leiponen P., Parkkari J., Palvanen M., Jarvinen M., 2006. A sideways fall and hip fracture. Bone 39, 383-384. Epub 2006 Feb 2028.

Keaveny T.M., Hoffmann P.F., Singh M., Palermo L., Bilezikian J.P., Greenspan S.L., Black D.M., 2008. Femoral bone strength and its relation to cortical and trabecular changes after treatment with PTH, alendronate, and their combination as assessed by finite element analysis of quantitative CT scans. Journal of Bone and Mineral Research 23, 1974-1982.

Keaveny T.M., Kopperdahl D.L., Melton L.J., 3rd, Hoffmann P.F., Amin S., Riggs B.L., Khosla S., 2010. Age-dependence of femoral strength in white women and men. Journal of Bone and Mineral Research 25, 994-1001.

Keaveny T.M., McClung M.R., Wan X., Kopperdahl D.L., Mitlak B.H., Krohn K., 2012. Femoral strength in osteoporotic women treated with teriparatide or alendronate. Bone 50, 165-170. Epub 2011 Oct 2017.

Keyak J.H., 2000. Relationships between femoral fracture loads for two load configurations. Journal of Biomechanics 33, 499-502.

Keyak J.H., 2001. Improved prediction of proximal femoral fracture load using nonlinear finite element models. Medical Engineering and Physics 23, 165-173

Keyak J.H., Falkinstein Y., 2003. Comparison of in situ and in vitro CT scan-based finite element model predictions of proximal femoral fracture load. Medical Engineering and Physics 25, 781-787

Keyak J.H., Kaneko T.S., Skinner H.B., Hoang B.H., 2007. The effect of simulated metastatic lytic lesions on proximal femoral strength. Clinical Orthopaedics and Related Research 459, 139-145

Keyak J.H., Koyama A.K., LeBlanc A., Lu Y., Lang T.F., 2009. Reduction in proximal femoral strength due to long-duration spaceflight. Bone 44, 449-453. Epub 2008 Dec 2003.

Keyak J.H., Rossi S.A., Jones K.A., Les C.M., Skinner H.B., 2001a. Prediction of fracture location in the proximal femur using finite element models. Medical Engineering and Physics 23, 657-664.

Keyak J.H., Rossi S.A., Jones K.A., Skinner H.B., 1998. Prediction of femoral fracture load using automated finite element modeling. Journal of Biomechanics 31, 125-133.

Keyak J.H., Sigurdsson S., Karlsdottir G., et al., 2011. Male-female differences in the association between incident hip fracture and proximal femoral strength: a finite element analysis study. Bone 48, 1239-1245. Epub 2011 Mar 1216.

Keyak J.H., Skinner H.B., Fleming J.A., 2001b. Effect of force direction on femoral fracture load for two types of loading conditions. Journal of Orthopaedic Research 19, 539-544.

Koivumaki J.E., Thevenot J., Pulkkinen P., Kuhn V., Link T.M., Eckstein F., Jamsa T., 2012. Ct-based finite element models can be used to estimate experimentally measured failure loads in the proximal femur. Bone 50, 824-829. Epub 2012 Jan 2028.

Lenaerts L., van Lenthe G.H., 2009. Multi-level patient-specific modelling of the proximal femur. A promising tool to quantify the effect of osteoporosis treatment. Philosophical Transactions Series A, Mathematical, Physical, and Engineering Sciences 367, 2079-2093.

Lewiecki E.M., Keaveny T.M., Kopperdahl D.L., Genant H.K., Engelke K., Fuerst T., Kivitz A., Davies R.Y., Fitzpatrick L.A., 2009. Once-monthly oral ibandronate improves biomechanical determinants of bone strength in women with postmenopausal osteoporosis. The Journal of Clinical Endocrinology and Metababolism 94, 171-180. Epub 2008 Oct 2007.

Lochmuller E.M., Muller R., Kuhn V., Lill C.A., Eckstein F., 2003. Can novel clinical densitometric techniques replace or improve DXA in predicting bone strength in osteoporosis at the hip and other skeletal sites? Journal of Bone and Mineral Research 18, 906-912.

Lotz J.C., Cheal E.J., Hayes W.C., 1991a. Fracture prediction for the proximal femur using finite element models: Part I--Linear analysis. J Biomed Eng 113, 353-360.

Lotz J.C., Cheal E.J., Hayes W.C., 1991b. Fracture prediction for the proximal femur using finite element models: Part II--Nonlinear analysis. J Biomed Eng 113, 361-365.

Martelli S., Taddei F., Schileo E., Cristofolini L., Rushton N., Viceconti M., 2012. Biomechanical robustness of a new proximal epiphyseal hip replacement to patient variability and surgical uncertainties: a FE study. Medical Engineering and Physics 34, 161-171. Epub 2011 Aug 2012.

Mnif H., Koubaa M., Zrig M., Trabelsi R., Abid A., 2009. Elderly patient's mortality and morbidity following trochanteric fracture. A prospective study of 100 cases. Orthopaedics&traumatology, surgery&research 95, 505-510. Epub 2009 Sep 2026.

Odgaard A., Kabel J., van Rietbergen B., Dalstra M., Huiskes R., 1997. Fabric and elastic principal directions of cancellous bone are closely related. Journal of Biomechanics 30, 487-495.

Ohman C., Baleani M., Pani C., Taddei F., Alberghini M., Viceconti M., Manfrini M., 2011. Compressive behaviour of child and adult cortical bone. Bone 49, 769-776. Epub 2011 Jul 2016.

Orwoll E.S., Marshall L.M., Nielson C.M., et al., 2009. Finite element analysis of the proximal femur and hip fracture risk in older men. Journal of Bone and Mineral Research 24, 475-483.

Pahr D.H., Zysset P.K., 2009a. A comparison of enhanced continuum FE with micro FE models of human vertebral bodies. Journal of Biomechanics 42, 455-462

Pahr D.H., Zysset P.K., 2009b. From high-resolution CT data to finite element models: development of an integrated modular framework. Computer Methods in Biomechanics and Biomedical Engineering 12, 45-57

Parkkari J., Kannus P., Palvanen M., Natri A., Vainio J., Aho H., Vuori I., Jarvinen M., 1999. Majority of hip fractures occur as a result of a fall and impact on the greater trochanter of the femur: a prospective controlled hip fracture study with 206 consecutive patients. Calcified Tissue International 65, 183-187.

Ridler T.W., Calvard S., 1978. Picture Thresholding Using an Iterative Selection Method. IEEE Transactions on Systems, Man and Cybernetics 8, 630-632

Rincon-Kohli L., Zysset P.K., 2009. Multi-axial mechanical properties of human trabecular bone. Biomechanics and Modeling in Mechanobiology 8, 195-208

Schileo E., Dall'ara E., Taddei F., Malandrino A., Schotkamp T., Baleani M., Viceconti M., 2008. An accurate estimation of bone density improves the accuracy of subject-specific finite element models. Journal of Biomechanics 41, 2483-2491

Schwartz A.V., Kelsey J.L., Sidney S., Grisso J.A., 1998. Characteristics of falls and risk of hip fracture in elderly men. Osteoporosis International 8, 240-246.

Steiger J.H., 1980. Tests for comparing elements of a correlation matrix. Psychological bullettin 87, 245-251

Trabelsi N., Yosibash Z., 2011. Patient-specific finite-element analyses of the proximal femur with orthotropic material properties validated by experiments. J Biomed Eng 133, 061001.

Varga P., Baumbach S., Pahr D., Zysset P.K., 2009. Validation of an anatomy specific finite element model of Colles' fracture. Journal of Biomechanics 42, 1726-1731

Viceconti M., Bellingeri L., Cristofolini L., Toni A., 1998. A comparative study on different methods of automatic mesh generation of human femurs. Medical Engineering and Physics 20, 1-10.

Viceconti M., Davinelli M., Taddei F., Cappello A., 2004. Automatic generation of accurate subject-specific bone finite element models to be used in clinical studies. Journal of Biomechanics 37, 1597-1605.

Viceconti M., Taddei F., Cristofolini L., Martelli S., Falcinelli C., Schileo E., 2012. Are spontaneous fractures possible? An example of clinical application for personalised, multiscale neuro-musculo-skeletal modelling. Journal of Biomechanics 45, 421-426. Epub 2011 Dec 2026.

WHO (1994) Assessment of fracture risk and its application to screening for postmenopausal osteoporosis. Technical Report Series. WHO, Geneve

Yosibash Z., Trabelsi N., Milgrom C., 2007. Reliable simulations of the human proximal femur by high-order finite element analysis validated by experimental observations. Journal of Biomechanics 40, 3688-3699. Epub 2007 Aug 3613.

Zysset P.K., Curnier A., 1996. A 3D damage model for trabecular bone based on fabric tensors. Journal of Biomechanics 29, 1549-1558

Zysset P.K., Rincon-Kohli L. (2006) An alternative fabric-based yield and failure criterion for treabecular bone. In Holzapfel G., Ogden R. (eds) Mechanics of biological tissue. Springer, Berlin, pp 457-470

Appendix: Material model for the QCT-based FE

The constitutive relationship used to define the material properties in the FE model was based on the more general elastic plastic damage constitutive law published by and Garcia et al. (Garcia, et al., 2009) which has been already used in a number of studies to model bone tissue (Chevalier, et al., 2009; Chevalier, et al., 2010; Graeff, et al., 2009; Varga, et al., 2009).

In the present study the following assumption were taken:

The damage evolution was slightly changed compared to Garcia and Zysset (Garcia, et al., 2009) by switching off plasticity (as in case of monotonic test its effect would be marginal compared to the one of damage) and reformulating the damage hardening function r^D (see below);

Bone was considered isotropic (in the implementation, the eigenvalues of the Fabric tensor were therefore: $m_1=m_2=m_3=1$) as no fabric information could be extracted from the QCT images;

Different behavior for high density elements were assumed for accounting for cortical bone by defining a Tissue Function TF (defined below);

The same power coefficient (k) was assumed for the bone volume fraction-elasticity and bone volume fraction-yield relationships.

The constitutive model can be represented by a primary linear spring, which defines the elastic properties of the intact bone, in series with a linear damageable spring, which accounts for elastic damage due to micro-cracks. The material nonlinearity is introduced by a scalar damage variable (D) which drives the isotropic reduction of stiffness and the hardening of bone once the element reaches the yield surface. D is defined between 0 (no

damage) and 1 (total damage) and is calculated during the simulations by the generalized Newton method at each increment.
The model is defined by an observable variable, the Green –Lagrange strain **E**, and the above mentioned internal variable D. The free energy potential ψ(**E**,D) and the total Piola-Kirchhoff 2 stress **S** then become:

$$\Psi(\boldsymbol{E}, D) = \frac{1}{2}(1-D)\boldsymbol{E}:\mathbb{S}\boldsymbol{E} + \boldsymbol{I}_{[\mathbf{0},\mathbf{1}[}(D) \tag{5.2}$$

$$\boldsymbol{S} = (1-D)\mathbb{S}\boldsymbol{E} \tag{5.3}$$

where the compliance tensor can be defined as:

$$\mathbb{E} = \mathbb{S}^{-1} = \frac{1}{TF}\left(\sum_{i=1}^{3}\frac{1}{\varepsilon_0}\boldsymbol{M_i}\otimes\boldsymbol{M_i} - \sum_{i,j=1;i\neq j}^{3}\frac{\upsilon_0}{\varepsilon_0}\boldsymbol{M_i}\otimes\boldsymbol{M_j} + \sum_{i,j=1;i\neq j}^{3}\frac{1}{\mu_0}\boldsymbol{M_i}\,\overline{\underline{\otimes}}\,\boldsymbol{M_j}\right) \tag{5.4}$$

where the second factor represents the description proposed by Garcia et al. (Garcia, et al., 2009) with the assumption of isotropic material. In that description ε_0, υ_0 and μ_0 represent the elastic constants (elastic modulus, shear modulus, and Poisson's ratio) for a pore-less material extrapolated from the experimental results obtained by Rincon-Kohli and Zysset (Rincon-Kohli and Zysset, 2009) who tested trabecular bone samples. However, due to the thick cortical bone in the femur, in the present study a tissue function (TF) was used to obtain meaningful results for high density bone (ρ>0.5). The TF is defined as a nonlinear scalar function for both compression and tension and provides, once extrapolated for pore-less bone (BV/TV=ρ=1), an elastic modulus equal to 24 GPa (Emax).

$$\begin{cases} TF(\rho, E_{max}, \varepsilon_0, k) = \rho^k & , \quad for\ \rho \leq 0.5 \\ TF(\rho, E_{max}, \varepsilon_0, k) = \rho^k + \dfrac{E_{max}-\varepsilon_0}{\varepsilon_0}\left(\dfrac{\rho-0.5}{0.5}\right)^{2k} & , \quad for\ \rho > 0.5 \end{cases} \tag{5.5}$$

where *k* is the porosity exponents of the density-based elasticity relationship. As example, Figure 5.8 shows the effect of TF on the elastic modulus.
The damage criterion was based on the one proposed by Garcia et al. (Garcia, et al., 2009), which was defined as a piecewise Hill criterion with different behavior for compressive and tensile properties:

$$Y(\boldsymbol{S}, D) = \sqrt{\boldsymbol{S}:\mathbb{F}_{\pm}\boldsymbol{S}} - r^D(D) \tag{5.6}$$

Where **S** is the stress and $F_{\pm}$ are the fourth-order tensors for compression (-) and tension (+) which introduce the asymmetric yield material properties of the bone tissue and are defined as:

$$\mathbb{F}_{\pm} = \frac{1}{TF^2}\left(\sum_{i=1}^{3}\frac{1}{(\sigma_0^{\pm})^2}\boldsymbol{M_i}\otimes\boldsymbol{M_i} - \sum_{i,j=1;i\neq j}^{3}\frac{\chi_0^{\pm}}{(\sigma_0^{\pm})^2}\boldsymbol{M_i}\otimes\boldsymbol{M_j} + \sum_{i,j=1;i\neq j}^{3}\frac{1}{2{\tau_0}^2}\boldsymbol{M_i}\,\overline{\otimes}\,\boldsymbol{M_j}\right) \tag{5.7}$$

and $r^D(D)$ is the damage hardening law which adapts the yield surface in function of the damage D and is defined as:

$$r^D(D) = 1 - (1-\alpha)e^{-kD} \tag{5.8}$$

Where the coefficient α represents the ratio between the yield and ultimate stress and was considered equal to 2/3. As for elasticity, the second factor of the tensors $F_{\pm}$ are taken from the description of Garcia et al. (Garcia, et al., 2009) for isotropic material. In that model the constants σ_0^{+} and σ_0^{-} represent the tensile and compressive strength, χ_0^{+} and χ_0^{-} represent the interaction coefficients and τ_0 represents the shear strength, all for pore-less material. However, in the same fashion as for elasticity, the yield surface was corrected with the TF to account for cortical bone and to obtain, once extrapolated for pore-less material, a compression ultimate stress equal to 266 MPa (Ohman, et al., 2011) and a tension ultimate stress equal to 200 MPa (Bayraktar, et al., 2004).
All the material constants for both elasticity (ε_0, υ_0, and μ_0) and yield (σ_0^{+}, σ_0^{-}, χ_0^{+}, χ_0^{-} and τ_0) were finally recomputed by interpolating the experimental results of Rincon-Kohli and Zysset (Rincon-Kohli and Zysset, 2009) with the newly defined TF and the above mentioned assumptions for pore-less material. The resulting material properties are reported in Table 5.1.

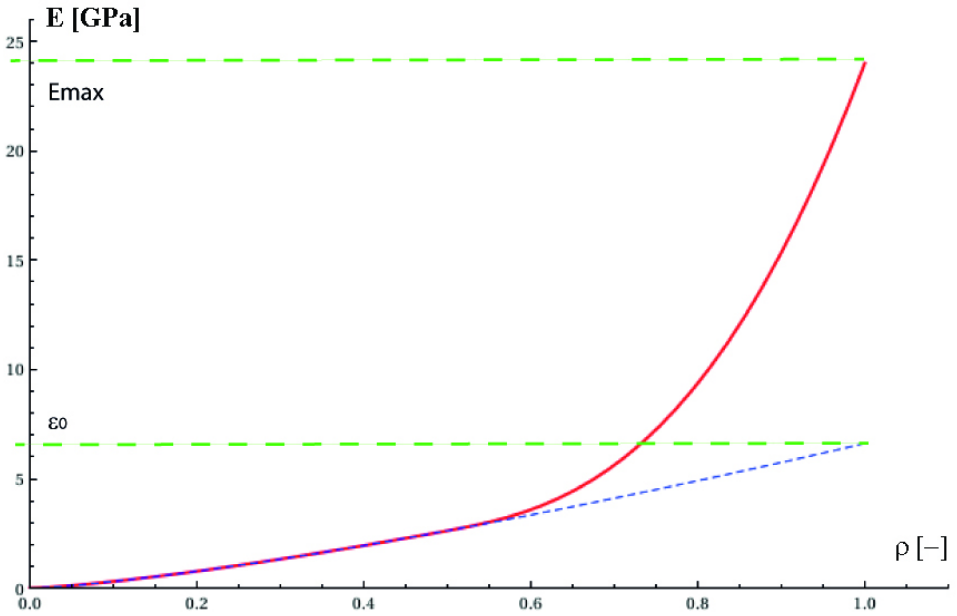

Figure 5. 8: Effect of the Tissue Function on the elastic modulus. Example of elastic modulus in function of the bone volume fraction. The solid red curve represents the new values obtained by using the TF correction while the blue dashed one represents the values computed without correction.

Chapter 6

DXA versus experiments for the human proximal femur

From the manuscript:

DXA predictions of human femoral mechanical properties depend on the load configuration

E. Dall'Ara [a]*, B. Luisier [a], R. Schmidt [b], M. Pretterklieber [c], F. Kainberger [d], P. Zysset [e], D. Pahr [a]

a Institute of Lightweight Design and Structural Biomechanics, Vienna University of Technology, Austria
b Department of Trauma Surgery, Medical University of Vienna, Austria
c Department of Applied Anatomy, Medical University of Vienna, Austria
d Department of Radiology, Medical University of Vienna, Austria
e Institute for Surgical Technology and Biomechanics, University of Bern, Switzerland

Submitted to: Clinical Biomechanics, 2012

Abstract

Background: the aim of this study was to evaluate the ability of DXA BMD measured in different regions of the proximal part of the human femur for predicting the mechanical properties of matched fresh frozen proximal femora tested in two different loading configurations.

Methods: 36 pairs of human femora were isolated, DXA scanned and tested until failure to simulate a fracture consequent to a fall on the side or a one-legged standing spontaneous fracture. The ability of the DXA output from four different regions of the proximal femur in predicting the femoral mechanical properties were measured and compared for the two loading scenarios.

Findings: the femoral ultimate force was well correlated for the two loading configurations (R^2=0.72, ultimate force in STANCE was approximately three times larger than the one measured in FALL). The femoral neck DXA BMD was the best correlated to the femoral ultimate force for both configurations. In particular, femoral neck BMD predicted significantly better femoral failure when simulating a fall than when simulating a standing configuration (R^2=0.80 vs R^2=0.66, P<0.05).

Interpretation: Neck BMD was found to be the best surrogate of femoral strength for both loading configurations and should therefore be considered as one of the key factors for discriminating femoral fracture risk *in vivo*. The better predictive ability of neck BMD for femoral strength if tested in a fall compared to a one-legged stance configuration suggests that DXA's clinical relevance may not be as high for spontaneous femoral fractures than for fractures associated to a fall.

Keywords: Biomechanics, Femur, BMD, Bone strength, Osteoporosis, Mechanical testing

6.1 Introduction

Osteoporosis is a common skeletal disease causing bone mass reduction and bone microstructural changes, which lead to a dramatic increase of lifetime fracture risk (Johnell and Kanis, 2006). In osteoporotic individuals, femoral fracture is a major clinical problem with high morbidity and mortality (Cummings and Melton, 2002; Mnif, et al., 2009). Estimation of the fracture risk is necessary to identify patients requiring treatment.

A fracture occurs when the applied load is higher than the one supported by the bone in that loading configuration. In most cases, femoral fractures are associated with an impact load due to a sideways fall (Greenspan, et al., 1998; Kannus, et al., 2006; Schwartz, et al., 1998) whereas only 2% of the falls can be considered as spontaneous (i.e. not related to any high- or low-energy trauma (Nyberg, et al., 1996; Parkkari, et al., 1999)). A recent computational biomechanics study of the lower limb showed that in the simultaneous presence of severe osteoporosis and degradation of neuro-motor control, a spontaneous hip fracture during physiological loading can not be excluded (Viceconti, et al., 2012). Consequently, both "one-legged standing" (following referred to as "STANCE") and "sideways falling" (following referred to as "FALL") loading conditions are of main interest to understand the mechanical resistance of the human femur (Keyak, 2000; Lochmuller, et al., 2003; Lotz and Hayes, 1990). Experimental and finite element studies have shown that loading direction affects femoral ultimate force, stiffness and strain distribution (Cristofolini, et al., 2007; Keyak, et al., 2001). In particular, if matched pairs of femora are tested, the fracture load in simulated one-legged stance was found to account for approximately 80% of the variance of the failure load in simulated fall (Keyak, 2000).

Bone Mineral Density (BMD) measured at the hip is considered as a surrogate of bone strength and therefore is used to define osteoporosis. Dual energy X-rays absorptiometry (DXA) is most frequently used to evaluate hip BMD for its low radiation dose and its low cost (Griffith and Genant, 2008). However, this technique allows only 2D measurements of bone mineral density without the capability of discriminating neither between bones (e.g. femoral head and iliac crest) nor between bone microstructures (trabecular and cortical bone). Therefore, densitometric measures performed in different regions of the femur with DXA have shown a wide range of coefficients of determination for predictions of femoral strength *in vitro* (range for FALL: 0.37-0.92 (Boehm, et al., 2008; Bouxsein, et al., 1999; Cheng, et al., 1997; Courtney, et al., 1994; Courtney, et al., 1995; Dragomir-Daescu, et al., 2011; Lochmuller, et al., 2003; Pinilla, et al., 1996; Roberts, et al., 2010); range for STANCE: 0.35-0.71 (Bousson, et al., 2006; Cody, et al., 1999; Kukla, et al., 2002; Lochmuller, et al., 2003; Lochmuller, et al., 1998). When comparing the femoral strength measured in two different loading conditions, performing tests on matched femora is recommended to account for BMD and femoral geometry (Cheng, et al., 2007; Gregory and Aspden, 2008). Interestingly, hitherto only two studies investigated the ability of BMD to predict femoral mechanical properties by testing pairs of femora in both one-legged stance and sideways fall. Keyak et al. (1998) tested 18 pairs of femora in both configurations and found that the intertrochanteric BMD predicted better the ultimate force in FALL configuration (R^2=0.82) compared to subcapital BMD in STANCE configuration (R^2=0.61). However, in that study BMD was computed from quantitative computed tomography (QCT) and was assessed only in the above mentioned regions. In another study, Lochmueller et al. (2003) tested approximately 120 pairs of femora in both configurations. They found that DXA neck BMD and BMC predicted better (not clearly if significantly) the femoral ultimate load in FALL than in STANCE configurations (R^2=0.40/0.52 vs R^2=0.53/0.45). However, in that study the femora were fixed in formalin

before testing. Even though it was previously shown that long term low percentile formalin fixation does not affect BMD (Lochmuller, et al., 2001) and mineral content (Edmondston, et al., 1994), it was shown to alter the Young's modulus, yield strain, ultimate strain and plastic energy absorption of cortical bone (Ohman, et al., 2008; Unger, et al., 2010) and ultrasound properties of human calcanei (Popperl, et al., 1999). The low predictive ability of the neck BMD reported in that study and the relatively high number of atypical fractures (crash fractures of the head or trochanter and shaft fractures were 25% of the tested samples) might be affected by the influence of formalin fixation on the femoral mechanical properties of bone. Therefore, it remains to be investigated if the same difference in the prediction ability of BMD for the different configurations would hold also for fresh frozen bones.

Femoral stiffness plays an important role in the designing of hip prosthesis and in the prediction of femoral strength with finite element models. While bone stiffness has been found to well correlate to the bone strength for human vertebrae (Dall'Ara, et al., 2010) and radii (Varga, et al., 2009), little is known about this relationship for the human femur and in particular about its dependence on the loading direction and BMD.

The aim of this study was to evaluate systematically the ability of DXA BMD and bone mineral content (BMC) measured in four different regions of the proximal femur for predicting the mechanical properties (both stiffness and ultimate force) of a large number of matched fresh frozen proximal femoral segments tested in two different loading configurations *in vitro*.

6.2 Materials and methods

6.2.1 Sample preparation

Left and right fresh frozen anatomic specimens of human femora were extracted from 40 voluntary bony donators at the Department of applied Anatomy, Center of Anatomy and Cell Biology, Medical University of Vienna, Austria. The pairs of femora that showed either deformations or previous damage were excluded, leaving 36 pairs for the study (17 males, 19 females with age 76±12 years, range 46-96). The ethics commission of the Medical University of Vienna approved all procedures applied during the present study. The femora were kept frozen at -20°C until the beginning of the sample preparation and in between the procedure steps. In each pair of femora, one was assigned to the "STANCE" and the other to the "FALL" group. Left and right femora were randomized for the groups to test the same number of left in STANCE and FALL. Soft tissues were carefully removed from the femoral shaft, greater trochanter and lesser trochanter. The proximal portion of each femur was isolated by cutting at 80 mm distally to the middle point of the lesser trochanter, perpendicularly to the proximal shaft axis (Fessy, et al., 1997). Polyurethane (PU) was used to embed the most distal 60 mm of the isolated proximal femur.

6.2.2 DXA analysis

Each sample was then submerged in 0.9% NaCl saline solution, exposed to vacuum for ten minutes to remove air bubbles and scanned with DXA (*Discovery QDR, Hologic Inc., USA*) in a custom made chamber. Total (Tot_BMD and Tot_BMC), neck (Neck_BMD and Neck_BMC), trochanteric (Troch_BMD and Troch_BMC) and intertrochanteric (Inter_BMD and Inter_BMC) BMD and BMC were computed with the standard

procedures used in clinics by an experienced DXA analyst. An example of DXA analysis is shown in Figure 6.1.

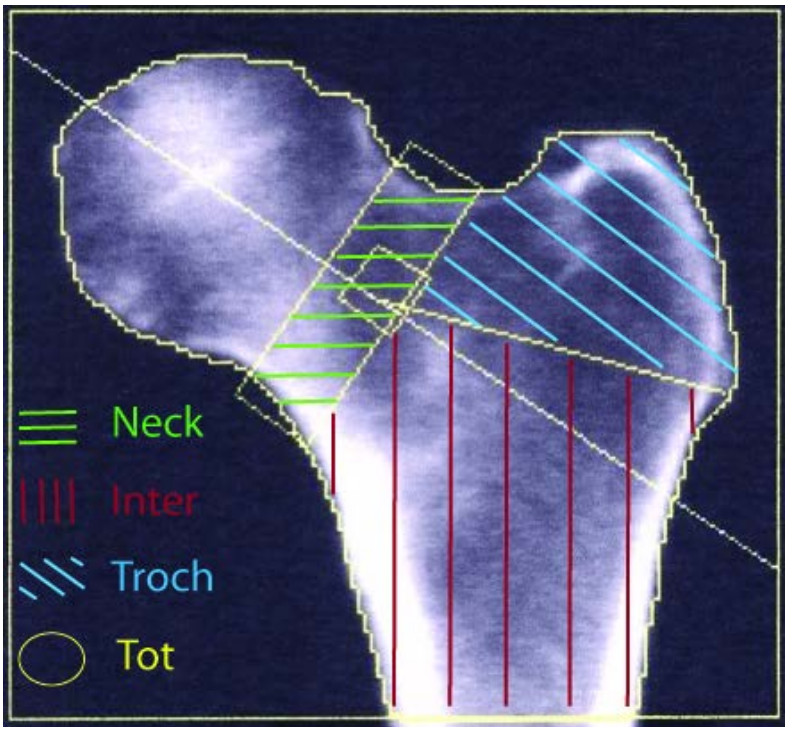

Figure 6. 1: Example of DXA analysis for one proximal femur.

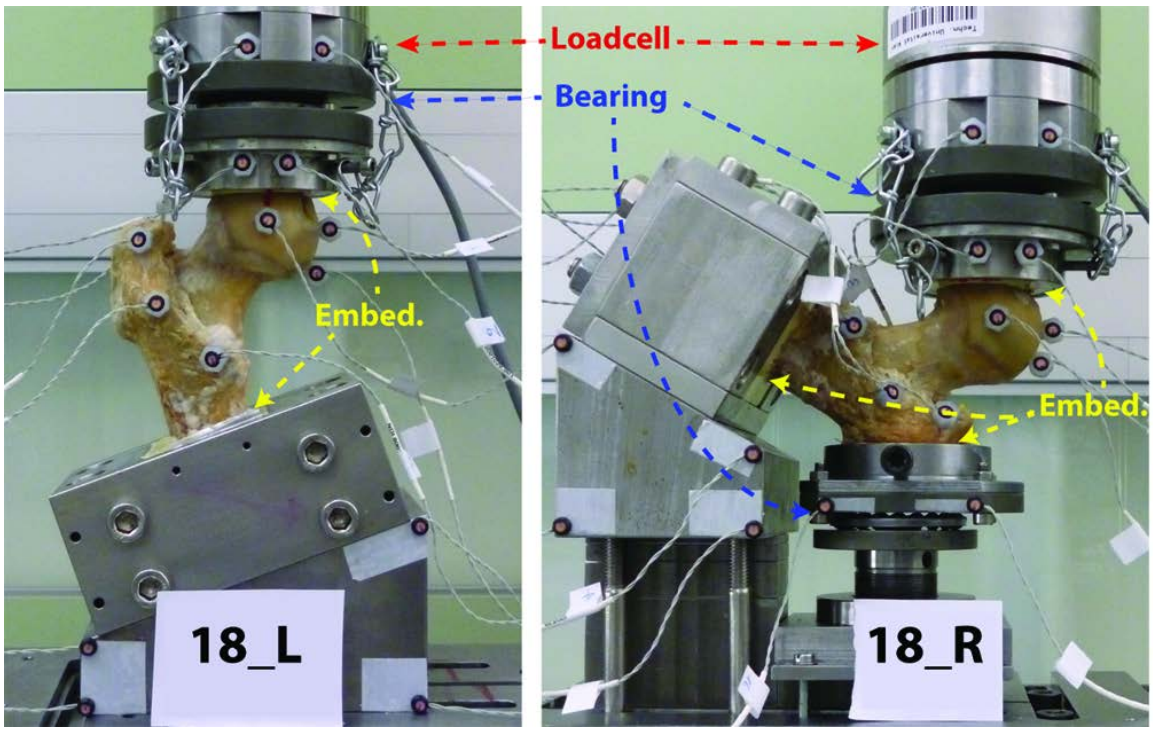

Figure 6. 2: Mechanical setup to simulate a one-legged stance (left) and a fall on the side backward (right). The output of the active markers attached to the bone and to the setup was used in another study (Chapter 5).

6.2.3 Mechanical tests

Each specimen was kept in 0.9% NaCl saline solution for at least four hours before testing and then carefully positioned in the machine as shown in Figure 6.2. In both configurations, the load was applied in the plane containing both neck and proximal shaft axes. The load was applied on the femoral head with an inclination of 70º or 20º from the proximal shaft axis for the FALL and STANCE configurations, respectively. To distribute the applied load, 10 mm of the proximal part of the femoral head in the STANCE configuration and 10 mm of the medial part of the femoral head in the FALL configuration were embedded in PU. Ten millimeters of the lateral part of the greater trochanter of the samples tested in FALL configuration were embedded in PU to distribute the reaction force during testing.
The shaft was fixed in both configurations. Furthermore, custom made bearings were designed and applied to the setup to allow the rotation and two translations in the plane perpendicular to the loading axis for the femoral head in STANCE configuration and for both femoral head and greater trochanter in the FALL configuration. The axial force was measured by means of a 100kN load cell (*U3 force transducer, HBM, Germany*) mounted above the bearing of the femoral head. A servo-hydraulic testing machine (*Mini-Bionix, MTS system, U.S.A.*) was used to compress the femoral head at a rate of 5mm/min until a clear failure was visible. However, in five cases (due to the dimension and the shape of the samples) the machine was stopped before a failure was visible to avoid contact between the parts of the setup and the femur. The femoral ultimate force (Fu) and stiffness (S) were defined as the maximum applied load and the maximum slope of the linear part of the "load-displacement" curve, respectively.

6.2.4 Post test radiographs and classification of fractures

After testing, the samples were placed in an angulated position of 15° antetorsion of the femoral neck, which corresponds to a supine position of the patient. Plain radiographs were performed along the anterior-posterior direction comparable to a pelvic AP view with the following settings: 70kV, density -2, under-the-table technique (*Philips Optimus X-Ray Generator®; Philips Medical Systems DMC GmbH, Hamburg, Germany*). The fracture sites were classified according to four anatomical regions, as in clinical routine: head, subcapital, neck and trochanter. Wherever the fracture location was in between two regions, the region involving the larger part of the fracture was considered as fracture site.

6.2.5 Statistics

Averages, standard deviations (SD), coefficients of determination (R^2) and standard errors of the estimate (SEE) were computed for all densitometric measurements (Tot_BMD, Neck_BMD, Troch_BMD, Inter_BMD, Tot_BMC, Neck_BMC, Troch_BMC, Inter_BMC) and mechanical properties (S, Fu) for the FALL and STANCE groups. Paired Student T-tests were used to compare the averages of the different variables for the groups FALL and STANCE (α=0.05). Linear regressions were used to correlate the densitometric measures with the experimental results and to correlate the experimental results to each other as from the analysis of the residuals a linear model was found to be appropriate. Pearson's correlation coefficients of the predictions were compared with the method suggested by Steiger (Steiger, 1980) for dependent samples (α=0.05).

6.3 Results

Due to technical problems during the DXA measurements, the BMD values of one pair of samples were not available and those samples were excluded. By analyzing the T-Score, 40% of the subjects were osteoporotic (T-Score<-2.5) and 31% were osteopenic (T-Score<1).
Averages and standard deviations of the densitometric quantities and experimental results for split groups are summarized in Table 6.1. In particular, the mean values of each densitometric measures were not statistically different for the two groups (Student paired T-tests: p>0.181). Both BMD ($0.86<R^2<0.91$, $0.97<Sl<1.03$, $0.002<Int(mg/cm^2)<0.021$) and BMC ($0.85<R^2<0.93$, $0.92<Sl<0.99$, $0.23<Int(mg)<1.48$) of the different regions computed for the femora of the two groups were well correlated.

	Stance	**Fall**	**p-value**
Tot_BMD [g/cm²]	0.70±0.18	0.71±0.20	*0.272*
Neck_BMD [g/cm²]	0.59±0.15	0.59±0.15	*0.595*
Troch_BMD [g/cm²]	0.53±0.16	0.53±0.17	*0.480*
Inter_BMD [g/cm²]	0.83±0.21	0.84±0.23	*0.221*
Tot_BMC [g]	30.3±10.3	31.0±10.6	*0.192*
Neck_BMC [g]	3.3±1.1	3.3±1.0	*0.607*
Troch_BMC [g]	7.3±2.9	7.4±2.9	*0.682*
Inter_BMC [g]	19.7±6.8	20.3±7.0	*0.181*
Fu [N]	8709±2929	3123±1143	***<0.001***
S [N/mm]	6284±1941	1639±455	***<0.001***

Table 6. 1: Overview of the densitometric measures and mechanical properties splitted for the two groups of femora tested in the different loading configurations. The third column shows the p-values from the paired Student's t-test used to compare the averages of the properties for the two groups.

The experiments showed in all cases a clear maximum of the load-displacement curve (Figure 6.3a). As expected, femoral stiffness was correlated with failure load for both STANCE (R^2=0.73) and FALL (R^2=0.73) (Figure 6.3b). The experimental ultimate force showed a correlation between the two loading configurations (R^2=0.72, SEE=0.74 kN, Figure 6.3c). In fact the ultimate force in the STANCE was approximately three times larger than the one measured in the FALL configuration (Fu_STANCE= 8.7±2.9 kN,

range: 3.54-14.42 kN; Fu_FALL=3.1±1.1 kN, range: 1.46-5.26 kN; $P<0.001$, Slope=0.33, Figure 6.3c and Table 6.1). Results of the failure analysis performed on the X-rays, showed that the samples tested in STANCE configuration failed mainly in the neck (44%) or in the subcapital region (36%), while only a few failed in the trochanteric region (8%) or in the head (3%). The samples tested in FALL configuration failed mainly in the femoral neck (64%) whereas the 17% failed in the trochanteric region, only 11% failed in the subcapital region and 3% in the femoral head. It was not possible to recognize the failure location of the remaining samples.

		Exp_Fu			***Exp_S***		
		STANCE	**FALL**	***p-value***	**STANCE**	**FALL**	***p-value***
DXA_BMD	***Neck***	0.66	0.80	***0.048***	0.46	0.65	*0.063*
	Tot	0.60	0.75	***0.033***	0.36	0.66	***0.013***
	Troch	0.59	[b] 0.69	*0.129*	0.43	0.68	***0.029***
	Inter	0.54	[b] 0.69	*0.056*	[b] 0.29	0.60	***0.014***
DXA_BMC	***Neck***	0.67	0.71 [a]	*0.341*	0.44	0.56	*0.152*
	Tot	0.64	0.66	*0.394*	0.36	0.58	***0.014***
	Troch	0.60	0.55 [a]	*0.302*	0.44	0.60	***0.038***
	Inter	0.55	0.62	*0.363*	[b] 0.27	0.51	***0.014***

Table 6. 2: Coefficients of determination (R^2) of the densitometric measures to predict experimental ultimate force (Fu) and stiffness (Exp_S) in the STANCE and FALL configurations. Significant differences between the R^2 for the two loading configurations are emphasized in "Bold". "a" represents significant differences between predictions of BMD and BMC for the different regions. "b" represents significant differences between prediction ability of the densitometric measures performed in the femoral neck and the ones performed in the other regions.

The correlations between the densitometric measures taken at the femoral neck and the ultimate force in STANCE and FALL configurations are reported in Figure 6.4 and the comparisons between the coefficients of determination of the predictions for ultimate force and stiffness in case of all densitometric measures are reported in Table 6.2. Ultimate force Fu was best predicted by Neck_BMC for STANCE (R^2=0.67, SEE=1.65kN) and by Neck_BMD for FALL (R^2=0.80, SEE=0.51kN). For the FALL configuration, BMD showed better predictions of Fu (in two cases the difference between the R^2 became significant, Table 6.2). In case of STANCE, BMC seemed to (not significantly) predict slightly better Fu compared to BMD. In both configurations, femoral neck properties were best predictors of Fu compared to the other regions (in two cases the differences between the R^2 became significant, Table 6.2). A similar trend was found for stiffness. However, the predictions of stiffness were lower for all densitometric measures ($R^2 \leq 0.68$) and the best predictor was Troch_BMD (R^2=0.68, SEE=0.25kN/mm) for FALL which was, however, not significantly different than the prediction of Neck_BMD (R^2=0.65, SEE=0.26kN/mm).
For all regions and for both BMD and BMC, the Pearson's correlation coefficients were systematically higher when predicting the Fu in the FALL configuration compared to the STANCE except for Troch_BMC. However, probably due to the limited number of femur pairs (36), the differences between the R^2 were significant in only two cases (for Neck_BMD and Tot_BMD, while for Inter_BMD the significance was close to the limit of 0.05). If the analysis were restricted to the samples that failed in the neck region for both configurations similar trends were found. In particular, Neck BMD predicted ultimate force for FALL configuration (R^2=0.89, SEE=0.47kN/mm) significantly better (P=0.012) than for STANCE configuration (R^2=0.68, SEE=1.62kN/mm).

6.4 Discussion

The aim of the present study was to compare the ability of BMD and BMC of different proximal femoral regions in predicting femoral mechanical properties tested in two loading configurations *in vitro*.
The BMD values for each region (Lochmuller, et al., 2000; Manske, et al., 2006; Pinilla, et al., 1996) and the measured femoral mechanical properties (Cristofolini, et al., 2007; Eckstein, et al., 2004; Keyak, 2001) found in the present study were consistent with the results of *in vitro* studies previously published. The average ultimate force for the STANCE configuration was higher than the peak forces due to physiological activities (walking, walking upstairs or downstairs (Bergmann, et al., 2001)) and in the same range of maximal forces due to stumbling (Bergmann, et al., 2004; Bergmann, et al., 2010), which might cause spontaneous fractures.
For both loading conditions, the testing setup was able to reproduce typical failure locations observed in clinical practice (Alffram, 1964): subcapital, neck and trochanteric fractures. Only in two cases the fracture was localized in the femoral head, which do not correspond to a typical fracture location. Experimental stiffness was shown to be a good predictor of ultimate force for both loading configurations (R^2=0.73). Since the paired groups of femora had similar shape and BMD, the difference between the slopes of the linear regressions split for STANCE (Sl=1.3) and FALL (Sl=2.1) can be explained by geometrical loading effects. The loading direction plays an important role in the stress distribution that induces different damage localization at higher loads.

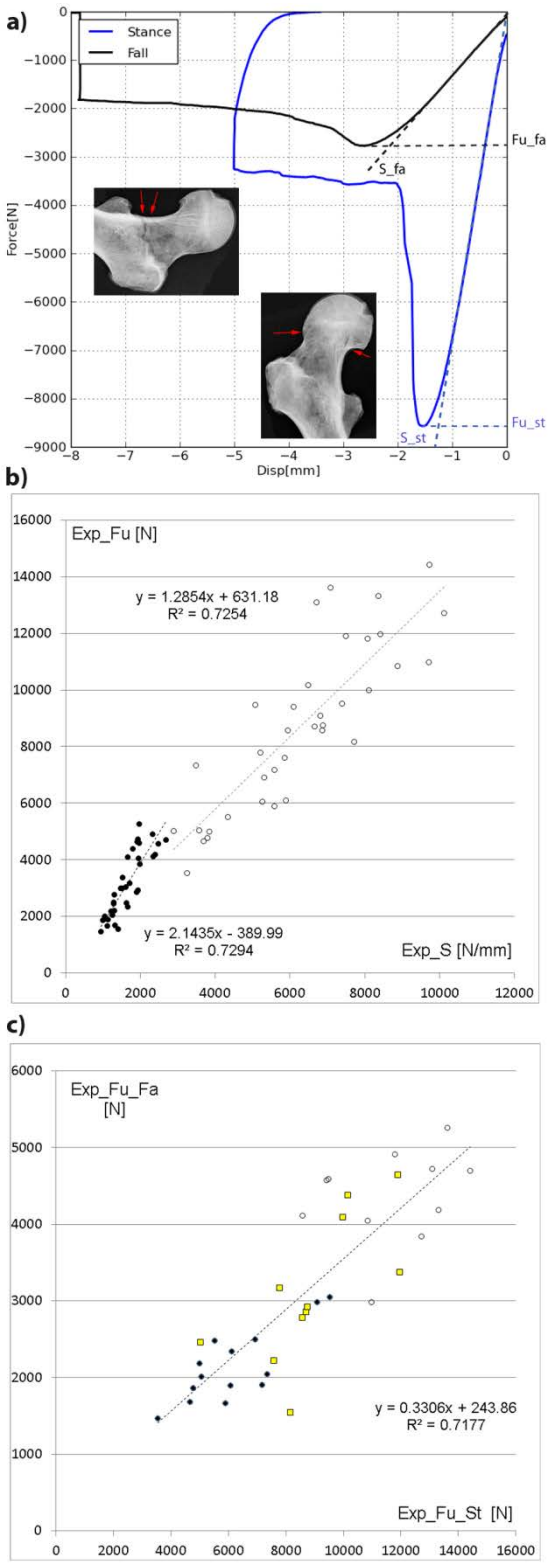

Figure 6. 3: Overview of the mechanical test results. a) Example of a pair of experimental curves for the STANCE and FALL configurations. The X-ray failure analysis is shown nearby. b) Correlation between stiffness and ultimate force computed from the experiments separated for testing configuration (FALL in filled circles, STANCE in open circles). c) Correlation between ultimate force of the samples tested in STANCE and the ones tested in FALL configurations (close circles, open squares and open circles represent osteoporotic, osteopenic and normal subjects, respectively).

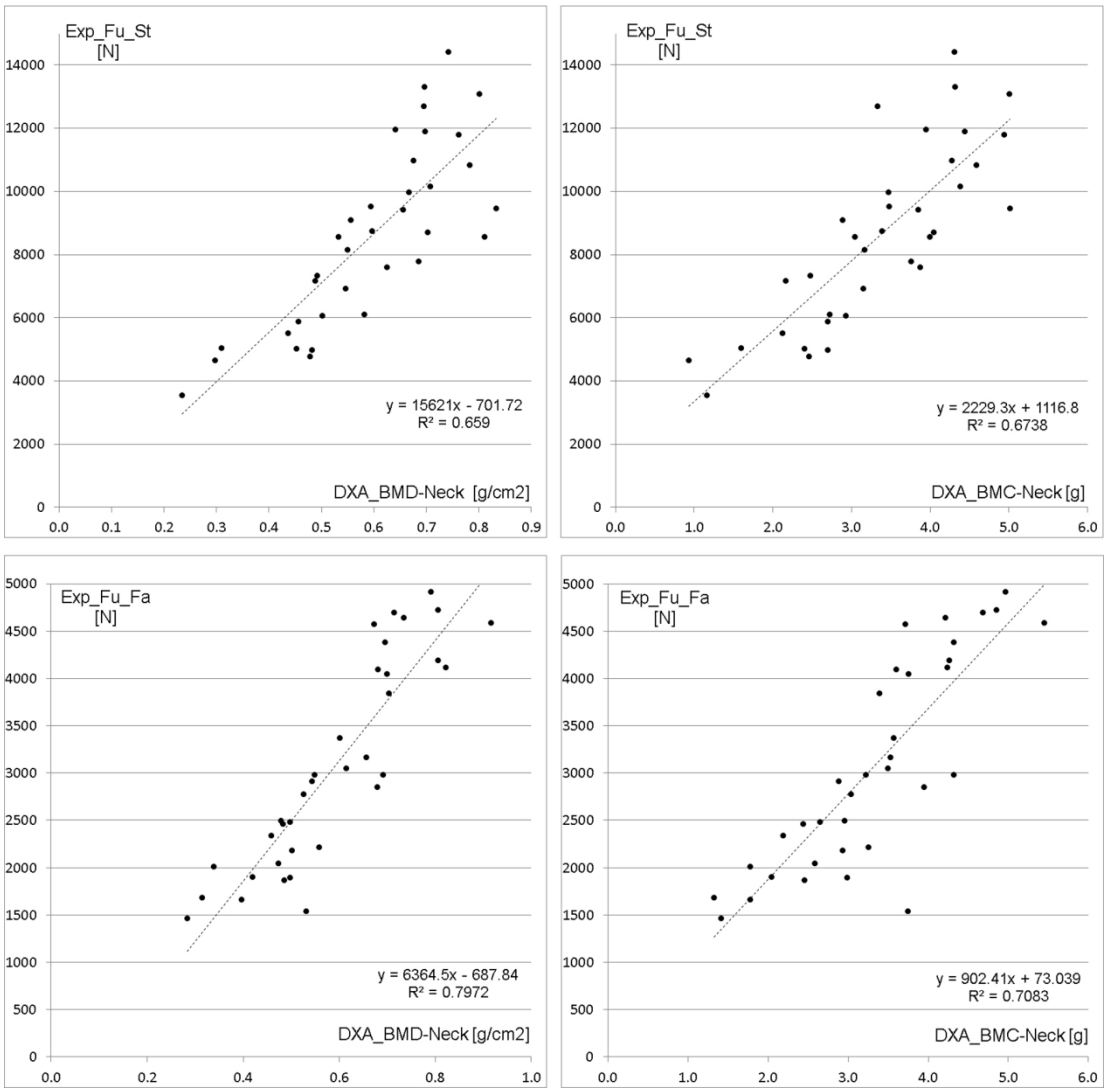

Figure 6. 4: Correlation between femoral ultimate force and DXA BMD (left) or BMC (right) measured in the neck. Correlations are reported for the samples tested in STANCE (top) and FALL configurations (bottom).

Indeed, even though the femora most frequently failed in the neck region in both configurations (44% for STANCE and 64% for FALL), the femora tested in STANCE showed a higher rate of subcapital fractures compared to the contralateral ones tested in FALL, which showed a higher rate of trochanteric fractures. While there is not a systematic agreement about the most common failure location induced by different testing setups used to test human femora *in vitro*, the high rate of neck fractures in STANCE and FALL found in the present study is not in agreement with the most common trend found in the literature where subcapital fractures were most frequent in STANCE (80% in Cristofolini et al. (2007), 69% in Cody et al. (1999), 83% in Keyak (2001)) and trochanteric fractures were most frequent in FALL (82% in Keyak (2001), 55% in Dragomir-Daescu et al. (2011)). The disagreement might be due to three main differences among the studies. First, the samples were positioned with different angles between the loading axis and the proximal shaft angle (in case of STANCE: 8° in Cristofolini et al. (2007), 25° in Cody et al. (1999) and 20° in the present study; in case of FALL: 80° in Dragomir-Daescu et al. (2011) vs 60°

in the present study) and between the loading axis and the femoral neck axis (in case of FALL: 70° in Keyak (2001) vs 0° in the present study). Second, different loading rates were used during the destructive testing (3-20 times slower in the present study compared to the above mentioned ones). Third, the mechanical setup was slightly different. In particular, the bearings included in our setup reduced the shear forces and the torque in the plane perpendicular to the loading axis both on the femoral head and on the greater trochanter. The translation of the femoral head under loading increased the lever arm and therefore the bending moment and the peak stresses in the neck. The ability of reproducing a fracture consistent with clinical observations in almost all femora tested in the present study (~95%) speaks for the good quality of the used mechanical setup.

The lower coefficient of determination between failure load measured in the two configurations (R^2=0.72) compared to the one found by Keyak et al. (2000) (R^2=0.81) might be due to different sample size (17 vs 36 pairs), different testing setup (in Keyak (2000) no bearing was added in the setup for removing any in plane forces or torsion) and different positioning of the proximal femora in the FALL configuration (angle between loading axis and neck axis 70º vs 0º). However, the fact that the slope of the linear regressions was similar to the one found in the present study (0.33 vs 0.38) strengthens the result that the human femur can resist three times higher loads in a one-legged stance configuration than in sideways fall. However, the relatively high SEE (0.74 kN) of the Fu-STANCE to Fu-FALL linear regression states that the ultimate force measured in STANCE can not be used to accurately predict the one measured in FALL.

As expected, the correlation of BMD and BMC between the samples tested in the two loading conditions was close to the 1:1 relationship and no significant differences were found between the mean values of all densitometric quantities computed for the two groups. The significant difference between the ultimate force computed for the two loading configurations reflects that femoral morphology is optimized for physiological loading. The limited correlation of BMD and BMC with ultimate load confirms that factors other than bone density and quantity contribute to femoral strength and therefore to femoral fracture risk. Known factors are: trabecular structure and orientation (Hansen, et al., 2011), cortical thickness and its distribution along the femur (Treece, et al., 2010), patient's ability to protect the hip during the fall (Feldman and Robinovitch, 2007), location and direction of the fall (Carpenter, et al., 2005), the amount of soft tissues between the bone and the impact surface (Nielson, et al., 2009), the height and weight of the subject, reduced agility and neuromuscular malfunction (Has, et al., 2006). This consideration is emphasised by the better ability of BMD and BMC of the different femoral regions (except for trochanteric BMC) to predict ultimate force and stiffness for the FALL than for STANCE configurations (in seven cases the differences became significant).

Furthermore, BMD systematically predicted better (or similarly, in a few cases) the femoral mechanical properties than BMC for all investigated regions. This contrasts with our previous study in the human spine, where ultimate force of vertebral bodies tested in axial compression was better predicted by measurements proportional to body mass (as BMC) compared to areal BMD (Dall'Ara, et al., 2012). We attribute this discrepancy to the distinct loading mode and the important role of trabecular bone in vertebral compression.

The femoral neck was the region that was better correlated to the femoral ultimate force for both configurations. In particular neck BMD predicted significantly better femoral failure load in FALL compared to both trochanteric and intertrochanteric BMD. This result is in line with the more frequent failure of the neck for samples tested in the FALL and with the results found by Lochmueller et al. (2003) who showed similar trend for formalin fixed femora.

All the above-mentioned results suggest that DXA neck BMD is a better surrogate of femoral strength when loaded as in a sideways fall than if loaded as in a one-legged stance configuration *in vitro* (R^2=0.80 vs R^2=0.66, $p<0.05$). If the statistical tests were performed on logarithmically transformed variables (to obtain more homogeneous variance distribution), the *P*-values slightly changed and in some cases the differences between the Pearson's coefficients lost of significance. However, we are confident that this effect is due to the relatively low sample size. It remains to be demonstrated if DXA neck BMD would be a better predictor of femoral fracture risk for fractures associated to a fall compared to the one for spontaneous fractures *in vivo*.

It is interesting to note that the prediction of femoral ultimate force with DXA neck BMD (R^2=0.66-0.80) measurements was similar to the one found for human thoracic and lumbar vertebrae from simulated (R^2=0.63-0.67 (Dall'Ara, et al., 2012)) or *in vitro* DXA (R^2=0.71-0.82 (Edmondston, et al., 1997; Lochmuller, et al., 2003)). This finding stresses that the densitometric measures are able to predict the 60-80% of the variation of bone strength but that other parameters such as structural and microstructural parameters, microdamage and loading conditions contribute to explain the remaining uncertainties.

The present study has some limitations. First, the muscular forces were not reproduced in the mechanical test. Especially the abductor muscles could change the stress distribution and therefore fracture location, stiffness and ultimate force of the femur in both configurations. However, it was previously shown with finite element models that the exclusion of the abductor forces in a simulated one-legged stance slightly overestimates the risk of fracture (Cristofolini, et al., 2007). Second, the samples were tested in quasi-static condition under a loading rate of 5mm/min to better control the experiments and the better recognize the bone failure. As bone is a viscoelastic material, tests performed at a loading rate closer to the physiological one for impact failure would lead to higher stiffness (Juszczyk, et al., 2011) and ultimate forces (Courtney, et al., 1994). Third, the DXA measurements were performed *in vitro* after isolation of the proximal femur. Therefore, the values of Tot BMD and Tot BMC were affected by the absence of the pelvis compared to the *in situ* case. Fourth, even though a substantial number of femora was tested (36 pairs), an increase in sample size would probably increase the number of significant differences between the compared coefficients of determination.

In conclusion, among all considered densitometric measures, femoral neck BMD was found to be the best *ex vivo* femoral strength predictor in both loading configurations. This result underlines that this measure should be considered as one of the key factors for discriminating femoral fracture risk *in vivo*. Moreover, femoral neck BMD was found to significantly better predict femoral ultimate force if tested in a fall compared to a one-legged stance configuration. The results suggest that DXA's ability of predicting spontaneous fractures may not be as good as for fractures associated to a fall.

Acknowledgements

The authors gratefully acknowledge Mr. Exler for having manufactured the experiment set-up tools, Prof Pettermann for the fruitful discussion, Mr. Fritz for the help while designing the setup, Mr. Seifert and Mr. Sallmutter for the help with sample preparation and Ms. Bojas, Ms. Huber, Ms. Nourzad, Ms. Weinelt ad Ms. Hofmann-Digruber for the help during the DXA analysis. We would like to thank Prof Mayr and Mr. Unger for the logistic help during the scanning.

Bibliography

Alffram P.A., 1964. An epidemiolologic study of cervical and trochanteric fractures of the femur in an urban population. Analysis of 1,664 cases with special reference to etiologic factors. Acta Orthopaedica Scandinavica Supplementum 65, 1-109.

Bergmann G., Deuretzbacher G., Heller M., Graichen F., Rohlmann A., Strauss J., Duda G.N., 2001. Hip contact forces and gait patterns from routine activities. Journal of Biomechanics 34, 859-871.

Bergmann G., Graichen F., Rohlmann A., 2004. Hip joint contact forces during stumbling. Langenbeck's Archives of Surgery 389, 53-59. Epub 2003 Nov 2019.

Bergmann G., Graichen F., Rohlmann A., Bender A., Heinlein B., Duda G.N., Heller M.O., Morlock M.M., 2010. Realistic loads for testing hip implants. Bio-medical Materials and Engineering 20, 65-75.

Boehm H.F., Horng A., Notohamiprodjo M., Eckstein F., Burklein D., Panteleon A., Lutz J., Reiser M., 2008. Prediction of the fracture load of whole proximal femur specimens by topological analysis of the mineral distribution in DXA-scan images. Bone 43, 826-831. Epub 2008 Aug 2007.

Bousson V., Le Bras A., Roqueplan F., Kang Y., Mitton D., Kolta S., Bergot C., Skalli W., Vicaut E., Kalender W., Engelke K., Laredo J.D., 2006. Volumetric quantitative computed tomography of the proximal femur: relationships linking geometric and densitometric variables to bone strength. Role for compact bone. Osteoporosis International 17, 855-864. Epub 2006 Mar 2018.

Bouxsein M.L., Coan B.S., Lee S.C., 1999. Prediction of the strength of the elderly proximal femur by bone mineral density and quantitative ultrasound measurements of the heel and tibia. Bone 25, 49-54.

Carpenter R.D., Beaupre G.S., Lang T.F., Orwoll E.S., Carter D.R., 2005. New QCT analysis approach shows the importance of fall orientation on femoral neck strength. Journal of Bone and Mineral Research 20, 1533-1542. Epub 2005 May 1516.

Cheng X., Li J., Lu Y., Keyak J., Lang T., 2007. Proximal femoral density and geometry measurements by quantitative computed tomography: association with hip fracture. Bone 40, 169-174. Epub 2006 Jul 2028.

Cheng X.G., Nicholson P.H., Boonen S., Brys P., Lowet G., Nijs J., Dequeker J., 1997. Effects of anteversion on femoral bone mineral density and geometry measured by dual energy X-ray absorptiometry: a cadaver study. Bone 21, 113-117.

Cody D.D., Gross G.J., Hou F.J., Spencer H.J., Goldstein S.A., Fyhrie D.P., 1999. Femoral strength is better predicted by finite element models than QCT and DXA. Journal of Biomechanics 32, 1013-1020.

Courtney A.C., Wachtel E.F., Myers E.R., Hayes W.C., 1994. Effects of loading rate on strength of the proximal femur. Calcified Tissue International 55, 53-58.

Courtney A.C., Wachtel E.F., Myers E.R., Hayes W.C., 1995. Age-related reductions in the strength of the femur tested in a fall-loading configuration. Journal of Bone and Joint Surgery Americal volume 77, 387-395.

Cristofolini L., Juszczyk M., Martelli S., Taddei F., Viceconti M., 2007. In vitro replication of spontaneous fractures of the proximal human femur. Journal of Biomechanics 40, 2837-2845

Cummings S.R., Melton L.J., 2002. Epidemiology and outcomes of osteoporotic fractures. Lancet 359, 1761-1767.

Dall'Ara E., Schmidt R., Pahr D., Varga P., Chevalier Y., Patsch J., Kainberger F., Zysset P., 2010. A nonlinear finite element model validation study based on a novel experimental technique for inducing anterior wedge-shape fractures in human vertebral bodies in vitro. Journal of Biomechanics 43, 2374-2380

Dall'Ara E., Pahr D., Varga P., Kainberger F., Zysset P., 2012. QCT-based Finite Element Models Predict Human Vertebral Strength in vitro Significantly Better than Simulated DEXA. Osteoporosis International 23, 563-572

Dragomir-Daescu D., Op Den Buijs J., McEligot S., Dai Y., Entwistle R.C., Salas C., Melton L.J., 3rd, Bennet K.E., Khosla S., Amin S., 2011. Robust QCT/FEA models of proximal femur stiffness and fracture load during a sideways fall on the hip. Annals of Biomedical Engineering 39, 742-755

Eckstein F., Wunderer C., Boehm H., Kuhn V., Priemel M., Link T.M., Lochmuller E.M., 2004. Reproducibility and side differences of mechanical tests for determining the structural strength of the proximal femur. Journal of Bone and Mineral Research 19, 379-385

Edmondston S.J., Singer K.P., Day R.E., Breidahl P.D., Price R.I., 1994. Formalin fixation effects on vertebral bone density and failure mechanics: an in-vitro study of human and sheep vertebrae. Clin Biomech 9, 175-179

Edmondston S.J., Singer K.P., Day R.E., Price R.I., Breidahl P.D., 1997. Ex vivo estimation of thoracolumbar vertebral body compressive strength: the relative contributions of bone densitometry and vertebral morphometry. Osteoporosis International 7, 142-148

Feldman F., Robinovitch S.N., 2007. Reducing hip fracture risk during sideways falls: evidence in young adults of the protective effects of impact to the hands and stepping. Journal of Biomechanics 40, 2612-2618. Epub 2007 Mar 2628.

Fessy M.H., Seutin B., Bejui J., 1997. Anatomical basis for the choice of the femoral implant in the total hip arthroplasty. Surgical and Radiologic Anatomy 19, 283-286.

Greenspan S.L., Myers E.R., Kiel D.P., Parker R.A., Hayes W.C., Resnick N.M., 1998. Fall direction, bone mineral density, and function: risk factors for hip fracture in frail nursing home elderly. American journal of medicine 104, 539-545.

Gregory J.S., Aspden R.M., 2008. Femoral geometry as a risk factor for osteoporotic hip fracture in men and women. Medical Engineering and Physics 30, 1275-1286. Epub 2008 Oct 1231.

Griffith J.F., Genant H.K., 2008. Bone mass and architecture determination: state of the art. Best Practice & Research Clinical Endocrinology & Metabolism 22, 737-764

Hansen S., Jensen J.E., Ahrberg F., Hauge E.M., Brixen K., 2011. The combination of structural parameters and areal bone mineral density improves relation to proximal femur strength: an in vitro study with high-resolution peripheral quantitative computed tomography. Calcified Tissue International 89, 335-346. doi: 310.1007/s00223-00011-09523-z. Epub 02011 Aug 00228.

Has B., Nagy A., Has-Schon E., Pavic R., Kristek J., Splavski B., 2006. Influence of instability and muscular weakness in ethiopathogenesis of hip fractures. Collegium Antropologicum 30, 823-827.

Johnell O., Kanis J.A., 2006. An estimate of the worldwide prevalence and disability associated with osteoporotic fractures. Osteoporososis International 17, 1726-1733

Juszczyk M.M., Cristofolini L., Viceconti M., 2011. The human proximal femur behaves linearly elastic up to failure under physiological loading conditions. Journal of Biomechanics 44, 2259-2266. Epub 2011 Jun 2230.

Kannus P., Leiponen P., Parkkari J., Palvanen M., Jarvinen M., 2006. A sideways fall and hip fracture. Bone 39, 383-384. Epub 2006 Feb 2028.

Keyak J.H., 2000. Relationships between femoral fracture loads for two load configurations. Journal of Biomechanics 33, 499-502.

Keyak J.H., 2001. Improved prediction of proximal femoral fracture load using nonlinear finite element models. Medical Engineering and Physics 23, 165-173

Keyak J.H., Skinner H.B., Fleming J.A., 2001. Effect of force direction on femoral fracture load for two types of loading conditions. Journal of Orthopaedic Research 19, 539-544.

Kukla C., Gaebler C., Pichl R.W., Prokesch R., Heinze G., Heinz T., 2002. Predictive geometric factors in a standardized model of femoral neck fracture. Experimental study of cadaveric human femurs. Injury 33, 427-433.

Lochmuller E.M., Krefting N., Burklein D., Eckstein F., 2001. Effect of fixation, soft-tissues, and scan projection on bone mineral measurements with dual energy X-ray absorptiometry (DXA). Calcified Tissue International 68, 140-145.

Lochmuller E.M., Miller P., Burklein D., Wehr U., Rambeck W., Eckstein F., 2000. In situ femoral dual-energy X-ray absorptiometry related to ash weight, bone size and density, and its relationship with mechanical failure loads of the proximal femur. Osteoporosis International 11, 361-367.

Lochmuller E.M., Muller R., Kuhn V., Lill C.A., Eckstein F., 2003. Can novel clinical densitometric techniques replace or improve DXA in predicting bone strength in osteoporosis at the hip and other skeletal sites? Journal of Bone and Mineral Research 18, 906-912.

Lochmuller E.M., Zeller J.B., Kaiser D., Eckstein F., Landgraf J., Putz R., Steldinger R., 1998. Correlation of femoral and lumbar DXA and calcaneal ultrasound, measured in situ with intact soft tissues, with the in vitro failure loads of the proximal femur. Osteoporosis International 8, 591-598.

Lotz J.C., Hayes W.C., 1990. The use of quantitative computed tomography to estimate risk of fracture of the hip from falls. The Journal of Bone and Joint Surgery American volume 72, 689-700.

Manske S.L., Liu-Ambrose T., de Bakker P.M., Liu D., Kontulainen S., Guy P., Oxland T.R., McKay H.A., 2006. Femoral neck cortical geometry measured with magnetic resonance imaging is associated with proximal femur strength. Osteoporosis International 17, 1539-1545. Epub 2006 Jul 1518.

Mnif H., Koubaa M., Zrig M., Trabelsi R., Abid A., 2009. Elderly patient's mortality and morbidity following trochanteric fracture. A prospective study of 100 cases. Orthopaedics&traumatology, surgery&research 95, 505-510. Epub 2009 Sep 2026.

Nielson C.M., Bouxsein M.L., Freitas S.S., Ensrud K.E., Orwoll E.S., 2009. Trochanteric soft tissue thickness and hip fracture in older men. J Clin Endocrinol Metab 94, 491-496

Nyberg L., Gustafson Y., Berggren D., Brannstrom B., Bucht G., 1996. Falls leading to femoral neck fractures in lucid older people. Journal of the American Geriatrics Society 44, 156-160.

Ohman C., Dall'Ara E., Baleani M., Van Sint Jan S., Viceconti M., 2008. The effects of embalming using a 4% formalin solution on the compressive mechanical properties of human cortical bone. Clin Biomech 23, 1294-1298

Parkkari J., Kannus P., Palvanen M., Natri A., Vainio J., Aho H., Vuori I., Jarvinen M., 1999. Majority of hip fractures occur as a result of a fall and impact on the greater

trochanter of the femur: a prospective controlled hip fracture study with 206 consecutive patients. Calcified Tissue International 65, 183-187.

Pinilla T.P., Boardman K.C., Bouxsein M.L., Myers E.R., Hayes W.C., 1996. Impact direction from a fall influences the failure load of the proximal femur as much as age-related bone loss. Calcified Tissue International 58, 231-235.

Popperl G., Lochmuller E., Becker H., Mall G., Steinlechner M., Eckstein F., 1999. Determination of calcaneal ultrasound properties ex situ: reproducibility, effects of storage, formalin fixation, maceration, and changes in anatomic measurement site. Calcified Tissue International 65, 192-197.

Roberts B.J., Thrall E., Muller J.A., Bouxsein M.L., 2010. Comparison of hip fracture risk prediction by femoral aBMD to experimentally measured factor of risk. Bone 46, 742-746. Epub 2009 Oct 2022.

Schwartz A.V., Kelsey J.L., Sidney S., Grisso J.A., 1998. Characteristics of falls and risk of hip fracture in elderly men. Osteoporosis International 8, 240-246.

Steiger J.H., 1980. Tests for comparing elements of a correlation matrix. Psychological bullettin 87, 245-251

Treece G.M., Gee A.H., Mayhew P.M., Poole K.E., 2010. High resolution cortical bone thickness measurement from clinical CT data. Medical Image Analysis 14, 276-290. Epub 2010 Jan 2025.

Unger S., Blauth M., Schmoelz W., 2010. Effects of three different preservation methods on the mechanical properties of human and bovine cortical bone. Bone 47, 1048-1053. Epub 2010 Aug 1021.

Varga P., Baumbach S., Pahr D., Zysset P.K., 2009. Validation of an anatomy specific finite element model of Colles' fracture. Journal of Biomechanics 42, 1726-1731

Viceconti M., Taddei F., Cristofolini L., Martelli S., Falcinelli C., Schileo E., 2012. Are spontaneous fractures possible? An example of clinical application for personalised, multiscale neuro-musculo-skeletal modelling. Journal of Biomechanics 45, 421-426. Epub 2011 Dec 2026.

Chapter 7

Conclusions

7.1 Original contributions

The aim of this thesis was to apply and validate specimen specific QCT-based homogenized FE models to predict the mechanical properties of the human vertebral body and proximal femur. One of the objectives of the thesis was to design experimental setups to test a large number of vertebrae and femora up to failure by inducing fractures typically observed in clinical practice. Furthermore, another goal was to compare the predictive ability of such models with the one of standard clinical tools used to evaluate the risk of fracture in patients. The studies presented in Chapters 2 to 6 were designed to answer specific research questions and provided the following results:

Chapter 2 showed a hierarchical methodology to estimate μCT BV/TV from QCT BMD for the full range of density. The procedure was defined for the human vertebra and then applied also to the human femur (Chapter 5). Even though the calibration equations found in the study is strictly dependent from the used scanning machines, the method presented is original and can be used to define similar equations for other anatomical sides, especially where the thin cortical shell does not allow to use standard methodologies like ash density measurements. The calibration equations found by using the presented methodology were then applied in the BV/TV-based hvFE models described in the following chapters (Chapter 4 for the vertebra and Chapter 5 for the femur);

Chapter 3 described a novel experimental setup to induce anterior wedge shape fractures to human vertebral body sections. The choice of testing vertebral body sections instead of full vertebrae was taken to better control the boundary conditions in the experiments and to have a better match between numerical simulations and experiments. Moreover, accurate stiffness measurements were performed by reducing the effect of the compliance of the setup/machine. From the numerical point of view nonlinear models were generated by adapting an already published procedure (Chevalier, et al., 2009) with novel and more complex boundary conditions. Furthermore, this chapter showed that the QCT-based hvFE models predict the vertebral failure load better (R^2=0.79) than the volumetric trabecular

BMD multiplied by the minimal cross-sectional area (minCSA) obtained with a standard clinical tool (Figure 3.8, R^2=0.70, QCTPro, Mindways, USA);

Chapter 4 presented how the hvFE model presented in the previous chapter could be used for future pre-clinical and clinical applications. In particular, it described a method to evaluate areal BMD by simulating DXA outputs generated from QCT scans. Moreover, it confirmed that FE as well as volumetric densitometric measurements like BMD, are better predictors of vertebral material properties, while BMC predicts better structural properties. Furthermore, it showed that an improvement of image resolution would not improve the predictive ability of densitometric measurements and could only enhance the prediction of vertebral body stiffness by using μFE models (from R^2=0.52 for hvFE to R^2=0.72 for μFE) while for the other mechanical properties only a small improvement could be shown for apparent properties (from R^2=0.71 to R^2=0.78 for modulus and from R^2=0.79 to R^2=0.88 for strength). Finally, it presented that, for both image resolutions, FE models (hvFE or μFE) are better predictors of vertebral mechanical properties than aBMD;

Chapter 5 described the experimental setup designed to induce proximal femoral fractures in two loading configurations. Moreover, it showed the procedure to generate QCT based hvFE models of the femur, by calibrating the QCT BMD with μCT BV/TV in the same fashion as shown in Chapter 2 for the vertebral body, and by adapting an already published constitutive model (Garcia, et al., 2009) for isotropic materials with thick cortical bone. The chapter showed that the hvFE models predict femoral failure load better than QCT based BMD for both STANCE (R^2=0.80 versus R^2=0.56) and FALL (R^2=0.85 versus R^2=0.68) configurations. Moreover, hvFE can provide qualitatively information about the damage localization and the kinematic of the femoral head;

Chapter 6 further investigated the experimental results of the human femora used to validate the hvFE models in Chapter 5. In particular, for every sample a DXA exam was performed and the data compared with the mechanical properties of the femora tested by simulating a spontaneous fracture or an accidental one, caused by a fall on the side. The result of this chapter showed that the neck BMD among all the other densitometric measurement (BMD and BMC in different location of the proximal femur) is the best predictor of the femoral mechanical properties (R^2=0.66 for STANCE and R^2=0.80 for FALL). Moreover, it demonstrated that DXA can predict better the femoral mechanical properties if tested in a simulated fall than if tested simulating a spontaneous fracture. Both results suggest that neck BMD should be included in the definition of the clinical tools to predict the risk of fracture and that the current clinical techniques might not be accurate in predicting spontaneous fractures.

7.2 General Discussion

This thesis was aimed to validate specimen specific QCT-based hvFE models of the human vertebra and femur. To do so a similar approach was used for the two anatomical sites:

- a relatively large set of bone samples (at the organ level) were prepared and stored fresh frozen,
- the samples were scanned with QCT and with HR-pQCT,
- the samples were examined with standard clinical tools (low resolution QCT or DXA),

- experimental setups were designed to be able to generate bone fractures which are typically observed in clinical practice,
- from the 3D QCT scans, hvFE models were generated to match the same boundary conditions of the experiments,
- the outcomes of the FE simulations and of the densitometric measurements were compared to the experimental results to evaluate the ability of the different tools to predict bone stiffness and failure load.

Based on this, the thesis was divided in two large parts. Chapters 2, 3 and 4 focused on the validation of the method for the vertebral body, while Chapters 5 and 6 focused on the proximal femur. In the next subsections the main strengths and limitations of this thesis will be discussed, considering the outcomes all together, without splitting between the two different anatomical sites.

7.2.1 Sample preparation

An important part of a study which aims to perform mechanical testing on bone samples, is the sample preparation. The samples tested in the above presented studies were collected from the Medical University of Vienna and all the procedures performed in the present thesis were approved by its ethics commission. Samples were extracted from the donors and frozen until the beginning of the preparation. In between each step of the procedure (preparation, scanning, testing, radiographies after test), the samples were kept frozen. Even though this choice made harder the sample handling and the necessity of a fully equipped lab to handle biological tissues with potential risk of infections, it was preferred to a chemical fixation/storage, such as formalin solutions, which might affect the bone mechanical properties (Ohman, et al., 2008; Unger, et al., 2010).

7.2.2 CT scanning and densitometry

Each sample was scanned with a QCT and with a HR-pQCT to extract the bone geometry and BMD information. In a second step this data were used to generate FE models. Even though it was not described in this thesis, the femora were scanned with HR-pQCT too and the data will be used in future studies. Furthermore, each sample underwent a densitometric exam (with DXA or with low resolution QCT) to verify if the FE models could improve the prediction of bone mechanical properties compared with the standard clinical tools used to estimate the RoF *in vivo*. Two chambers were designed and manufactured to perform the scans (with QCT, HR-pQCT and DXA) of each sample in saline solution (0.9% NaCl) in order to simulate the presence of soft tissues, which were removed during their dissection from the spine and from the hip. A fundamental step of the procedure was to leave the samples inside the scanning chambers under vacuum for at least ten minutes before scanning. This simple step assured to obtain almost air bubbles-free scans. In fact, the air bubbles, having a very low HU value, would lead to an underestimation of the averaged BMD value of the elements in which they would be contained and therefore affect their mechanical properties. To reduce the effect of the few remaining air bubbles in the scans, the BMD values lower than -100 mgHA/cc were set equal to -100 mgHA/cc. The QCT and densitometric scanning procedures were defined such as the ones used during standard clinical analysis, without optimizing the machine settings to obtain the best image quality. This decision was taken to obtain hvFE models which are as close as possible to the ones which might be generated from *in vivo* scans.

7.2.3 Mechanical testing

The setups used in this thesis were designed to optimize the accuracy of the validation procedure. In fact, the main source of error in an FE validation study is neither the experimental nor the computational parts, but in most cases comes from their comparison. In fact, we can generate very complex models or extremely well designed experiments but if we do not have an accurate match between them, our validation study will not be successful and we might misinterpret the final outcomes. In the process of designing a validation study for predicting bone mechanical properties at the organ level the researcher should ask himself many questions like: Does the model represent accurately the boundary conditions of the experimental setup? Are those boundary conditions not too far from the ones observed *in vivo* to simulate a meaningful loading scenario and, thus, are typical fractures obtained? Do the assumptions taken in the model (e.g. about the material property, boundary conditions, etc.) resemble the tested samples (absence of damage induced during the sample preparation, presence of pathologies whose effect on the bone mechanical properties is not clear, …)? Do the experimental errors affect significantly the measured quantities? And so on.
With these considerations in mind, the experimental setups designed in this thesis were found to produce reliable outcomes. In particular, they induced fractures typically observed in clinical practice for both vertebrae and femora. For the femur we were able to simulate both spontaneous fractures which might happen in a one-legged stance position and accidental fractures which might occur with the femur in a position representative to a fall on the greater trochanter. Moreover, thanks to a meticulous sample preparation and scanning procedures, we were able to reproduce well the boundary conditions in the FE models to match the ones observed or imposed during the experiments. We evaluated not only the bone strength (which is the simplest outcome of an experimental test as can be accurately measured with a load-cell in series to the tested bone) but also the bone stiffness, which is a fundamental property when designing implants, evaluating the effect of drug treatments, etc. However, this measurement is not trivial due, in most cases, to the presence of machine and setup compliances which act as springs in series to the specimen to be tested. As described in detail in Chapter 3 and 5, displacement sensors (LVDTs or infrared markers) were added to the setups to accurately measure also the bone stiffness.

7.2.4 Generation of hvFE models

For both anatomical sites, the QCT images were cropped and rotated to match the position of the samples during the experiments. Afterwards they were coarsened to the final required elements size (1.3^3 mm^3 for the vertebra and 3^3 mm^3 for the femur) and converted to BV/TV scale by proper calibration. Finally, the image voxels were directly converted into hexahedron elements and the right boundary conditions applied. This method guaranteed a fast preprocessing of the data, with a minor user interaction. The procedures to extract the bone geometry for FE models from QCT scans were based on previously published studies (Chevalier, et al., 2008; Keyak, et al., 2001). Moreover, material nonlinearities were driven by using an already published constitutive model (Garcia, et al., 2009). In that model, the bone material properties were assigned by entering BV/TV and fabric information in each element and it was tested on HR-pQCT images of the lumbar vertebra. However, in the present thesis, the constitutive model had to be adapted to compensate for lower resolution of the original QCT images and for the thick cortical bone which can be found in the proximal femur.

Calibration of BV/TV

A new methodology to calibrate QCT BMD with μCT BV/TV was developed for bones with a thin cortical shell as the vertebral body. This methodology was extensively described and applied to six human vertebral bodies in Chapter 2 and then applied to three femora in Chapter 5. The results of those studies suggest that a unique calibration equation can be used for both anatomical sites. The equations found for human vertebra and femur are reported below.
Vertebrae:

$$BV/_{TV} = \begin{cases} \sim 0, & BMD < -100 \\ 0.094 * \mathrm{BMD} - 0.030, & -100 \leq BMD \leq 1061 \\ 100, & BMD > 1061 \end{cases} \quad (7.1)$$

Femora:

$$BV/_{TV} = \begin{cases} \sim 0, & BMD < -100 \\ 0.093 * \mathrm{BMD} + 1.077, & -100 \leq BMD \leq 1064 \\ 100, & BMD > 1064 \end{cases} \quad (7.2)$$

Constitutive model

The definition of a novel constitutive model valid for human trabecular and cortical bone was beyond the aim of this study. Therefore, an elastic-damage constitutive model developed for bone and implemented in the FE solver used in the present study (*Abaqus 6.8-6.11, Simulia, Dassault Systemes, Velizy-Villacoublay, France*) was used (Garcia, et al., 2009). However, this model considers bone such as an orthotropic material in function of fabric and BV/TV, and it was developed for the human vertebra which has a preponderant portion of trabecular bone. Therefore, it was necessary to adapt the model for samples in which it was not possible to extract fabric information (based on QCT images) and where cortical bone plays and important role (such as the proximal femur). For the human vertebra the bone was assumed as transverse isotropic with main direction coincident with the cranio-caudal axis of the vertebral body (Chevalier, et al., 2009). No correction was done for cortical bone and the material properties to define the elastic and yield behaviour were taken without any correction from the literature (Rincon-Kohli and Zysset, 2009). For the femur the bone was considered as isotropic and a correction was performed to take into account for the thick cortical bone. In particular the experimental results found by (Rincon-Kohli and Zysset, 2009) were used to define a new set of material properties which would lead to meaningful results if extrapolated for pore-less material. For more details please refer to the Appendix of the Chapter 5. In both cases the hvFE predictions of ultimate strength were in good quantitative agreement with the experimental results and therefore the above mentioned assumptions seemed to be well undertaken.

7.2.5 Prediction ability of the hvFE models

hvFE were able to predict approximately 80% of the variability of the experimental ultimate force *in vitro* both for vertebral bodies (R^2=0.79, as reported in Chapter 3) and for femora (R^2=0.80 for STANCE and R^2=0.85 for FALL, as reported in Chapter 5). In both cases fair quantitative predictions were obtained (Slope=0.86, Intercept=0.723 kN for the vertebral bodies, Slope=1.29, Intercept=2.472 kN for the femora tested in STANCE and

Slope=0.91, Intercept=0.713 kN for the femora tested in FALL; reported in Chapters 3 and 5).
Moreover, these predictions were found to be better, in most cases significantly, than the BMD or BMC computed from the QCT scans with standard clinical tool or from the images used to generate the hvFE models ($0.34<R^2<0.70$ for the vertebral body, $0.56<R^2<0.74$ for the femur in STANCE and $0.66<R^2<0.71$ for the femur in FALL; reported in Chapters 3, 4 and 5) or than the densitometric results obtained from the clinical (simulated, in case of vertebrae) DXA ($0.63<R^2<0.67$ for the vertebral body, $0.54<R^2<0.66$ for the femur in STANCE and $0.55<R^2<0.80$ for the femur in FALL; reported in Chapters 4 and 6).

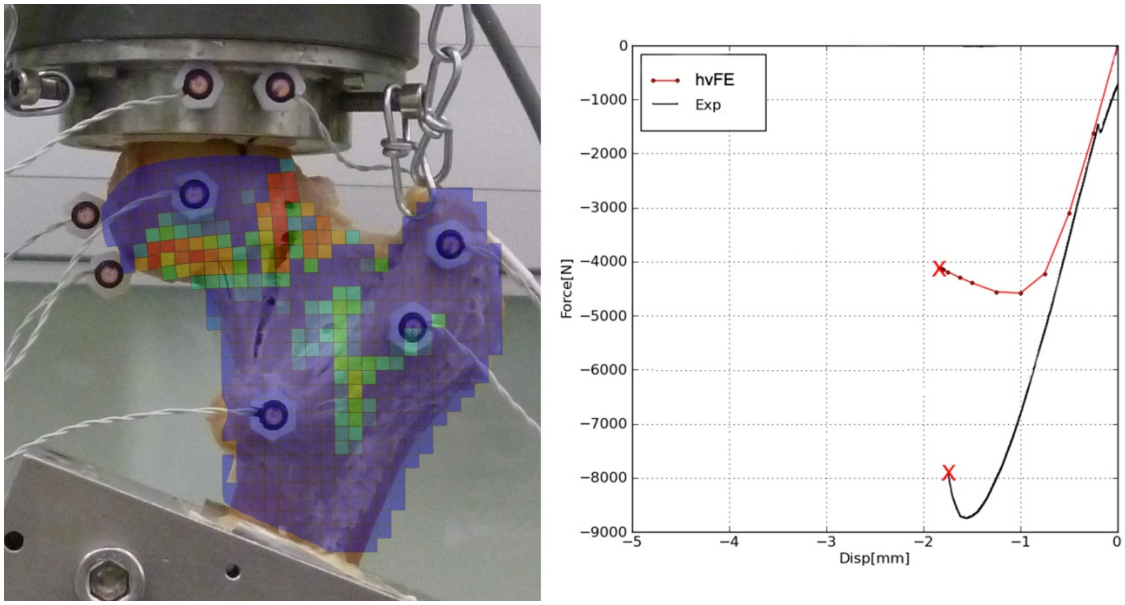

Figure 7. 1: Left: A picture taken of one of the fractured femora tested in stance configuration superimposed to the prediction of the damage distribution computed with the specimen-specific hvFE model (cropped section parallel to the frontal plane). Right: Comparison between load-displacement curves extracted from the hvFE (red) and experiments (black). The "X" represent the loading step from which the images shown on the left were taken.

Additionally, the hvFE models provided meaningful qualitative information about the load-displacement curves and about the failure localization for both anatomical sites (Figure 7.1).

7.2.6 Limitations of the study

This thesis has some limitations which might be improved in future studies. First, the calibration equation shown in Chapter 2 was found to be dependent from the subject. Some possible variables affecting the outcomes the calibration equation might be the range of BMD, the average cortical thickness, the bone geometry, the fat content, etc. Even if not reported in Chapter 5, a similar trend was found for the femur even though in that study only two subjects were considered (Dall'Ara, et al., 2012). Therefore, to obtain a more general equation more subjects should be included in the analysis.
Second, as already mentioned in the previous chapters, the QCT and DXA scans were performed *in vitro* in a custom made chamber to simulate soft tissues around the scanned

bone. However, the image quality of the same bones scanned *in situ* or *in vivo* might be lower due to the artifacts introduced by the other bones (for example the pelvis) which were removed during the dissection of the samples. A previous study (Keyak and Falkinstein, 2003) showed that the differences in the ultimate force predicted by hvFE models of the proximal femora based on *in situ* or *in vitro* scans can be up to 13%. Nevertheless, this value could change from model to model. Therefore, scanning the bones *in situ* before dissection would guarantee images closer to the *in vivo* situation. On the other side it would mean to scan whole cadavers, enhancing the logistical difficulties in scanning, its cost, and its ethical implications. Alternatively, the usage of a body phantom to simulate the human body during an *in vitro* scan might be an easier and cheaper solution to reduce differences between *in situ* and *in vitro* scans.
Third, a few technical refinements could be done on the experimental setups. For example a multi-axial load-cell could be used to measure also the transverse forces and the moments for both vertebral and femoral tests to increase the number of measurements used for validating the hvFE models. Moreover, the usage of a digitizer would have improved the match between the position of the infrared markers used to track the displacements of a few points of the femur (refer to Chapter 5) and their position in the hvFE models.
Fourth, even though the goal of this thesis was to minimize the time necessary to extract the bone geometry from the QCT scans and to mesh it for generating nonlinear QCT-based hvFE models, the definition of a smooth mesh might help to improve the prediction of the fracture location for both anatomical sites (and displacement of the femoral head in case of the femur). Moreover, the predictions of femoral stiffness might be improved by modelling a specimen specific cartilage layer. In this thesis the cartilage was not included in the model because it was not possible to segment it from the saline solution around the femora used to simulate the soft tissues. A possible option in future studies would be to perform an additional magnetic resonance scan of each sample, which could be registered to the QCT images, to obtain the thickness of the cartilage layer. Yet, this modification of the design of the study would largely increase the project's cost and time.

7.3 Outlook

It is well accepted that new methods to improve the prediction of femoral and vertebral fractures are needed to help clinicians to decide which patients require to be treated against bone loss. The results of this Thesis demonstrated that the subject specific Nonlinear QCT-based Finite Element method is superior to the current Bone Densitometry for prediction of vertebral and femoral strength *in vitro*. However, there is still a missing link in the computational chain to be able to evaluate the patient's risk of fracture by using the hvFE models: the estimation of the most critical loading scenario. For example, this information can be included in the model by evaluating the direction and the magnitude of the joint forces with instrumented implants (Bergmann, et al., 2004) or by estimating the joints and muscle forces in certain loading conditions with muskuloskeletal models (Lund, et al., 2012). Once the most critical loading scenario is estimated for each patient and for each bone, the computation of the bone strength in such configuration with the hvFE presented in this Thesis can be used to estimate the risk of fracture of each specific bone. Even though it is likely that a better estimation of the bone strength would improve the estimation of the risk of fracture, this remains to be demonstrated through clinical studies. Thanks to their high degree of automation, the models proposed here could be directly used in large clinical studies to estimate, for example, the risk of fracture or to investigate the

effect of drug treatments on the bone strength. Nevertheless, the next sections (*7.3.1* and *7.3.2*) report possible modifications and adaptations of the presented models which might be taken to improve their outcomes and applicability in a clinical environment. Finally, section *7.3.3* will underline how the large amount of experimental data acquired during this study will be helpful in the future to validate and compare different models based on QCT images.

7.3.1 Clinical and Pre-clinical application of the hvFE models

The hvFE models that were developed and validated in this thesis for the human vertebra and femur were designed to be applied without major modifications in further pre-clinical and clinical studies for *in vivo* scans. Some possible applications include the study of the effect of drug treatments on the bone mechanical properties of patients, the effect of bone lytic metastasis, etc.
However, some modifications might be necessary before a clinical application:

- The effect of *in vitro* vs *in situ* or *in vivo* scans should be investigated to understand possible effects on the hvFE results due to a higher noise in the original QCT images;
- In case of the femur a proper automatic or semi-automatic algorithm should be defined to be able to segment the femoral head from the hip joint without a major interaction of the operator. In case of the vertebrae a proper procedure to select how and where to isolate the vertebral body from the CT scan should be developed;
- Suitable visualization software should be designed to be able to apply the presented procedures to generate, run and evaluate the hvFE in a fast and simple way.

7.3.2 Model improvements

The model itself could be improved trying not to increase the pre-processing, computational and post-processing times. Possible improvements which might be applied to the model and whose effect should be studied in details might be the following.

- According to the results of Chapter 2, the scatter in the QCT BMD to BV/TV calibration equation is associated with the dimension of the region where those quantities are measured. Therefore, averaging the BMD value on a larger region might improve the predictions of the hvFE models, by reducing the scatter in the material properties which might lead to stress concentrators and unrealistic concentration of the damage;
- A more complex mesh which would represent the bone geometry more realistically might improve the prediction of the homogenized FE models. In particular, a smooth mesh composed by tetrahedral elements might lead to more accurate predictions of the local mechanical properties (Viceconti, et al., 1998) and probably of the damage distribution;
- The definition of different material properties for the cortical and trabecular bone microstructures might improve the prediction of the fracture location. This option could be implemented by using the software used by (Engelke, et al., 2010) to segment between trabecular and cortical bone in the QCT images;
- For the proximal femur, the definition of anisotropic (at least transversal isotropic) material properties based on the estimation of the principal trabecular orientation might become feasible in the next years thanks to the progresses in the image processing field. The inclusion of this information might on one hand site improve

the prediction of bone strength and on the other side explain the larger underestimation of it in case of one legged stance configuration;

- As shown for the vertebrae in Chapter 4, a similar study could be replicated to investigate the effect of an improved CT resolution on the predictive ability of densitometric and numerical methods for the mechanical properties of the proximal femur.

7.3.3 Experimental datasets

The large datasets of experimental data and QCT/HR-pQCT 3D images could be used as a benchmark to validate any other models based on such inputs which will be developed and/or improved in the future. In particular, they could be used to compare the different methodologies developed to generate QCT or HR-pQCT based FE models. This consideration is not limited to FE models but also to, for example, structural engineering methods which can be applied to the CT images by using the beam theory (Whealan, et al., 2000) to compute bone mechanical properties.

Bibliography

Bergmann G., Graichen F., Rohlmann A., 2004. Hip joint contact forces during stumbling. Langenbeck's Archives of Surgery 389, 53-59. Epub 2003 Nov 2019.

Chevalier Y., Charlebois M., Pahra D., Varga P., Heini P., Schneider E., Zysset P., 2008. A patient-specific finite element methodology to predict damage accumulation in vertebral bodies under axial compression, sagittal flexion and combined loads. Computer Methods in Biomechanics and Biomedical Engineering 11, 477-487

Chevalier Y., Pahr D., Zysset P.K., 2009. The role of cortical shell and trabecular fabric in finite element analysis of the human vertebral body. J Biomed Eng 131, 111003

Dall'Ara E., Pahr D., Zysset P., 2012. QCT-BMD to MicroCT-BV/TV calibration relationships are similar for human vertebra and femur. Journal of Biomechanics 45, S450

Engelke K., Fuerst T., Dasic G., Davies R.Y., Genant H.K., 2010. Regional distribution of spine and hip QCT BMD responses after one year of once-monthly ibandronate in postmenopausal osteoporosis. Bone 46, 1626-1632. Epub 2010 Mar 1610.

Garcia D., Zysset P.K., Charlebois M., Curnier A., 2009. A three-dimensional elastic plastic damage constitutive law for bone tissue. Biomechanics and Modeling in Mechanobiology 8, 149-165

Keyak J.H., Falkinstein Y., 2003. Comparison of in situ and in vitro CT scan-based finite element model predictions of proximal femoral fracture load. Medical Engineering and Physics 25, 781-787

Keyak J.H., Rossi S.A., Jones K.A., Les C.M., Skinner H.B., 2001. Prediction of fracture location in the proximal femur using finite element models. Medical Engineering and Physics 23, 657-664.

Lund M.E., de Zee M., Andersen M.S., Rasmussen J., 2012. On validation of multibody musculoskeletal models. Proceedings of the Institute of Mechanical Engineering Part H 226, 82-94

Ohman C., Dall'Ara E., Baleani M., Van Sint Jan S., Viceconti M., 2008. The effects of embalming using a 4% formalin solution on the compressive mechanical properties of human cortical bone. Clin Biomech 23, 1294-1298

Rincon-Kohli L., Zysset P.K., 2009. Multi-axial mechanical properties of human trabecular bone. Biomechanics and Modeling in Mechanobiology 8, 195-208

Unger S., Blauth M., Schmoelz W., 2010. Effects of three different preservation methods on the mechanical properties of human and bovine cortical bone. Bone 47, 1048-1053. Epub 2010 Aug 1021.

Viceconti M., Bellingeri L., Cristofolini L., Toni A., 1998. A comparative study on different methods of automatic mesh generation of human femurs. Medical Engineering and Physics 20, 1-10.

Whealan K.M., Kwak S.D., Tedrow J.R., Inoue K., Snyder B.D., 2000. Noninvasive imaging predicts failure load of the spine with simulated osteolytic defects. Journal of Bone and Joint Surgurey American volume 82, 1240-1251

Curriculum Vitae

ENRICO DALL'ARA

Birth: 4th February 1981, Cesena (FC), Italy
Nationality: Italian
Current Address: Eisvogelgasse 6/24, 1060, Vienna, Austria
Email: edallara@ilsb.tuwien.ac.at
Tel number: +436648985833
Languages: Italian *(mother tongue)*, English *(fluent)*, German *(basic)*

Education

2008-2012 *PhD Mechanical Engineering*, TU-Wien, Austria
2000-2006 *MSc Mechanical Engineering*, University of Bologna, Italy

Professional Activities and Awards

2008-today *Laboratory Manager*, TU-Wien, Austria
2009 ***Best Poster Award*** of the Austrian Society of Mineral Research
2006-2007 *Junior Researcher*, Rizzoli Orthopedic Institute, Bologna, Italy

Selected Publications in Peer Reviewed Journals (chronological order, out of 23)

Öhman C, Baleani M, Perilli E, Tassani S**, Dall'Ara E**, Baruffaldi F, Viceconti M: "*Mechanical testing of cancellous bone from the femoral head: experimental errors due to off-axis measurements*"; JBiomech. 2007;40(11):2426-33.

Dall'Ara E, Öhman C, Baleani M, Viceconti M: "*The effect of tissue condition and applied load on Vickers hardness of human trabecular bone*"; JBiomech. 2007;40(14):3267-70.

Schileo E, **Dall'Ara E**, Taddei F, Malandrino A, Schotkamp T, Baleani M, Viceconti M: *"An accurate estimation of bone density improves the accuracy of subject-specific Finite Element Models"* JBiomech. 2008;41(11):2483-91.

Dall'Ara E, Schmidt R, Pahr D, Varga P, Chevalier Y, Patsch J, Kainberger F, Zysset P: *"A nonlinear finite element model validation study based on a novel experimental technique for inducing anterior wedge-shape fractures in human vertebral bodies in vitro"*; JBiomech. 2010;43(12):2374-2380

Varga P, **Dall'Ara E**, Pahr D, Pretterklieber M, Zysset P: *"Validation of an HR-pQCT-based homogenized finite element approach using mechanical testing of ultra-distal radius sections"*; BiomechModelMechanobiol. 2011; 10(4): 431-44

Dall'Ara E, Varga P, Pahr D, Zysset P: *"Full Range Calibration of local QCT BMD for Human Vertebral Body with registered Micro-CT images"*; MedPhys 2011; 38 (5): 2602-2609

Dall'Ara E, Pahr D, Varga P, Kainberger F, Zysset P*: "QCT-based Finite Element Models predict the Human Vertebral Apparent Strength and Stiffness significantly better than DXA"*; OsteoporosInt 2012; 23(2): 563-572

Pahr D, **Dall'Ara E**, Varga P, Zysset P: *"HR-pQCT based homogenized finite element models provide quantitative predictions of experimental vertebral body stiffness and strength with the same accuracy as μFE models"*; CMBBE. 2012, 15(7): 711-720

Dall'Ara E, Öhman C, Baleani M, Viceconti M: *"Is the hardness of human trabecular bone the same for normal and osteoarthritic subjects?"*; JBiomech 2011; 44 (8): 1593-1598

Dall'Ara E, Schmidt R, Zysset P: *"Microindentation can discriminate between damaged and intact human bone tissue"*; Bone. 2012; 50(4): 925-929

Maquer G, **Dall'Ara E**, Zysset P: *"Removal of the cortical endplates has little effect on ultimate load and damage distribution in QCT-based voxel models of human lumbar vertebrae under axial compression"*; JBiomech 2012; 45(9): 1733-1738

Dall'Ara E, Luisier B, Schmidt R, Pretterklieber M, Kainberger K, Zysset P, Pahr D: *"DXA predictions of human femoral mechanical properties depend on the load configuration"*, Bone 2013; 52(1): 27-38

Pahr D, Schwiedrzik J, **Dall'Ara E**, Zysset P: *"Clinical versus pre-clinical FE models for vertebral body strength predictions"*, **Submitted *(Invited)*** to special issue of JMBBM

Dall'Ara E, Luisier B, Schmidt R, Kainberger K, Zysset P, Pahr D: *"A nonlinear QCT-based finite element model validation study for the human femur tested in two configurations in vitro"*, **Accepted** in Bone

Selected Conferences Contributions (chronological order, out of 27)

Dall'Ara E, Öhman C, Baleani M, Viceconti M: *"Osteoarthritis Affects Hardness Of Human Trabecular Bone Tissue";* ESB 2008 Lucern; Talk

Dall'Ara E, Schmidt R, Pahr D, Varga P, Chevalier Y, Patsch J, Kainberger F, Zysset P: *"An improved technique for inducing compression fractures of vertebral bodies in vitro"*; ECTS 2009 Vienna; Poster

Dall'Ara E, Varga P, Pahr D, Zysset P: *"Local BMD calibration of human vertebrae QCT using registered Micro-CT images"*; ECTS 2010 Glasgow; Poster

Dall'Ara E, Schmidt R, Zysset P: *"Microindentation can discriminate between damaged and intact human bone tissue"*; ESB 2010 Edinburgh; Talk

Dall'Ara E, Pahr D, Varga P, Kainberger F, Zysset P: *"Comparison between clinical diagnostic tools and QCT-based Finite Element models for predicting human vertebral apparent strength in vitro"*; ASBMR 2010 Toronto, Poster

Dall'Ara E, Pahr D, Varga P, Kainberger F, Zysset P: *"Vertebral Strength Prediction With An Increased QCT Resolution: Densitometry Versus FEA"*; ECTS 2011 Athens; Poster

Pahr D, **Dall'Ara E**, Varga P, Zysset P: *"HR-pQCT based homogenized finite element models provide quantitative predictions of experimental vertebral body stiffness and strength with the same accuracy as μFE models"*; ISB 2011 Brussels; Talk

Dall'Ara E, Pahr D, Zysset P: *"QCT-BMD to microCT-BV/TV calibration relationships are similar for human vertebra and femur"*; ESB 2012 Lisbon, Talk

Dall'Ara E, Luisier B, Pretterklieber M, Kainberger K, Zysset P, Pahr D: *"A Non-linear Finite Element model Validation study for the Human Femur"*; ECCOMAS 2012 Vienna, Talk